THE UNIVERSITY OF WARWICK

Library Declaration and Deposit Agreement

1. STUDENT DETAILS

Please complete the following:

Full name: ……

University ID number: ……

2. THESIS DEPOSIT

2.1 I understand that under my registration at the University, I am required to deposit my thesis with the University in BOTH hard copy and in digital format. The digital version should normally be saved as a single pdf file.

2.2 The hard copy will be housed in the University Library. The digital version will be deposited in the University's Institutional Repository (WRAP). Unless otherwise indicated (see 2.3 below) this will be made openly accessible on the Internet and will be supplied to the British Library to be made available online via its Electronic Theses Online Service (EThOS) service.
[At present, theses submitted for a Master's degree by Research (MA, MSc, LLM, MS or MMedSci) are not being deposited in WRAP and not being made available via EthOS. This may change in future.]

2.3 In exceptional circumstances, the Chair of the Board of Graduate Studies may grant permission for an embargo to be placed on public access to the hard copy thesis for a limited period. It is also possible to apply separately for an embargo on the digital version. (Further information is available in the *Guide to Examinations for Higher Degrees by Research*.)

2.4 *If you are depositing a thesis for a Master's degree by Research, please complete section (a) below. For all other research degrees, please complete both sections (a) and (b) below:*

(a) Hard Copy

I hereby deposit a hard copy of my thesis in the University Library to be made publicly available to readers (please delete as appropriate) EITHER immediately OR after an embargo period of ……..... months/years as agreed by the Chair of the Board of Graduate Studies.

I agree that my thesis may be photocopied. YES / NO (*Please delete as appropriate*)

(b) Digital Copy

I hereby deposit a digital copy of my thesis to be held in WRAP and made available via EThOS.

Please choose one of the following options:

EITHER My thesis can be made publicly available online. YES / NO (*Please delete as appropriate*)

OR My thesis can be made publicly available only after…..[date] (Please give date)
YES / NO (*Please delete as appropriate*)

OR My full thesis cannot be made publicly available online but I am submitting a separately identified additional, abridged version that can be made available online.
YES / NO (*Please delete as appropriate*)

OR My thesis cannot be made publicly available online. YES / NO (*Please delete as appropriate*)

3. GRANTING OF NON-EXCLUSIVE RIGHTS

Whether I deposit my Work personally or through an assistant or other agent, I agree to the following:

Rights granted to the University of Warwick and the British Library and the user of the thesis through this agreement are non-exclusive. I retain all rights in the thesis in its present version or future versions. I agree that the institutional repository administrators and the British Library or their agents may, without changing content, digitise and migrate the thesis to any medium or format for the purpose of future preservation and accessibility.

4. DECLARATIONS

(a) I DECLARE THAT:

- I am the author and owner of the copyright in the thesis and/or I have the authority of the authors and owners of the copyright in the thesis to make this agreement. Reproduction of any part of this thesis for teaching or in academic or other forms of publication is subject to the normal limitations on the use of copyrighted materials and to the proper and full acknowledgement of its source.

- The digital version of the thesis I am supplying is the same version as the final, hard-bound copy submitted in completion of my degree, once any minor corrections have been completed.

- I have exercised reasonable care to ensure that the thesis is original, and does not to the best of my knowledge break any UK law or other Intellectual Property Right, or contain any confidential material.

- I understand that, through the medium of the Internet, files will be available to automated agents, and may be searched and copied by, for example, text mining and plagiarism detection software.

(b) IF I HAVE AGREED (in Section 2 above) TO MAKE MY THESIS PUBLICLY AVAILABLE DIGITALLY, I ALSO DECLARE THAT:

- I grant the University of Warwick and the British Library a licence to make available on the Internet the thesis in digitised format through the Institutional Repository and through the British Library via the EThOS service.

- If my thesis does include any substantial subsidiary material owned by third-party copyright holders, I have sought and obtained permission to include it in any version of my thesis available in digital format and that this permission encompasses the rights that I have granted to the University of Warwick and to the British Library.

5. LEGAL INFRINGEMENTS

I understand that neither the University of Warwick nor the British Library have any obligation to take legal action on behalf of myself, or other rights holders, in the event of infringement of intellectual property rights, breach of contract or of any other right, in the thesis.

Please sign this agreement and return it to the Graduate School Office when you submit your thesis.

Student's signature: .....…… Date: .....

Synthesis of DNA–polymer conjugates using RAFT polymerisation

by

Thomas Robert Wilks

A thesis submitted in partial fulfilment of the requirements

for the degree of Doctor of Philosophy in Chemistry

University of Warwick, Department of Chemistry

August 2013

Table of Contents

Acknowledgements

First, I must thank Rachel, my supervisor, whose constant support has kept me sane and enabled me to finish this thesis. I must also thank her for letting me follow my own ideas, even if in some cases they turned out to be dead ends.

I am very grateful to the University of Warwick for providing me with the resources I needed to complete my research, and to the Chancellor's Scholarship in particular for funding my studies. Thanks also go to all the technical and support staff in the Department of Chemistry for all the invaluable support and advice they have provided, and to everyone who has contributed to this work (particularly Jon Bath and Jan Willem de Vries).

A huge thank you to all the members of the O'Reilly group for helping me throughout the course of my PhD – your varied perspectives and constructive criticisms helped me get around many seemingly intractible problems. Particular thanks must go to Helen Willcock for proof-reading this thesis and for giving me plenty of encouragement during the process – both were completely invaluable.

I would like to thank my family and friends for getting me through what has been, at times, a very challenging three and a half years. Without you, I doubt I would ever have submitted this thesis. In particular, my wife Esme has stood more than can reasonably be expected of any partner and I doubt I will ever be able to repay her for her constant love, encouragement and emotional support.

Finally, thank you to my son Freddie, whose arrival has helped put everything in perspective.

Declaration

This thesis is submitted to the University of Warwick in support of my application for the degree of Doctor of Philosophy. It has been composed by myself and has not been submitted in any previous application for any degree.

The work presented (including data generated and data analysis) was carried out by the author except in the cases outlined below:

- The tetrazine compounds **10** and **12** were synthesised by Claire Hansell at the University of Warwick.
- The norbornene-terminated poly(NIPAM) used in Chapter 4 was synthesised by the group of Prof. Filip Du Prez of the University of Ghent.
- The TEM images in Chapter 5 and Chapter 6, and the AFM images in Chapter 7 were acquired by Joseph Patterson of the University of Warwick.
- The alkyne CTA (**15**) used in Chapter 5 and Chapter 6 was synthesised by Prof. Rachel O'Reilly of the University of Warwick.
- The AFM studies in Chapter 6 were conducted by Dr. Jeffery Raymond of Texas A&M University.

Parts of this thesis have been submitted for publication by the author in the following scientific journals:

- *ACS Nano* (Chapter 5 and Chapter 6) – DOI: 10.1021/nn402642a
- *Chemical Communications* (Chapter 7)

Signed _____ Date _____

Abstract

The use of reversible addition–fragmentation chain transfer (RAFT) polymerisation for the production of DNA–polymer conjugates is explored.

Chapter 1 gives a general introduction to the field of DNA–polymer conjugates, their potential applications and methods for their synthesis. The need for a general, solution-phase technique for DNA–polymer conjugation is highlighted.

In Chapters 2-5, the use of a number of different strategies for the production of DNA–polymer conjugates is described. Amide coupling (Chapter 2) is found to produce the desired products only under very specific reaction conditions. The thiol–alkene Michael addition reaction (Chapter 3) is found to afford DNA–polymer conjugates in aqueous solution with high yield; however, attempts to replicate this using organic solvents are not successful. The inverse electron-demand Diels–Alder reaction between tetrazine and norbornene (Chapter 4) is explored and found to produce DNA–polymer conjugates in high yield in organic solvents; however, the precursor compounds are time-consuming to prepare and so the generality of this approach is limited. Finally, the copper-catalysed azide–alkyne cycloaddition (Chapter 5) is found to be an excellent method for the production of a wide range of DNA–polymer conjugates.

Chapter 6 describes the use of the DNA segment of a DNA–polymer conjugate to assemble a discrete three dimensional nanostructure – a DNA tetrahedron – incorporating the temperature-responsive polymer poly(*N*-isopropylacrylamide). These hybrid structures are found to be able to stabilise the formation of discrete, well-defined polymer nanoparticles at elevated temperatures.

Chapter 7 describes the use of a non-covalent interaction (intercalation) to produce DNA–polymer conjugates. The effect of polymer molecular weight and structure on the strength of this interaction are explored. Finally, intercalation is exploited to template the formation of discrete polymer particles on a DNA strand.

Abbreviations

3-HPA	3-Hydroxypicolinic acid
4-AM	4-Acryloyl morpholine
AAm	Acrylamide
Acr	Acridine
AFM	Atomic force microscopy
AIBN	2,2'-Azobis(2-methylpropionitrile)
APMA	(3-aminopropyl)methacrylamide
ATRP	Atom transfer radical polymerisation
BiPy	2,2'-Bipyridine
BP	Base pair
CA	Citric acid
CDI	1,1'-Carbonyldiimidazole
CMC	Critical micelle concentration
CPG	Controlled pore glass bead
CRP	Controlled radical polymerisation
cryoEM	Cryogenic electron microscopy
cryoTEM	Cryogenic transmission electron microscopy
CTA	Chain transfer agent
ctDNA	Calf thymus DNA
CuAAC	Copper-catalysed azide–alkyne cycloaddition

Đ Dispersity

DA Diels–Alder

DA_{inv} Inverse electron demand Diels–Alder

DCC *N*,*N*'-Dicyclohexylcarbodiimide

DCM Dichloromethane

DDMAT 2-(Dodecylthiocarbonothioylthio)-2-methylpropionic acid

D_h Hydrodynamic diameter

DI De-ionised

DIPEA *N*,*N*-Diisopropylethylamine

DLLA D,L-Lactic acid

DLS Dynamic light scattering

DMA Dimethylacrylamide

DMAc *N*,*N*-Dimethylacetamide

DMAP 4-(Dimethylamino)pyridine

DMF *N*,*N*-Dimethylformamide

DMPP Dimethylphenylphosphine

DMSO Dimethyl sulfoxide

DNA Deoxyribonucleic acid

DP Degree of polymerisation

dsDNA Double stranded DNA

DTNB 5,5'-Dithiobis(2-nitrobenzoate)

EDCI *N*-(3-Dimethylaminopropyl)-*N*'-ethylcarbodiimide hydrochloride

EDTA Ethylenediaminetetraacetic acid

EPHP 1-Ethylpiperidine hypophosphite

ESI Electrospray ionisation

FAM 6-Carboxyfluorescein

FC Ferrocene

FRET Förster resonance energy transfer

FTIR Fourier transform infrared

GM Glycomonomer

GO Graphene oxide

HATU 1-[*bis*(Dimethylamino)methylene]-1*H*-1,2,3-triazolo[4,5-*b*]pyridinium 3-oxid hexafluorophosphate

HBTU *O*-(Benzotriazol-1-yl)-*N*,*N*,*N*',*N*'-tetramethyluronium hexafluorophosphate

HEMA Hydroxyethyl methacrylate

HOBt 1-Hydroxybenzotriazole

HPLC High-performance liquid chromatography

HPMA (2-Hydroxypropyl)methacrylamide

HR High resolution

IR Infrared

K_a Equilibrium binding constant

LbL Layer-by-layer

LC Liquid chromatography

LCST Lower critical solution temperature

LD Linear dichroism

LPO Lauroyl peroxide

MA Methyl acrylate

MAAm Methacrylamide

MAH Maleic anhydride

Mal Maleimide

MALDI-ToF Matrix-assisted laser desorption/ionisation time-of-flight

MMA Methyl methacrylate

M_n Number average molecular weight

MOPS 3-(*N*-Morpholino)propanesulfonic acid

MS Mass spectrometry

MVE Methylvinyl ether

MWCO Molecular weight cut-off

NAS *N*-Acryloyl succinimide

Nb Norbornene

NHPMI *N*-(*n*-Hexyl)-2-pyridylmethanimine

NHS *N*-Hydroxysuccinimide

NIPAM *N*-Isopropylacrylamide

NMP Nitroxide-mediated polymerisation

NMP 1-Methyl-2-pyrrolidinone

NMR Nuclear magnetic resonance

NVC *N*-Vinyl caprolactam

NVP *N*-Vinyl pyrrolidone

OEGMA Oligo(ethylene glycol) methacrylate

P4-AM Poly(4-acryloyl morpholine)

PAA Phenylacetylene alcohol

PAGE Poly(acrylamide) gel electrophoresis

PBS Phosphate buffer solution

PCL Poly(ε-caprolactone)

PCR Polymerase chain reaction

PDA Photodiode array

PDMA Poly(dimethylacrylamide)

PEG Poly(ethylene glycol)

PEGA Poly(ethylene glycol) acrylate

PEGMA Poly(ethylene glycol) methacrylate

PEI Poly(ethyleneimine)

PFO Poly(9,9-di-n-octylfluorenyl-2,7-diyl)

PFP Pentafluorophenyl

PFS Poly(ferrocenylsilane)

PIC Polyion complex

PLG Propargyl-L-glutamate

PMDETA *N*,*N*,*N*',*N*',*N*''-Pentamethyldiethylenetriamine

PMMA Poly(methyl methacrylate)

PNIPAM	Poly(NIPAM)
PPE	Poly(*para*-phenyleneethynylene)
PPO	Poly(propylene oxide)
PS	Poly(styrene)
PTFE	Poly(tetrafluoroethylene)
PyBOP	(Benzotriazol-1-yloxy)tripyrrolidinophosphonium hexafluorophosphate
PyBroP	Bromotripyrrolidinophosphonium hexafluorophosphate
RAFT	Reversible addition–fragmentation chain transfer
RI	Refractive index
RNA	Ribonucleic acid
RT	Room temperature
SDS	Sodium dodecyl sulfate
SEC	Size exclusion chromatography
SPAAC	Strain-promoted azide–alkyne cycloaddition
ssDNA	Single stranded DNA
Sty	Styrene
TAMRA	Carboxytetramethylrhodamine
TCEP	*tris*(2-Carboxyethyl)phosphine
TEA	Triethylamine
TEAA	Triethylammonium acetate
TEGA	Tri(ethylene glycol) methyl ether acrylate

TEM Transmission electron microscopy

THF Tetrahydrofuran

THPTA *tris*-(Hydroxypropyltriazolylmethyl)amine

T_m Melting temperature

TNB 5-Thio(2-nitrobenzoate)

Tris 2-Amino-2-(hydroxymethyl)-1,3-propanediol

Tz Tetrazine

UV Ultraviolet

VAc Vinyl acetate

Chapter 1

Introduction

The importance of the nanoscopic world

Nature has made good use of the subtle forces of evolution and over the billions of years that life has existed on this planet has developed a truly astounding degree of complexity. Variation at the macroscopic level is the most immediately obvious manifestation of this diversity, but beneath everything that we are able to see with the naked eye lies an ocean of micro- and nanoscopic structures, and it is these that are ultimately responsible for the proliferation and divergent forms of life on Earth.

From the materials scientist's point of view, natural systems have the enviable quality of being precisely structured from the level of single atoms to that of whole ecosystems. While we have developed highly efficient, complex and versatile ways to manipulate small molecules – indeed, to the point at which the possibility of 'dialling in' a molecule of interest and having it produced to order is now seriously being mooted (although it is still some way off)[*] – and arguably can be said to have equalled Nature in our ability to produce complex microscopic objects,[1] we still lack the ability to produce absolutely precise structures on the nanometre scale. It is this regime, illustrated in Figure 1.1, that is the target of much of today's cutting edge materials science research.

Natural systems, by contrast, excel when it comes to controlled organisation on this length scale. Although in many cases assembly is controlled by (comparatively) simple hydrophobic/hydrophilic interactions (for example in cell membranes and vesicles), the most complex structures – enzymes, viruses, the ribosome, the DNA double helix – rely on precise manipulation of intra- and intermolecular interactions, achieved by absolute control

[*] http://www.dial-a-molecule.org/wp/

of primary structure and fine-tuning of the energetics of the system. What is perhaps most remarkable is that all life (and its diversity) derives from the shuffling of just four nucleic acid bases and twenty-three amino acids.

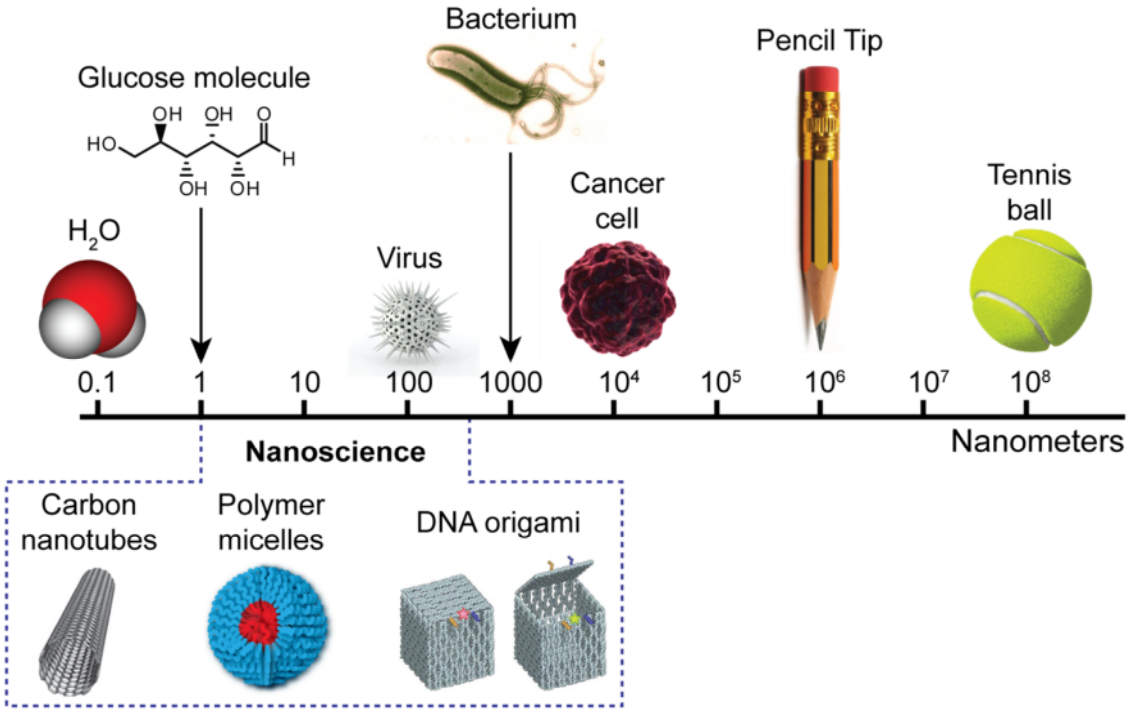

Figure 1.1 Illustration of the size regime targeted by nanoscience and nanomaterials research.

From a materials science point of view, proteins and nucleic acids represent nothing more than polymers of zero dispersity (that is, they have a single molecular weight rather than a range) in which the monomer sequence is known absolutely. In contrast to Nature, materials scientists have many fewer limitations when it comes to the palette of monomers from which they are free to choose, so in principle our ability to produce complex nanostructures should be commensurately greater. However, two limitations have presented themselves that have hindered the ability of the scientific community in achieving this goal. The first is that although the laws governing chemical interactions are well known and understood the ability to apply these laws in highly complex polymeric systems has yet to be realised. Indeed, it is still not possible to predict the structure that a given amino acid sequence will adopt (although significant advances have been made in the field of the design of protein tertiary structure[2]), so the possibility of using manmade

monomers to design, *ab initio*, a complex, perfectly-defined structure remains for now a distant dream. The second problem is that polymerisation techniques have yet to progress to a stage whereby the production of sequence-defined, monodisperse products is a realistic prospect. However, materials scientists have made significant advances in creating complex nanoscale objects from polymeric building blocks, and one of the reasons for this has been the introduction of controlled polymerisation techniques, which have allowed access to those building blocks.

Nanostructures from block copolymers

The most basic interaction exploited by materials scientists – and in particular polymer chemists – is the incompatibility between hydrophilic and hydrophobic groups, and their partitioning in an aqueous environment. It is this interaction that is responsible for the formation of micelles from surfactants such as sodium dodecyl sulfate (SDS), and vesicles and bilayers from phospholipids (Figure 1.2). In most examples taken from Nature, these amphiphilic compounds take the form of a polar head group attached to a hydrophobic hydrocarbon chain.

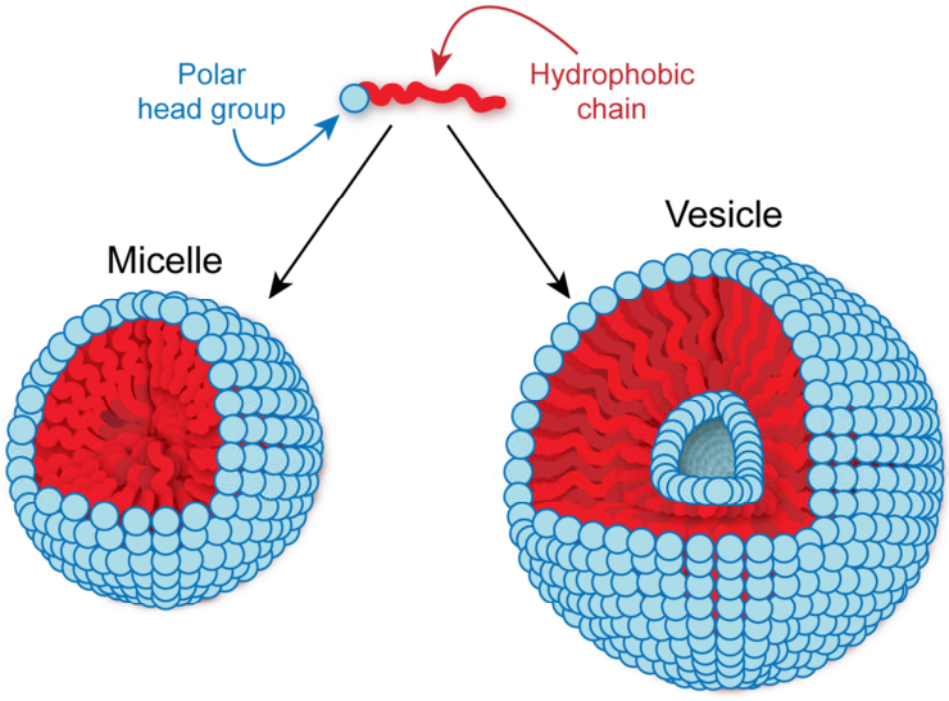

Figure 1.2 Structures of a micelle and a vesicle formed from a small molecule amphiphile.

However, the hydrophilic head group can also be polymeric, and so polymer chemists can exploit this effect by covalently linking two chains of differing solvophilicity – that is, by the synthesis of amphiphilic diblock copolymers. Upon dissolution in water, the hydrophobic and hydrophilic domains partition and discrete structures may be formed – the morphology adopted depends on the amount of space taken up by the two domains, usually known as the packing parameter (Figure 1.3).[3]

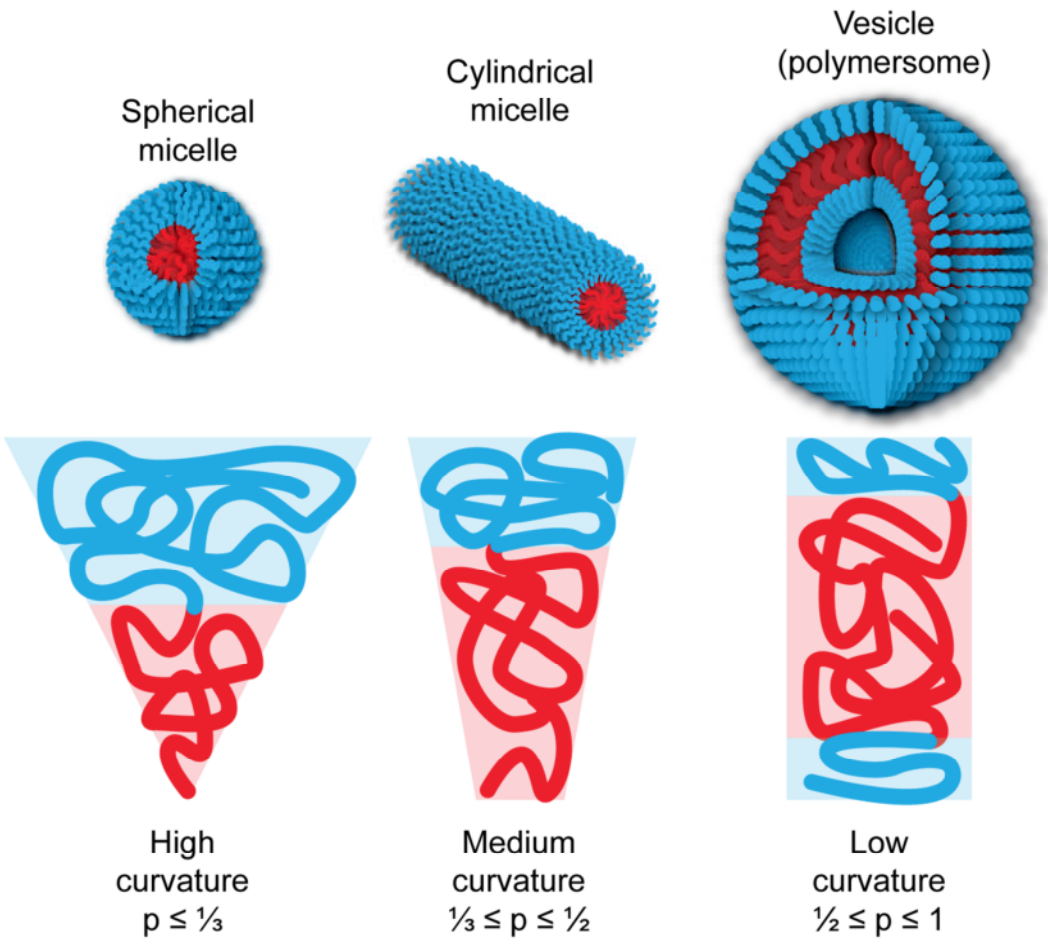

Figure 1.3 Schematic representation of the different structures adopted by amphiphilic diblock copolymers in water. The morphology depends on the packing parameter, p, which is a measure of the volume occupied by the hydrophobic part of the polymer chain (red). Adapted from Blanazs, Armes and Ryan.[3]

For conventional AB-type block copolymers, spherical micelles and vesicles (also known as polymersomes) are the most commonly-targeted structures, and there is an abundance of literature on the subject.[3,4] More complex systems have been devised, wherein one or more of the polymer blocks has a responsive character: this allows the packing parameter to be

changed upon application of an external stimulus, thus effecting a morphology change, be it from unimers to vesicles, unimers to micelles, micelles to vesicles, or *vice versa*.[5-7] Cylindrical micelles have also been created by exploiting the packing parameter effect, but this morphology represents more of a challenge as it is only favoured within a relatively narrow window.[8]

A much larger degree of structural variation can be accessed if more than two polymeric blocks are employed – for example in ABC- or ABA-type block copolymers. Hamburger-shaped micelles have been reported,[9] as have toroidal,[10] helical,[11] tubular,[12] and ribbon-shaped structures, and a plethora of less well-defined morphologies such as 'octopuses' and various bilayer assemblies.[13] All of these examples, however, rely on the same basic principle of the incompatibility between hydrophilic and hydrophobic chains in an aqueous milieu. The reader is directed to an excellent review on the subject for more information.[3]

Recently, polymer chemists have begun to move away from the use of the packing parameter as the main driver for nanoscale structure formation. An excellent example of the use of a new interaction to control polymer assembly comes from the work of Manners *et al.*, who used the crystalline nature of poly(ferrocenylsilane) to create very well-defined cylindrical micelles of controlled length and diameter (Figure 1.4).[14]

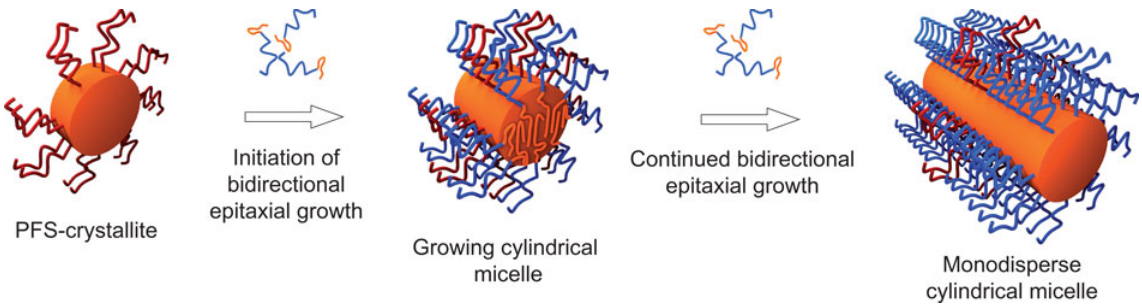

Figure 1.4 Cylindrical micelles of poly(ferrocenylsilane) (PFS) grown by crystallisation-driven self-assembly (from Manners *et al.*).[14]

Here the driving force for structure formation is not the packing parameter of the polymers involved but the crystallisation of the core block. Further manipulation of this phenomenon has even allowed the growth of asymmetric ABC-type cylinders, which

contain discrete domains of different polymers in the shell.[15] Petzetakis *et al.* have also made use of this crystallisation-driven self-assembly method by employing the semicrystalline polymer poly(L-lactide) as the core-forming block.[16]

Another interesting example was demonstrated by Hawker *et al.*, who used the addition of gold nanoparticles to induce a morphology transition from spherical to ellipsoidal in surfactant-stabilised structures made of poly(styrene-*b*-2-vinylpyridine).[17] Here, control of interfacial interactions between the two polymeric blocks and the surfactant was key in driving the shape change.

A few examples also exist of the use of hydrogen bonding interactions to create novel morphologies for block copolymer self-assemblies.[18-21] However, most of the literature in this area concerns the production of vesicular or spherical micellar particles.[22] Clearly, these examples have only touched the surface of what is possible and there remains a huge amount of scope for the use of different molecular interactions for the production of novel polymeric architectures.

The rise of DNA as a nanoscale building block

While amino acids are Nature's building block of choice for the production of 3D nanoscale architectures, the sheer number and complexity of the possible interactions in protein structures means they are not quite so appealing to materials scientists. DNA, by contrast, is used *in vivo* solely for the storage and transfer of genetic information, and almost all natural DNA is found in the archetypal double helix structure. However, DNA structures capable of advanced functions such as catalysis have been created in the laboratory,[23] and this molecule is capable of forming highly complex shapes – Nature has simply evolved a better alternative (in the shape of proteins) and so has no need to make use of this latent complexity. To materials scientists, however, DNA presents a huge advantage over peptides: it has a much more limited number of components (the four bases adenine, guanine, thymine and cytosine – A, G, T and C) and a small number of

highly specific, stable interactions (A pairs with T; G with C – see Figure 1.5). These features mean it is much simpler to predict the structure formed by a given DNA sequence or combination of sequences, and it is therefore an ideal material for the construction of complex nanoscale objects.

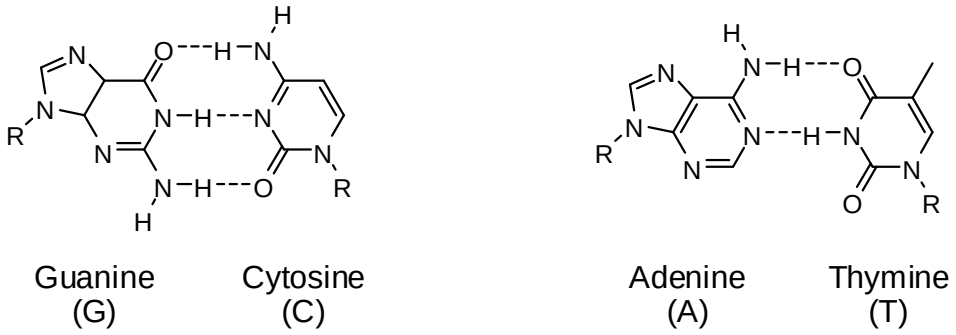

Figure 1.5 The Watson–Crick base pairs that control the assembly of double stranded DNA.

The idea of using DNA as an alternative programmable material was first suggested by Seeman, and developed much later by Rothemund into the field of DNA origami.[24,25] The original (and still much-used) concept of DNA origami is that a long single strand of DNA (typically derived from a bacterial genome) can be folded into any desired shape by the addition of so-called 'staple' strands, which act – as their name suggests – to pinch different regions of the long strand together. Perhaps the simplest structure that can be made in this manner is a DNA tile (see Figure 1.6), which is composed of parallel double helices tied together by staple strands that cross over from one helix to its neighbour.

This relatively simple concept has been developed into something approaching an art-form, with a wealth of complex structures such as the 'tensegrity triangle' and a 'locked' DNA box now accessible, as well as others incorporating 3D curvature.[26-28] Much smaller structures have also been created including tetrahedra,[29] prisms,[30] and cubes.[31] Hand in hand with this explosion in structural diversity, the use of DNA to perform complex functions such as computation,[32,33] chemical synthesis,[34,35] drug delivery,[36] and transport of cargo along a track,[37] has emerged as an important area of materials research. However, while DNA nanotechnology has provided access to a huge range of novel nanostructures,

and has undoubtedly been shown to be a powerful tool in materials chemistry, there remains a significant barrier to it having a truly profound impact outside of the research community: cost. Indeed, to make just a few nanomoles of the DNA box with a controllable lid cost nearly €10 000.* Although the cost of DNA synthesis will continue to fall, for now this means that the use of these structures for practical applications such as drug delivery or computing is not viable.

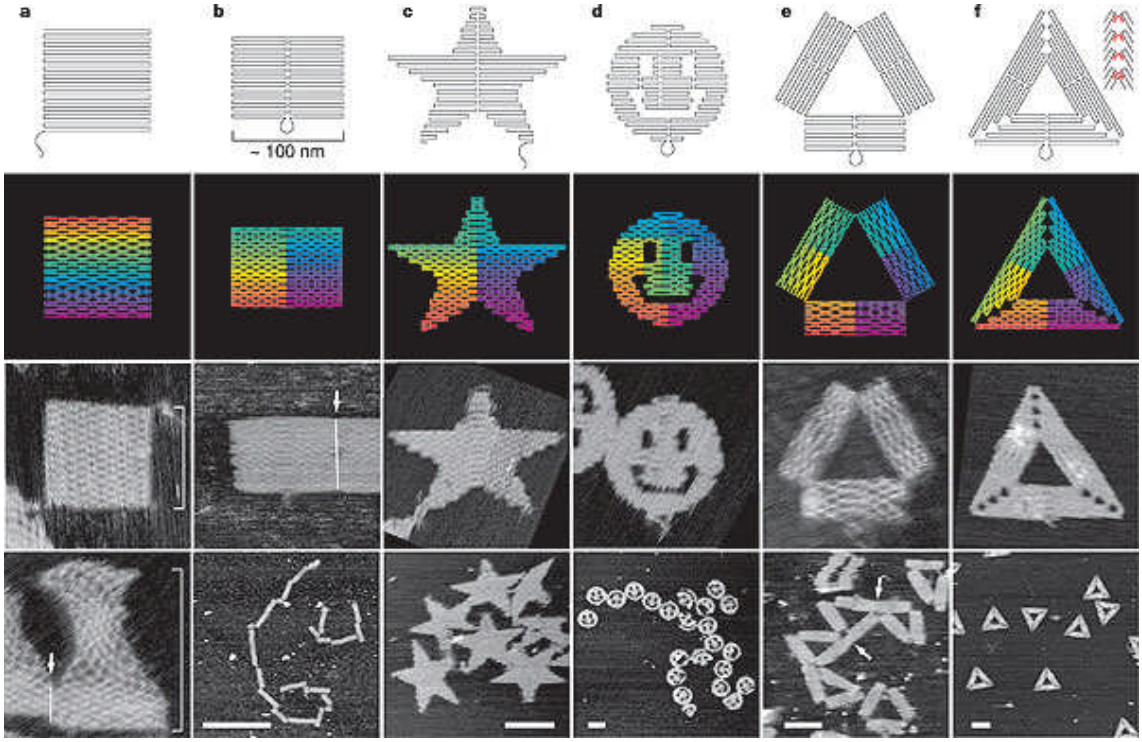

Figure 1.6 DNA tiles of different shapes assembled using the principles of DNA origami (from Rothemund).[25]

Covalent attachment of polymers to DNA

How can the problem of DNA cost be addressed? One idea is to replace some of the DNA with a cheaper material such as a polymer. The polymer then forms the bulk of the overall material, whilst the DNA is retained at key points to direct the precise assembly of the structure or to provide an addressable recognition site. This approach is exemplified by the 'programmable atom equivalents' of Mirkin *et al.*, wherein short DNA strands are tethered to the surface of inorganic or polymeric nanoparticles – assembly of these

* Conversation with the author, Kurt Gothelf.

particles is then directed by the hybridisation of complementary DNA sequences (Figure 1.7).[38-40]

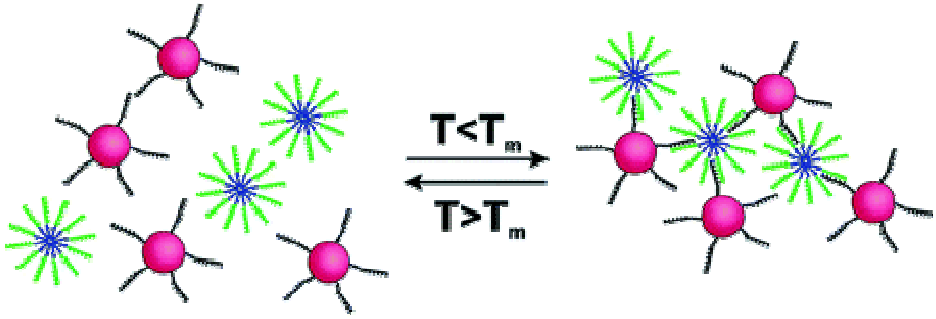

Figure 1.7 Programmed assembly of DNA-functionalised gold nanoparticles (pink) with DNA-containing polymer micelles (blue and green). The two populations of particles contained complementary DNA sequences and aggregated when mixed at room temperature. Upon heating above the melting temperature of the DNA the individual particles were released. From Mirkin *et al.*[39]

Polymers in particular are attractive for conjugation to DNA since they are capable (as discussed above) of forming well-defined nanostructures themselves. In addition, they also give access to a wide range of stimuli-responsive behaviours inaccessible to purely DNA-based structures.

Early research into the conjugation of short DNA strands with synthetic polymers was concerned primarily with the employment of polymers as "stealth" vehicles, wherein low circulation times and poor cell penetration *in vivo* might be overcome by concealing DNA in a biocompatible polymer package. Preliminary work utilised an ionic interaction wherein polyion complex (PIC) micelles were formed on mixing DNA (a poly*anion*) with a diblock copolymer containing a poly*cationic* block and an inert hydrophilic block. Alternatively, the DNA could be directly conjugated to the hydrophilic polymer and then mixed with a polycation. Neutralisation of charges and self-assembly in aqueous solutions yielded PIC micelles containing the polyion (DNA–polymer) complex as the core with an encapsulating hydrophilic shell (Figure 1.8).[41,42] Subsequent work in this area has seen the development of PIC micelles with targeting ligands on their periphery,[43] and degradable hydrophilic shells

to help increase the rate of DNA release.[44-46] The particles have also been used for therapeutic applications by encapsulating anti-sense DNA in the core.[47]

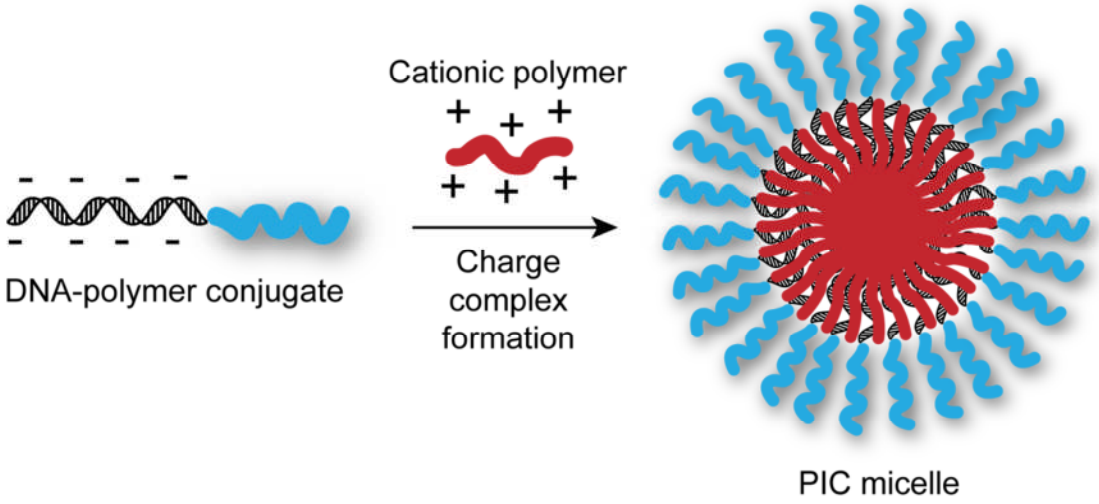

Figure 1.8 Schematic of the process used to make polyion complex (PIC) micelles. A DNA strand conjugated to a hydrophilic polymer (blue) is mixed with a cationic polymer (red). The DNA and cationic polymer combine to form a hydrophobic charge neutral complex that aggregates to form the core of the micelle.

Research has also been directed towards the attachment of hydrophilic polymers to DNA for other applications that do not involve precise higher-order assembly of the polymer segment. Stayton *et al.* attached complementary DNA sequences to poly(*N*-isopropylacrylamide) (poly(NIPAM)) and streptavidin to create a non-covalently linked polymer–protein hybrid that could be used for affinity precipitation of biotin (which binds to the protein) upon raising of the solution temperature above the polymer's cloud point.[48] The group of Matyjaszewski has also attached complementary DNA strands to poly(NIPAM) and Green Fluorescent Protein to create a non-covalently linked polymer–protein conjugate. Poly(NIPAM) has also been used for the affinity precipitation of the following species: double stranded DNA (by the formation of a triple helix),[49] single stranded DNA (by hybridisation with the complementary strand),[50,51] genotoxins,[52] and DNA-binding proteins.[53-55] The temperature-responsive nature of this polymer has also proved useful for the assembly of nanoparticles capable of hybridisation-induced aggregation, creating DNA sensors that are highly sensitive to even single base pair

mismatches.[56,57] Interestingly, DNA hybridisation events have been observed to increase the cloud point temperature of poly(NIPAM) in solution,[58] and conjugation of this polymer affords DNA that is more resistant to nuclease degradation *in vitro*.[59]

In the area of PIC micelles, the principal goal is the placement of DNA in the hydro*phobic* core of a water-dispersed micelle. Such an approach, however, is somewhat counter-intuitive when one considers that DNA is a wholly hydro*philic* molecule under normal physiological conditions, a property essential to its biological function.

Other hydrophilic polymers have been attached to DNA, and this has led to conjugates for use in a diverse range of applications. These include carriers for delivery of small interfering RNA,[60] DNA detection,[61-64] sandwich hybridisation and other diagnostic assays,[65-67] protein binding,[68] affinity electrophoresis,[69] DNA-coated surfaces,[70] DNA microarrays,[71,72] antiviral and therapeutic compounds,[73-75] and bioelectronics containing conductive polymers.[76]

Covalent conjugation of DNA to hydrophilic polymer blocks has been achieved through a number of aqueous phase conjugation strategies such as carbodiimide linkage,[42] disulfide formation,[58,75,77-81] thiol–maleimide Michael addition,[44-46,69] *via* the ribose ring,[68,73,74] and by photo-crosslinking with an intercalating group situated at the polymer chain-end.[54,55,82,83] A large body of work also exists concerning the incorporation of DNA into hydrogels by copolymerisation with monomers such as acrylamide;[84] however, these will not be discussed here and the reader is directed to a recent review should they wish to find out more.[85] All the approaches used to date are listed in Table 1.1, with details of the conjugation chemistries shown in Scheme 1.1 and Scheme 1.2. This gives an idea of the relatively narrow range of polymers that have been used, with a large preponderance for poly(ethylene glycol)- (PEG) and poly(NIPAM)-based conjugates. Yields also vary widely, depending both on the nature of the polymer and the conjugation chemistry employed. However, a number of techniques now exist that afford DNA–hydrophilic polymer conjugates in high yields (greater than 50 %).

Table 1.1 List of hydrophilic polymers conjugated to DNA, showing the techniques used. Yields are given as a range of the values quoted in the referenced works. Polymer abbreviations: PEG = poly(ethylene glycol), PCL = poly(caprolactone), 4-AM = 4-acryloyl morpholine, NAS = *N*-acryloyl succinimide, GM = glycomonomer, HEMA = hydroxyethyl methacrylate, HPMA = (2-hydroxypropyl)methacrylamide, APMA = (3-aminopropyl)methacrylamide, NIPAM = *N*-isopropylacrylamide, DLLA = D,L-lactic acid, GA = glycolic acid, OEGMA = oligo(ethylene glycol) methacrylate, PEGA = poly(ethylene glycol) acrylate, PEGMA = poly(ethylene glycol) methacrylate, PLG = propargyl-L-glutamate. Solvent abbreviations: MeCN = acetonitrile, DCM = dichloromethane, DMF = *N*,*N*-dimethylformamide. CPG = controlled pore glass bead. CuAAC = Copper-catalysed azide–alkyne cycloaddition. SPAAC = strain-promoted azide–alkyne cycloaddition

Polymer	Conjugation chemistry	Solvent	Phase	Yield / %
Elastin-like polypeptide	Amide coupling[86]	Water	Solution	-
Oligo(ethylene glycol)	Phosphoramidite[87]	MeCN	Solid support	-
PEG	Amide coupling[41-43,47]	Water	Solution	61-90
	Amide coupling + thiol Michael addition[88]	Water	Solution	98
	CuAAC[89]	Water	Solution	-
	Disulfide formation[79,81]	Water	Solution	61-75
	Thiol Michael addition[44-46]	Water	Solution	63-89
	Phosphoramidite[61,90]	MeCN	Solid support	-
PEG-*b*-PCL	Phosphoramidite[91]	DCM	Solid support	7
Poly(4-AM-*co*-NAS)	Growth from CPG[65]	MeCN	Solid support	-
Poly(acrylamide)	Thiol Michael addition[69]	Water	Solution	74
Poly(aspartamide)	SPAAC[60]	Water	Solution	98
Poly(GM)	Disulfide formation[80]	Water	Solution	97
Poly(HEMA)	Polym. from DNA[70]	Water	Solid support	-
Poly(HPMA-*s*-APMA)	Disulfide formation[75]	Water	Solution	89
Poly(L-lysine)	Reductive amination[68,73,74]	Water	Solution	-

Table 1.1 (continued)

Polymer	Conjugation chemistry	Solvent	Phase	Yield / %
Poly(NIPAM)	Amide coupling[48,49]	Water	Solution	15
	Amide coupling + thiol Michael addition[88]	Water	Solution	42
	Disulfide formation[58,77]	Water	Solution	70
	Photocrosslinking[54,55,82,83]	Water	Solution	36
	Phosphoramidite[90]	MeCN	Solid support	-
Poly(NIPAM-*co*-PA-*co*-NAS)	Amide coupling[92]	Water	Solution	-
Poly(OEGMA)	Polym. from DNA[70]	Water	Solid support	-
	CuAAC[93]	Water	Solution	-
Poly(PEGA)	Disulfide formation[78]	Water	Solution	88
Poly(PEGMA)	CuAAC[93]	Water	Solution	>99
Poly(PLG)	CuAAC[94]	Water	Solution	-
Poly(pyrrole)	Amide coupling[76]	DMF	Solution	-
	Ionic complex[64]	Water	Solution	-

When it comes to conjugation of hydrophobic polymers, however, there are far fewer examples of high-yielding coupling reactions. DNA is not very amenable to the procedures required for its conjugation to hydrophobic polymer segments (incompatibility with common organic solvents and the low efficiency of macromolecular coupling being the two biggest hurdles). As such, the generation of polymer–DNA hybrids for assembly into nanostructures containing hydrophobic polymer cores and DNA as the hydrophilic shell has only been investigated by a very small number of research groups. To date, *efficient* attachment of DNA to water-insoluble polymers has only been achieved using solid-phase synthetic strategies wherein DNA is grown from polymer chains tethered to the support,[65-67,71,72] by coupling phosphoramidite-functionalised hydrophobic polymer to bound DNA,[39,61,63,87,90,91,95-105] or by using extremely high concentrations of DNA.[62,106] Table 1.2

provides a summary of the approaches used thus far in this area. In almost all cases where hydrophobic polymers have been successfully conjugated, the use of a solid support was necessary to achieve acceptable yields.

Table 1.2 List of hydrophobic polymers conjugated to DNA, showing the techniques used. Yields are given as a range of the values quoted in the referenced works. Polymer abbreviations: PFO = poly(9,9-di-n-octylfluorenyl-2,7-diyl), MAH = maleic anhydride, MVE = methylvinyl ether, Nb-Sty = norbornene styrene, Nb-Acid = norbornene carboxylic acid, Nb-PAA = norbornene phenylacetylene alcohol, Nb-FC = norbornene ferrocene, PPE = poly(*para*-phenyleneethynylene). Solvent abbreviations: THF = tetrahydrofuran, DMSO = dimethyl sulfoxide.

Polymer	Conjugation chemistry	Solvent	Phase	Yield / %
PFO	Phosphoramidite	DCM	Solid support	25
Poly(benzyl ether) dendron	Phosphoramidite[95]	THF	Solid support	-
Poly(DLLA-*co*-GA)	Amide coupling[106]	DMSO	Solution	75
Poly(ethylene-*alt*-MAH)	Growth from CPG[67]	MeCN	Solid support	-
Poly(MAH-*alt*-MVE)	Growth from CPG[66]	MeCN	Solid support	-
Poly(Nb-Sty-*b*-Nb-Acid)	Amide coupling[107]	DMF	Solution	-
	Amide coupling[108]	$CHCl_3$	Solution	-
Poly(Nb-PAA)	Phosphoramidite[96]	$CHCl_3$	Solid support	30
Poly(Nb-Fc-*b*-Nb-PAA)	Phosphoramidite[63]	MeCN	Solid support	30
Poly(styrene)	Phosphoramidite[39]	DMF	Solid support	4
	Amide coupling[89]	MeCN	Solid support	-
	Amide coupling + thiol Michael addition[88,109]	THF	Solution	10
Poly(TBA-*co*-4-AM)	Growth from CPG[71,72]	MeCN	Solid support	-
PPE	Amide coupling[62]	Water	Solution	-
PPO	Phosphoramidite[90,97-104]	MeCN	Solid support	32-41
	Phosphoramidite[105]	DCM	Solid support	-

Amide coupling

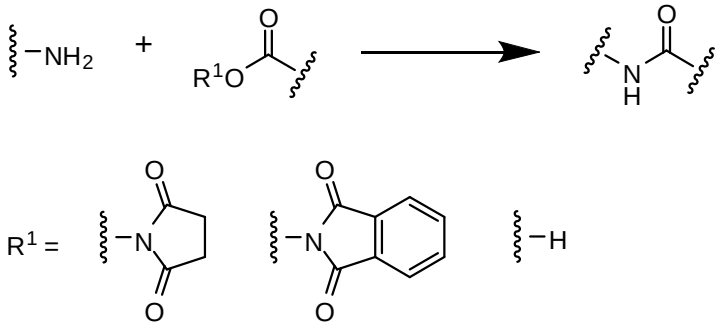

Amide coupling + thiol-ene

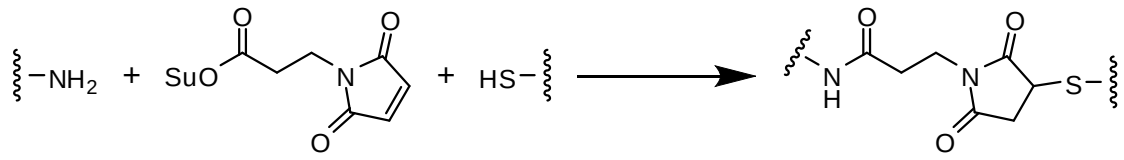

CuAAC

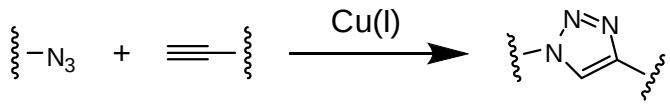

Disulfide formation

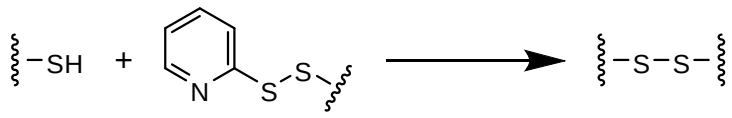

Growth from CPG

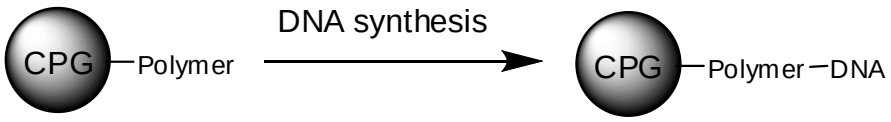

Ionic complex

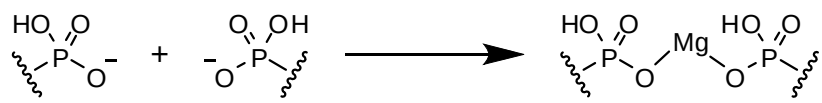

Scheme 1.1 Details of the conjugation chemistries used for the synthesis of DNA block copolymers.

Phosphoramidite

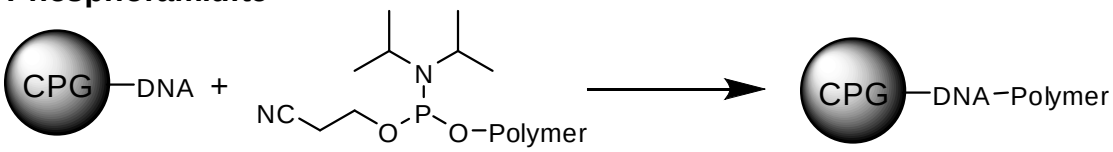

Photocrosslinking

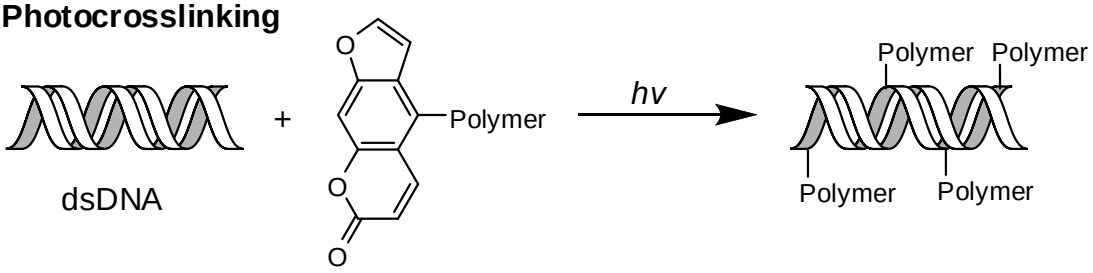

Polymerisation from DNA

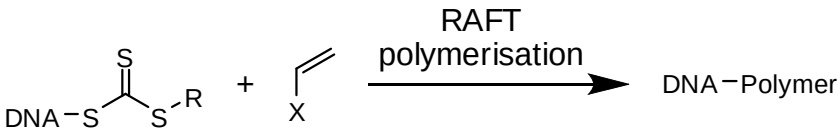

Reductive amination

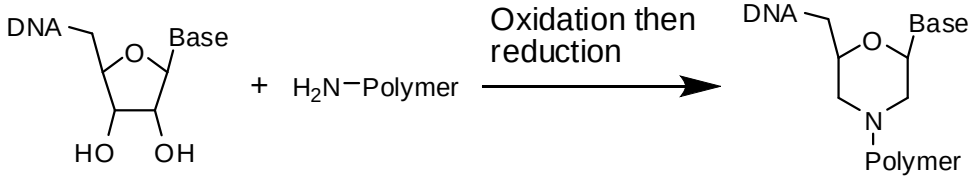

SPAAC

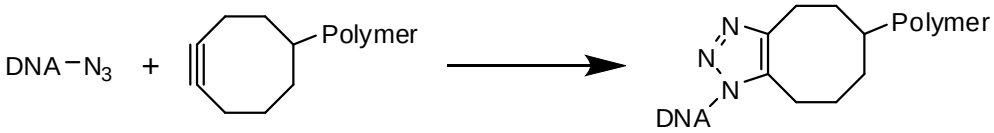

Thiol-ene

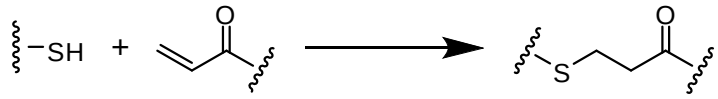

Scheme 1.2 Details of the conjugation chemistries used for the synthesis of DNA block copolymers.

Despite the inherent difficulties in linking DNA to hydrophobic polymer segments, this approach has realised the creation of a new family of amphiphilic diblock copolymers, wherein the hydrophilic block is replaced by a short single stranded DNA (ssDNA) segment (usually ~22 nucleotides in length). With correct tailoring of block ratios, these amphiphiles behave in a fashion analogous to their purely polymeric cousins and assemble into micellar structures in aqueous solution. In contrast to the PIC micelles discussed above, these assemblies have ssDNA exposed at their surface, leaving its unique functionality free for further manipulation.

One of the first examples of this approach came from Mirkin *et al.*, who synthesised poly(styrene)–DNA conjugates, which were found to assemble in aqueous solution into well-defined micelles.[39] The ssDNA located in the coronae of the micelles could then be used for the reversible formation of hybrid materials by mixing with gold nanoparticles bearing the complementary sequence of ssDNA (Figure 1.7). Matyjaszewski *et al.* also demonstrated the reversible formation of higher-order structures by functionalising star-shaped polymers with ssDNA.[93]

A large amount of the work in the area of DNA–polymer micelles has been performed by the group of Andreas Herrmann. Using poly(propylene oxide) (PPO) as the hydrophobic segment, micelles have been constructed with the ability to template organic reactions,[98] synergistically deliver anti-cancer therapeutics,[97] and act as templates for the deposition of protein coats to create virus-like delivery vehicles.[102] All of these applications rely on the unique interactions of the DNA segment. The same research group also found that a shape change from spherical to rod-like micelles could be achieved by the addition of different lengths of DNA complementary to that found in the micelles' coronae (Figure 1.9),[101] and also that the difference in shape had a drastic effect on the uptake of the particles by cells.[103] Hybrid micelles[99] and vesicles[100] have also been created by co-assembly of their DNA–polymer conjugates with PEG-*b*-PPO copolymers and lipids respectively. The lipid vesicles were of particular interest as the introduction of a photo-sensitizer by hybridisation

of a complementary strand bearing the appropriate group meant that the structures could be ruptured by exposure to UV irradiation.

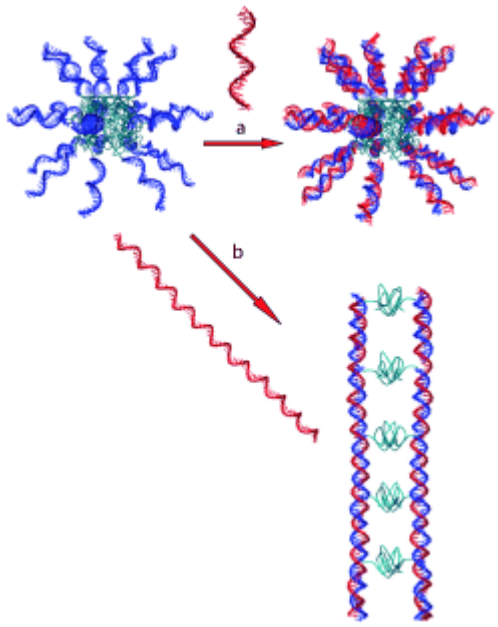

Figure 1.9 DNA-containing micelles synthesised by Herrmann *et al.*[101] Addition of a short strand of DNA complementary to that found in the shell of the micelle resulted in retention of the spherical morphology (a). However, addition of a strand of DNA containing multiple repeats of the complementary sequence led to the formation of rod-like structures (b).

Gauffre *et al.* synthesised DNA–polymer micelles containing a poly(caprolactone) core.[91] These particles could be selectively bound to and released from a surface coated with ssDNA by use of DNA hybridisation and de-hybridisation events, leading to potential applications in surface patterning.

Another interesting application came from Caruso *et al.*, who conjugated short repeat units of adenine (poly(A)) or thymine (poly(T)) to the surface of micelles composed of poly(NIPAM-*co*-propargyl acrylate-*co*-*N*-acryloyl succinimide) using amide coupling chemistry.[92] The poly(A)- and poly(T)-functionalised micelles were then used in a layer-by-layer deposition process on silica nanoparticles. Poly(T) was first deposited on the silica, and poly(A)-functionalised micelles were then added. These formed a layer by hybridisation of the DNA segments. Poly(T)-functionalised micelles were then added and the structure built up by repeating the process up to five times. The particles were capped with PEG,

and the silica template removed to create multi-functional DNA–polymer microcapsules (Figure 1.10).

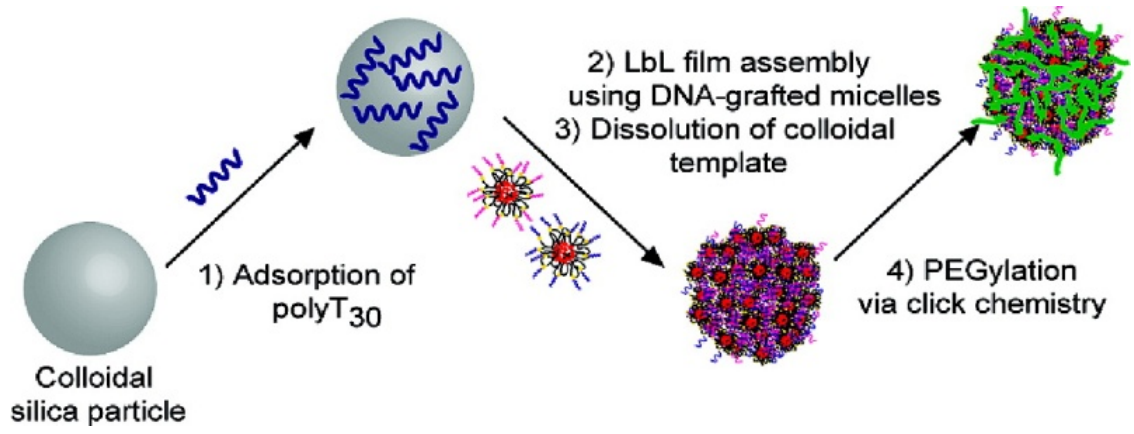

Figure 1.10 Hybrid DNA–polymer microcapsules synthesised by Caruso *et al.*[92] 1) A silica nanoparticle is functionalised with poly(thymine). 2) Micelles containing poly(adenine) or poly(thymine) are added in alternating steps to build up several layers. 3) The silica template is removed. 4) The surface of the hollow capsules is functionalised with PEG.

One of the most exciting features of micelles incorporating ssDNA in the corona is that it becomes possible to use biological tools – such as enzymes – for their manipulation. Herrmann *et al.* neatly demonstrated this by incorporating primers for the polymerase chain reaction into the coronae of their micelles. Upon incubation under PCR conditions the DNA was elongated from just 22 nucleotides in length to over one thousand, thus giving access to DNA–polymer conjugates with a much longer DNA segment than can be accessed by solid phase synthesis techniques.[88] The same group also used enzymatic ligation (stitching together of two DNA sequences) to elongate the DNA segment of several other DNA–polymer conjugates.[90]

Perhaps the most elegant use of this approach, however, was developed by Gianneschi *et al.*, who used enzymatic degradation of DNA to induce a morphology change from spherical micelles to rods (Figure 1.11).[108] The micelles were assembled from a diblock copolymer containing a hydrophobic poly(norbornene-styrene) segment and a hydrophilic section composed of a brush copolymer containing DNA side-arms. When the micelles were incubated with a 'DNAzyme' (a DNA-based structure that severs another DNA

strand at a specific location), the DNA arms were cut. This had the effect of drastically reducing the packing parameter of the hydrophilic segment, inducing the change to a rod-shaped morphology. The spherical shape could be restored by addition of a strand of DNA containing a region whose sequence was complementary to that of the shortened DNA arms. Hybridisation with this additional strand effectively restored the length of the arms, causing the packing parameter to change once more and restoring the original shape of the particles. The same group also discovered that the DNA contained within the micelles was much less vulnerable to nuclease degradation, presumably because the dense packing of the chains prevented binding of the enzyme.[107]

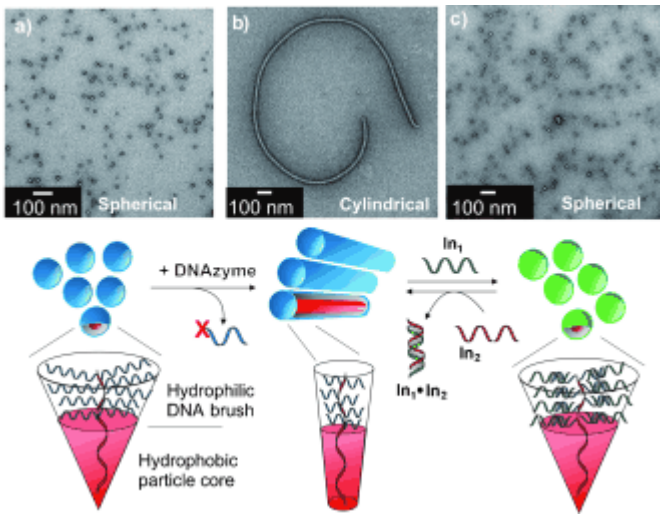

Figure 1.11 'Shape-shifting' micelles designed by Gianneschi *et al.*[108] Spherical micelles are formed by a block copolymer containing a poly(norbornene-styrene) core and a shell composed of a brush with DNA side arms (a). Upon incubation with a DNAzyme, which shortens the DNA arms, a switch to a cylindrical morphology is achieved (b). Re-extension of the arms can be achieved by addition of a long strand of DNA containing a region that is complementary to the shortened arms contained in the particles (c).

Liu *et al.* created pH-responsive DNA–polymer micelles by clever design of the DNA sequence contained in the particles' coronae. Incorporation of a long run of cytosine residues led to the formation of spherical micelles at high pH but formation of an 'i-motif' structure involving two DNA–polymer conjugates at low pH, resulting in a switch to a rod-like morphology (Figure 1.12).[104]

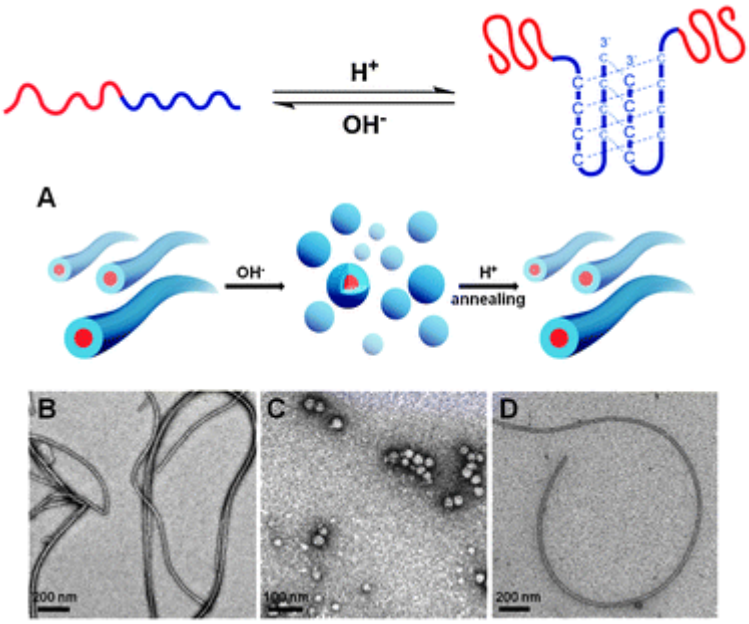

Figure 1.12 pH-responsive DNA-containing micelles synthesised by Liu *et al.*[104] At high pH, the DNA contained in the micelle's corona exists as a single strand, leading to the formation of spherical particles (C). Lowering the pH causes the DNA to pair up to form 'i-motif' structures, resulting in a switch to a rod-like morphology (B and D).

The above study neatly demonstrated that DNA structures beyond the double helix could be used to give DNA–polymer conjugates added functionality. However, the use of the DNA strand for the assembly of more complex structures remains relatively under-explored, which is somewhat surprising given the multitude of architectures that are now available thanks to the development of DNA origami (see above). Sleiman *et al.* have begun to explore this area, using DNA cubes and nanotubes for the precise 3D arrangement of polymer domains (Figure 1.13).[89,110]

The research into DNA–polymer conjugates reviewed above clearly demonstrates the great potential of this field to yield novel nanoscale materials. However, the difficulties with the production of these conjugates (particularly containing hydrophobic polymers) has meant that relatively few research groups – and in particular those concerned primarily with polymer synthesis rather than biomaterials – have ventured into this area. Whilst solid phase synthesis has allowed for the production of DNA–polymer conjugates in relatively high yields and is efficient (in most cases), its reliance on expensive solid-phase DNA

synthesis equipment limits its accessibility to the wider community of polymer chemists, underlining the necessity for the development of robust, efficient solution-phase strategies.

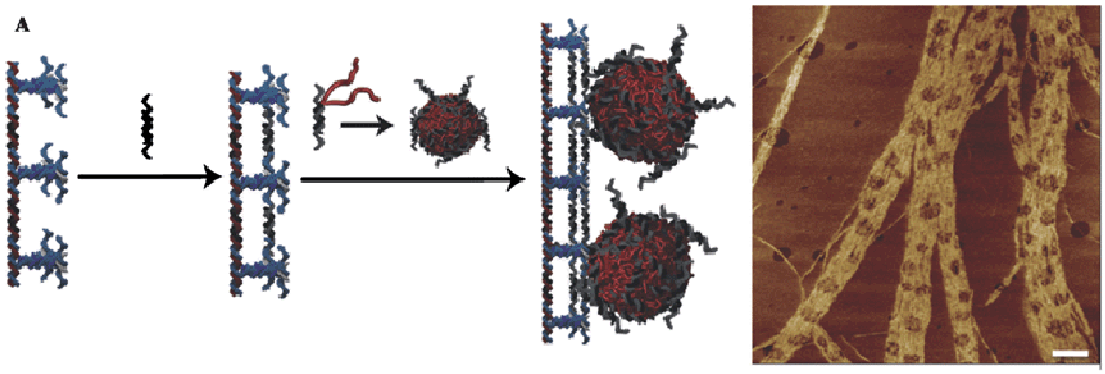

Figure 1.13 Use of a DNA template to organise polymer domains, as demonstrated by Sleiman *et al.*[89] A long DNA rod (left) bearing single stranded DNA domains is functionalised by addition of polymer particles (red spheres) bearing the complementary DNA strand. Organisation of the polymer domains was observed by atomic force microscopy (right-hand panel).

Non-covalent methods for the attachment of polymers to DNA

Up to this point, only the covalent attachment of polymers to DNA strands has been discussed. However, in some situations, such as delivery of therapeutic DNA, it may be that physical attachment of the polymer is not desirable. The double-helical structure of double stranded DNA (dsDNA) is well known and contains a number of sites where non-covalent binding may occur (Figure 1.14). Firstly, there are the major and minor grooves, formed by the asymmetric positioning of the phosphate backbone on the DNA bases (right of Figure 1.14). Secondly, the space between the base pairs of DNA can also serve as a binding site for large, planar aromatic molecules such as acridine and ethidium bromide. However, there are almost no reported uses of these interactions to form DNA–polymer conjugates – this area undoubtedly contains huge potential for the synthesis of interesting new materials and is discussed at greater length in Chapter 7.

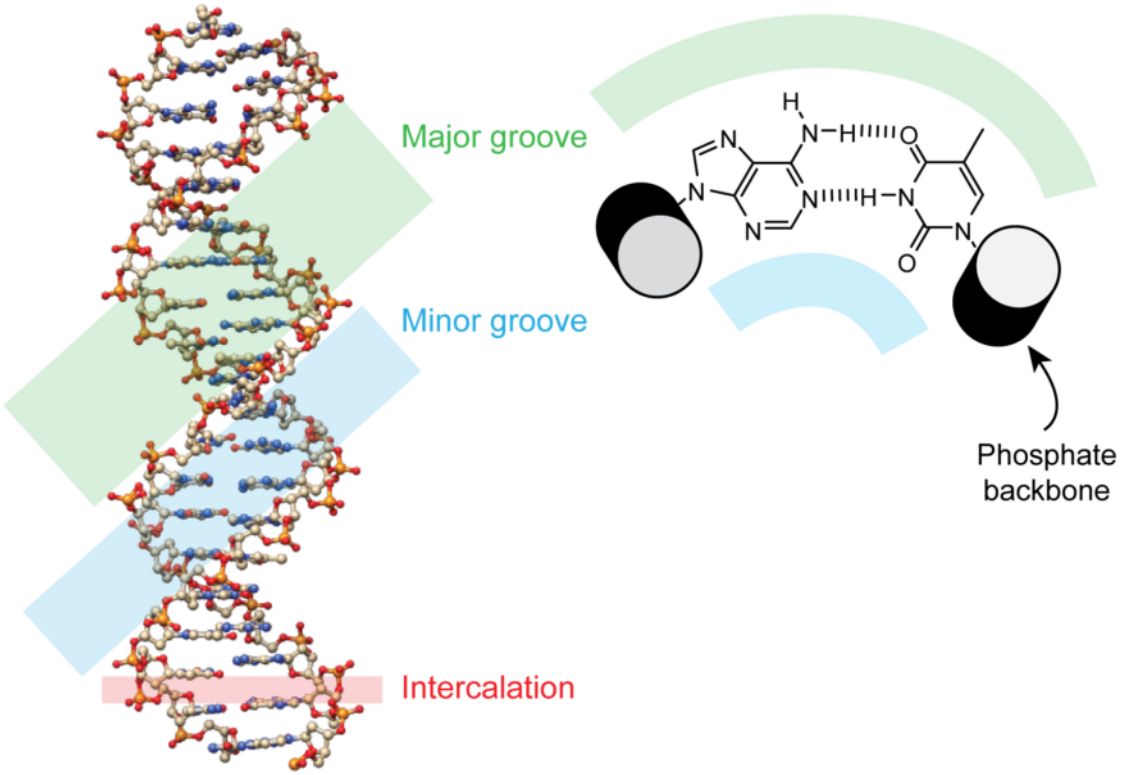

Figure 1.14 The structure of the B-form of dsDNA showing potential sites for non-covalent binding. These include binding in the major (green) or minor (blue) grooves, which are formed by the asymmetric positioning of the phosphate backbone on the DNA bases (right). Intercalation (red) between the base pairs is also possible.

Controlled radical polymerisation

None of the complexity that has been achieved thus far using block copolymer self-assembly would have been possible were it not for the introduction of controlled polymerisation techniques, which made the synthesis of the necessary building blocks possible. While living techniques such as anionic and cationic polymerisation have been available for some time[111-113] for the synthesis of well-defined polymers (that is, polymers in which the molecular weight – and therefore the number of repeat units – can be targeted and the distribution of chain lengths is narrow), these methods have a number of drawbacks. Firstly, they require extremely stringent reaction conditions (rigorous exclusion of oxygen and water in particular) and extensive and usually laborious purification of monomers, initiators and solvents. Secondly, the range of monomer functionality that is tolerated is small, which necessarily limits the possibilities for novel structure formation.

It has only been with the relatively recent introduction of controlled radical polymerisation (CRP) techniques that materials chemists have gained access to a truly diverse range of multifunctional polymers. Nitroxide-mediated polymerisation (NMP),[114] atom transfer radical polymerisation (ATRP)[115] and reversible addition–fragmentation chain transfer (RAFT)[116] polymerisation are the three most popular techniques in use today, and all share the same basic mechanistic principal (Scheme 1.3). This is that there is an active species (P•), which is capable of monomer addition, which is in equilibrium with a dormant species (P–X), which is inert towards polymerisation. By tuning the equilibrium such that the concentration of the active species is kept low, chain termination is minimised and the addition of monomer units is slowed, giving rise to a controlled polymerisation.

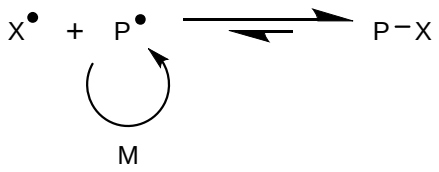

Scheme 1.3 The basic mechanistic principal of controlled radical polymerisation. The active species (P•) is in equilibrium with the dormant species (P–X). Addition of monomer (M) only occurs with the active species. P–X is favoured in the equilibrium, which leads to a low concentration of the active species, giving rise to a controlled polymerisation.

NMP, while a useful technique for some monomers, is somewhat limited by the functionality it can tolerate.[117] ATRP and RAFT, by contrast, are both excellent techniques for the polymerisation of a huge range of functional monomers. One major difference between the two is that while use of a functional ATRP initiator leads to functionalisation of just one end of the polymer chain, the nature of the chain transfer agent (CTA) in RAFT polymerisation means that both ends of the polymer can be modified without the requirement for further manipulations (see Scheme 1.4). Because of the flexibility of the design of the RAFT CTA (for more of which, see below), this technique is also capable of the controlled polymerisation of a wider range of monomers than ATRP. For both of these reasons, and because of the particular expertise of the O'Reilly research group, RAFT was

chosen as the polymerisation technique to be used for the work that follows.

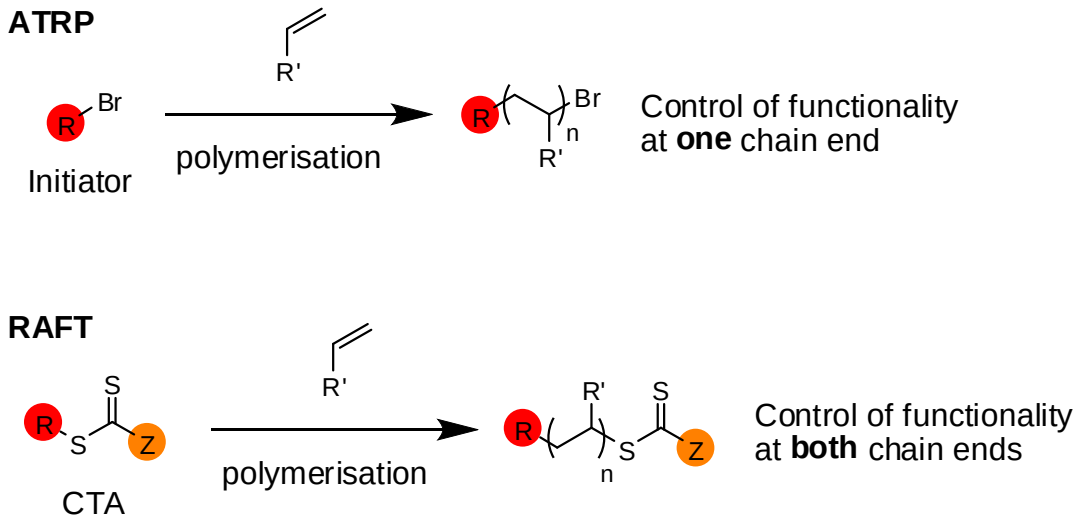

Scheme 1.4 Location of functional groups introduced by the initiator/CTA in polymers produced by ATRP and RAFT. ATRP allows the control of functionality at one chain end only by varying the R group. RAFT, however, allows functionalisation of both chain ends, since the R and Z groups can both be varied.

As has been mentioned, RAFT polymerisation relies on the use of an appropriate CTA to control the process of monomer addition. The basic structure of a CTA is shown in Figure 1.15, and consists of a central thiocarbonylthio group flanked by two groups commonly referred to as R and Z. By convention, the R group ends up at the α terminus of the polymer chain, and the Z group at the ω terminus.

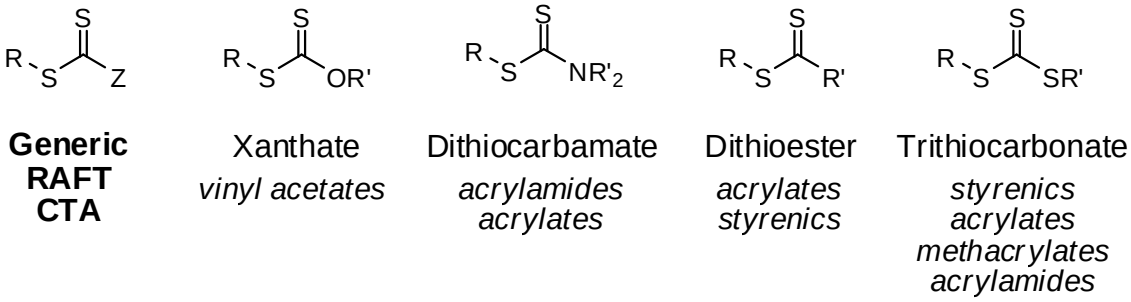

Figure 1.15 Structure of a generic RAFT CTA (left), and the structures of a xanthate, dithiocarbamate, dithioester and trithiocarbonate. The types of monomer that are usually polymerised with control are indicated below each class of CTA in italics.

Thanks to extensive work by a number of research groups, CTAs are relatively simple to

synthesise,[118] and broadly fall into one of four classes: dithioesters, trithiocarbonates, dithiocarbamates, and xanthates. As shown in Figure 1.15, each is particularly suited to the polymerisation of different classes of monomer, with xanthates representing a good choice for less activated monomers such as vinyl acetate, and trithiocarbonates for more activated monomers such as acrylates and styrenics.

The mechanism of RAFT is rather complex,[119,120] and has not been fully elucidated, with a number of phenomena yet to be explained.[121] (An in-depth discussion of the mechanism is beyond the scope of this work, but a number of thorough reviews have been published on the subject[121,122]) However, the proposed process (as depicted in Scheme 1.5) is largely accepted by the polymer chemistry community to be a good enough approximation, and it provides effective rationalisation for most, if not all, of the experimental observations.

The first step is initiation. This may take the form of auto-initiation (for example styrene at 110°C) or, more commonly, involves the use of a separate initiator such as 2,2'-azobis(2-methylpropionitrile) (AIBN). Whichever is chosen, the initiating radical species (I•) is produced. This then combines with several monomer units to produce short oligomeric radicals (P_n•).

The next phase is the pre-equilibrium, wherein P_n• combines with the CTA (**1**) to form an equilibrium with an intermediate species (**2**). **2** can then decompose in one of two ways: either by direct reversal to re-form **1**; or by ejection of the R group radical (R•) to form the CTA–oligomer species (**3**). With ejection of R•, the next phase can begin, known as re-initiation. Here, R• combines with the monomer to create another oligomeric radical (P_m•). This rapidly leads to the final phase, the main equilibrium, in which P_m• combines with **3** to form an intermediate (**4**) containing two growing polymer chains (P_n and P_m). It should be noted at this point that **4** represents the dormant state of polymerisation process – the growing polymer chains therefore spend most of their time locked into this complex. **4** can

then either decompose back to **3** and $P_m\bullet$, or to **5** and $P_n\bullet$. Because P_m and P_n are essentially indistinguishable, which way the decomposition occurs is determined at random.

Initiation:

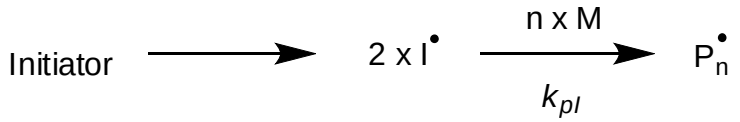

Propagation:

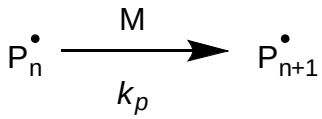

Pre-equilibrium:

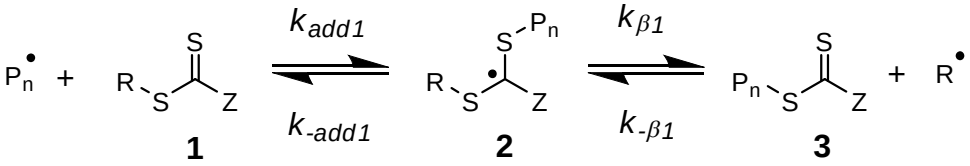

Re-initiation:

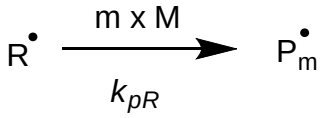

Main equilibrium:

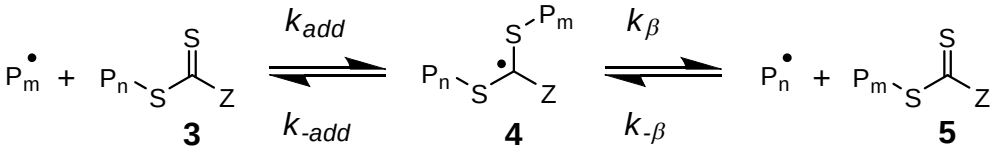

Termination:

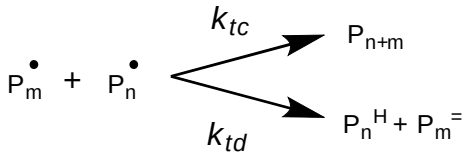

Scheme 1.5 The proposed mechanism of the RAFT polymerisation process.

Polymerisation only occurs when the growing polymer chain is not locked into **3**, **4** or **5**, and it is the constant shuttling between these structures, and the fact that the polymer

chains spend most of their time in a dormant state, that gives rise to the controlled nature of the polymerisation. Termination can occur by polymer–polymer coupling, but this is minimised by the low concentration of radicals in solution at any one time. It is this possibility for termination by combination of polymeric radicals that results in RAFT being termed a pseudo- rather than a true living polymerisation process.

Examination of the mechanism of RAFT polymerisation reveals the importance of the CTA structure in maintaining control of the process. The R group must be designed such that fragmentation to produce the radical is favoured in the pre-equilibrium. It must also be capable of rapid re-initiation with the monomer. This requires a delicate balance between stability (an overly reactive radical is a poor leaving group and so will not be favoured in the pre-equilibrium) and reactivity (radicals that are too stable may not re-initiate). The Z group has a more subtle effect, since it tunes the electronics of all the CTA species involved (**1**-**5**), thereby shifting the positions of the key equilibria. This is the reason that different classes of CTA are appropriate for different classes of monomer. A nice example to demonstrate this is a 'switchable' CTA designed by Benaglia *et al.* – the electronics of the system, and therefore the types of monomer it is able to polymerise with control, can be controlled by simple protonation and deprotonation of a pyridine ring (Scheme 1.6).[123]

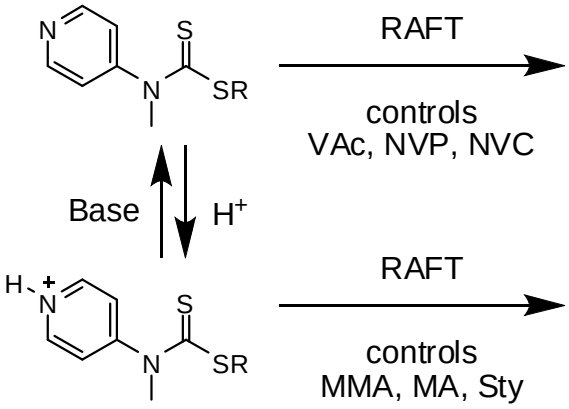

Scheme 1.6 A pH-switchable RAFT CTA designed by Benaglia *et al.*[123] In the deprotonated state, the CTA controls the polymerisation of less activated monomers such as vinyl acetate (VAc), *N*-vinyl pyrrolidone (NVP) and *N*-vinyl caprolactam (NVC). Once protonated, the change in electronic structure results in the controlled polymerisation of more activated monomers such as methyl methacrylate (MMA), methyl acrylate (MA) and styrene (Sty).

Project aims

The first key aim of this work was to identify a conjugation chemistry that would afford DNA–polymer conjugates in high yields in solution, in solvents compatible with hydrophobic polymers and using functional groups that were straightforward to incorporate into a DNA strand (or that could be purchased from a commercial supplier already attached to the DNA). It was hoped that this would provide a more accessible route to DNA–polymer conjugates for the wider materials science community.

The second goal of this work was to use the DNA segment of a DNA–polymer conjugate to form a complex nanoscale DNA-based structure, and then to use a stimulus-responsive polymer segment to induce additional structure formation in response to an external cue. In this way it was hoped that the unique properties of *both* parts of the DNA–polymer conjugate could be exploited.

The third and final aim of this work was to explore the use of a non-covalent interaction to produce DNA–polymer hybrid materials.

References

(1) Daicho, Y.; Murakami, T.; Hagiwara, T.; Maruo, S. *Opt. Mater. Express* **2013**, *3*, 875.

(2) Gradišar, H.; Božič, S.; Doles, T.; Vengust, D.; Hafner-Bratkovič, I.; Mertelj, A.; Webb, B.; Šali, A.; Klavžar, S.; Jerala, R. *Nat. Chem. Biol.* **2013**, *9*, 362.

(3) Blanazs, A.; Armes, S. P.; Ryan, A. J. *Macromol. Rapid Commun.* **2009**, *30*, 267.

(4) Klok, H.-A.; Lecommandoux, S. *Adv. Mater.* **2001**, *13*, 1217.

(5) Doncom, K. E. B.; Hansell, C. F.; Theato, P.; O'Reilly, R. K. *Polym. Chem.* **2012**, *3*, 3007.

(6) Moughton, A. O.; Patterson, J. P.; O'Reilly, R. K. *Chem. Commun.* **2011**, *47*, 355.

(7) Shen, L.; Du, J.; Armes, S. P.; Liu, S. *Langmuir* **2008**, *24*, 10019.

(8) Bang, J.; Jain, S.; Li, Z.; Lodge, T. P.; Pedersen, J. S.; Kesselman, E.; Talmon, Y. *Macromolecules* **2006**, *39*, 1199.

(9) Li, Z.; Hillmyer, M. A.; Lodge, T. P. *Macromolecules* **2005**, *39*, 765.

(10) Pochan, D. J.; Chen, Z.; Cui, H.; Hales, K.; Qi, K.; Wooley, K. L. *Science* **2004**, *306*, 94.

(11) Zhong, S.; Cui, H.; Chen, Z.; Wooley, K. L.; Pochan, D. J. *Soft Matter* **2008**, *4*, 90.

(12) Yu, K.; Eisenberg, A. *Macromolecules* **1998**, *31*, 3509.

(13) Jain, S.; Bates, F. S. *Macromolecules* **2004**, *37*, 1511.

(14) Gilroy, J. B.; Gädt, T.; Whittell, G. R.; Chabanne, L.; Mitchels, J. M.; Richardson, R. M.; Winnik, M. A.; Manners, I. *Nat. Chem.* **2010**, *2*, 566.

(15) Rupar, P. A.; Chabanne, L.; Winnik, M. A.; Manners, I. *Science* **2012**, *337*, 559.

(16) Petzetakis, N.; Dove, A. P.; O'Reilly, R. K. *Chem. Sci.* **2011**, *2*, 955.

(17) Jang, S. G.; Audus, D. J.; Klinger, D.; Krogstad, D. V.; Kim, B. J.; Cameron, A.; Kim, S.-W.; Delaney, K. T.; Hur, S.-M.; Killops, K. L.; Fredrickson, G. H.; Kramer, E. J.; Hawker, C. J. *J. Am. Chem. Soc.* **2013**, *135*, 6649.

(18) Chebotareva, N.; Bomans, P. H. H.; Frederik, P. M.; Sommerdijk, N. A. J. M.; Sijbesma, R. P. *Chem. Commun.* **2005**, 4967.

(19) Bazzi, H. S.; Sleiman, H. F. *Macromolecules* **2002**, *35*, 9617.

(20) Sun, Z.; Bai, F.; Wu, H.; Schmitt, S. K.; Boye, D. M.; Jiang, Z.; Wang, J.; Fan, H. *Chem. A Eur. J.* **2009**, *15*, 11128.

(21) Deng, R.; Liu, S.; Li, J.; Liao, Y.; Tao, J.; Zhu, J. *Adv. Mater.* **2012**, *24*, 1889.

(22) Kuo, S.-W. *Polym. Int.* **2009**, *58*, 455.

(23) Breaker, R. R. *Nat. Biotechnol.* **1997**, *15*, 427.

(24) Seeman, N. C. *J. Theor. Biol.* **1982**, *99*, 237.

(25) Rothemund, P. W. K. *Nature* **2006**, *440*, 297.

(26) Liu, D.; Wang, M.; Deng, Z.; Walulu, R.; Mao, C. *J. Am. Chem. Soc.* **2004**, *126*, 2324.

(27) Andersen, E. S.; Dong, M.; Nielsen, M. M.; Jahn, K.; Subramani, R.; Mamdouh, W.; Golas, M. M.; Sander, B.; Stark, H.; Oliveira, C. L. P.; Pedersen, J. S.; Birkedal, V.; Besenbacher, F.; Gothelf, K. V.; Kjems, J. *Nature* **2009**, *459*, 73.

(28) Han, D.; Pal, S.; Nangreave, J.; Deng, Z.; Liu, Y.; Yan, H. *Science* **2011**, *332*, 342.

(29) Goodman, R. P.; Schaap, I. A. T.; Tardin, C. F.; Erben, C. M.; Berry, R. M.; Schmidt, C. F.; Turberfield, A. J. *Science* **2005**, *310*, 1661.

(30) He, X.; Dong, L.; Wang, W.; Lin, N.; Mi, Y. *Chem. Commun.* **2013**, *49*, 2906.

(31) Chen, J.; Seeman, N. C. *Nature* **1991**, *350*, 631.

(32) Seelig, G.; Soloveichik, D.; Zhang, D. Y.; Winfree, E. *Science* **2006**, *314*, 1585.

(33) Qian, L.; Winfree, E. *Science* **2011**, *332*, 1196.

(34) Rozenman, M. M.; Liu, D. R. *ChemBioChem* **2006**, *7*, 253.

(35) McKee, M. L.; Milnes, P. J.; Bath, J.; Stulz, E.; Turberfield, A. J.; O'Reilly, R. K. *Angew. Chem., Int. Ed.* **2010**, *49*, 7948.

(36) Douglas, S. M.; Bachelet, I.; Church, G. M. *Science* **2012**, *335*, 831.

(37) Wang, C.; Ren, J.; Qu, X. *Chem. Commun.* **2011**, *47*, 1428.

(38) Mirkin, C. A.; Letsinger, R. L.; Mucic, R. C.; Storhoff, J. J. *Nature* **1996**, *382*, 607.

(39) Li, Z.; Zhang, Y.; Fullhart, P.; Mirkin, C. A. *Nano Lett.* **2004**, *4*, 1055.

(40) Hurst, S. J.; Hill, H. D.; Macfarlane, R. J.; Wu, J.; Dravid, V. P.; Mirkin, C. A. *Small*

2009, *5*, 2156.

(41) Jeong, J. H.; Kim, S. W.; Park, T. G. *J. Control. Release* **2003**, *93*, 183.

(42) Jeong, J. H.; Kim, S. W.; Park, T. G. *Bioconjugate Chem.* **2003**, *14*, 473.

(43) Jeong, J. H.; Kim, S. H.; Kim, S. W.; Park, T. G. *J. Biomater. Sci., Polym. Ed.* **2005**, *16*, 1409.

(44) Oishi, M.; Sasaki, S.; Nagasaki, Y.; Kataoka, K. *Biomacromolecules* **2003**, *4*, 1426.

(45) Oishi, M.; Nagatsugi, F.; Sasaki, S.; Nagasaki, Y.; Kataoka, K. *ChemBioChem* **2005**, *6*, 718.

(46) Oishi, M.; Nagasaki, Y.; Itaka, K.; Nishiyama, N.; Kataoka, K. *J. Am. Chem. Soc.* **2005**, *127*, 1624.

(47) Jeong, J. H.; Kim, S. H.; Kim, S. W.; Park, T. G. *Bioconjugate Chem.* **2005**, *16*, 1034.

(48) Fong, R. B.; Ding, Z.; Long, C. J.; Hoffman, A. S.; Stayton, P. S. *Bioconjugate Chem.* **1999**, *10*, 720.

(49) Costioli, M. D.; Fisch, I.; Garret-Flaudy, F.; Hilbrig, F.; Freitag, R. *Biotechnol. Bioeng.* **2003**, *81*, 535.

(50) Umeno, D.; Mori, T.; Maeda, M. *Chem. Commun.* **1998**, 1433.

(51) Takeshi, M.; Daisuke, U.; Mizuo, M. *Biotechnol. Bioeng.* **2001**, *72*, 261.

(52) Umeno, D.; Maeda, M. *Anal. Sci.* **1997**, *13*, 553.

(53) Maeda, M.; Nishimura, C.; Inenaga, A.; Takagi, M. *React. Polym.* **1993**, *21*, 27.

(54) Umeno, D.; Kawasaki, M.; Maeda, M. *Bioconjugate Chem.* **1998**, *9*, 719.

(55) Soh, N.; Umeno, D.; Tang, Z.; Murata, M.; Maeda, M. *Anal. Sci.* **2002**, *18*, 1295.

(56) Takarada, T.; Imaizumi, E.; Kino, K.; Yoshimoto, K.; Ogasawara, S.; Kanayama, N.; Maeda, M. *Nucleic Acids Symp. Ser.* **2007**, *51*, 305.

(57) Tang, Z.; Takarada, T.; Sato, Y.; Maeda, M. *Chem. Lett.* **2004**, *33*, 1602.

(58) Sugawara, Y.; Tamaki, T.; Ohashi, H.; Yamaguchi, T. *Soft Matter* **2013**, *9*, 3331.

(59) Murata, M.; Kaku, W.; Anada, T.; Sato, Y.; Kano, T.; Maeda, M.; Katayama, Y. *Bioorg. Med. Chem. Lett.* **2003**, *13*, 3967.

(60) Takemoto, H.; Miyata, K.; Hattori, S.; Ishii, T.; Suma, T.; Uchida, S.; Nishiyama, N.; Kataoka, K. *Angew. Chem., Int. Ed.* **2013**, *52*, 6218.

(61) Immoos, C. E.; Lee, S. J.; Grinstaff, M. W. *J. Am. Chem. Soc.* **2004**, *126*, 10814.

(62) Lee, K.; Povlich, L. K.; Kim, J. *Adv. Funct. Mater.* **2007**, *17*, 2580.

(63) Gibbs, J. M.; Park, S.-J.; Anderson, D. R.; Watson, K. J.; Mirkin, C. A.; Nguyen, S. T. *J. Am. Chem. Soc.* **2005**, *127*, 1170.

(64) Thompson, L. A.; Kowalik, J.; Josowicz, M.; Janata, J. *J. Am. Chem. Soc.* **2002**, *125*, 324.

(65) Minard-Basquin, C.; Chaix, C.; D'Agosto, F.; Charreyre, M.-T.; Pichot, C. *J. Appl.*

Polym. Sci. **2004**, *92*, 3784.

(66) Chaix, C.; Minard-Basquin, C.; Delair, T.; Pichot, C.; Mandrand, B. *J. Appl. Polym. Sci.* **1998**, *70*, 2487.

(67) Minard-Basquin, C.; Chaix, C.; Pichot, C. *Nucleosides, Nucleotides Nucleic Acids* **2001**, *20*, 895.

(68) Bayard, B.; Bisbal, C.; Lebleu, B. *Biochemistry* **1986**, *25*, 3730.

(69) Kanayama, N.; Shibata, H.; Kimura, A.; Miyamoto, D.; Takarada, T.; Maeda, M. *Biomacromolecules* **2009**, *10*, 805.

(70) He, P.; He, L. *Biomacromolecules* **2009**, *10*, 1804.

(71) de Lambert, B.; Chaix, C.; Charreyrex, M.-T.; Laurent, A.; Aigoui, A.; Perrin-Rubens, A.; Pichot, C. *Bioconjugate Chem.* **2005**, *16*, 265.

(72) de Lambert, B.; Chaix, C.; Charreyre, M.-T.; Martin, T.; Aigoui, A.; Perrin-Rubens, A.; Pichot, C.; Mandrand, B. *Anal. Biochem.* **2008**, *373*, 229.

(73) Lemaitre, M.; Bayard, B.; Lebleu, B. *Proc. Natl. Acad. Sci. U. S. A.* **1987**, *84*, 648.

(74) Leonetti, J. P.; Rayner, B.; Lemaitre, M.; Gagnor, C.; Milhaud, P. G.; Irnbach, J. L.; Lebleua, B. *Gene* **1988**, *72*, 323.

(75) York, A. W.; Huang, F.; McCormick, C. L. *Biomacromolecules* **2010**, *11*, 505.

(76) Korri-Youssoufi, H.; Garnier, F.; Srivastava, P.; Godillot, P.; Yassar, A. *J. Am. Chem. Soc.* **1997**, *119*, 7388.

(77) Boyer, C.; Bulmus, V.; Davis, T. P. *Macromol. Rapid Commun.* **2009**, *30*, 493.

(78) Heredia, K. L.; Nguyen, T. H.; Chang, C.-W.; Bulmus, V.; Davis, T. P.; Maynard, H. D. *Chem. Commun.* **2008**, 3245.

(79) Oishi, M.; Hayama, T.; Akiyama, Y.; Takae, S.; Harada, A.; Yamasaki, Y.; Nagatsugi, F.; Sasaki, S.; Nagasaki, Y.; Kataoka, K. *Biomacromolecules* **2005**, *6*, 2449.

(80) Vázquez-Dorbatt, V.; Tolstyka, Z. P.; Chang, C.-W.; Maynard, H. D. *Biomacromolecules* **2009**, *10*, 2207.

(81) Lee, S. H.; Kim, S. H.; Park, T. G. *Biochem. Biophys. Res. Commun.* **2007**, *357*, 511.

(82) Umeno, D.; Kiji, M.; Murata, M.; Maeda, M. *Polym. J. (Tokyo, Jpn.)* **1999**, *31*, 1109.

(83) Iwataki, T.; Yoshikawa, K.; Kidoaki, S.; Umeno, D.; Kiji, M.; Maeda, M. *J. Am. Chem. Soc.* **2000**, *122*, 9891.

(84) Umeno, D.; Kano, T.; Maeda, M. *Anal. Chim. Acta* **1998**, *365*, 101.

(85) Wang, Z.-G.; Ding, B. *Adv. Mater.* **2013**, *25*, 3905.

(86) Fluegel, S.; Buehler, J.; Fischer, K.; McDaniel, J. R.; Chilkoti, A.; Schmidt, M. *Chem. A Eur. J.* **2011**, *17*, 5503.

(87) Carneiro, K. M. M.; Aldaye, F. A.; Sleiman, H. F. *J. Am. Chem. Soc.* **2009**, *132*, 679.

(88) Safak, M.; Alemdaroglu, F. E.; Li, Y.; Ergen, E.; Herrmann, A. *Adv. Mater.* **2007**, *19*, 1499.

(89) Carneiro, K. M. M.; Hamblin, G. D.; Hanni, K. D.; Fakhoury, J.; Nayak, M. K.; Rizis, G.; McLaughlin, C. K.; Bazzi, H. S.; Sleiman, H. F. *Chem. Sci.* **2012**, *3*, 1980.

(90) Ayaz, M. S.; Kwak, M.; Alemdaroglu, F. E.; Wang, J.; Berger, R.; Herrmann, A. *Chem. Commun.* **2011**, *47*, 2243.

(91) Talom, R. M.; Fuks, G.; Kaps, L.; Oberdisse, J.; Cerclier, C.; Gaillard, C.; Mingotaud, C.; Gauffre, F. *Chem. A Eur. J.* **2011**, *17*, 13495.

(92) Cavalieri, F.; Postma, A.; Lee, L.; Caruso, F. *ACS Nano* **2009**, *3*, 234.

(93) Averick, S.; Paredes, E.; Li, W.; Matyjaszewski, K.; Das, S. R. *Bioconjugate Chem.* **2011**, *22*, 2030.

(94) Chen, P.; Li, C.; Liu, D.; Li, Z. *Macromolecules* **2012**, *45*, 9579.

(95) Wang, L.; Feng, Y.; Sun, Y.; Li, Z.; Yang, Z.; He, Y.-M.; Fan, Q.-H.; Liu, D. *Soft Matter* **2011**, *7*, 7187.

(96) Watson, K. J.; Park, S.-J.; Im, J.-H.; Mirkin, C. A. *J. Am. Chem. Soc.* **2001**, *123*, 5592.

(97) Alemdaroglu, F. E.; Alemdaroglu, N. C.; Langguth, P.; Herrmann, A. *Adv. Mater.* **2008**, *20*, 899.

(98) Alemdaroglu, F. E.; Ding, K.; Berger, R.; Herrmann, A. *Angew. Chem., Int. Ed.* **2006**, *45*, 4206.

(99) Kwak, M.; Musser, A. J.; Lee, J.; Herrmann, A. *Chem. Commun.* **2010**, *46*, 4935.

(100) Rodríguez-Pulido, A.; Kondrachuk, A. I.; Prusty, D. K.; Gao, J.; Loi, M. A.;

Herrmann, A. *Angew. Chem., Int. Ed.* **2013**, *52*, 1008.

(101) Ding, K.; Alemdaroglu, F. E.; Börsch, M.; Berger, R.; Herrmann, A. *Angew. Chem., Int. Ed.* **2007**, *46*, 1172.

(102) Kwak, M.; Minten, I. J.; Anaya, D.-M.; Musser, A. J.; Brasch, M.; Nolte, R. J. M.; Müllen, K.; Cornelissen, J. J. L. M.; Herrmann, A. *J. Am. Chem. Soc.* **2010**, *132*, 7834.

(103) Alemdaroglu, F. E.; Alemdaroglu, N. C.; Langguth, P.; Herrmann, A. *Macromol. Rapid Commun.* **2008**, *29*, 326.

(104) Zhao, Z.; Wang, L.; Liu, Y.; Yang, Z.; He, Y.-M.; Li, Z.; Fan, Q.-H.; Liu, D. *Chem. Commun.* **2012**, *48*, 9753.

(105) Kwak, M.; Gao, J.; Prusty, D. K.; Musser, A. J.; Markov, V. A.; Tombros, N.; Stuart, M. C. A.; Browne, W. R.; Boekema, E. J.; ten Brinke, G.; Jonkman, H. T.; van Wees, B. J.; Loi, M. A.; Herrmann, A. *Angew. Chem., Int. Ed.* **2011**, *50*, 3206.

(106) Jeong, J. H.; Park, T. G. *Bioconjugate Chem.* **2001**, *12*, 917.

(107) Rush, A. M.; Thompson, M. P.; Tatro, E. T.; Gianneschi, N. C. *ACS Nano* **2013**, *7*, 1379.

(108) Chien, M.-P.; Rush, A. M.; Thompson, M. P.; Gianneschi, N. C. *Angew. Chem., Int. Ed.* **2010**, *49*, 5076.

(109) Sowwan, M.; Faroun, M.; Mentovich, E.; Ibrahim, I.; Haboush, S.; Alemdaroglu, F. E.; Kwak, M.; Richter, S.; Herrmann, A. *Macromol. Rapid Commun.* **2010**, *31*, 1242.

(110) McLaughlin, C. K.; Hamblin, G. D.; Hänni, K. D.; Conway, J. W.; Nayak, M. K.;

Carneiro, K. M. M.; Bazzi, H. S.; Sleiman, H. F. *J. Am. Chem. Soc.* **2012**, *134*, 4280.

(111) Szwarc, M.; Levy, M.; Milkovich, R. *J. Am. Chem. Soc.* **1956**, *78*, 2656.

(112) Szwarc, M. *Nature* **1956**, *178*, 1168.

(113) Higashimura, T.; Kishiro, O. *Polym. J. (Tokyo, Jpn.)* **1977**, *9*, 87.

(114) Hawker, C. J. *J. Am. Chem. Soc.* **1994**, *116*, 11185.

(115) Matyjaszewski, K.; Gaynor, S.; Wang, J.-S. *Macromolecules* **1995**, *28*, 2093.

(116) Chiefari, J.; Chong, Y. K.; Ercole, F.; Krstina, J.; Jeffery, J.; Le, T. P. T.; Mayadunne, R. T. A.; Meijs, G. F.; Moad, C. L.; Moad, G.; Rizzardo, E.; Thang, S. H. *Macromolecules* **1998**, *31*, 5559.

(117) Nicolas, J.; Guillaneuf, Y.; Lefay, C.; Bertin, D.; Gigmes, D.; Charleux, B. *Prog. Polym. Sci.* **2013**, *38*, 63.

(118) Skey, J.; O'Reilly, R. K. *Chem. Commun.* **2008**, 4183.

(119) Moad, G.; Rizzardo, E.; Thang, S. H. *Aust. J. Chem.* **2005**, *58*, 379.

(120) Perrier, S.; Takolpuckdee, P. *J. Polym. Sci., Part A: Polym. Chem.* **2005**, *43*, 5347.

(121) Klumperman, B.; van den Dungen, E. T. A.; Heuts, J. P. A.; Monteiro, M. J. *Macromol. Rapid Commun.* **2010**, *31*, 1846.

(122) Moad, G.; Rizzardo, E.; Thang, S. H. *Aust. J. Chem.* **2006**, *59*, 669.

(123) Benaglia, M.; Chiefari, J.; Chong, Y. K.; Moad, G.; Rizzardo, E.; Thang, S. H. *J. Am. Chem. Soc.* **2009**, *131*, 6914.

Chapter 2

DNA–polymer conjugation using amide coupling techniques

2.1 Introduction

Efficient coupling of amines to carboxylic acids has long been an important target for the synthetic chemist. Amides are ubiquitous in many natural products – the most important examples being proteins – and can be made by a simple condensation reaction. However, this lacks the specificity, control and functional group tolerance necessary for the construction of large, complex biomolecules such as peptides. The process is also an equilibrium, so high yields can be challenging to obtain. To circumvent these problems it is necessary to increase the reactivity of the acid, and over the years a number of different methods have been developed to this end.

Perhaps the most common is the use of the acyl chloride Scheme 2.1, which was first introduced by Schotten and Baumann at the end of the 19th century.[1,2]

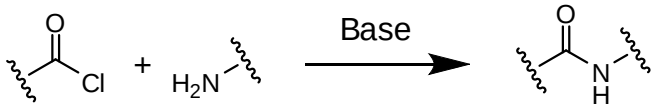

Scheme 2.1 Formation of an amide from an amine and an acyl chloride.

The main advantage of this approach is its simplicity: only the amine and acyl chloride are required (plus an auxiliary base to trap the HCl generated) and the reaction proceeds rapidly and irreversibly at room temperature. However, the generation of the acyl chloride involves harsh conditions (specifically the use of thionyl chloride) which may lead to degradation or loss of other functional groups present in the parent carboxylic acid. Acyl chlorides are also highly susceptible to hydrolysis and will react with even weak

nucleophiles, so unwanted side reactions can be a problem when dealing with heterofunctional compounds.

A second popular method for amide synthesis uses 1,1'-carbonyldiimidazole (CDI).[3] Carboxylic acids react rapidly with this reagent at room temperature (release of CO_2 gas provides an entropic driving force for the reaction) to produce the intermediate imidazolide (Scheme 2.2, step 1). Whilst it is possible to isolate this compound, more commonly the reaction is carried out in the presence of a primary or secondary amine, resulting in one pot formation of the desired amide (Scheme 2.2, step 2).

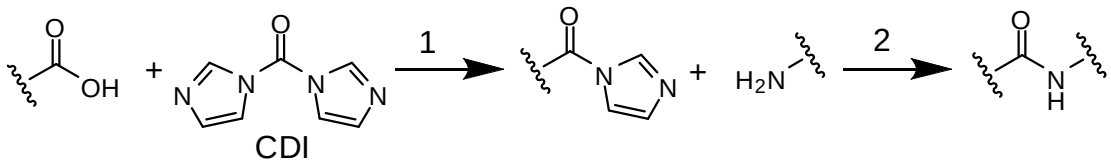

Scheme 2.2 Formation of an amide from a carboxylic acid and an amine *via* the imidazolide using CDI.

This approach may be preferable to the use of thionyl chloride as it can be performed in one step (no isolation of the intermediate is required), CDI is less reactive than thionyl chloride and therefore easier to handle, and there is greater specificity for reaction with amines over alcohols or other nucleophiles. However, hydrolysis of the intermediate can still lead to lower than expected yields.

Perhaps the most important class of amide coupling reagents is the carbodiimides, which were first used in this context as early as 1955.[4] Their popularity stems from their high specificity, resistance to hydrolysis (indeed, water can be used as the reaction solvent) and ease of use (the by-products can often simply be filtered off). A huge range of coupling agents is available to mediate the process (illustrated in Scheme 2.3): *N*-(3-dimethylaminopropyl)-*N*'-ethylcarbodiimide hydrochloride (EDCI) and *N*,*N*'-dicyclohexylcarbodiimide (DCC) are two typical examples, but more advanced reagents such as *O*-(benzotriazol-1-yl)-*N*,*N*,*N*',*N*'-tetramethyluronium hexafluorophosphate

(HBTU) (see Figure 2.1) are also available that preclude the use of 1-hydroxybenzotriazole (HOBt) (a potentially hazardous material that is used to deactivate the coupling intermediate and reduce racemisation). This large variety also means that an appropriate reagent can be found for most acid/amine pairings, even in cases when the latter is rather deactivated (for example in aniline).[5]

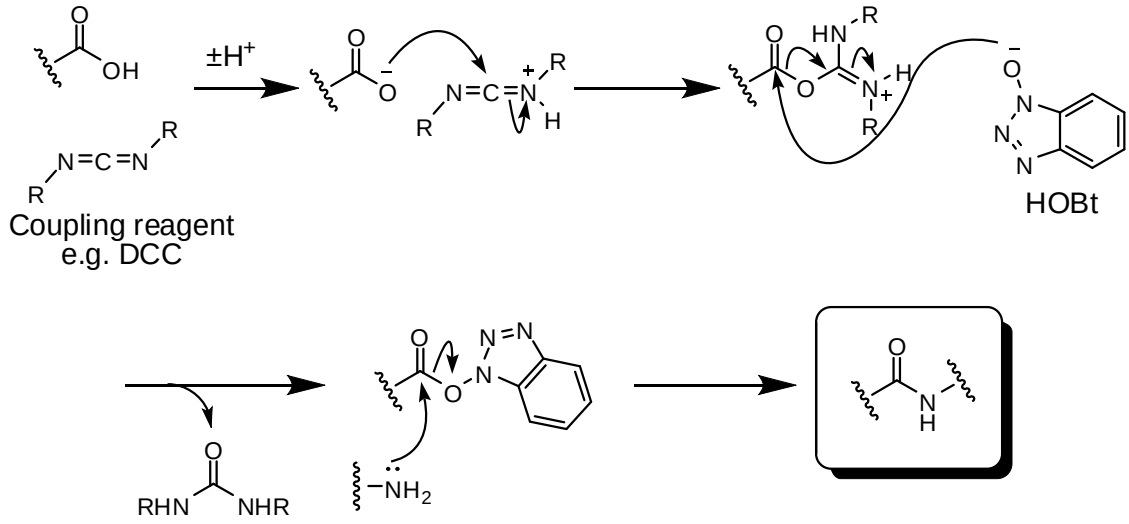

Scheme 2.3 The mechanism of the amide–carboxylic acid coupling reaction as mediated by a generic carbodiimide coupling reagent in the presence of HOBt.

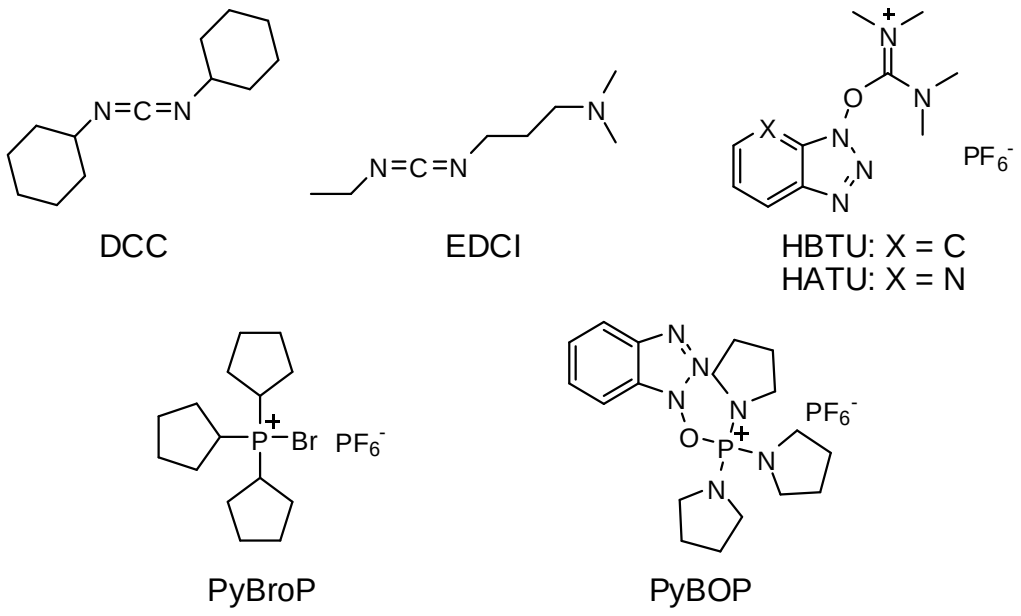

Figure 2.1 Structures of the coupling agents used in this study.

Other coupling agents, based on phosphorous (sometimes in combination with a triazole group – see Figure 2.1), have also been devised. In these cases, formation of the phosphine oxide provides a driving force for the reaction, and the intermediate is highly reactive towards even hindered amines.[6,7]

In the context of DNA–polymer coupling, this reaction has already been utilised successfully to attach a number of polymers to short oligonucleotides.[8-11] Park *et al* achieved DNA coupling to hydrophobic poly(D,L-lactic-*co*-glycolic acid) in good yield by pre-activating the polymer using DCC and *N*-hydroxysuccinimide (NHS).[8] However, this approach required very high DNA concentrations (2 mM) to be effective and has not so far been used successfully for the conjugation of more hydrophobic polymers such as poly(styrene). All other reports have performed the conjugation in water using hydrophilic polymers, and in these cases the conjugation reaction appears to work more effectively, producing higher yields at lower DNA concentrations.[9-11] Given that for small molecule reactions, amide–acid coupling often works just as well in organic solvents as it does in water, this is perhaps surprising – although perhaps less so considering that the solubility of DNA in most organic solvents is low. Furthermore, an exploration of the use of different coupling agents has yet to appear in the literature, with all of the before cited publications utilising the common EDCI (or DCC)/ NHS coupling reagent combination.

From the point of view of accessibility, the amide coupling route to DNA–polymer conjugates is attractive because amine-functionalised DNA is one of the most common – and therefore cheapest – modifications available from commercial suppliers. The DNA can be used 'as received': a potentially very attractive feature for synthetic and materials labs with no experience of DNA manipulation.

It was decided that an extensive study should be carried out into the use of different coupling reagents and solvents to attach amine-functionalised DNA to acid-functionalised polymers to determine the optimum coupling conditions.

2.2 Results & Discussion

2.2.i Synthesis of carboxylic acid-functionalised polymers

Since the thiocarbonyl thio groups present in RAFT chain transfer agents (CTAs) degrade in the presence of amines, it has always been difficult to incorporate this group into polymers synthesised using this CRP technique. By contrast, carboxylic acid groups are stable under RAFT polymerisation conditions and can be incorporated into the CTA. 2-(Dodecylthiocarbonothioylthio)-2-methylpropionic acid (DDMAT) is a widely used CTA, which has been shown to control the polymerisation of a large variety of monomers, and which contains a free carboxylic acid group in its structure (see Figure 2.2). It was envisaged that polymers produced using this CTA could be coupled to amine-functionalised DNA.

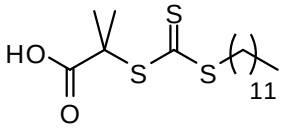

DDMAT

Figure 2.2 The structure of 2-(Dodecylthiocarbonothioylthio)-2-methylpropionic acid (DDMAT).

Poly(NIPAM), poly(styrene) and poly(NIPAM-*b*-styrene) were thus synthesised using RAFT polymerisation, with DDMAT as the CTA. As outlined in Table 2.1, good control over molecular weight was achieved, with all polymers having a low dispersity (i.e. below 1.2). All polymers retained the trithiocarbonate group, as evidenced by the overlap of the refractive index (RI) and UV (309 nm) size exclusion chromatography (SEC) traces (the trithiocarbonate group has a characteristic absorbance at 309 nm). As previously discussed, the trithiocarbonate group present in the product polymers is vulnerable to degradation by amines. It was thought that this might interfere with the DNA coupling reaction, so, using a previously reported method,[12] this group was substituted for a hydrogen atom (Figure 2.3), effectively removing all functionality from this end of the polymer. To confirm the successful removal of the end group, the SEC UV traces at 309 nm were compared before

and after the reaction.

Table 2.1 Polymers produced by RAFT polymerisation with DDMAT as the CTA. THF was used as the SEC eluent in all cases. [a] PMMA calibration standards. [b] PS calibration standards. [c] Degrees of polymerisation (DPs) of NIPAM and styrene blocks respectively. [*] Determined by end group analysis using the integrals of the SC*H*$_2$ peak of the trithiocarbonate group and the NC*H* (poly(NIPAM)) or phenyl (poly(styrene)) polymer peak.

Polymer	Type	DP^{NMR}	M_n^{NMR} / kDa*	M_n^{SEC} / kDa	Đ
P1	poly(NIPAM)[a]	50	6.0	5.3	1.14
P2	poly(styrene)[b]	49	5.5	4.9	1.06
P3	poly(NIPAM-*b*-styrene)[b]	49/47[c]	10.4	9.0	1.11

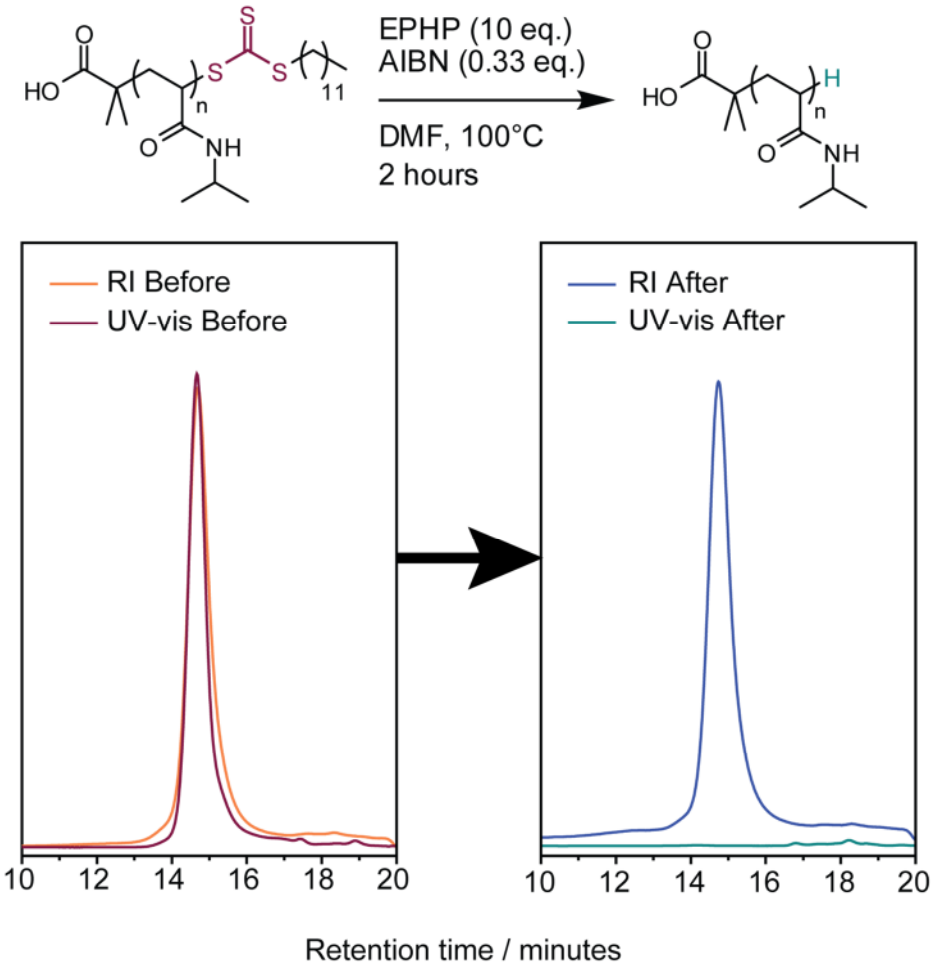

Figure 2.3 Removal of the trithiocarbonate group from poly(NIPAM) using 1-Ethylpiperidine hypophosphite (EPHP) and AIBN. Left panel: UV-vis (309 nm) and RI SEC traces before end group removal. Right panel: SEC traces after end group removal.

As Figure 2.3 shows, no product was detected at this wavelength after the reaction, indicating greater than 99 % removal of the RAFT end-group, but the RI trace remained essentially the same i.e. there was no unwanted polymer–polymer coupling. The ^{1}H NMR spectra were also compared before and after the reaction. Removal of the trithiocarbonate group resulted in the disappearance of the signal at 3.06 ppm attributed to the adjacent CH_2 group. Performing the NMR in d_6-DMSO confirmed that the carboxylic acid group survived the end group removal process (see Figure 2.4).

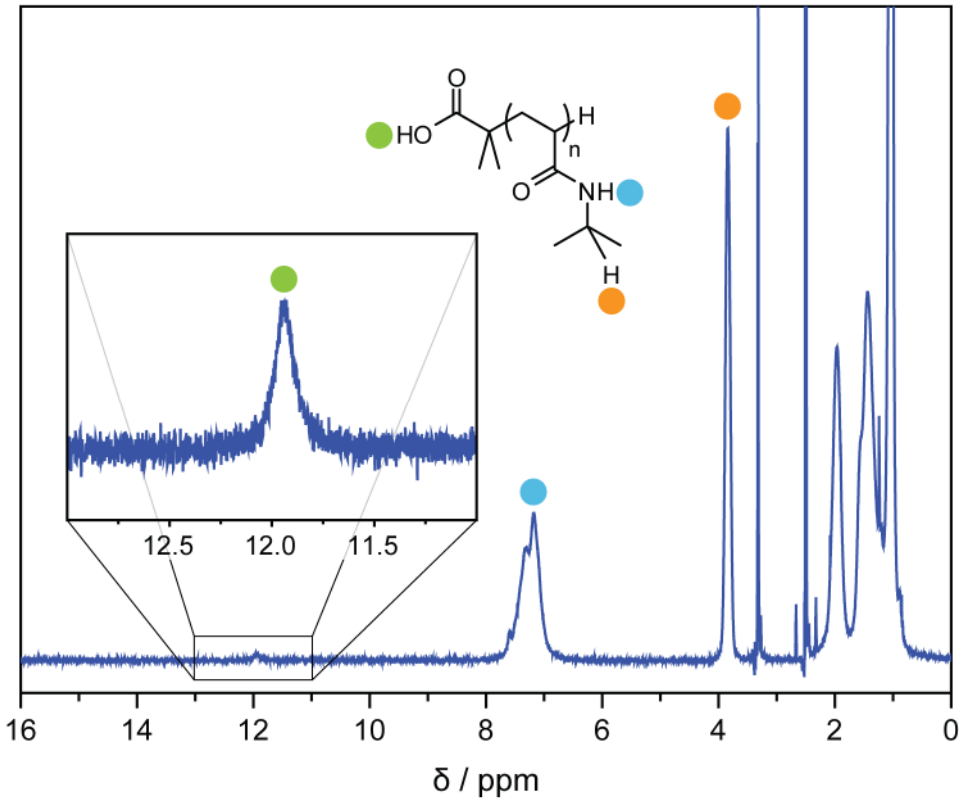

Figure 2.4 ^{1}H NMR spectrum confirming the presence of the carboxylic acid after the removal of the trithiocarbonate group from poly(NIPAM) using EPHP. Solvent: d_6-DMSO.

In addition, poly(NIPAM) was synthesised with varying degrees of polymerisation (DP) – ranging from 50 to 196 – in order that the effect of polymer chain length on coupling efficiency could be tested. It was also envisaged that different block lengths of poly(NIPAM) would give rise to different morphologies in the final DNA–polymer conjugates. The properties of the polymers synthesised are summarised in Table 2.2.

Table 2.2 Poly(NIPAM) of varying DP produced by RAFT. Dimethylformamide (DMF) was used as the SEC eluent in each case, with PMMA calibration standards. * Determined by end group analysis.

Polymer	Type	DP^{NMR}	M_n^{NMR} / kDa*	M_n^{SEC} / kDa	Đ
P4a	poly(NIPAM)	50	6.0	5.1	1.18
P4b		97	11.3	10.4	1.14
P4c		196	22.5	20.0	1.18

2.2.ii Coupling of carboxylic acid-functionalised polymers to s0–NH_2 DNA

With the carboxylic acid-functionalised polymers in hand, coupling of amine-functionalised DNA (s0–NH_2) was attempted. The DNA strand s0–NH_2 was designed to have no secondary structure at room temperature and was 22 nucleotides in length, with the base sequence shown in Figure 2.5.

s0–NH_2 = 5'- H_2N-GCC CGA AAT ACC CCG TTA GAA A -3'

Figure 2.5 Base sequence of the DNA strand s0–NH_2 used in this work.

Since the primary aim of this work was to find an *accessible* way of conjugating polymers to DNA, it was decided to work at DNA concentrations not above 10 μM. This meant that reactions could be carried out on a practical scale (i.e. 10 μL or above) without using too much material – an important consideration given the high cost of functional DNA. Coupling to the carboxylic acid-functionalised poly(NIPAM) (H–poly(NIPAM)–CO_2H) synthesised above was attempted using a variety of solvents and either EDCI or DCC as coupling agent as detailed in Table 2.3.

The coupling agents were added in a 100-fold excess relative to the amine group and the reaction left overnight to proceed. Each reaction mixture was then diluted with 5 × glycerol loading buffer and water, and analysed by 15 % native poly(acrylamide) gel electrophoresis (PAGE).

Table 2.3 Coupling agents and solvents tested for the conjugation of poly(NIPAM)–CO_2H to s0–NH_2. A * indicates that the coupling agent was not highly soluble in the solvent used. 100 equivalents of *N*,*N*-diisopropylethylamine (DIPEA) as an auxiliary base were used in all cases.

Reaction #	Coupling agent	Solvent
1a	EDCI/HOBt	DMF
1b*		THF
1c		MeCN
1d*		NMP
1e		DMSO
2a	DCC/HOBt	DMF
2b		THF
2c		MeCN
2d		NMP
2e		DMSO

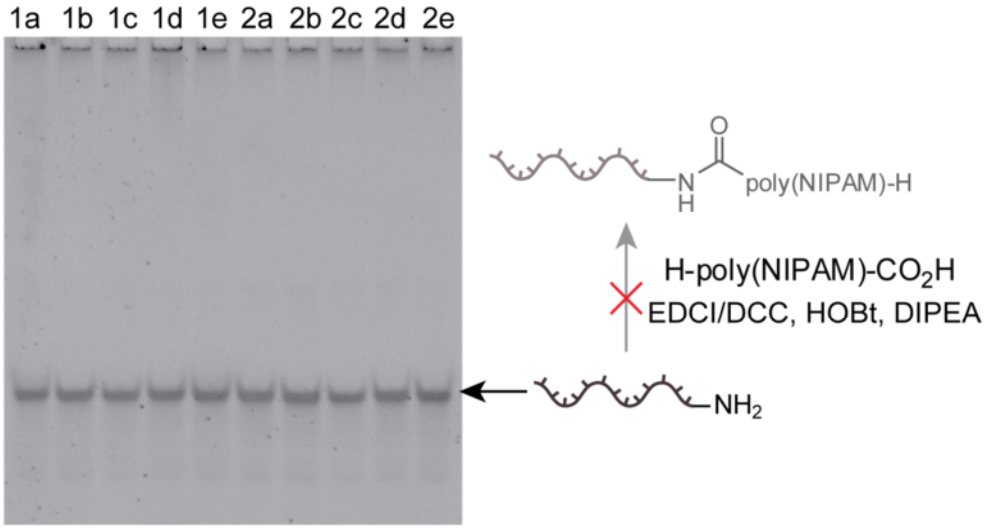

Figure 2.6 15 % native PAGE analysis of the DNA–polymer conjugation reactions detailed in Table 2.3, employing DCC and EDCI as amide coupling reagents. The only band observed was due to the starting material s0–NH_2, indicating that the expected product had failed to form.

Figure 2.6 shows a typical PAGE gel for the analysis of these reactions. The narrow band

due to the starting material s0–NH_2 could clearly be seen; however, there was no evidence of any DNA–polymer conjugate, which was expected to appear as a broad, low-mobility band. These reactions were repeated a number of times using different concentrations of coupling agent, temperatures and auxiliary bases, but in no case was the desired product observed.

It was hypothesised that the reaction was failing because of the low concentrations employed: the activated esters formed by EDCI and DCC were not reactive enough for the coupling reaction with the s0–NH_2 to take place before hydrolysis occurred. More reactive coupling agents are available so it was decided to trial these under identical conditions to those above. HBTU and 1-[Bis(dimethylamino)methylene]-1*H*-1,2,3-triazolo[4,5-*b*]pyridinium 3-oxid hexafluorophosphate (HATU) (see Figure 2.1) are popular coupling reagents and often recommended for 'difficult' coupling reactions,[5] and were therefore employed as shown in Table 2.4.

Table 2.4 Coupling agents and solvents tested for the conjugation of poly(NIPAM)–CO_2H to s0–NH_2. A * indicates that the coupling agent was not highly soluble in the solvent used. 100 equivalents of DIPEA as auxiliary base were used in all cases.

Reaction #	Coupling agent	Solvent
3a	HBTU	DMF
3b*		THF
3c		MeCN
3d*		NMP
3e		DMSO
4a	HATU	DMF
4b*		THF
4c		MeCN
4d		NMP
4e		DMSO

PAGE analysis of the crude reaction mixtures was conducted as before, and showed successful formation of the conjugate when DMF was the reaction solvent – see Figure 2.7. Analysis of the PAGE results using densitometry (Figure 2.8) gave an approximate yield of the conjugate of 25 %.

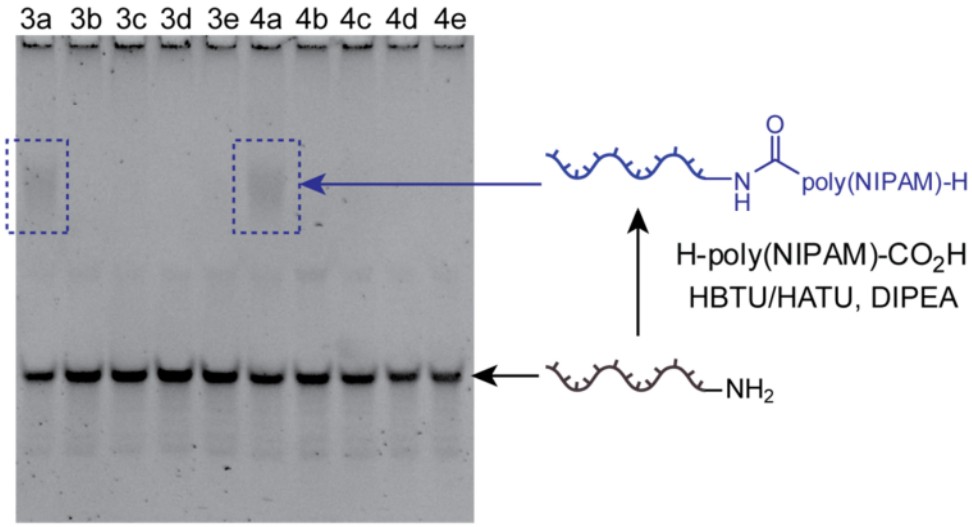

Figure 2.7 15 % native PAGE analysis of the DNA–polymer conjugation reactions detailed in Table 2.4, employing HBTU and HATU as amide coupling reagents. The band due to the starting material s0–NH_2 was still the main band observed; however, in the case of reactions 3a and 4a another, slow-migrating band was also observed, which was attributed to the DNA–polymer conjugate.

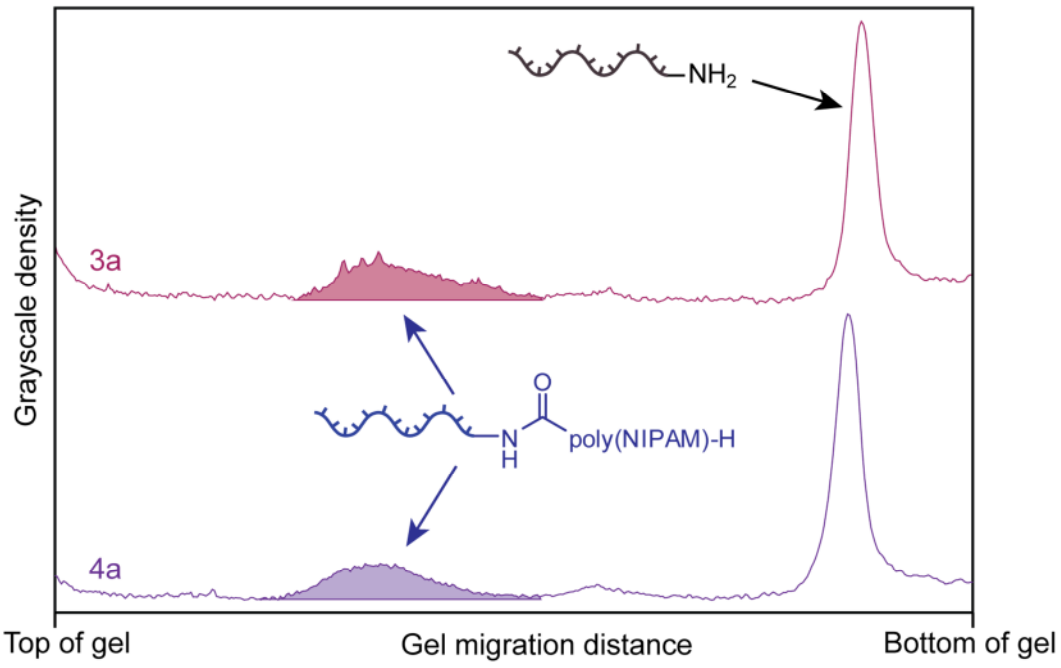

Figure 2.8 Densitometric analysis of lanes 3a and 4a in Figure 2.7. The DNA–polymer conjugate was clearly visible as a low-mobility band.

It is interesting that the reaction solvent had such a dramatic effect on the efficiency of the reaction. The polarity of the solvent has often been observed to alter the reactivity of activated esters, but NMP and DMSO are both highly polar (with polarity indices of 6.7 and 7.2 respectively – both higher than DMF),[13] yet no coupling was observed when they were employed. A possible explanation was that DMF played a catalytic role in the reaction, as it can in the production of acyl chlorides.[14,15] A further possibility is that the solubility of the end group had a significant effect on the yield.

Two further coupling reagents were tested. (Benzotriazol-1-yloxy)tripyrrolidino-phosphonium hexafluorophosphate (PyBOP) and bromotripyrrolidinophosphonium hexa-fluorophosphate (PyBroP) (see Figure 2.1) are phosphorous-based coupling agents often used in peptide synthesis. Both form a highly activated intermediate, which is reactive towards even hindered amines. It was hypothesised that increasing the reactivity of the activated acid would increase the efficiency of the DNA–polymer coupling reaction, so this was attempted as described in Table 2.5.

Table 2.5 Coupling agents and solvents tested for the conjugation of poly(NIPAM)–CO_2H to s0–NH_2. 100 equivalents of DIPEA as auxiliary base were used in all cases.

Reaction #	Coupling agent	Solvent
5a	PyBOP	DMF
5b		THF
5c		MeCN
5d		NMP
5e		DMSO
6a	PyBroP	DMF
6b		THF
6c		MeCN
6d		NMP
6e		DMSO

Despite the increased activity of the coupling agents, PAGE analysis revealed that no DNA–polymer conjugate was formed under any of the above conditions.

2.2.iii The effect of polymer molecular weight on coupling efficiency

Experiments were carried out to determine whether the degree of polymerisation (and therefore the molecular weight) of the polymer used had any effect on the efficiency of the coupling reaction. To this end, the synthesis of conjugates containing poly(NIPAM) with DPs of 97 and 196 was attempted using the conditions identified above, with HATU or HBTU as the coupling agent and DMF as the solvent. However, in no cases were the conjugates observed (Figure 2.9). It also proved very difficult to repeat the synthesis of the lower DP conjugate (reactions 3a and 4a above), despite increasing the purity of the solvent and DNA. The best yield obtained in the repeat experiments was 5 % (as assessed by PAGE densitometry), but only for the lower DP polymer (see Figure 2.9). This led to the conclusion that conjugate-formation under these conditions was highly sensitive to small perturbations.

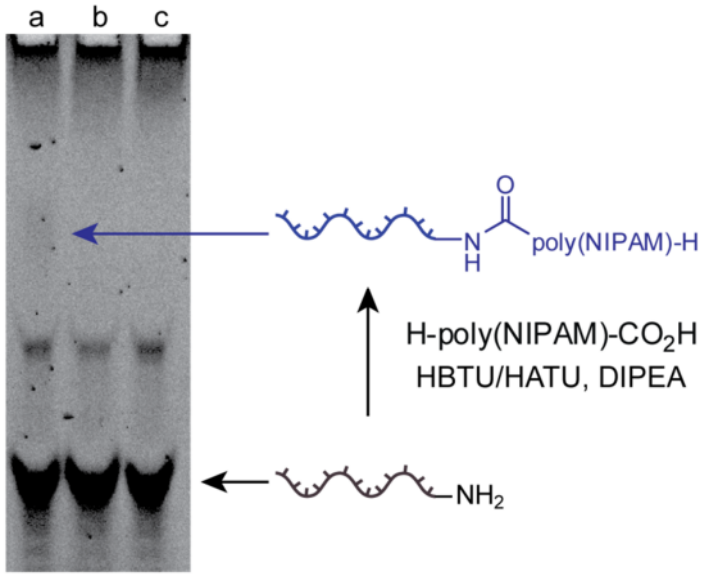

Figure 2.9 15 % native PAGE analysis of attempted conjugation of **P4a-c** to s0–NH_2. Polymers used were as follows: lane a – **P4a**; lane b – **P4b**; lane c – **P4c**. A very low yield (~5 %) of the conjugate was visible as a faint band in lane a only.

Whilst the utmost was done to attempt to control all the variables involved, eventually it

was decided that the irreproducibility of the results coupled with the less than impressive yields meant that this chemistry was not suitable for achieving the stated goals of the project.

2.2.iv Coupling with a hydrophobic polymer

Conjugation reactions were also attempted using the poly(styrene) and poly(styrene-*b*-NIPAM) synthesised in Section 2.2.i, with HBTU or HATU as the coupling reagent. Reaction mixtures were analysed by 2 % agarose gel electrophoresis, but under no conditions was the conjugate product observed. In these cases it is thought that the efficiency of the chemistry was not sufficient to overcome the incompatibility between the hydrophobic polymer and DNA.

2.2.v Synthesis of polymers containing an activated ester end group

Recently, pentafluorophenyl (PFP) esters have been used for the functionalisation of polymers produced by RAFT.[16-19] The more established NHS esters have also been shown to be very useful in polymer functionalisation.[20] Previous work in the O'Reilly group has shown that pre-activated species such as these may be more effective for modification of s0–NH_2 with small molecules than generating the activated ester *in situ*.* It is hypothesised that this is because the formation of the activated ester results in the production of by-products, which later inhibit the attack of the amine and/or cause its degradation. It was therefore reasoned that conjugation of s0–NH_2 to polymers containing a pre-activated acid group may be more efficient than the coupling agent-mediated process described above.

Two activated ester-functionalised CTAs (**6** and **7**) were thus synthesised, as shown in Scheme 2.4. Both were used to polymerise NIPAM with good control over molecular weight and dispersity – Table 2.6 gives a summary. The presence of the PFP group was confirmed by ^{19}F NMR spectroscopy by observing the appearance of broad signals at −152.9, −158.0 and −162.3 ppm attributable to the PFP group attached to the polymer.

* Unpublished work.

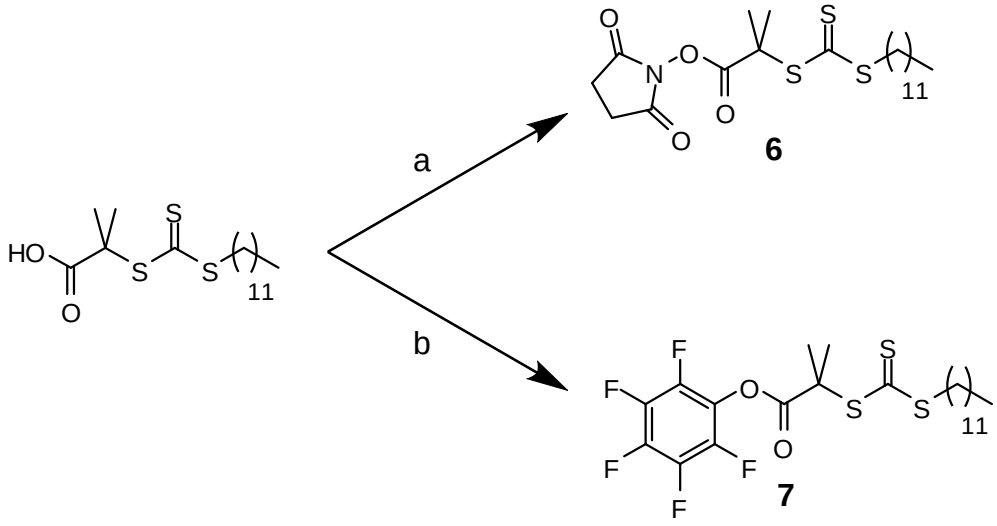

Scheme 2.4 Synthesis of activated ester CTAs **6** (NHS–DDMAT) and **7** (PFP–DDMAT): a) i. NHS, DCM, 4°C, N_2, 2 hours; ii. rt, 48 hours; b) Pentafluorophenyl trifluoroacetate (1.2 eq), DIPEA (2 eq), DMF, 0°C, N_2, 1 hour.

Table 2.6 Poly(NIPAM) synthesised using CTAs **6** and **7**. * Determined by end group analysis using ^{1}H NMR spectroscopy. † Determined by DMF SEC, PMMA calibration standards. ‡ Determined by ^{19}F and ^{1}H NMR spectroscopy using trifluorotoluene as an external standard.

Polymer	CTA used	M_n^{NMR*} / kDa	$M_n^{SEC†}$ / kDa	Đ†	Incorporation of activated ester
P5	**6** (NHS)	11.1	9.6	1.10	>99%*
P6	**7** (PFP)	8.8	7.8	1.10	80-95%‡

By introducing an external standard with both fluorine and hydrogen NMR peaks (in this case trifluorotoluene), it was possible to estimate the degree of PFP functionalisation – around 80-95% – as shown in Figure 2.10. The presence of the NHS group was confirmed by ^{1}H NMR spectroscopy by comparing the integral of the signal at 2.85 ppm (attributable to the two CH_2 groups on the succinimide group) to that of the signal at 3.30 ppm (due to the CH_2 group adjacent to the trithiocarbonate group at the opposite end of the polymer).

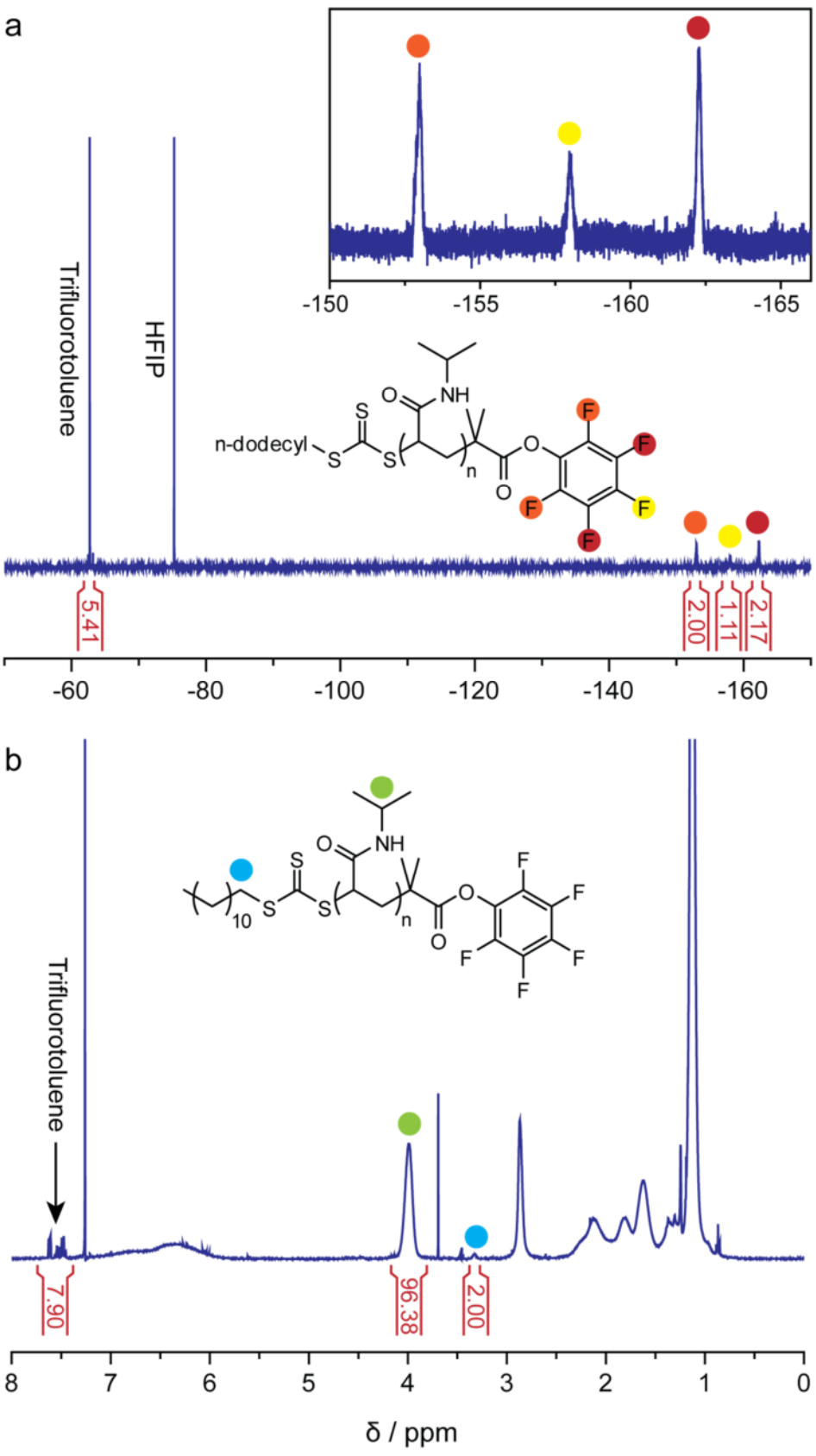

Figure 2.10 a) ^{19}F and b) ^{1}H NMR spectra of poly(NIPAM) containing a PFP activated ester (**P6**). Incorporation of the PFP group was quantified by comparing the integrals of, a) the fluorine signals of the PFP group, and, b) the hydrogen signals of the CH_2 group adjacent to the trithiocarbonate, with an external standard (trifluorotoluene). Solvent: $CDCl_3$.

2.2.vi Assessing the reactivity of the PFP end group

To confirm the reactivity of the PFP group at the polymer chain end, a study using a small molecule amine was undertaken. **P6** was dissolved in one of three NMR solvents – d_7-DMF, d_6-DMSO or d_8-THF – and a small excess of benzylamine was added. The reactions were left overnight at room temperature. ^{1}H NMR showed the appearance of a new peak around 5 ppm (although this was solvent-dependent) due to the CH_2 group adjacent to the newly-formed amide group, and ^{19}F NMR showed the complete absence of any PFP ester peaks, concomitant with the appearance of new peaks due to the pentafluorophenol formed during the reaction – see Figure 2.11. It was therefore concluded that the PFP end group was present and reactive under mild conditions towards primary amines.

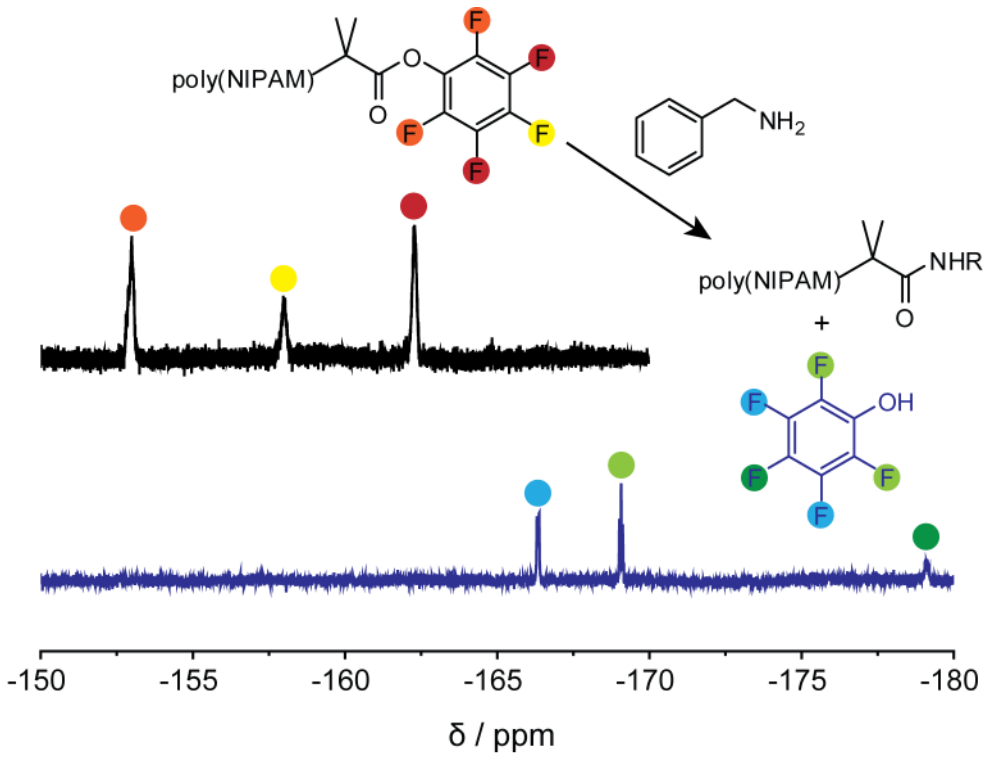

Figure 2.11 ^{19}F NMR spectrum of **P6**, showing the release of pentafluorophenol upon exposure to benzylamine. R = Bn. Solvent: $CDCl_3$.

2.2.vii Removal of the trithiocarbonate group

As previously mentioned, the trithiocarbonate group present in the PFP- and NHS-capped polymers synthesised above was vulnerable to aminolysis by primary amines. It was

therefore desirable to remove it. Initially, this was attempted using 1-Ethylpiperidine hypophosphite (EPHP) as described earlier in the chapter. PFP-capped poly(NIPAM) was mixed with EPHP and AIBN in 1,4-dioxane[*], degassed and heated to 100°C for two hours. The product polymer was isolated by precipitation into diethyl ether cooled using an ice bath (dialysis was inappropriate in this case because water would have hydrolysed the activated ester). Although ^{1}H NMR and SEC showed the disappearance of the trithiocarbonate group as previously described, ^{19}F NMR also revealed the complete loss of the PFP activated ester. It seems likely that this problem arose from the donation of a hydrogen atom from EPHP, leading to the release of pentafluorophenol, although no further study was carried out to confirm this. Instead, a different strategy was sought that did not rely on the use of a hydrogen donor.

AIBN alone has often been used in the literature to remove RAFT polymer end groups. Upon heating in the presence of this radical initiator, the end group dissociates from the polymer (as would normally occur in the main equilibrium of the RAFT process – see Scheme 1.5); in the absence of any monomer, the polymer is re-capped by the huge excess of AIBN radicals. However, this process can be rather inefficient, with up to 40 % of the end groups remaining after work-up. This is because, once AIBN has attacked the trithiocarbonate, it is a better leaving group than the polymeric radical, so the reaction is unable to reach completion. Since the polymer was to be added in a large excess to the s0–NH_2, it was important to get a much higher efficiency of end group removal.

Recently, Rizzardo *et al.* have shown that the use of lauroyl peroxide (LPO) in combination with AIBN can dramatically enhance the efficiency of end group removal.[21] LPO is a much better leaving group than AIBN and reacts quickly with the trithiocarbonate group to produce the polymeric radical, which is then mopped up by the high concentration of AIBN radicals. Use of LPO alone is not effective because it causes the polymeric radical to

[*] Dioxane was used instead of DMF since the latter typically contains a low concentration of primary amine (as a result of solvent degradation, which can be accelerated by the presence of molecular sieves used to remove water), which could have led to unwanted side-reactions with the activated ester.

be produced so fast that bimolecular coupling occurs, which manifests itself as a high molecular weight shoulder in SEC analysis and a broadening of dispersity. In the present case it would also have led to the incorporation of two PFP groups in some chains, which may have caused unexpected results upon addition of s0–NH_2. The trithiocarbonate groups were thus removed from the termini of the PFP- and NHS-capped poly(NIPAM) samples by heating at 80°C in the presence of AIBN and LPO at high dilution in toluene (see Scheme 2.5).

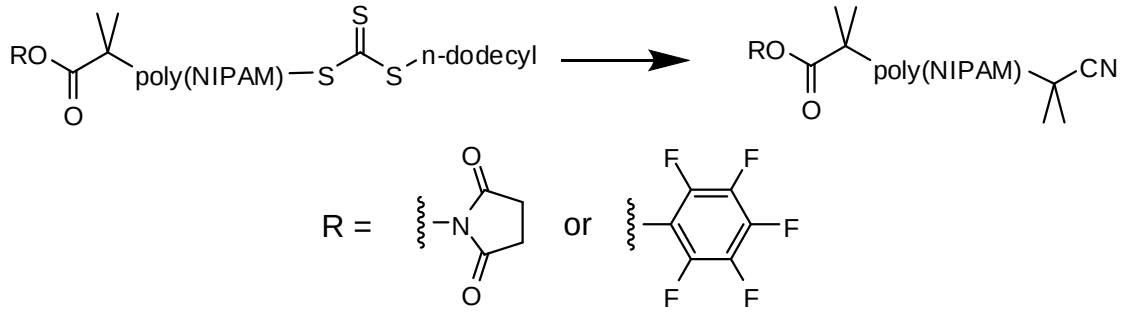

Scheme 2.5 Removal of the trithiocarbonate group from activated ester-containing poly(NIPAM) using AIBN and LPO. Reaction conditions: AIBN (100 eq.), LPO (4 eq.), toluene, 80°C, N_2, 5 hours.

In the case of **P6**, ^{1}H NMR confirmed the loss of the CH_2 group adjacent to the trithiocarbonate (see Figure 2.12) and DMF SEC using an inline UV-vis detector set to 309 nm (the characteristic absorbance of the sulfur-containing end group) provided further verification of the efficiency of the reaction (see Figure 2.13). Finally, ^{19}F NMR showed that the activated ester survived the reaction intact (see Figure 2.14).

For **P5**, DMF SEC once again revealed the loss of the signal at 309 nm due to the trithiocarbonate. ^{1}H NMR confirmed both the loss of the SCH_2 group and the retention of the succinimide group, which has a characteristic signal at 2.86 ppm (see Figure 2.15).

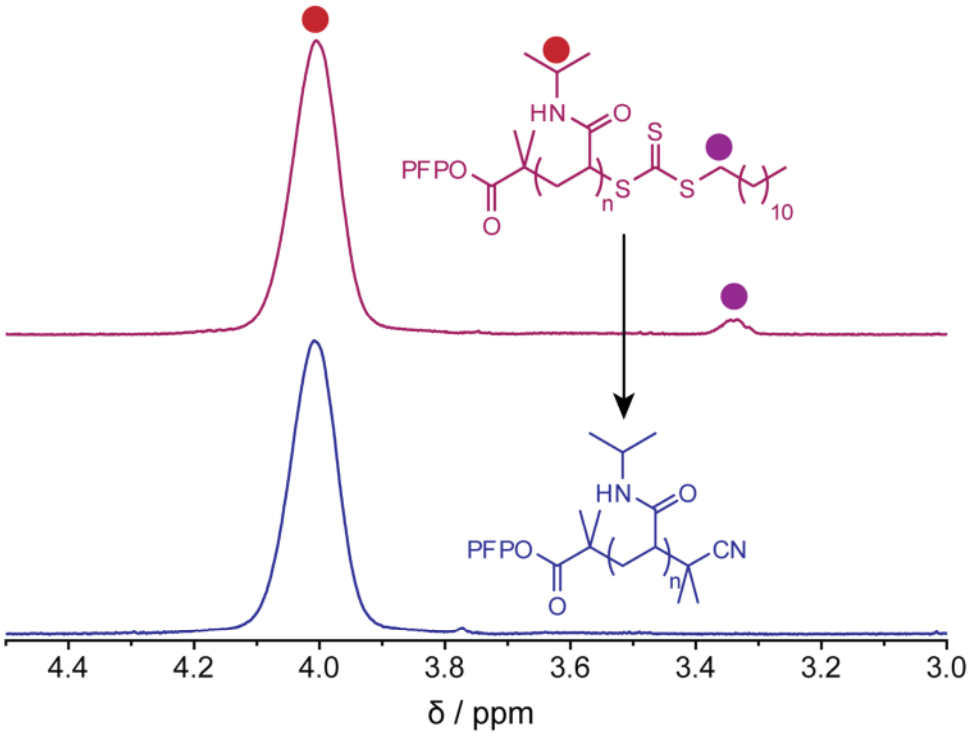

Figure 2.12 ^{1}H NMR spectrum showing the substitution of the trithiocarbonate group of **P6** using AIBN and LPO. Completion of the reaction is indicated by complete loss of the signal at around 3.3 ppm, which is attributed to the CH_2 group adjacent to the trithiocarbonate. Solvent: $CDCl_3$.

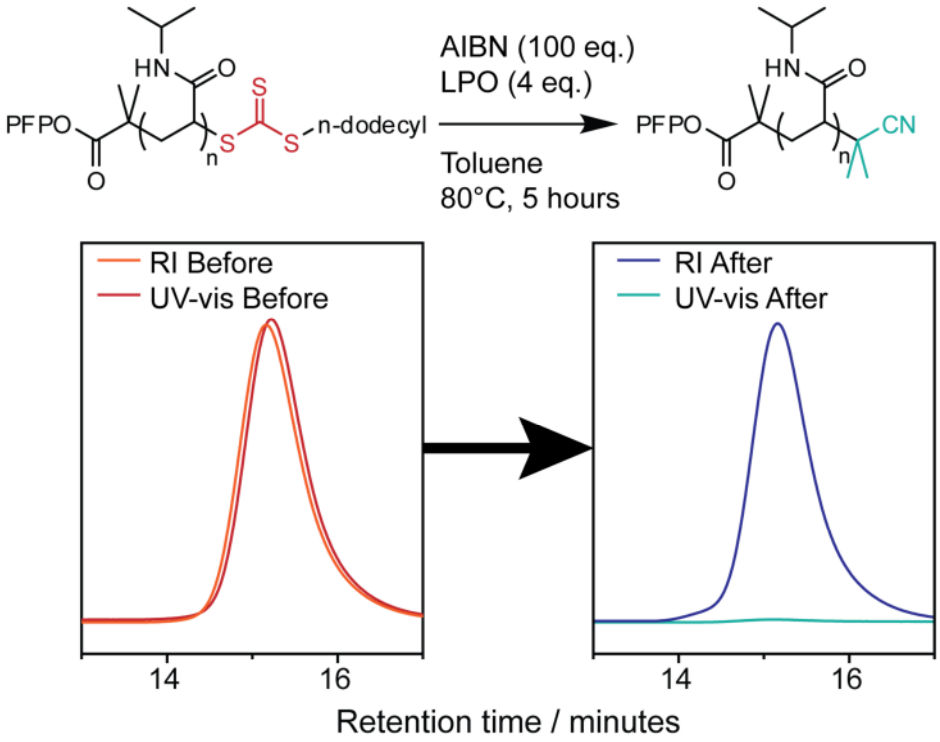

Figure 2.13 DMF SEC traces showing the loss of the signal at 309 nm (due to the trithiocarbonate group) upon substitution of the end group of **P6** with AIBN. In both chromatograms the UV-vis trace was scaled by the same amount relative to the RI.

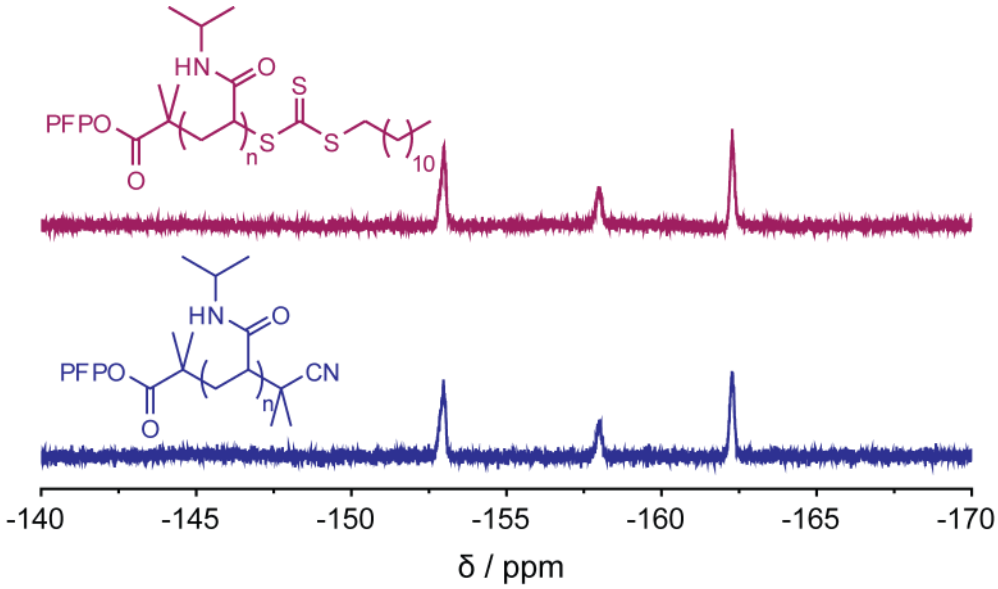

Figure 2.14 ^{19}F NMR spectrum showing the retention of the PFP activated ester group upon removal of the trithiocarbonate from **P6** using AIBN and LPO. Solvent: $CDCl_3$.

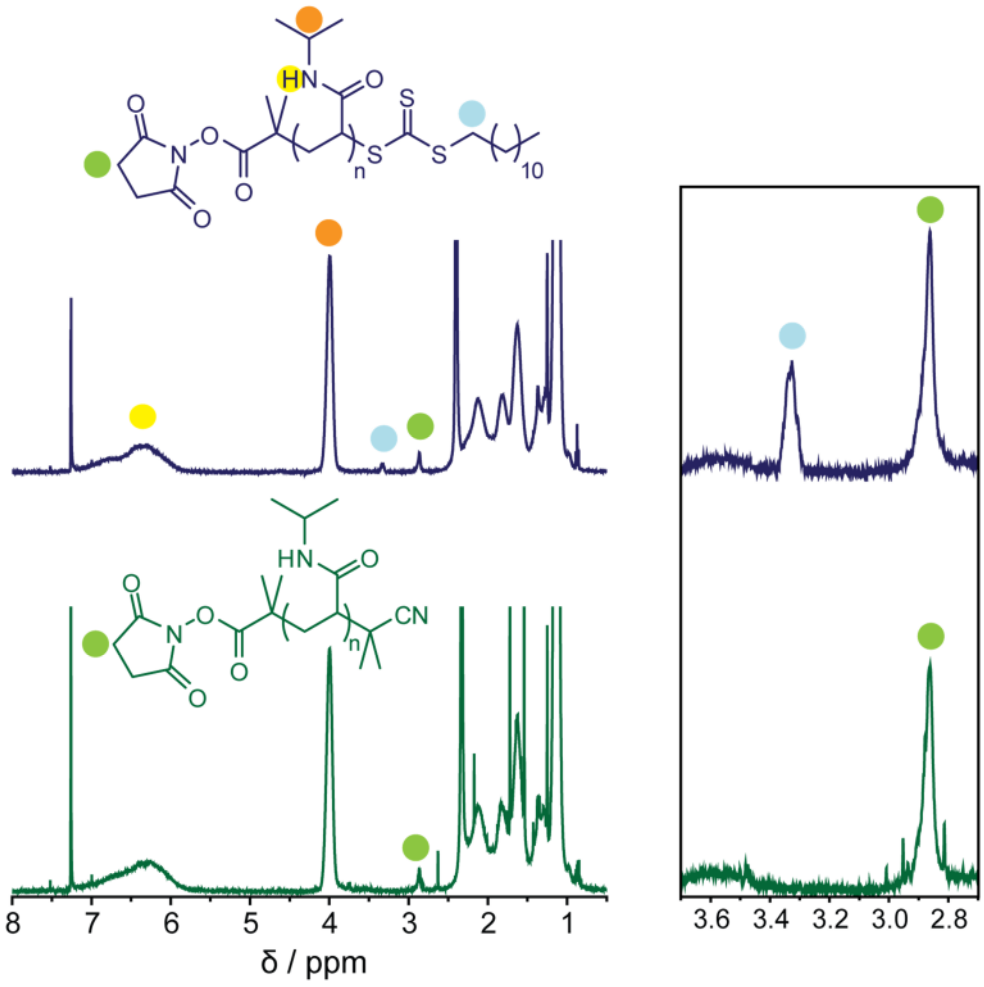

Figure 2.15 ^{1}H NMR spectrum showing the retention of the NHS activated ester group and the removal of the trithiocarbonate from **P5** upon exposure to AIBN and LPO. Solvent: $CDCl_3$.

2.2.viii Coupling of activated ester-containing polymers to s0–NH_2

Having confirmed that the activated esters remained intact following end group removal, coupling to s0–NH_2 was then attempted under various reaction conditions (summarised in Table 2.7).

However, under none of these conditions was the expected product observed. It is clear that, under these conditions, neither of the activated esters used were reactive enough for the DNA conjugate to form. Instead, hydrolysis and/or degradation occurred before the attack of the amine.

It was hypothesised that the low reactivity of the s0–NH_2 arose from the amine being buried within the tertiary structure of the DNA, which as a single strand in solution should adopt a random coil type conformation. To test this theory, the s0–NH_2 DNA strand was hybridised with its complement (s0') to give the double stranded species (dss0–NH_2). The structure of dss0–NH_2 should be a rigid rod with the amine group at one end. It was hoped that this would result in the reactive group being more available for attack on the activated ester. The duplex dss0–NH_2 was formed by mixing s0–NH_2 and s0' in NaCl solution, heating to 95°C to break all hydrogen bonding interactions, then cooling to room temperature slowly to allow controlled formation of the correct hydrogen bonds. 15 % native PAGE analysis confirmed the successful formation of the duplex (see Figure 2.16).

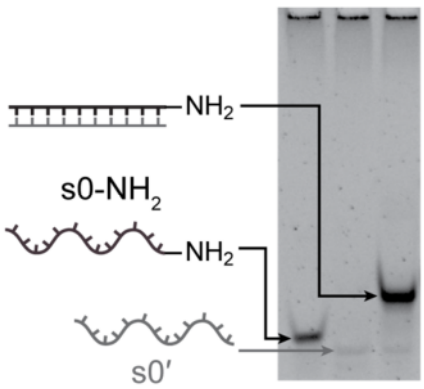

Figure 2.16 15 % native PAGE analysis showing the formation of the duplex dss0–NH_2 (right hand lane) from s0–NH_2 (left hand lane) and s0' (centre lane).

Table 2.7 Reaction conditions tested for the conjugation of **P6** (reactions 5 and 7) and **P5** (reactions 6 and 8) to s0–NH_2. All experiments were carried out at room temperature overnight. TEA = Triethylamine. DMAc = *N*,*N*-Dimethylacetamide.

Reaction #	[DNA] / μM	Catalyst	Eq. of polymer	Solvent
5/6a	10	-	100	DMF
5/6b				DMAc
5/6c				NMP
5/6d			10	DMF
5/6e				DMAc
5/6f				NMP
5/6g			1	DMF
5/6h				DMAc
5/6i				NMP
5/6j		TEA (0.1 M)	100	DMF
5/6k				DMAc
5/6l				NMP
5/6m			10	DMF
5/6n				DMAc
5/6o				NMP
5/6p			1	DMF
5/6q				DMAc
5/6r				NMP
7/8a	100	-	10	DMF
7/8b				DMAc
7/8c				NMP
7/8d			1	DMF
7/8e				DMAc
7/8f				NMP
7/8g		TEA (0.1 M)	10	DMF
7/8h				DMAc
7/8i				NMP
7/8j			1	DMF
7/8k				DMAc
7/8l				NMP

The mixture was diluted to a final DNA concentration of 10 μM in one of several organic solvents (see Table 2.8) and the activated ester-capped poly(NIPAM) added. The reaction was allowed to proceed overnight at room temperature and then analysed by 15 % native PAGE.

Table 2.8 Solvents used for the attempted coupling of **P5** and **P6** to the DNA duplex dss0–NH_2. The activated esters used were PFP (reaction 9) and NHS (reaction 10).

Reaction #	Solvent
9/10a	DMF
9/10b	DMAc
9/10c	NMP
9/10d	MeCN

As Figure 2.17 shows, no conjugate was formed under any of these conditions. This led to the conclusion that the pre-activation of the acid group was not effective in increasing the efficiency of the amide coupling reaction when forming DNA–polymer conjugates. The PFP and succinimide groups were simply too stable to undergo substitution with such a low concentration of amine.

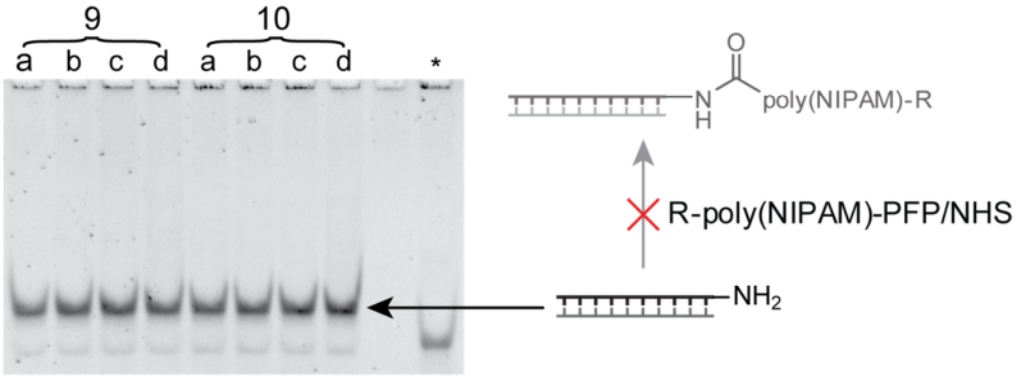

Figure 2.17 15 % native PAGE analysis of the reactions mixtures detailed in Table 2.8. Lane * contains s0–NH_2 DNA. R = $C(CH_3)_2CN$. Some s0–NH_2 is visible in lanes 9a-d and 10a-d, indicating that it was added in a slight excess when the duplex was formed.

2.3 Conclusions

Conjugation of acid-functionalised poly(NIPAM) to amine-functionalised DNA was achieved at low DNA concentrations in an organic milieu using the coupling agents HBTU and HATU, with a yield of around 25 %. The reaction only proceeded when DMF was used as the solvent, and was unsuccessful in any of the other organic solvents tested. The yield of the reaction was found to be highly sensitive to the purity of the reagents used. Conjugation of the more hydrophobic poly(styrene) was unsuccessful. Polymers were synthesised containing either an NHS or PFP activated ester at their chain end, but these groups were found to be too unreactive to facilitate the DNA–polymer conjugation reaction. Finally, use of double stranded rather than single stranded DNA was found to have no effect on the yield of the conjugation reaction.

2.4 Experimental

2.4.i Materials & Methods

For general materials and methods details, see the Appendix. 2-(Dodecylthiocarbonothioylthio)-2-methylpropionic acid (DDMAT) was synthesised using a previously published procedure and recrystallised from acetone/water.[22] *N*-isopropylacrylamide (NIPAM) was recrystallised from hexane and stored at 4°C. 2,2'-Azobis(2-methylpropionitrile) (AIBN) was purchased from Wako Pure Chemical Indutries and recrystallised twice from methanol and stored in the dark at 4°C. Styrene was passed through a neutral alumina column prior to use to remove the radical inhibitor. 18 MΩ water was obtained using a MilliQ™ Simplicity system. Dialysis membranes were purchased from Spectra/Por® and soaked in 18 MΩ water before use. The DNA strands s0–NH_2 and s0' were purchased from Integrated DNA Technologies, Inc. and re-suspended in 18 MΩ water to a concentration of 200 μM before use. Syringe filters were purchased from Gilson Scientific Ltd. Silica gel for column chromatography and all NMR solvents were purchased from Apollo Scientific Ltd. MOPS buffer consisted of 100 mM 3-(*N*-morpholino)propanesulfonic acid adjusted to the desired pH with 1 M HCl or NaOH. PBS consisted of 100 mM potassium phosphate – the desired pH was achieved by mixing appropriate amounts of the monobasic and dibasic versions (both at 100 mM). All other chemicals were purchased from Sigma-Aldrich Corporation and used as received.

2.4.ii Synthesis of poly(NIPAM) using DDMAT

Polymers containing a carboxylic acid end-group were synthesised using the CTA DDMAT. A typical procedure was as follows. DDMAT (0.032 g, 0.09 mmol), NIPAM (1.000 g, 8.84 mmol) and AIBN (0.003 g, 0.02 mmol) were dissolved in 1,4-dioxane (3 mL). The solution was rigorously de-gassed by four successive freeze-pump-thaw cycles, sealed under nitrogen and heated at 65°C for 32 hours. The reaction mixture was allowed to cool and the solvent then removed *in vacuo*. The solid was taken up in the minimum volume of

THF possible and the polymer product precipitated into diethyl ether (200 mL) at room temperature. The product was isolated by filtration as a light yellow solid (0.708 g, 71 %)* and analysed by DMF SEC using PMMA calibration standards (M_n 10 400 Da, Đ 1.14). ^{1}H NMR (300 MHz, $CDCl_3$) δ 7.00-5.50 (br s, PNIPAM N*H*), 4.10-3.80 (br s, PNIPAM NC*H*$(CH_3)_2$), 2.40-0.73 (br m, polymer backbone *H*) ppm.

2.4.iii Synthesis of poly(styrene) using DDMAT

DDMAT (70 mg, 0.19 mmol) was dissolved in styrene (1 g, 9.60 mmol) and transferred to an oven-dried ampoule. The solution was rigorously degassed by four successive freeze-pump-thaw cycles and then stirred under N_2 at 110°C for 34 hours. The gel-like residue was dissolved in the minimum amount of THF (~3 mL) and the product precipitated into MeOH (300 mL) cooled with dry ice. The product was washed on the filter with successive portions of cold MeOH and isolated as a yellow solid (0.694 g, 69 %) and analysed by SEC using THF as the eluent and PMMA calibration standards (M_n 4 900 Da, Đ 1.06). ^{1}H NMR (400 MHz, $CDCl_3$) δ 7.40-6.20 (br m, PS aryl *H*), 3.27 (br t, end group SC*H*$_2$), 2.50-1.00 (br m, PS backbone *H*), 0.90 (t, end group S$(CH_2)_{11}$C*H*$_3$) ppm.

2.4.iv Chain extension of poly(styrene) with NIPAM

Poly(styrene) was chain extended with NIPAM as follows. Polystyrene (PS) (0.500 g, 0.10 mmol), NIPAM (0.577 g, 5.10 mmol) and AIBN (0.003 g, 0.02 mmol) were dissolved in 1,4-dioxane (3 mL) and rigorously degassed by 5 successive freeze-pump-thaw cycles, then stirred under nitrogen at 65°C for 26 hours. The solvent was then removed *in vacuo*, the residue re-dissolved in the minimum amount of THF (~1 mL) and the product precipitated into diethyl ether (300 mL). After filtration and drying the product was isolated as a light yellow solid (0.561 g, 61 %) and analysed by SEC using THF as the eluent and PMMA calibration standards (M_n 9 000 Da, Đ 1.11). ^{1}H NMR (300 MHz, $CDCl_3$) δ 7.40-5.50 (br m, PS aryl *H*), 4.12-3.88 (br s, PNIPAM NC*H*$(CH_3)_2$), 2.50-0.50 (br m, polymer backbone

* Percentage yields were calculated from the final monomer conversion, which was assessed by ^{1}H NMR spectroscopy at the end of the polymerisation.

H) ppm.

2.4.v Removal of the RAFT end group using EPHP

The trithiocarbonate end group was removed from poly(NIPAM) as follows.[12] Poly(NIPAM)$_{50}$ (0.200 g, 0.01 mmol), 1-ethylpiperidine hypophosphite (EPHP) (0.060 g, 0.33 mmol) and AIBN (2 mg, 10 μmol) were dissolved in anhydrous DMF (5 mL) and transferred to an oven-dried ampoule. The solution was rigorously degassed by three successive freeze-pump-thaw cycles and then stirred under nitrogen at 100°C for 2 hours. Water (20 mL) was added and the solution dialysed (MWCO 1 kDa) against 18 MΩ water, with five water changes. The solution was freeze-dried to yield a white powder (0.150 g, 75 %), which was analysed by SEC using DMF as the eluent and PMMA calibration standards (M_n 6 800 Da, Đ 1.06). ^{1}H NMR (400 MHz, d_6-DMSO) δ 11.93 (br s, end group CO_2H), 8.00-6.40 (br m, PNIPAM N*H*), 3.84 (br s, PNIPAM NHC*H*$(CH_3)_2$), 2.40-0.50 (br m, polymer backbone *H*) ppm.

End group removal from poly(NIPAM) samples of various molecular weights was achieved using the same method, keeping the concentration and number of equivalents of EPHP and AIBN constant. For poly(styrene) and poly(styrene-*b*-NIPAM) samples, the same procedure was followed except for purification, which was as follows: the reaction solvent was removed *in vacuo*, the residue re-dissolved in THF (1 mL) and the product precipitated in diethyl ether (300 mL) cooled with dry ice. The precipitate was washed on the filter with ice-cold water (3 × 10 mL) to remove EPHP by-products and the product collected as a white solid and dried under vacuum at 40°C.

2.4.vi DNA–polymer conjugation using amide coupling reagents

For a full list of the coupling agents and solvents tested, see Table 2.3 and Table 2.4. A general procedure follows; unless otherwise stated, stock solutions were made up in the appropriate reaction solvent. The acid-functionalised polymer (1 μL, 10 mM in DMF), coupling agents (1 μL, 10 mM) and s0–NH_2 (0.5 μL, 200 μM in water) were mixed and the

solution topped up to 9.5 μL with the appropriate reaction solvent. DIPEA (0.5 μL, 20 mM) was added, and the mixture vortexed briefly then left overnight at room temperature. Water (70 μL) and 5 × glycerol loading buffer (20 μL) were added and the mixture analysed by 15 % native PAGE.

2.4.vii Synthesis of NHS–DDMAT, 6

NHS–DDMAT, **6**, was synthesised as follows.[20] DDMAT (0.500 g, 1.37 mmol), NHS (0.158 g, 1.37 mmol) and DCC (0.283 g, 1.37 mmol) were dissolved in dichloromethane and the mixture stirred for 48 hours. The cloudy mixture was filtered through a 0.45 μm PTFE syringe filter and the retentate washed with CH_2Cl_2 (5 mL). This process was then repeated. The solvent was removed *in vacuo* and the residue dissolved in a small amount of ethyl acetate. The solution was purified by silica gel column chromatography, eluting with a mixture of ethyl acetate and pet. ether 40-60 (1:1). The product fractions (R_f = 0.53) were collected and the solvent removed *in vacuo* to afford **6** as a yellow solid (0.502 g, 79 %). ^{1}H NMR (400 MHz, $CDCl_3$) δ 3.30 (t, *J* = 7 Hz, 2H, SC*H*$_2$), 2.81 (br s, 4H, C*H*$_2$(C=O)N), 1.87 (s, 6H, C(C*H*$_3$)$_2$), 1.68 (quint, *J* = 7 Hz, 2H, SCH$_2$C*H*$_2$), 1.38 (m, 2H, C*H*$_2$CH$_3$), 1.25 (br s, 16H, SCH$_2$CH$_2$(C*H*$_2$)$_8$), 0.88 (t, *J* = 7 Hz, 3H, CH$_2$C*H*$_3$) ppm. ^{13}C NMR (150 MHz, $CDCl_3$) δ 218.8 (*C*=S), 169.1 (*C*=OO), 168.7 (NHS *C*=O), 54.3 (*C*(CH$_3$)$_2$), 37.2 (S*C*H$_2$), 31.9 (SCH$_2$*C*H$_2$), 29.6, 29.5, 29.4, 29.3, 29.1, 29.0, 27.8, 25.4 (NHS *C*H$_2$), 25.3 (C(*C*H$_3$)$_2$), 22.7 (*C*H$_2$CH$_3$), 14.1 (S(CH$_2$)$_{11}$*C*H$_3$) ppm. IR (ν_{max} / cm^{-1}): 2917, 2848, 1777, 1736, 1203, 1074, 811. ESI HR MS calcd. for $C_{21}H_{35}NO_4S_3$ [M+Na]$^+$ 484.1626 Da; observed 484.1619 Da.

2.4.viii Synthesis of PFP–DDMAT, 7

PFP–DDMAT, **7**, was synthesised as follows. DDMAT (0.500 g, 1.37 mmol) was added to an oven-dried schlenk flask, which was then evacuated and refilled with nitrogen three times. Anhydrous DMF (7.5 mL) was added *via* syringe and the flask cooled to 0°C with an ice bath. DIPEA (354 μL, 2.74 mmol) was then added *via* syringe, followed by dropwise

addition of pentafluorophenyl trifluoroacetate (283 μL, 1.65 mmol). After one hour stirring at 0°C, the flask was opened to the air and diethyl ether (30 mL) was added, followed by a 1 M solution of HCl (30 mL). The organic layer was collected and washed with water (2 × 30 mL) and brine (30 mL). The solvent was removed *in vacuo* to give a yellow oily residue, which was then purified by silica gel column chromatography, eluting with a mixture of ethyl acetate and pet. ether 40-60 (gradient from 5-10 % ethyl acetate). The fractions containing the product (R_f = 0.81) were combined and the solvent removed *in vacuo* to yield CTA **7** as a yellow oil (0.686 g, 94 %). ^{1}H NMR (400 MHz, $CDCl_3$) δ 3.31 (t, *J* = 7 Hz, 2H, SCH_2), 1.86 (s, 6H, $C(CH_3)_2$), 1.69 (quint, *J* = 7 Hz, 2H, SCH_2CH_2), 1.40 (m, 2H, CH_2CH_3), 1.26 (br s, 16H, $SCH_2CH_2(CH_2)_8$), 0.88 (t, *J* = 7 Hz, 3H, CH_2CH_3) ppm. ^{13}C NMR (150 MHz, $CDCl_3$) δ 219.9 (*C*=S), 169.6 (*C*=O), 142.1 (t), 140.4 (t), 138.7 (t), 137.0 (t) (PFP *C*s), 55.4 ($C(CH_3)_2$), 37.2 (SCH_2), 31.9, 29.6, 29.5, 29.4, 29.3, 29.1, 29.0, 28.9, 27.8, 25.4 ($C(CH_3)_2$), 22.7 (CH_2CH_3), 14.1 ($S(CH_2)_{11}CH_3$) ppm. ^{19}F NMR (375 MHz, $CDCl_3$) −151.5 (d, 2F, ortho *F*), −157.7 (t, 2F, para *F*), −162.3 (t, 2F, meta *F*) ppm. IR (ν_{max} / cm^{-1}): 2925, 2854, 1779, 1517, 1079, 992, 815. ESI HR MS calcd. for $C_{23}H_{31}F_5O_2S_3$ $[M+H]^+$ 531.1486 Da; observed 531.1480 Da.

2.4.ix Synthesis of poly(NIPAM) using NHS– and PFP–DDMAT

Polymerisation of NIPAM with **6** was conducted as follows. NHS–DDMAT, **6**, (0.041 g, 0.09 mmol), NIPAM (1.000 g, 8.84 mmol) and AIBN (0.002 g, 0.01 mmol) were dissolved in 1,4-dioxane (1.5 mL) and transferred to an oven-dried ampoule. The mixture was subjected to three freeze-pump-thaw cycles and sealed under an atmosphere of nitrogen. It was then placed in an oil bath preheated to 65°C. After 2 hours the ampoule was removed and the reaction quenched by opening it to the air and cooling with liquid nitrogen. The solution was poured into pet. ether 40-60 (80 mL) cooled in an ice bath and the precipitant collected by filtration. The product was then dissolved in THF (1 mL) and the process repeated 5 more times. Finally, the isolated solid was dissolved in THF (1 mL) and precipitated into diethyl ether (80 mL) cooled in an ice bath. The product was isolated by

filtration, dried *in vacuo* and isolated as a yellow powder (0.335 g, 36 %) and analysed by DMF SEC using PMMA calibration standards (M_n 9 610 Da, Đ 1.10). ^{1}H NMR (400 MHz, $CDCl_3$) δ 7.36-5.55 (br m, PNIPAM N*H*), 4.00 (br s, PNIPAM C*H*$(CH_3)_2$), 3.33 (br m, 2H, SCH_2), 2.86 (br s, 4H, CH_2(C=O)N), 2.64-0.80 (br m, PNIPAM backbone *H*), 0.88 (t, *J* = 7 Hz, 3H, S$(CH_2)_{11}CH_3$) ppm.

PFP–DDMAT, **7**, was also used to polymerise NIPAM using an identical procedure. The product was collected as a yellow solid (0.266 g, 32 %) and analysed by DMF SEC using PMMA calibration standards (M_n 7 760 Da, Đ 1.10). ^{1}H NMR (400 MHz, $CDCl_3$) δ 7.40-5.70 (br m, PNIPAM N*H*), 4.00 (br s, PNIPAM C*H*$(CH_3)_2$), 3.35 (br m, 2H, SCH_2), 2.65-0.75 (br m, PNIPAM backbone *H*), 0.88 (t, *J* = 7 Hz, 3H, S$(CH_2)_{11}CH_3$) ppm. ^{19}F NMR (375 MHz, $CDCl_3$) δ −153.0 (br m, 2F, PFP end group F_{ortho}), −158.0 (br m, 1F, PFP end group F_{para}), −162.3 (br m, 2F, PFP end group F_{meta}) ppm.

2.4.x Modification of poly(NIPAM)–PFP with benzylamine

Poly(NIPAM) containing a PFP end group (M_n 9 540 Da, Đ 1.18) (5.8 mg, 0.5 μmol) was dissolved in d_8-THF (1 mL) and ^{1}H and ^{19}F NMR spectra recorded. Benzylamine (0.55 μL, 5.0 μmol) was added and the reaction left for 2 hours. The ^{1}H and ^{19}F NMR spectra were recorded again and showed that the reaction had reached 100 % conversion. ^{1}H NMR (400 MHz, d_8-THF) (end of reaction) δ 7.73-6.55 (br m, PNIPAM N*H*), 7.35-7.10 (m, excess benzylamine), 4.50 (s, 2H, PNIPAM end group PhCH_2NHC=O), 3.98 (br s, PNIPAM C*H*$(CH_3)_2$), 3.78 (s, excess benzylamine), 2.72-0.84 (br m, PNIPAM backbone *H*) ppm. ^{19}F NMR (375 MHz, d_8-THF) δ −166.3 (dd, *J* = 18, 9 Hz, 2F, PFP-OH F_{meta}), −169.1 (t, *J* = 21 Hz, 2F, PFP-OH F_{ortho}), −179.1 (m, 1F, PFP-OH F_{para}) ppm.

2.4.xi Removal of the trithiocarbonate group using AIBN and LPO

Poly(NIPAM)–PFP (100 mg, 0.01 mmol), AIBN (187 mg, 1.14 mmol) and LPO (18 mg, 0.05 mmol) were dissolved in dry toluene (28 mL) and the solution degassed by three freeze-pump-thaw cycles and then sealed under nitrogen. The mixture was heated to 80°C

for five hours, then allowed to cool to room temperature. The solvent was removed *in vacuo* and the residue resuspended in THF (1 mL), which was then poured into pet. ether 40-60 (15 mL) cooled with an ice bath. The precipitated product was collected by filtration and dried under vacuum to give a white powder (71 mg, 71 %), which was analysed by DMF SEC using PMMA calibration standards (M_n 8 170 Da, Đ 1.11). ^{1}H NMR (400 MHz, $CDCl_3$) δ 8.00-5.50 (br m, PNIPAM N*H*), 4.00 (br s, PNIPAM C*H*$(CH_3)_2$), 3.00-0.50 (br m, PNIPAM backbone *H*) ppm. ^{19}F NMR (375 MHz, $CDCl_3$) δ −153.0 (br m, 2F, PFP end group F_{ortho}), −158.0 (br m, 1F, PFP end group F_{para}), −162.3 (br m, 2F, PFP end group F_{meta}) ppm.

The trithiocarbonate group was removed from poly(NIPAM)–NHS using the same method to yield a white powder (61 mg, 61 %), which was analysed by DMF SEC using PMMA calibration standards (M_n 9 780 Da, Đ 1.11). ^{1}H NMR (400 MHz, $CDCl_3$) δ 7.40-5.40 (br m, PNIPAM N*H*), 4.00 (br s, PNIPAM C*H*$(CH_3)_2$), 2.86 (br s, 4H, C*H*$_2$(C=O)N), 2.60-0.80 (br m, PNIPAM backbone *H*) ppm.

2.4.xii Attempted conjugation of poly(NIPAM)–PFP and –NHS to s0–NH_2

The reaction solvents tested were: DMF, DMAc, NMP and MeCN. The polymer (9.5 μL, 10, 100 or 1000 μM in the reaction solvent) was mixed with s0–NH_2 (0.5 μL, 200 μM in water) or dss0–NH_2 (0.5 μL, 200 μM in 70 mM NaCl solution) and left overnight at room temperature. 5 × glycerol loading buffer (20 μL) and water (70 μL) were added and the reaction mixture analysed by 15 % native PAGE.

2.4.xiii Formation of the duplex dss0–NH_2

s0–NH_2 (6.31 μL, 3.17 mM in water) and s0' (17.09 μL, 1.17 mM in water) were mixed in 70 mM NaCl solution (76.6 μL). The solution was heated to 95°C for four minutes and then allowed to cool slowly to room temperature. The mixture was analysed by 15 % native PAGE.

2.5 References

(1) Schotten, C. *Ber. Dtsch. Chem. Ges.* **1884**, *17*, 2544.

(2) Baumann, E. *Ber. Dtsch. Chem. Ges.* **1886**, *19*, 3218.

(3) Staab, H. A. *Angew. Chem., Int. Ed.* **1962**, *1*, 351.

(4) Sheehan, J. C.; Hess, G. P. *J. Am. Chem. Soc.* **1955**, *77*, 1067.

(5) Valeur, E.; Bradley, M. *Chem. Soc. Rev.* **2009**, *38*, 606.

(6) Coste, J.; Le-Nguyen, D.; Castro, B. *Tetrahedron Lett.* **1990**, *31*, 205.

(7) Coste, J.; Frerot, E.; Jouin, P. *J. Org. Chem.* **1994**, *59*, 2437.

(8) Jeong, J. H.; Park, T. G. *Bioconjugate Chem.* **2001**, *12*, 917.

(9) Jeong, J. H.; Kim, S. H.; Kim, S. W.; Park, T. G. *Bioconjugate Chem.* **2005**, *16*, 1034.

(10) Fong, R. B.; Ding, Z.; Long, C. J.; Hoffman, A. S.; Stayton, P. S. *Bioconjugate Chem.* **1999**, *10*, 720.

(11) Lee, K.; Povlich, L. K.; Kim, J. *Adv. Funct. Mater.* **2007**, *17*, 2580.

(12) Moughton, A. O.; Stubenrauch, K.; O'Reilly, R. K. *Soft Matter* **2009**, *5*, 10.

(13) Snyder, L. R. *J. Chromatogr. Sci.* **1978**, *16*, 223.

(14) Bosshard, H. H.; Mory, R.; Schmid, M.; Zollinger, H. *Helv. Chim. Acta* **1959**, *42*, 1653.

(15) Montalbetti, C. A. G. N.; Falque, V. *Tetrahedron* **2005**, *61*, 10827.

(16) Roth, P. J.; Haase, M.; Basché, T.; Theato, P.; Zentel, R. *Macromolecules* **2009**, *43*, 895.

(17) Wiss, K. T.; Theato, P. *J. Polym. Sci., Part A: Polym. Chem.* **2010**, *48*, 4758.

(18) Gibson, M. I.; Fröhlich, E.; Klok, H.-A. *J. Polym. Sci., Part A: Polym. Chem.* **2009**, *47*, 4332.

(19) Singha, N. K.; Gibson, M. I.; Koiry, B. P.; Danial, M.; Klok, H.-A. *Biomacromolecules* **2011**, *12*, 2908.

(20) Li, H.; Bapat, A. P.; Li, M.; Sumerlin, B. S. *Polym. Chem.* **2011**, *2*, 323.

(21) Chen, M.; Moad, G.; Rizzardo, E. *J. Polym. Sci., Part A: Polym. Chem.* **2009**, *47*, 6704.

(22) Skey, J.; O'Reilly, R. K. *Chem. Commun.* **2008**, 4183.

Chapter 3

DNA–polymer conjugation using the thiol Michael addition reaction

---

3.1 Introduction

Thiols are well known to react with alkene groups. Indeed, the process forms the basis for one of the most important industrial processes ever invented: the vulcanisation of rubber.[1] However, it is only recently that this reaction has become a popular method for the modification of polymers post-polymerisation.[2-7] The reaction may proceed with one of two distinct mechanisms (Scheme 3.1): a radical process that requires an initiator and UV irradiation or heat; or a Michael-type nucleophilic addition, commonly in the presence of a suitable catalyst such as a phosphine.[8,9]

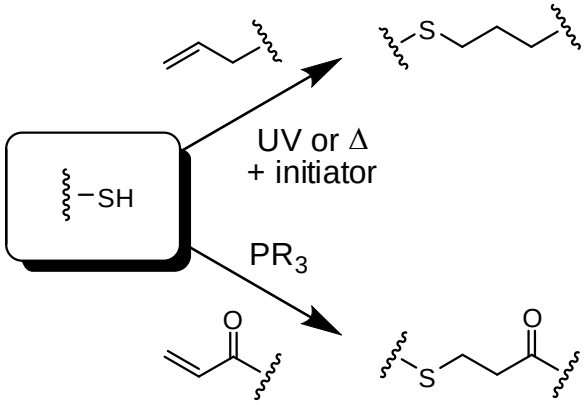

Scheme 3.1 Illustration of the two routes available for the reaction between a thiol and an alkene. Top: reaction with a terminal alkene in the presence of a radical initiator under UV irradiation or at high temperature. Bottom: reaction with an acrylate/acrylamide group via a Michael addition in the presence of a phosphine catalyst (other Michael acceptors and catalysts may also be used).

All polymers produced using the RAFT process have a terminal sulphur-containing group, independent of what kind of CTA is used to mediate the polymerisation. This can

straightforwardly be transformed into a thiol group using either aminolysis[4,10,11] or a reducing agent such as sodium borohydride[12,13] (see Scheme 3.2). All RAFT polymers can therefore be viewed as containing a protected thiol.

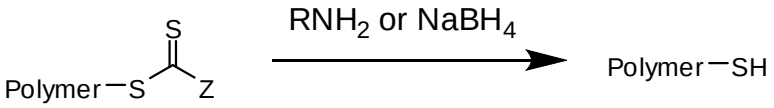

Scheme 3.2 Transformation of the end group of a polymer synthesised using RAFT into a thiol.

Since DNA can be vulnerable to degradation by UV radiation,[14] the second route was chosen for this work. In order for the reaction to proceed, the ene compound must be a Michael acceptor. In most polymer work, acrylates (and occasionally methacrylates) have become the molecules of choice for this reaction.[15,16] The maleimide group has also received considerable attention for its rapid reaction with thiols.[9,10,17-21] There is also a significant body of work in the scientific literature showing that (meth)acrylamides can also undergo efficient thiol Michael addition reactions. In the case of acrylamides, reactions have been reported using phosphine,[22] inorganic bases,[23] and primary,[9,24] secondary[25] or tertiary[26-28] amines as the catalyst – in other words, under very similar conditions to those used for acrylates. In the case of methacrylamides there are fewer examples, but enough to suggest the potential of this group as a highly reactive ene compound.[29-33] In the context of DNA–polymer conjugation, this is an important point because methacrylamide-functionalised DNA is already commercially available (the intended use is as a polymerisable group, for incorporation of DNA into acrylamide hydrogels for affinity separation of complementary oligonucleotides). Furthermore, with the availability and low price of amine-functionalised DNA, acrylamide-functionalised DNA should be easily accessible from acrylic acid *via* standard amide coupling routes. These reactive groups, in combination with thiol-terminated polymers produced using the RAFT polymerisation process, potentially provide a straightforward route to DNA–polymer conjugates. However, to date there have been no reports of the use of the thiol–(meth)acrylamide

Michael addition reaction in this context.

DNA–polymer conjugation has previously been realised using the thiol–maleimide[34] and thiol–acrylate[35] Michael addition reactions, but has only ever been reported in an aqueous environment. Yields were good (around 90 % in the case of the maleimide reaction) but required a relatively high DNA concentration of 0.1 mM, and the use of water as the reaction solvent precluded the conjugation of hydrophobic polymers. Given that polymer–polymer coupling in organic solvents has been achieved using thiol Michael addition chemistry, it was reasoned that an exploration of reaction conditions could yield some interesting results in the area of DNA–polymer conjugation. DNA strands functionalised with a methacrylamide, acrylamide or maleimide group were therefore targeted in the following work, and tested for their reaction with thiol-terminated polymers.

3.2 Synthesis of thiol-terminated polymers

Thiol-terminated polymers were synthesised by stirring with sodium borohydride and purified by dialysis against 18 MΩ water. The poly(NIPAM) samples detailed in Table 3.1 were used and successful removal of the trithiocarbonate end group was confirmed by SEC, using the method described in Chapter 2 – Figure 3.1 shows an example. Some disulfide coupling was observed – this manifested itself as a high molecular weight shoulder in the SEC trace at double the molecular weight of the original polymer. In principle, this was reversible and the free thiol could have been released by the addition of a reducing agent such as *tris*(2-carboxyethyl)phosphine (TCEP).

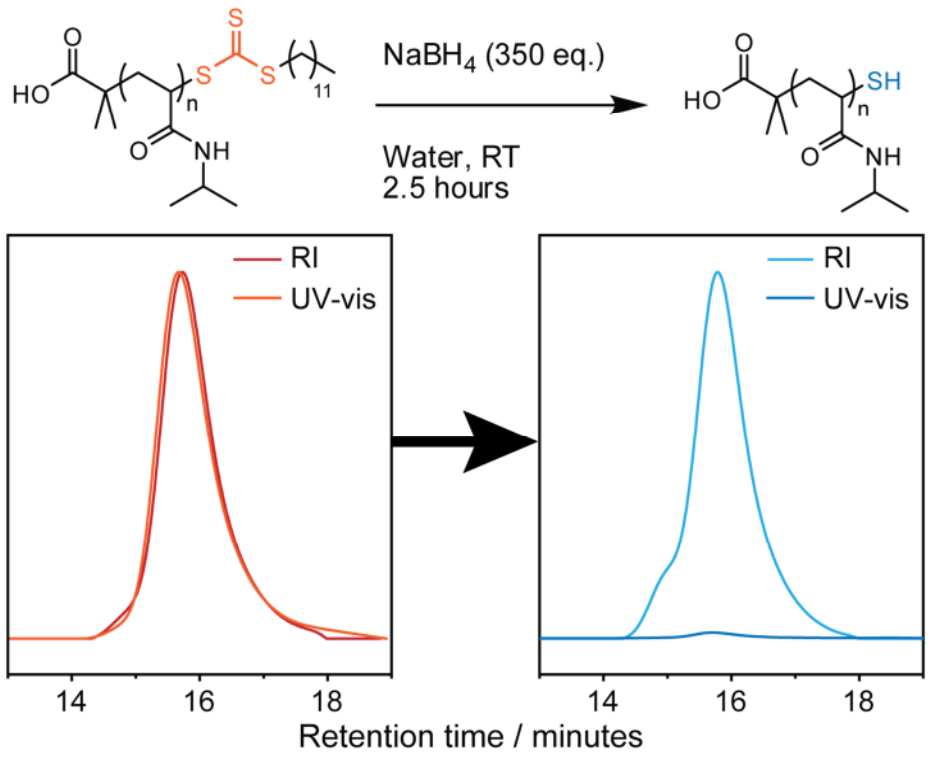

Figure 3.1 SEC traces showing the removal of the trithiocarbonate group from poly(NIPAM) using sodium borohydride in water. The refractive index (RI) trace remains essentially unchanged (except for a small high molecular weight shoulder due to disulfide coupling) while the intensity of the UV-vis trace (recorded at 309 nm – the absorbance maximum for the trithiocarbonate) drops almost to zero. RI traces were normalised; UV-vis traces were then scaled by the same amount as their respective RI traces and overlaid.

To further confirm the presence of the free thiol, Ellman's assay was performed on all samples.[36,37] This assay uses the compound 5,5'-dithiobis(2-nitrobenzoate) (DTNB or

Ellman's reagent), which readily undergoes thiol–disulfide exchange with free thiols, as shown in Scheme 3.3.

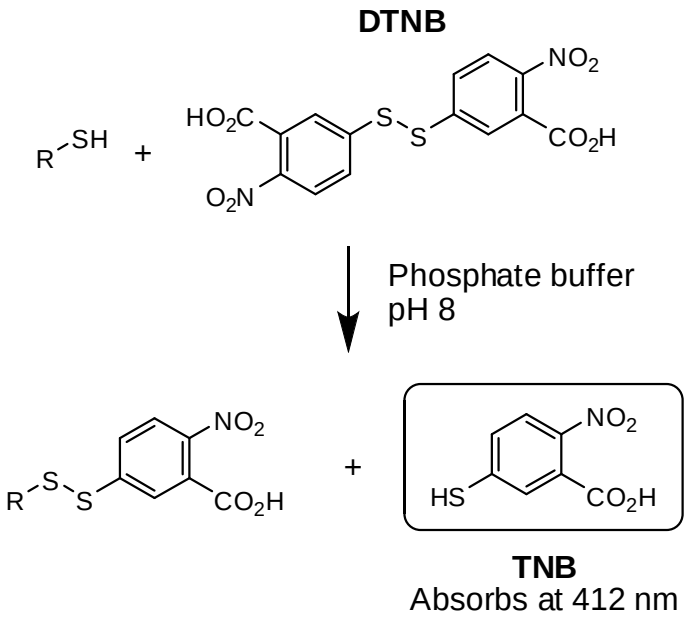

Scheme 3.3 The reaction used to determine thiol content of a substrate (R–SH) in Ellman's assay. Both disulfides have very low absorption at 412 nm, whereas 5-thio(2-nitrobenzoate) (TNB) has very high absorption at this wavelength.

The reaction produces another disulfide and 5-thio(2-nitrobenzoate) (TNB). TNB has a strong absorbance at 412 nm, whereas the disulfide species exhibit very little absorption at this wavelength. Since one molecule of TNB is generated for every thiol present in the mixture, the concentration of thiol before addition of DTNB can be inferred by calculating the concentration of TNB from the A_{412} value of the solution and the known extinction coefficient of TNB at this wavelength (ε = 14 150 M^{-1} cm^{-1} in phosphate buffer) using the Beer−Lambert law – $A = \varepsilon cl$, where c is the concentration of the absorbing species and l is the path length of the UV-vis cell. There are a number of sources of error when calculating thiol concentrations using this method. Firstly, the extinction coefficients are taken from the literature, and it may or may not be a reasonable assumption that they are the same in the system under investigation. Secondly, degradation of DTNB occurs due to ambient light, and this may lead to inaccurate results if the assay is not performed quickly and under low-light conditions. Finally, to make a meaningful comparison with the expected

concentration of thiol, the molecular weight of the material under investigation must be known, and the sample should be free from contaminants so that a given number of moles can be accurately weighed out. These factors mean a significant degree of error is associated with the numbers presented below.

To calculate an estimate of the thiol content of the polymers, a known concentration of polymer, calculated using the molecular weight as determined by ^{1}H NMR spectroscopy, was made up; Ellman's assay was then performed on the solution and the concentration of thiol calculated as outlined above. The polymer and thiol concentrations were then compared, to give the percentage incorporation of thiol – Table 3.1 details the properties of the polymers synthesised. In all cases the amount of free thiol was greater than 25 %, which was deemed high enough for DNA conjugation experiments since the polymer was to be added in excess – in all experiments below the equivalents of polymer actually refers to the equivalents of thiol (for example, when **P7** was used 200 equivalents of polymer were needed to give 100 equivalents of thiol, and so on).

Table 3.1 Properties of thiol-terminated poly(NIPAM) synthesised for this work. DMF was used as the SEC eluent in all cases with PMMA calibration standards. Thiol content was measured using Ellman's assay and is given as a percentage of what was predicted based on the molecular weight of the original polymer.

Polymer	DP^{NMR}	M_n^{SEC} / kDa		Đ		Thiol content / %
		Before	After	Before	After	
P7	50	5.1	5.7	1.18	1.17	47
P8	97	10.4	11.7	1.14	1.23	37
P9	196	20.0	21.4	1.18	1.30	27

3.3 Couplings using the thiol Michael addition reaction

3.3.i Coupling to methacrylamide-functionalised DNA

DNA functionalised with a methacrylamide group (Figure 3.2) is commercially available, so the s0 sequence was purchased with this modification at the 5' end (s0–MAAm). To ascertain the reactivity of s0–MAAm, it was combined with a small molecule thiol – in this case the amino acid cysteine – in the presence of varying amounts of a water soluble phosphine catalyst (TCEP) in buffer solution at pH 8.0 and the reaction followed by high-performance liquid chromatography (HPLC). Table 3.2 outlines the conditions tested.

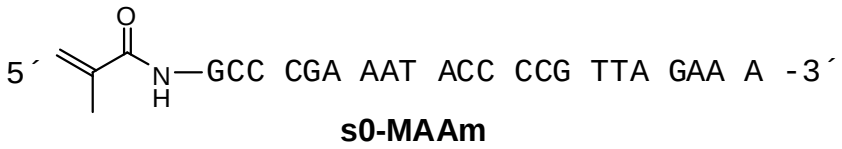

Figure 3.2 Structure of s0–MAAm.

Table 3.2 Reaction conditions tested and yields for the reaction of cysteine with s0–MAAm in potassium phosphate buffer solution at pH 8.0. The concentrations of DNA and cysteine were kept constant at 50 μM and 10 mM respectively. The equivalents of TCEP were measured relative to the methacrylamide group.

Reaction #	Eq. TCEP	Yield
1a	0.01	15 %
1b	0.1	13 %
1c	0.5	14 %
1d	1	14 %
1e	10	16 %
1f	100	23 %

As Figure 3.3 shows, after twenty-four hours a small additional peak could be seen in the HPLC chromatogram – this was attributed to the product of the reaction of cysteine with s0–MAAm (Scheme 3.4). A control experiment was conducted wherein s0–MAAm was mixed with TCEP alone – no shift in retention time or additional peaks were observed.

Interestingly, the amount of TCEP present appeared to make no difference to the yield, suggesting that the catalyst was unnecessary.

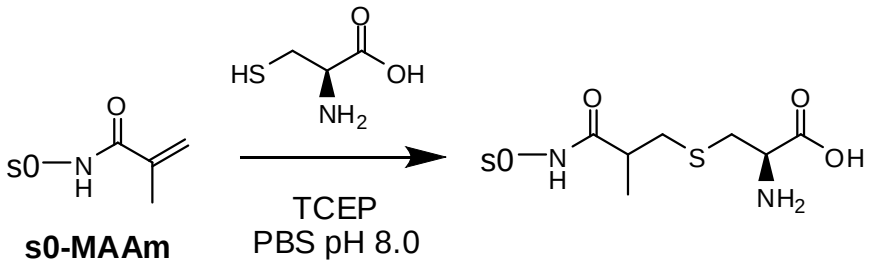

Scheme 3.4 Reaction of s0–MAAm with cysteine. PBS = Phosphate buffer solution.

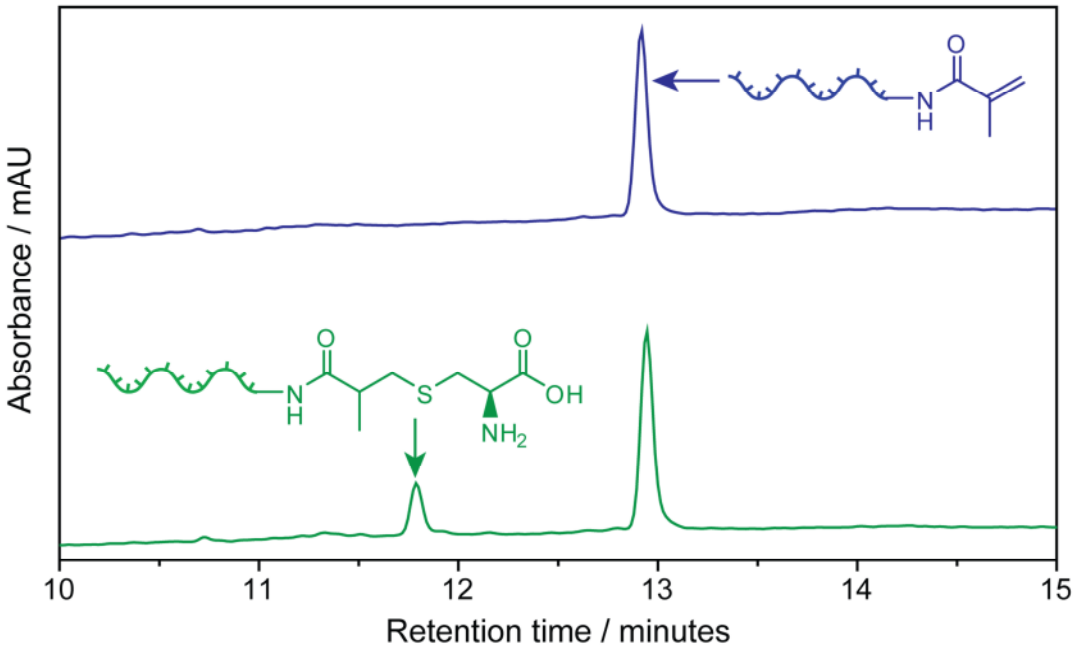

Figure 3.3 HPLC chromatogram showing the appearance of a new peak when cysteine (200 eq.) was reacted with s0–MAAm DNA (at a concentration of 10 μM) in phosphate buffer at pH 8.0, in the presence of TCEP (10 eq.).

Having shown that a reaction can take place between a thiol and the methacrylamide DNA (although slow and low yielding), conjugation to thiol-terminated polymers was next attempted. Initially, the reaction was attempted as outlined in Scheme 3.5 in the absence of any catalyst (see Table 3.3).

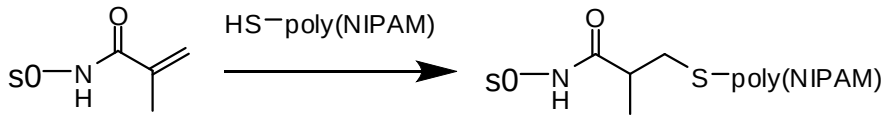

Scheme 3.5 Reaction of thiol-terminated poly(NIPAM) (**P7-9**) with methacrylamide-functionalised DNA (s0–MAAm).

Table 3.3 Reaction conditions tested for the conjugation of thiol-terminated poly(NIPAM) to s0–MAAm in the absence of any catalyst. The concentrations of DNA and polymer were kept constant at 10 μM and 1 mM respectively. The reactions were run at 40°C for twenty-four hours.

Reaction #	Solvent	Polymer
2a	PBS pH 8.0	**P7**
2b		**P8**
2c		**P9**
2d	DMF	**P7**
2e		**P8**
2f		**P9**
2g	DMSO	**P7**
2h		**P8**
2i		**P9**

However, after heating at 40°C overnight 15 % native PAGE analysis revealed that none of the expected DNA–polymer conjugate had been formed. The conjugation was then attempted in the presence of TCEP (Table 3.4). However, once again no product was observed by native PAGE analysis.

Table 3.4 Reaction conditions tested for the conjugation of thiol-terminated poly(NIPAM) to s0–MAAm in the presence of TCEP (100 μM). The concentrations of DNA and polymer were kept constant at 10 μM and 1 mM respectively. The reactions were run at 40°C for twenty-four hours. MOPS = 3-(*N*-Morpholino)propanesulfonic acid buffer.

Reaction #	Solvent	Polymer
3a		**P7**
3b	MOPS pH 8.0	**P8**
3c		**P9**
3d		**P7**
3e	DMF	**P8**
3f		**P9**

It was thought that formation of the thiol group should be attempted *in situ*, so poly(NIPAM) containing a terminal dithioester group (synthesised using the alkyne-containing CTA described in Chapter 5) was mixed with s0–MAAm in the presence of hexylamine and TEA (which should have cleaved the dithioester to release a thiol as illustrated in Scheme 3.6 – these reagents also served to catalyse the thiol Michael addition reaction itself).

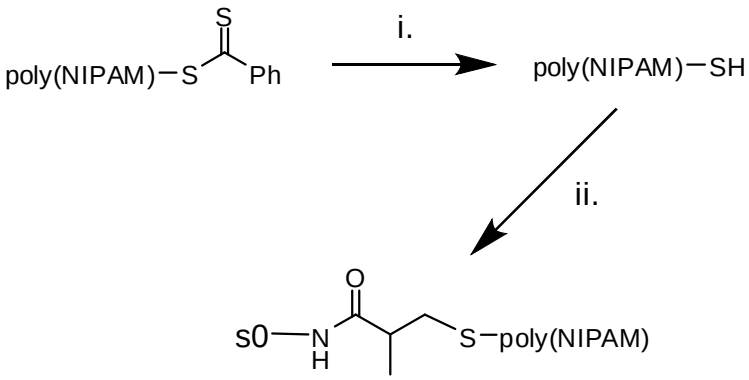

Scheme 3.6 Conjugation of poly(NIPAM) to s0–MAAm DNA by *in situ* reduction of the dithioester end group to a thiol: i) hexylamine/TEA (100 mM); ii) s0–MAAm (10 μM). The concentration of polymer was kept constant at 1 mM and the reactions were run for twenty-four hours at room temperature under a blanket of nitrogen.

It was important to use a dithioester-terminated polymer rather than one of the

trithiocarbonate-terminated polymers synthesised above, because upon aminolysis it produces only one thiol, which is situated at the polymer chain terminus. Aminolysis of a trithiocarbonate leads to the generation of two thiols, one of which is a small molecule and therefore capable of interfering with the coupling to DNA. Again, several solvents were tested as outlined in Table 3.5. However, no product was observed.

Table 3.5 Reaction conditions trialled for the *in situ* reduction of dithioester-terminated poly(NIPAM) in the presence of s0–MAAm as outlined in Scheme 3.6.

Reaction #	Solvent
4a	MOPS pH 8.0
4b	DMF
4c	DMSO

A thorough investigation of the reaction conditions was then carried out (Table 3.6), exploring the effects of varying the amount of polymer used, the temperature of the conjugation reaction and the use of mixed solvent systems. Once again, no product was observed under any of the conditions tested (Figure 3.4).

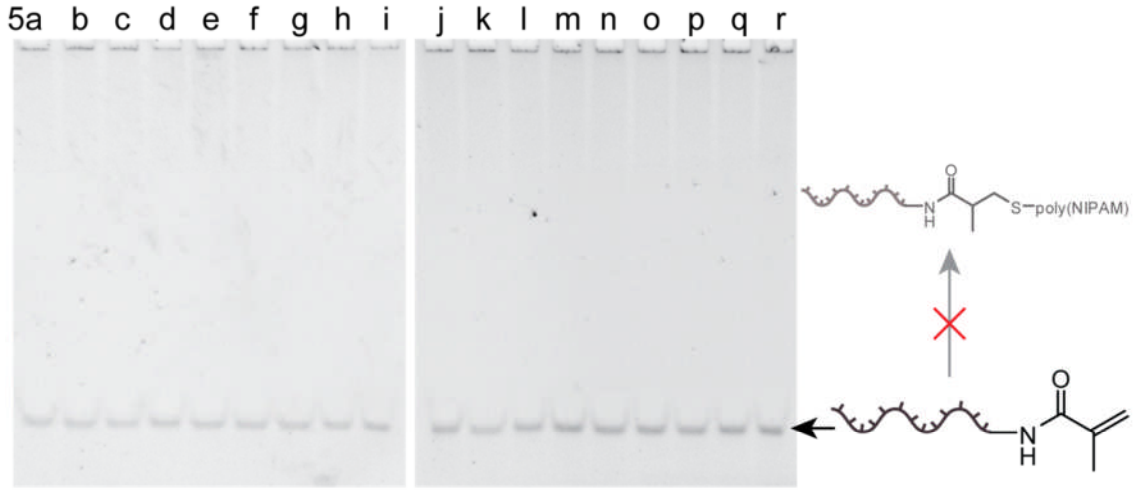

Figure 3.4 15 % native PAGE analysis of the reaction mixtures detailed in Table 3.6. The product was expected to appear as a broad, low-mobility band but under no conditions was it observed.

Table 3.6 Further reaction conditions trialled for the conjugation of thiol-terminated poly(NIPAM) (**P7**) to s0–MAAm. The DNA concentration was kept constant at 10 μM. Polymer equivalents were measured relative to the methacrylamide group.

Reaction #	Temperature	Solvent	Eq. polymer
5a			1
5b		H_2O/DMF	10
5c			100
5d			1
5e	RT	DMF	10
5f			100
5g			1
5h		NMP	10
5i			100
5j			1
5k		H_2O/DMF	10
5l			100
5m			1
5n	40°C	DMF	10
5o			100
5p			1
5q		NMP	10
5r			100

Finally, the use of a different catalyst – dimethylphenylphosphine (DMPP) – was explored (Table 3.7). This has been shown to be a potent catalyst for the thiol Michael addition reaction in organic solvents.[8] Due the air-sensitive nature of the catalyst, all reactions were conducted in degassed solvents under nitrogen.

Table 3.7 Reaction conditions trialled for the conjugation of thiol-terminated poly(NIPAM) (**P7**) to s0–MAAm using DMPP as catalyst. The DNA concentration was kept constant at 10 μM and all reactions were conducted at room temperature under an atmosphere of nitrogen for twenty-four hours.

Reaction #	Solvent	Eq. DMPP	Eq. polymer
6a	DMF	1	10
6b			100
6c		20	10
6d			100
6e	NMP	1	10
6f			100
6g		20	10
6h			100
6i	DMSO	1	10
6j			100
6k		20	10
6l			100

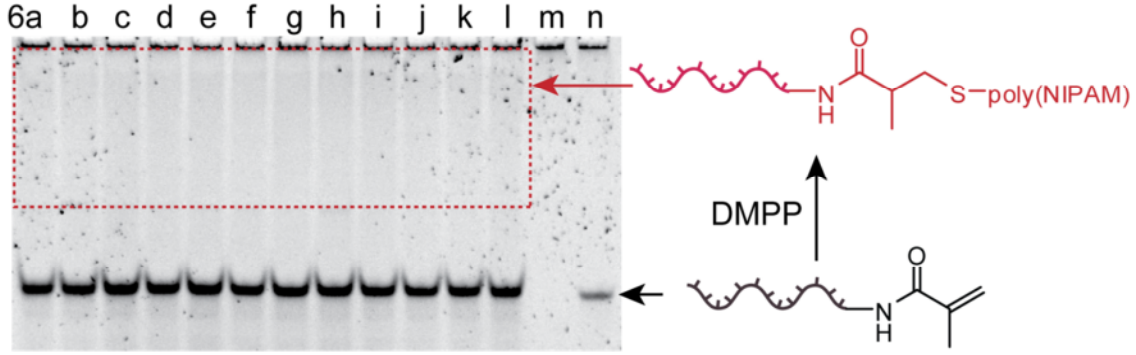

Figure 3.5 15 % native PAGE analysis of the reaction mixtures detailed in Table 3.7. A broad, low-mobility band is just visible, possibly indicating the formation of the desired product.

15 % native PAGE analysis of the reaction mixtures suggested that a very small amount of the conjugate may have been formed (see Figure 3.5), but yields were below 5 % in all cases (as assessed by densitometry, an example of which is shown in Figure 3.6).

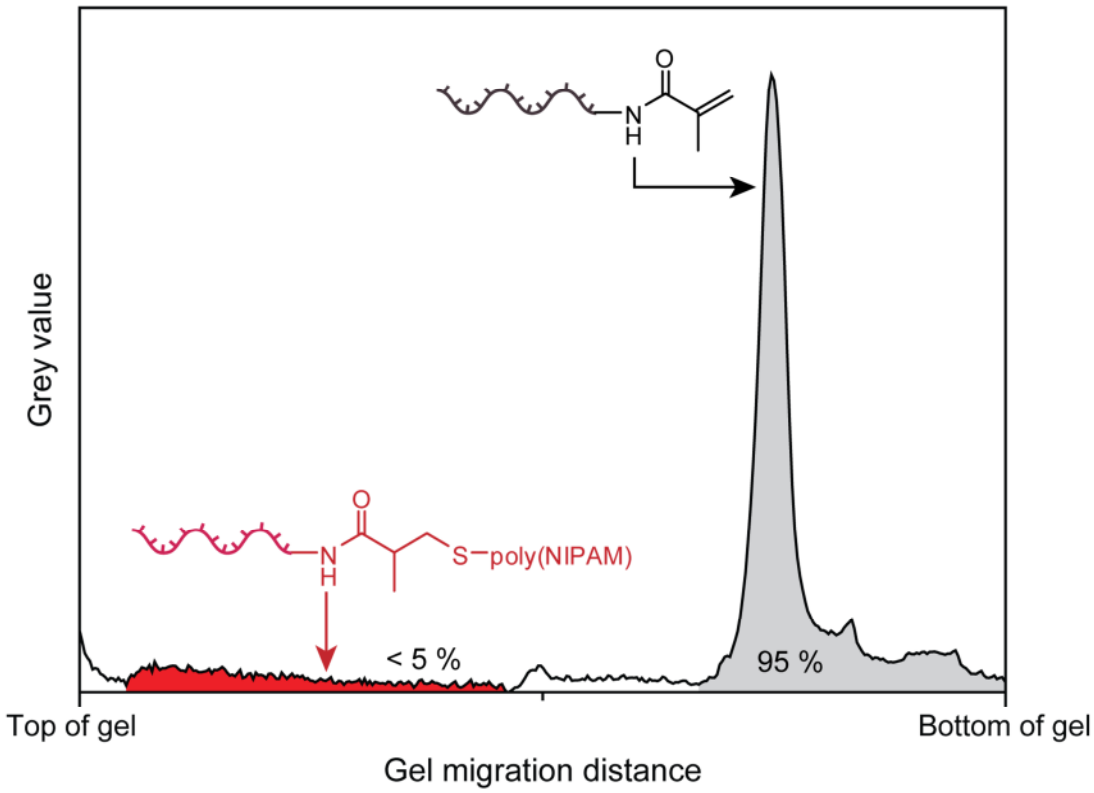

Figure 3.6 Densitometric analysis of Figure 3.5, lane 6e. A small hump is visible at low migration distance, which was attributed to a very low yield of the DNA–polymer conjugate. Yields (given as percentage values) were estimated by comparing the areas under each peak.

3.3.ii Synthesis and purification of s0–acrylamide

Having achieved only very low yields using the methacrylamide-functionalised DNA, the use of the more reactive acrylamide group was explored. Acrylamide-functionalised DNA is not currently commercially available, so it was synthesised from s0–NH_2 DNA and acrylic acid using EDCI and HOBt as coupling agents (see Scheme 3.7).

Purification of the very messy reaction mixture by HPLC (Figure 3.7) afforded the product, which was analysed by LC-MS and had the expected mass of 6 930 Da. It is thought that the many side products observed in the synthesis of s0–AAm were a result of unwanted reactions with the acrylamide.

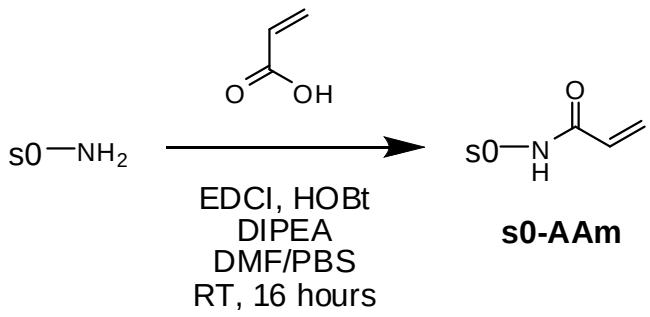

Scheme 3.7 Synthesis of an acrylamide-functionalised DNA strand (s0–AAm) from s0–NH_2 DNA and acrylic acid using EDCI and HOBt as coupling agents. Yield: 20 % after HPLC purification.

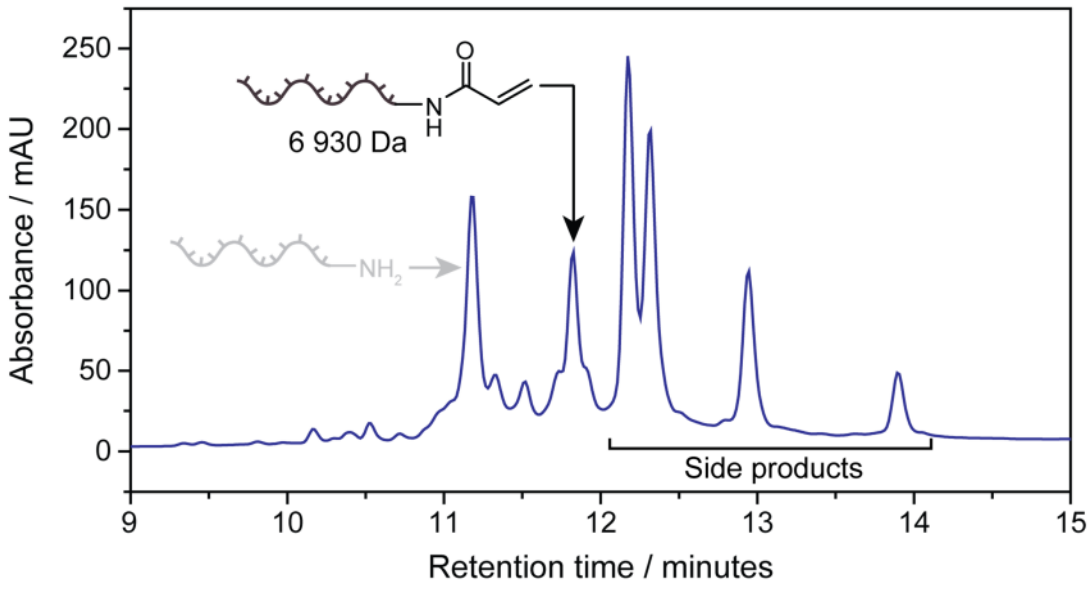

Figure 3.7 HPLC chromatogram of the reaction mixture during the synthesis of s0–AAm (black) from s0–NH_2 (grey). A number of side products were also observed, but were successfully removed by HPLC purification. The product was identified by LC-MS.

As for the methacrylamide version, s0–AAm was coupled to cysteine. A similar peak shift was observed, and the yield remained low despite increasing the amount of TCEP catalyst. Identical polymer couplings were attempted, but no product was observed in any case, even when using the more active catalyst DMPP. It was decided that a different type of ene compound should be used, so maleimide was investigated as a potentially more active alternative to (meth)acrylamide.

3.4 Thiol–maleimide conjugation

3.4.i Synthesis of Maleimide-functionalised DNA

Maleimide-functionalised DNA (s0–Mal) is not commercially available, so the desired product was synthesised using a bifunctional adapter, **8**, as shown in Scheme 3.8.

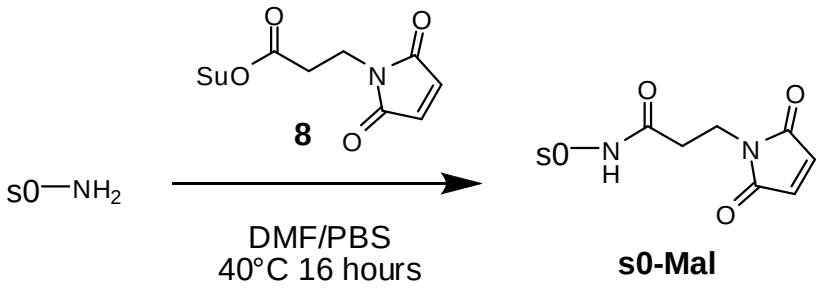

Scheme 3.8 Synthesis of maleimide-functionalised DNA (s0–Mal). Isolated yield: 63 %.

Formation of the product was followed by HPLC, which showed a clear shift in the retention time of the DNA peak from 10.0 to 11.5 minutes, with almost quantitative yield of the product, s0–Mal (Figure 3.8).

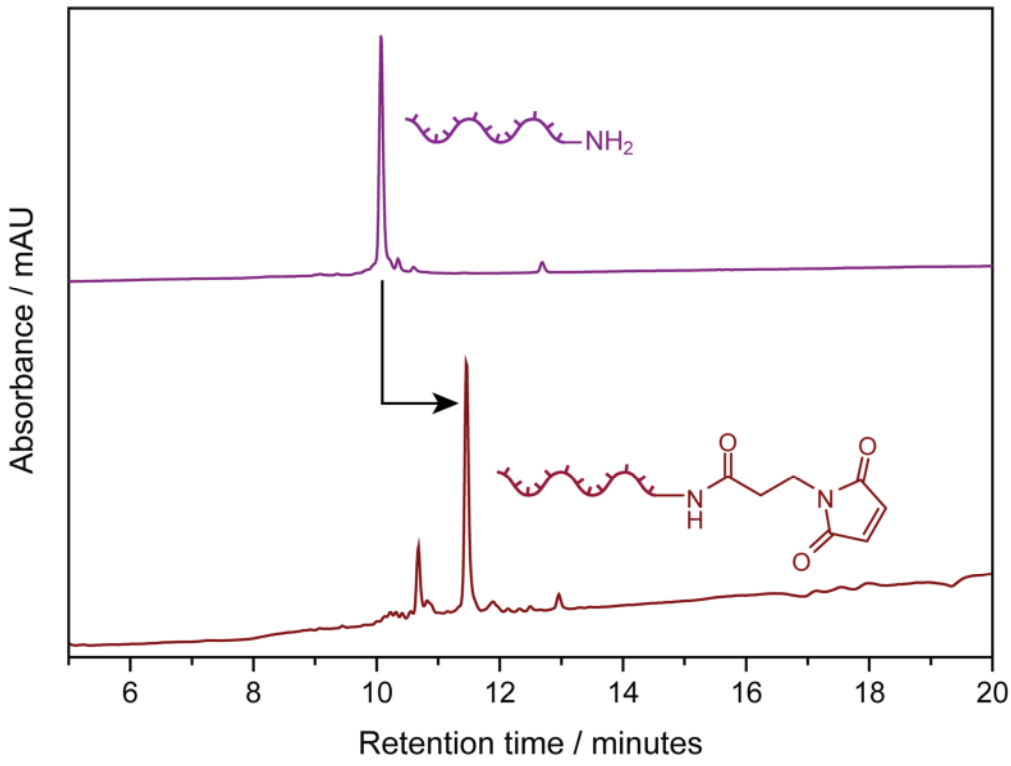

Figure 3.8 HPLC chromatogram showing the shift in retention time of the DNA peak during the synthesis of s0–Mal.

The product peak was collected and analysed by ESI-MS. However, the observed mass did not correspond exactly with that expected, despite several attempts to purify and de-salt the sample further (Figure 3.9).

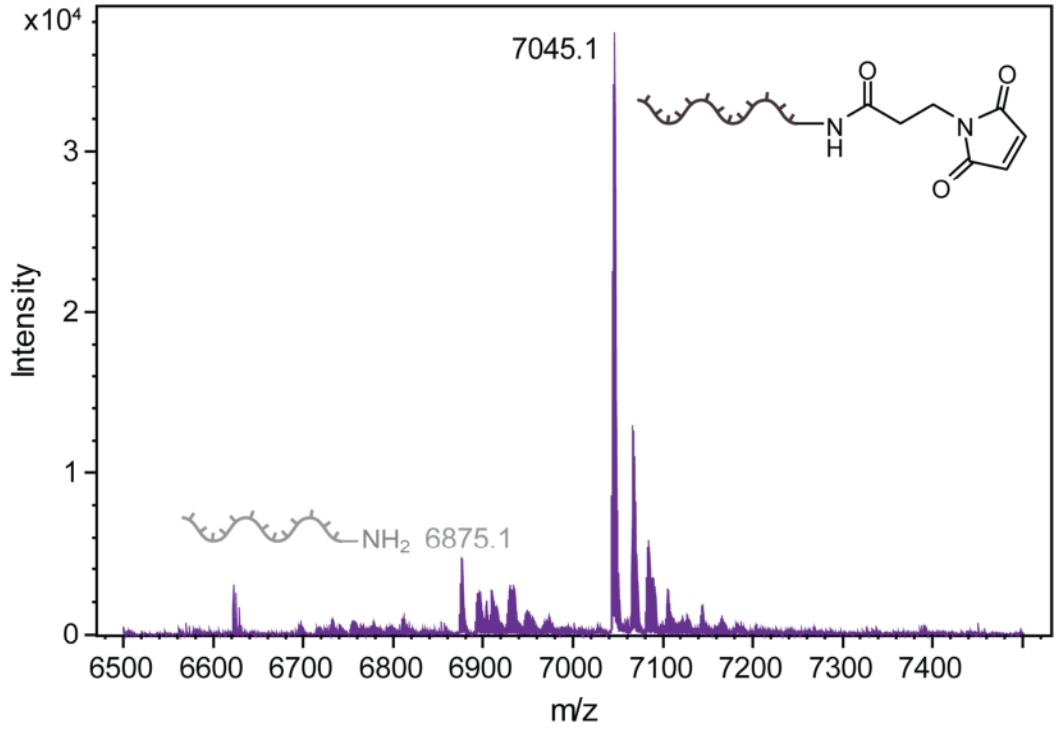

Figure 3.9 ESI MS spectrum of s0–Mal. Some starting material was still visible, as were several multiply-sodiated species. The expected mass of the product was 7 027.7 Da.

It was thought that the amine may have been reacting with the maleimide rather than the activated ester, so control experiments were carried out to rule out this possibility. First, the unactivated maleimide, **9**, was synthesised according to a modified literature procedure (Scheme 3.9).[38] This was then mixed with s0–NH_2 and any changes monitored by HPLC.

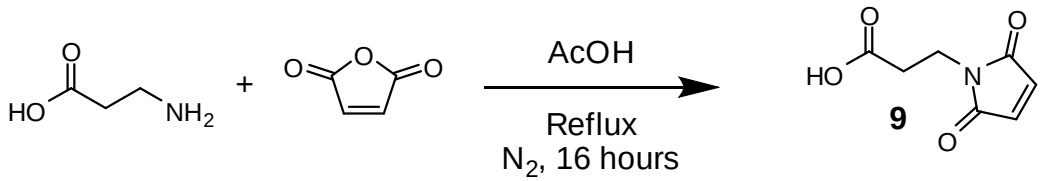

Scheme 3.9 Synthesis of the maleimide acid, **9**.

No change in retention time was observed after 16 hours (see Figure 3.10), so it was concluded that the amine will not react with the maleimide in the absence of coupling

agents.

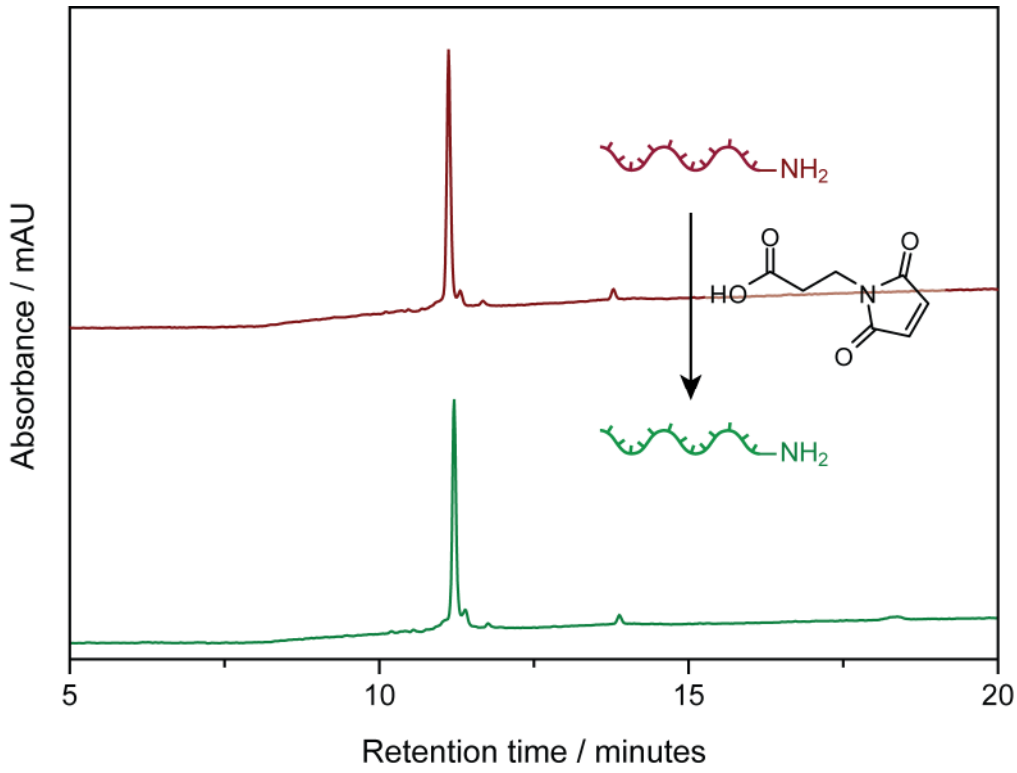

Figure 3.10 HPLC chromatogram showing that no reaction occurs between s0–NH_2 and the maleimide, **9**, in the absence of coupling agents.

Next, coupling of **9** to s0–NH_2 was attempted using standard EDCI/HOBt coupling conditions in PBS/DMF solution. After one hour, HPLC showed a clear peak shift. The product peak was collected and analysed by MALDI-ToF MS. The mass of the product was found to be 7 046 Da, which corresponded to that found for the product produced using the bifunctional adapter, **8**.

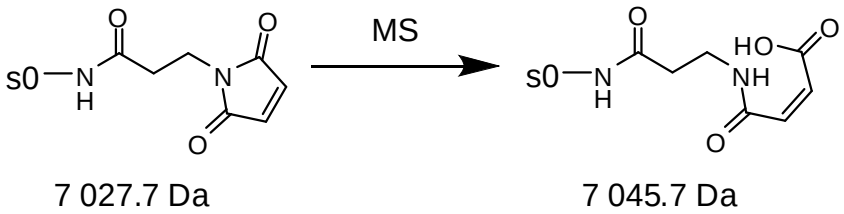

Scheme 3.10 Proposed structural change of s0–Mal under mass spectrometry conditions.

Having discounted the possibility of the amine reacting with the maleimide group, the most likely explanation for the disparity in the molecular weights was that hydrolysis of the

maleimide group was taking place within the MS machine to give a product with the observed mass (see Scheme 3.10).

3.4.ii Coupling of thiol-terminated polymers to maleimide-functionalised DNA

Having confirmed the successful formation of both of the conjugate precursors, conjugation reactions were first attempted under aqueous conditions. An elevated pH was employed to enhance the nucleophilicity of the thiol, as well as a slightly raised temperature. The number of equivalents of polymer was varied as described in Table 3.8.

Table 3.8 Reaction conditions trialled for the conjugation of thiol-terminated poly(NIPAM) (**P7-9**) to s0–Mal. All reactions were conducted at 40°C in MOPS buffer, pH 8. The DNA concentration remained constant at 10 μM.

Reaction #	Polymer (DP)	Polymer eq.
7a		2
7b		5
7c	**P7** (50)	25
7d		100
7e		500
7f		2
7g		5
7h	**P8** (97)	25
7i		100
7j		500
7k		2
7l		5
7m	**P9** (196)	25
7n		100
7o		500

After sixteen hours, the reaction mixtures were diluted with glycerol loading buffer and analysed by 15 % native PAGE (Figure 3.11). Slower-migrating, broader bands were visible in all lanes, implying that the conjugate had formed in all cases. Higher molecular weight polymers led to slower-migrating bands in the gel – this was as expected since gel electrophoresis separates species with the same charge based on molecular weight. The increase in breadth of the bands was attributed to the introduction of size dispersity by the polymer segment (the starting material DNA is a single molecule and therefore has no size dispersity).

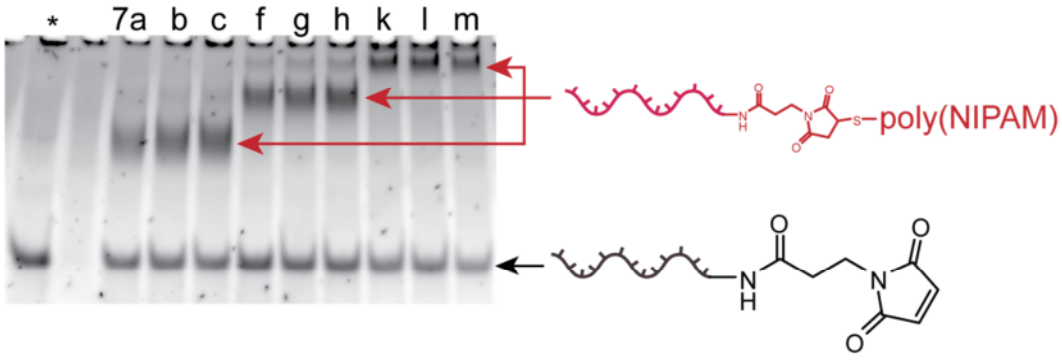

Figure 3.11 15 % PAGE analysis of the corresponding crude reaction mixtures detailed in Table 3.8 (for example, lane g corresponds to reaction 7g). Three distinct sets of new bands were observed, corresponding to conjugates containing different molecular weights of poly(NIPAM) (increasing from left to right). Lane * contained the s0–Mal species for comparison.

To prove that the conjugates had formed by reaction of the thiol group with the maleimide, and not with the activated ester (as was suggested above), they were mixed with a high concentration of a primary amine (2-amino-2-(hydroxymethyl)-1,3-propanediol – Tris base). It was reasoned that this would break any unstable thioester bonds whilst leaving the stronger thioether bonds intact, as illustrated in Scheme 3.11.

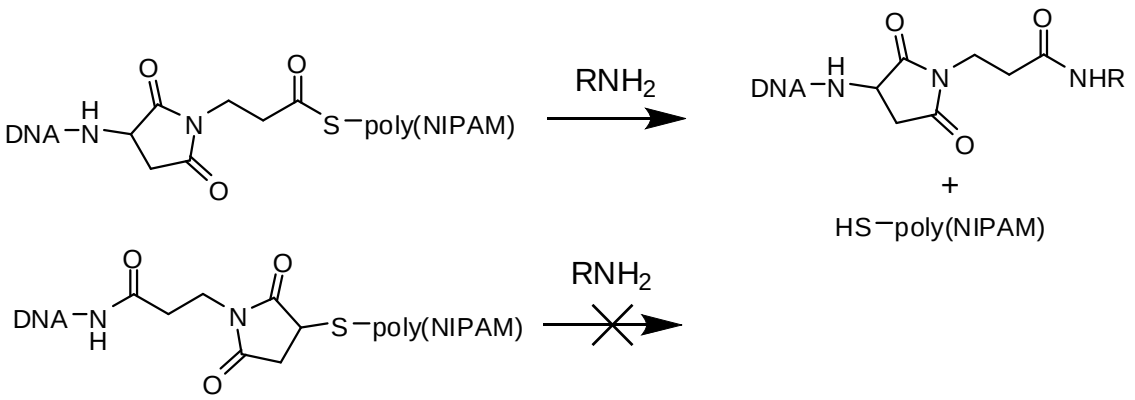

Scheme 3.11 Expected reactions of the thioester linkage (top) and the thioether linkage (bottom) with a primary amine (RNH_2).

As Figure 3.12 shows, no change in the PAGE results was observed upon incubation of the conjugates with the primary amine – it was therefore concluded that the desired conjugation product had been obtained. Had the incorrect linkage been formed, the PAGE results should have indicated the loss of the slower-migrating band due to the DNA–polymer conjugate.

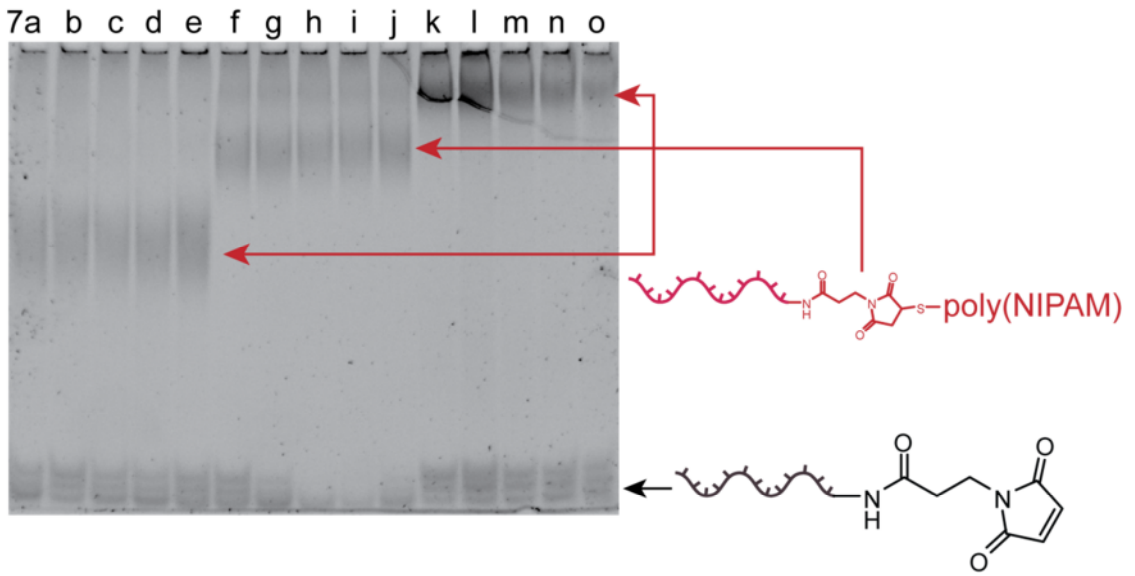

Figure 3.12 15 % PAGE analysis of the reactions detailed in Table 3.8 after exposure to 100 mM Tris base for sixteen hours. Comparison to Figure 3.11 revealed that little to no degradation of the DNA–polymer conjugate was occurring.

Densitometry was used to calculate approximate yields of the conjugation reactions performed in MOPS buffer (see Table 3.8 for conditions and Table 3.9 for yields). These

data suggested that once the number of equivalents of polymer used was greater than five there was no further increase in the yield of the reaction, with the maximum efficiency being around 50 %. This limit was attributed to degradation of the maleimide group under the slightly basic reaction conditions, and may also be due to unwanted side reactions of the thiol, which are likely to increase in proportion to the concentration of polymer – that is, even if the concentration was raised significantly, the benefit due to the increased rate of reaction with the maleimide group was offset by the increased rate of formation of thiol by-products.

Table 3.9 Yields for the DNA–poly(NIPAM) coupling reactions conducted in MOPS buffer at 40°C. Yields were calculated by densitometry (see experimental section for details).

Reaction #	Conjugate yield
7a	48 %
7b	53 %
7c	52 %
7d	57 %
7e	56 %
7f	38 %
7g	46 %
7h	56 %
7i	58 %
7j	50 %
7k	25 %
7l	31 %
7m	42 %
7n	51 %
7o	53 %

Table 3.10 Reaction conditions trialled for the conjugation of thiol-terminated poly(NIPAM) with s0–Mal. The DNA concentration was 10 μM for all reactions, with a 100-fold excess of polymer and DIPEA (where appropriate). Reactions were performed at 40°C for sixteen hours.

Reaction #	Solvent	DIPEA?
8a	DMF	
8b	THF	
8c	NMP	No
8d	DMSO	
8e	MeCN	
8f	DMF	
8g	THF	
8h	NMP	Yes
8i	DMSO	
8j	MeCN	

Having successfully formed the DNA–polymer conjugate in an aqueous milieu, the use of organic solvent systems was explored. Five different organic solvents were tested, both with and without an auxiliary base (in this case DIPEA), as summarised in Table 3.10. As Figure 3.13 shows, no product was observed for any of the solvents trialled.

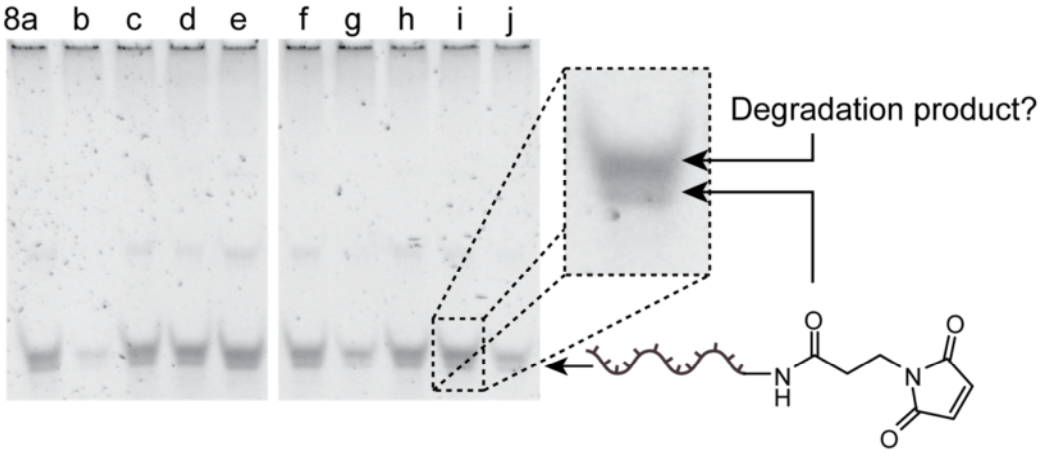

Figure 3.13 15 % native PAGE analysis of the crude reaction mixtures detailed in Table 3.10 showing that the conjugation of thiol-terminated poly(NIPAM) to s0–Mal DNA did not work in various organic solvents. Splitting of the band due to the starting material implied degradation of the maleimide group was occurring. Under identical conditions in MOPS buffer the conjugate was produced in around 50 % yield.

In all cases, the starting material band (bottom of gel) was observed to be split in two. This implied that the maleimide group was reacting with a small molecule or degrading under the reaction conditions before being able to react with the thiol on the polymer chain. Examination of the reaction mixture containing DMF by HPLC revealed the appearance of a number of new peaks (Figure 3.14), confirming that the maleimide group was indeed degrading under the reaction conditions.

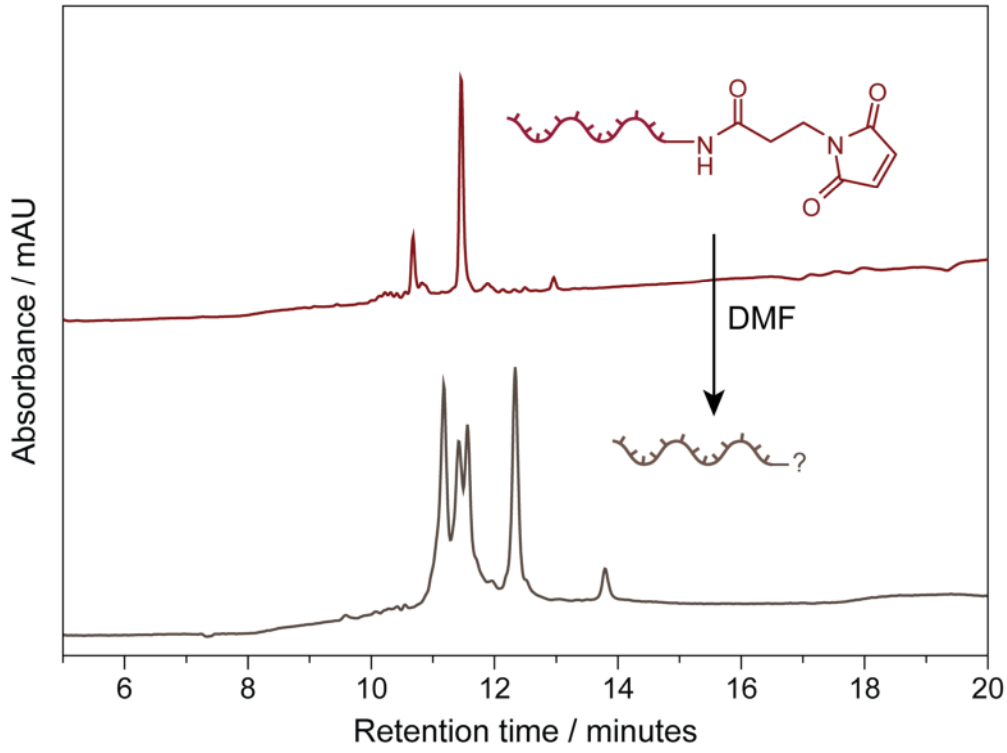

Figure 3.14 HPLC chromatograms of s0–Mal DNA before (top, red) and after (bottom, brown) incubation in DMF for 24 hours.

Having attempted DNA–polymer conjugation using methacrylamide-, acrylamide- and maleimide-functionalised DNA in a number of organic solvents and observed only very slight evidence of the formation of a product, it was concluded that the thiol Michael addition reaction was not going to provide a successful route to the desired conjugates.

3.5 Conclusions

Commercially-available methacrylamide-functionalised DNA was shown to react with the amino acid cysteine under basic aqueous conditions in the presence of a low concentration of the phosphine catalyst TCEP. However, use of thiol-capped poly(NIPAM) (synthesised by treatment of the trithiocarbonate-terminated polymer with sodium borohydride) in place of cysteine resulted in a very low yield of the DNA–polymer conjugate. Acrylamide-functionalised DNA was then synthesised from amine-functionalised DNA and acrylic acid; it also reacted with cysteine in the presence of TCEP, but no product was observed when the thiol-terminated poly(NIPAM) was used. Finally, maleimide-functionalised DNA was synthesised. It reacted with thiol-containing poly(NIPAM) to give the DNA–polymer conjugate in up to 50 % yield in buffer solution. However, use of organic solvents resulted in degradation of the maleimide group and no DNA–polymer conjugation was observed.

3.6 Experimental

3.6.i Materials & Methods

For general materials and methods details, see the Appendix. The DNA strand s0-MAAm was purchased from Integrated DNA Technologies, Ltd. and resuspended in 18 MΩ water to a final concentration of 200 μM before use (the purity was first confirmed by HPLC). 3-Maleimidopropionic acid *N*-hydroxysuccinimide ester (**8**) was purchased from Alfa Aesar and used as received. NAP-5 and -10 sephadex columns were purchased from GE Healthcare. All other chemicals were purchased from Sigma Aldrich, Ltd. and used as received.

3.6.ii Polymer end group removal using $NaBH_4$

The trithiocarbonate group present in poly(NIPAM) synthesised with DDMAT was reduced using a previously reported procedure.[39] An example procedure follows. Trithiocarbonate-terminated poly(NIPAM) (0.200 g, 0.03 mmol) was dissolved in water (20 mL) and sodium borohydride (0.378 g, 10.00 mmol) was added. The mixture was stirred at room temperature for 2.5 hours with vigorous stirring, then dialysed against 18 MΩ water for 4 days incorporating 5 water changes. The solution was then freeze-dried to obtain the thiol-terminated product (**P7**) as a white solid (0.131 g, 66 %) and analysed by DMF SEC using PMMA calibration standards (M_n 5 740 Da, PDI 1.17). ^{1}H NMR (400 MHz, $CDCl_3$) δ 7.20-5.50 (br s, PNIPAM N*H*), 3.99 ppm (br s, PNIPAM NC*H*$(CH_3)_2$), 3.20-0.50 (br m, polymer backbone *H*) ppm. **P8** and **P9** were synthesised using an identical procedure.

3.6.iii Ellman's assay

Ellman's assay was carried out as follows. Ellman's reagent (0.4 mg mL^{-1}) was dissolved in potassium phosphate buffer solution (100 mM, pH 8.0) to give Ellman's solution. The polymer under investigation (1 mg) was dissolved in water (600 μL) which had been purged with nitrogen for 30 minutes. This solution was then diluted with 1.2 mL of potassium

phosphate buffer solution (100 mM, pH 8.0). Finally, 200 μL of Ellman's solution was added and the solution mixed. The absorbance at 412 nm was recorded and the concentration of thiol determined by using the extinction coefficient of Ellman's solution (ε_{412} = 14 150 M^{-1} cm^{-1}). Finally, the percentage incorporation of thiol was calculated by comparing the calculated concentration to the theoretical concentration (which assumes one thiol group per polymer chain).

3.6.iv Reaction of s0–MAAm with cysteine

The methacrylamide-functionalised DNA strand s0–MAAm was reacted with cysteine under the following conditions. s0–MAAm (2.5 μL, 200 μM in water, 0.5 nmol) was mixed with TCEP (0.5 μL, various concentrations in water) and cysteine (7 μL, 10 mM in phosphate buffer pH 8.0) and left for 48 hours at room temperature. The reaction solution (1 μL) was then mixed with 18 MΩ water (49 μL) and analysed by HPLC, which showed a new peak with a retention time of 11.8 minutes attributed to the cysteine-functionalised DNA product.

3.6.v Conjugation of poly(NIPAM)–SH to s0–MAAm without catalyst

s0–MAAm (0.5 μL, 200 μM in water, 0.1 nmol) was added to thiol-terminated poly(NIPAM) (**P7**, **P8** or **P9**) (10 μL, 1 mM in the reaction solvent) and the mixture shaken for 24 hours at 40°C. The reaction mixture was then analysed by 15 % native PAGE. The reaction was also attempted with fewer equivalents of polymer and at room temperature.

3.6.vi Conjugation of poly(NIPAM)–SH to s0–MAAm with TCEP catalyst

s0–MAAm (0.5 μL, 200 μM in water, 0.1 nmol) was added to a 10 μL solution of TCEP (10 mM) and thiol-terminated poly(NIPAM) (**P7**, **P8** or **P9**) (1 mM) and the solution shaken at 40°C for 24 hours. The reaction mixture was then analysed by 15 % native PAGE.

3.6.vii *In situ* aminolysis of poly(NIPAM) in the presence of s0–MAAm

s0–MAAm (0.57 μL, 173 μM in water, 0.1 nmol) was mixed with hexylamine (4 μL,

100 mM in the reaction solvent), TEA (4 μL, 100 mM in the reaction solvent), dithioester-terminated poly(NIPAM) (**P13** – see Chapter 5) (1 μL, 10 mM in the reaction solvent, 10 nmol) and the reaction solvent (0.43 μL, MOPS pH 8.0, DMF or DMSO). After being left at room temperature overnight under an atmosphere of nitrogen, the reaction mixture was analysed by 15 % native PAGE.

3.6.viii Conjugation of poly(NIPAM)–SH to s0–MAAm with DMPP catalyst

s0–MAAm (0.58 μL, 173 μM in water, 0.1 nmol) was mixed with DMPP (5 μL, various concentrations in the reaction solvent) and thiol-terminated poly(NIPAM) (**P7**) (5 μL, various concentrations in the reaction solvent). The solution was left for 24 hours at room temperature under an atmosphere of nitrogen and then analysed by 15 % native PAGE, which revealed the formation of the DNA–polymer conjugate in approximately 5 % yield (as assessed by densitometry).

3.6.ix Synthesis of s0–AAm

Acrylamide-functionalised DNA (s0–AAm) was synthesised from amine-functionalised DNA (s0–NH_2) as follows. Acrylic acid (16.7 μL, 600 mM in DMF, 10 μmol), EDCI (16.7 μL, 600 mM in DMF, 10 μmol), HOBt (16.7 μL, 600 mM in DMF, 10 μmol) and DIPEA (1.7 μL, 10 μmol) were mixed and incubated at room temperature for thirty minutes. Phosphate buffer pH 8.0 (47.0 μL) and s0–NH_2 (3.2 μL, 3.17 mM in water, 10 nmol) were added and the mixture left at room temperature for 24 hours. The excess small molecules and DMF were removed by extraction with dichloromethane (3 × 200 μL). The aqueous layer was isolated and topped up to a final volume of 100 μL with water. The product was isolated by HPLC, with a yield of 20 % as quantified by UV-vis spectroscopy using the known extinction coefficient of the starting material DNA at 260 nm.

3.6.x Conjugation of poly(NIPAM)–SH to s0–AAm

Conjugation of thiol-terminated poly(NIPAM) (**P7**-**9**) to s0–AAm was attempted using identical conditions to those employed above for s0–MAAm. No product was observed

under any of the conditions used.

3.6.xi Synthesis of s0–Mal using the bifunctional adapter, 8

s0–NH_2 (1000 μL, 200 μM in water, 200 nmol), **8** (53.6 mg, 200 mmol) and DIPEA (35 μL, 200 mmol) were mixed in DMF (1000 μL) and the reaction shaken overnight at 40°C. The excess small molecules were then removed using a NAP-10 Sephadex column and the collected solution concentrated *in vacuo* and purified by HPLC. The product was isolated as a single fraction, with an isolated yield of 63 % as quantified by UV-vis spectroscopy using the known extinction coefficient of the starting material DNA at 260 nm.

3.6.xii 3-maleimidopropionic acid, 9

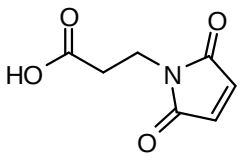

3-Maleimidopropionic acid, **9**, was synthesised as follows.[38] β-Alanine (1 g, 11.22 mmol) and maleic anhydride (1 g, 10.20 mmol) were refluxed in acetic acid (150 mL) for 16 hours. The solution was then allowed to cool to room temperature and the acetic acid removed by freeze-drying. The crude product was dissolved in acetone and the cloudy solution filtered through a 0.45 μm nylon syringe filter. The filtrate was purified by silica gel flash column chromatography, eluting with acetone to give a crude product (R_f 0.69). Excess acetic acid was removed by co-evaporation with toluene. The residue was then dissolved in a small amount of methanol and purified by silica gel column chromatography, eluting with a mixture of dichloromethane and ethyl acetate (9:1). The product (R_f 0.17) was isolated after removal of the solvent as a crystalline white powder (0.58 g, 34 %). ^{1}H NMR (400 MHz, d_6-DMSO) 12.39 (s, 1H, CO_2H), 7.07 (s, 2H, C=C-*H*), 3.67 (t, J = 7 Hz, 2H, NCH_2), 2.55 (t, J = 7 Hz, 2H, CH_2CO_2H) ppm. ^{13}C NMR (100 MHz, d_6-DMSO) 172.0 (CO_2H), 170.7 (N*C*=O), 134.6 (*C*=C), 33.3 (NCH_2), 32.4 (CH_2CO_2H) ppm.

3.6.xiii Reaction of s0–NH_2 with compound 9

s0–NH_2 DNA (2.5 μL, 200 μM in water, 0.5 nmol) and **9** (1.7 μL, 600 mM in DMF, 1 μmol) were mixed in pH 7.5 potassium phosphate buffer (2.5 μL) and DMF (3.3 μL) and shaken overnight at room temperature. HPLC analysis revealed that no reaction had taken place after 24 hours.

3.6.xiv Synthesis of s0–Mal using compound 9

Compound **9** (100 μL, 600 mM in DMF), EDCI (100 μL, 600 mM in DMF), and HOBt (100 μL, 600 mM in DMF) were mixed. To 50 μL of this solution were added pH 7.5 potassium phosphate buffer (25 μL) and s0–NH_2 DNA (25 μL, 200 μM in water, 5 nmol). DIPEA (1.7 μL, 10 μmol) was added and the mixture shaken at room temperature for one hour. Excess small molecules were removed using a NAP-5 sephadex column and the filtrate concentrated *in vacuo*, then purified by HPLC. The product was isolated as a single peak, dried down and resuspended in water to give a final isolated yield of 50 %. The yield was quantified by UV-vis spectroscopy using the known extinction coefficient of the starting material DNA at 260 nm.

3.6.xv Conjugation of poly(NIPAM)–SH to s0–Mal

s0–Mal (25 μL, 20 μM in MOPS buffer pH 8.0, 0.5 nmol) was mixed with thiol-terminated poly(NIPAM) (**P7**, **P8** or **P9**) (25 μL, various concentrations in MOPS buffer pH 8.0) and the solution incubated at 40°C for 24 hours. Analysis of the reaction mixtures by 15 % native PAGE revealed that the DNA–polymer conjugate (visible as a broad, low-mobility band) had been formed in up to 58 % yield.

3.6.xvi Degradation of s0–poly(NIPAM) conjugates by a primary amine

The DNA–polymer conjugates synthesised using s0–Mal (above) were tested for their resistance to degradation by a primary amine (Tris). A sample of each of the reaction mixtures from Section 3.6.xv (9 μL) was mixed with Tris (1 μL, 1 M in water) and incubated at room temperature for 24 hours. Analysis by 15 % native PAGE showed the

DNA–polymer conjugate resisted degradation by the amine.

3.6.xvii Conjugation of poly(NIPAM)–SH to s0–Mal in organic solvents

s0–Mal (2 μL, 50 μM in water, 0.1 nmol) was mixed with **P7** (1 μL, 10 mM in the reaction solvent) and DIPEA (0.5 μL, 20 mM in the reaction solvent) and the reaction solvent (DMF, THF, NMP, DMSO or MeCN – 6.5 μL). The solution was left for 24 hours at room temperature and then analysed by 15 % native PAGE. The reaction mixture was also analysed by HPLC to assess the degree of degradation of the maleimide group.

3.7 References

(1) Posner, T. *Ber. Dtsch. Chem. Ges.* **1905**, *38*, 646.

(2) Doncom, K. E. B.; Hansell, C. F.; Theato, P.; O'Reilly, R. K. *Polym. Chem.* **2012**, *3*, 3007.

(3) Willcock, H.; O'Reilly, R. K. *Polym. Chem.* **2010**, *1*, 149.

(4) Boyer, C.; Davis, T. P. *Chem. Commun.* **2009**, 6029.

(5) Sumerlin, B. S.; Vogt, A. P. *Macromolecules* **2010**, *43*, 1.

(6) Huang, X.; Boyer, C.; Davis, T. P.; Bulmus, V. *Polym. Chem.* **2011**, *2*, 1505.

(7) van Hensbergen, J. A.; Burford, R. P.; Lowe, A. B. *J. Polym. Sci., Part A: Polym. Chem.* **2013**, *51*, 487.

(8) Li, G.-Z.; Randev, R. K.; Soeriyadi, A. H.; Rees, G.; Boyer, C.; Tong, Z.; Davis, T. P.; Becer, C. R.; Haddleton, D. M. *Polym. Chem.* **2010**, *1*, 1196.

(9) Chan, J. W.; Hoyle, C. E.; Lowe, A. B.; Bowman, M. *Macromolecules* **2010**, *43*, 6381.

(10) Boyer, C.; Granville, A.; Davis, T. P.; Bulmus, V. *J. Polym. Sci., Part A: Polym. Chem.* **2009**, *47*, 3773.

(11) Boyer, C.; Bulmus, V.; Davis, T. P. *Macromol. Rapid Commun.* **2009**, *30*, 493.

(12) Kim, B. J.; Given-Beck, S.; Bang, J.; Hawker, C. J.; Kramer, E. J. *Macromolecules* **2007**, *40*, 1796.

(13) Spruell, J. M.; Levy, B. A.; Sutherland, A.; Dichtel, W. R.; Cheng, J. Y.; Stoddart, J. F.; Nelson, A. *J. Polym. Sci., Part A: Polym. Chem.* **2009**, *47*, 346.

(14) Ballari, R. V.; Martin, A. *Food Chem.* **2013**, *141*, 2130.

(15) Kade, M. J.; Burke, D. J.; Hawker, C. J. *J. Polym. Sci., Part A: Polym. Chem.* **2010**, *48*, 743.

(16) Espeel, P.; Goethals, F.; Driessen, F.; Nguyen, L.-T. T.; Du Prez, F. E. *Polym. Chem.* **2013**, *4*, 2449.

(17) Mantovani, G.; Lecolley, F.; Tao, L.; Haddleton, D. M.; Clerx, J.; Cornelissen, J. J. L. M.; Velonia, K. *J. Am. Chem. Soc.* **2005**, *127*, 2966.

(18) Pounder, R. J.; Stanford, M. J.; Brooks, P.; Richards, S. P.; Dove, A. P. *Chem. Commun.* **2008**, 5158.

(19) Li, M.; De, P.; Gondi, S. R.; Sumerlin, B. S. *J. Polym. Sci., Part A: Polym. Chem.* **2008**, *46*, 5093.

(20) Tao, L.; Kaddis, C. S.; Loo, R. R. O.; Grover, G. N.; Loo, J. A.; Maynard, H. D. *Macromolecules* **2009**, *42*, 8028.

(21) Galibert, M.; Renaudet, O.; Dumy, P.; Boturyn, D. *Angew. Chem., Int. Ed.* **2011**, *50*, 1901.

(22) Friscourt, F.; Ledin, P. A.; Mbua, N. E.; Flanagan-Steet, H. R.; Wolfert, M. A.; Steet, R.; Boons, G.-J. *J. Am. Chem. Soc.* **2012**, *134*, 5381.

(23) Zhou, F.; Ding, M.; Zhou, J. *Org. Biomol. Chem.* **2012**, *10*, 3178.

(24) Rim, C.; Son, D. Y. *Tetrahedron Lett.* **2009**, *50*, 4161.

(25) Wabnitz, T. C.; Yu, J.-Q.; Spencer, J. B. *Chem. A Eur. J.* **2004**, *10*, 484.

(26) Roy, R.; Baek, M.-G.; Rittenhouse-Olson, K. *J. Am. Chem. Soc.* **2001**, *123*, 1809.

(27) Thadke, S. A.; Kar, M.; Gupta, S. S.; Hotha, S. *Carbohydr. Res.* **2011**, *346*, 1511.

(28) Schoenmakers, R. G.; van de Wetering, P.; Elbert, D. L.; Hubbell, J. A. *J. Control. Release* **2004**, *95*, 291.

(29) Lin, C.-H.; Yang, K.-S.; Pan, J.-F.; Chen, K. *Tetrahedron Lett.* **2000**, *41*, 6815.

(30) Tseng, T.-C.; Wu, M.-J. *Tetrahedron: Asymmetry* **1995**, *6*, 1633.

(31) Rana, N. K.; Singh, V. K. *Org. Lett.* **2011**, *13*, 6520.

(32) Nishide, K.; Ohsugi, S.-i.; Shiraki, H.; Tamakita, H.; Node, M. *Org. Lett.* **2001**, *3*, 3121.

(33) Muro, E.; Pons, T.; Lequeux, N.; Fragola, A.; Sanson, N.; Lenkei, Z.; Dubertret, B. *J. Am. Chem. Soc.* **2010**, *132*, 4556.

(34) Oishi, M.; Nagatsugi, F.; Sasaki, S.; Nagasaki, Y.; Kataoka, K. *ChemBioChem* **2005**, *6*, 718.

(35) Oishi, M.; Nagasaki, Y.; Itaka, K.; Nishiyama, N.; Kataoka, K. *J. Am. Chem. Soc.* **2005**, *127*, 1624.

(36) Ellman, G. L. *Arch. Biochem. Biophys.* **1958**, *74*, 443.

(37) Segui, F.; Qiu, X.-P.; Winnik, F. M. *J. Polym. Sci., Part A: Polym. Chem.* **2008**, *46*, 314.

(38) Song, H. Y.; Ngai, M. H.; Song, Z. Y.; MacAry, P. A.; Hobley, J.; Lear, M. J. *Org. Biomol. Chem.* **2009**, *7*, 3400.

(39) Scales, C. W.; Convertine, A. J.; McCormick, C. L. *Biomacromolecules* **2006**, *7*, 1389.

Chapter 4

DNA–polymer conjugation using the tetrazine–norbornene inverse electron demand Diels–Alder reaction

---

4.1 Introduction

The Diels–Alder (DA) reaction is perhaps one of the best known in synthetic chemistry.[1] Normally, an electron-rich diene reacts with an electron-poor dienophile to yield the cyclic product (Scheme 4.1). The process typically requires heat or a catalyst, and a reverse DA reaction is possible (usually by increasing the temperature).

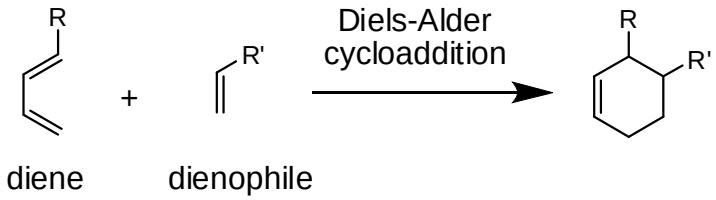

Scheme 4.1 A typical Diels–Alder cycloaddition reaction between an electron-rich diene and an electron-poor dienophile.

The reaction has been used for the highly efficient conjugation of polymers in solution.[2-4] However, there are no reports of it having been used for the purposes of DNA–polymer conjugation, probably because the extremes of temperature required are not desirable, and the synthesis of precursor compounds functionalised with the appropriate groups is not straightforward.

It is possible, however, to remove the need for elevated temperatures and the use of catalysts by using an electron-*poor* diene and an electron-*rich* dienophile, in what is termed an inverse electron demand Diels–Alder (DA_{inv}) reaction. A prime example of this is the reaction between tetrazine (Tz) and norbornene (Nb) to give a pyradizine (Scheme 4.2).[5]

The diene is contained within the Tz ring and is highly electron-poor due to the presence of the four nitrogen heteroatoms. The dienophile is the Nb group, which is both electron rich (in the sense that it has no electron-withdrawing substituents) and strained (providing an enthalpic driving force for the reaction).

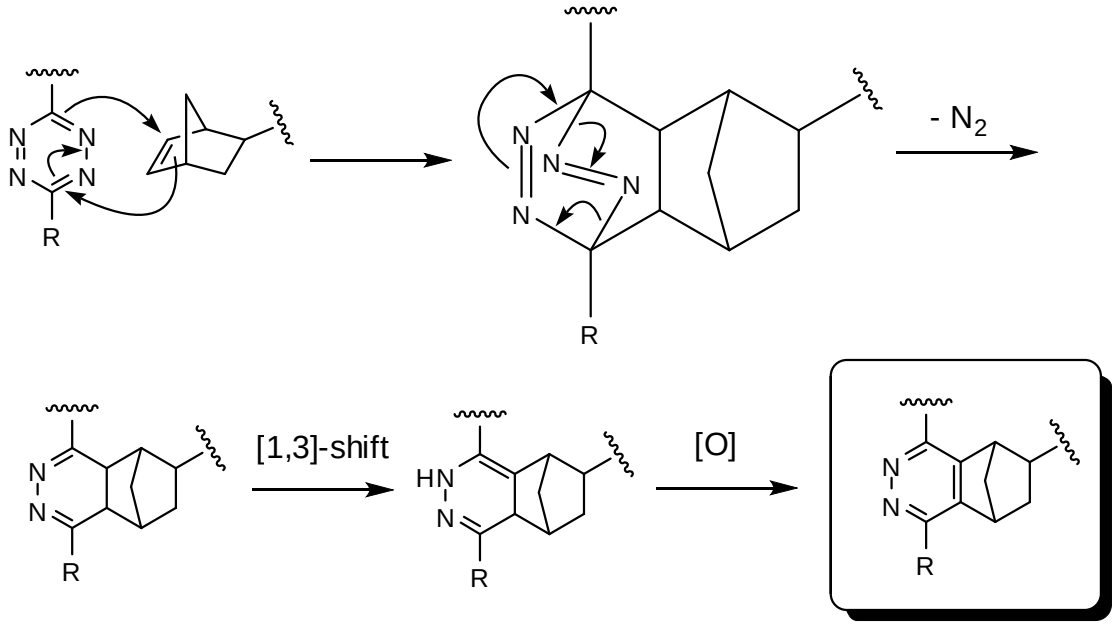

Scheme 4.2 The mechanism of the DA_{inv} reaction between tetrazine and norbornene.

The mechanism proceeds by an initial [4 + 2] cycloaddition (the DA_{inv} reaction) between the Tz and Nb groups. This is followed by a retro-DA reaction that expels a molecule of nitrogen (and provides a powerful entropic driving force for the reaction). Importantly, this step also means that the reaction is irreversible, unlike most DA processes. A [1,3]-hydride shift then occurs to afford the dihydropyradizine, which can be isolated. More commonly, though, oxidation occurs either by addition of an oxidant or simply by prolonged exposure to air to give the pyradizine product. The stability of the Tz (and therefore its reactivity) can be tuned by altering the R group attached directly to the ring.[6,7]

The Tz–Nb DA_{inv} reaction has been recently used for protein modification,[8] cell imaging (Figure 4.1),[9-11] post-assembly functionalisation of polymer micelles,[12] and labelling of quantum dots.[13] Importantly for this work, the modification of DNA with small molecules has also been demonstrated using this chemistry.[14] These studies have shown it to be highly

efficient in a range of solvents (both organic and aqueous) and orthogonal towards other reactive groups commonly found in biomolecules. Furthermore, recent work in the O'Reilly group has revealed that the DA_{inv} reaction between Tz and norbornene Nb (see Scheme 4.2) is efficient for the conjugation of macromolecules in solution.[15]

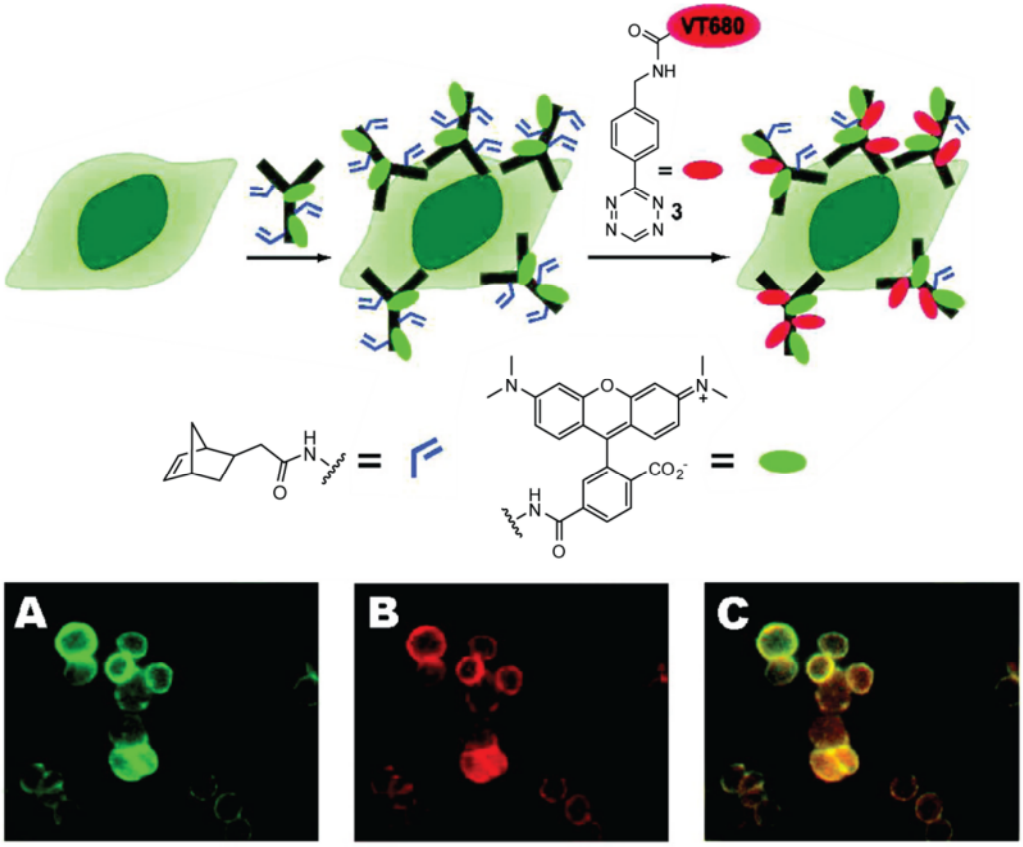

Figure 4.1 Labelling of live cells using the Tz–Nb DA_{inv} reaction. Cells were targeted with an antibody containing rhodamine (green) and norbornene. A Tz compound containing another dye molecule (red) was then introduced. Confocal microscopy (A, B and C) showed highly specific labelling of only the targeted cells.[9]

Given the obvious advantages of this chemistry, and the fact that it has not previously been reported, it was decided that DNA–polymer conjugation should be attempted. The only downside of this technique is that synthesis of the precursor molecules is far from trivial. It was decided, therefore, to attempt the coupling both ways round – that is, with the Tz group located on a DNA strand and the Nb group on a polymer and *vice versa*.

4.2 Results & Discussion

4.2.i Synthesis of s0–Tz

In order to obtain Tz-functionalised DNA, it was first necessary to synthesise an adapter containing the Tz group. This was obtained by activating the Tz–acid, **10**, with *N*-hydroxysuccinimide (NHS) to give Tz–NHS, **11**, as shown in Scheme 4.3. ^{1}H (Figure 4.2) and ^{13}C NMR spectroscopy both showed the expected peaks, including the four protons from the NHS group.

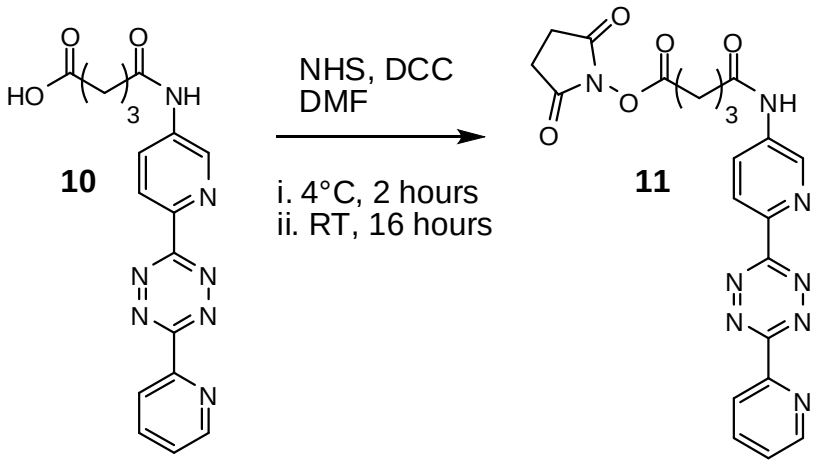

Scheme 4.3 Synthesis of Tz–NHS (**11**). Yield: 38 %.

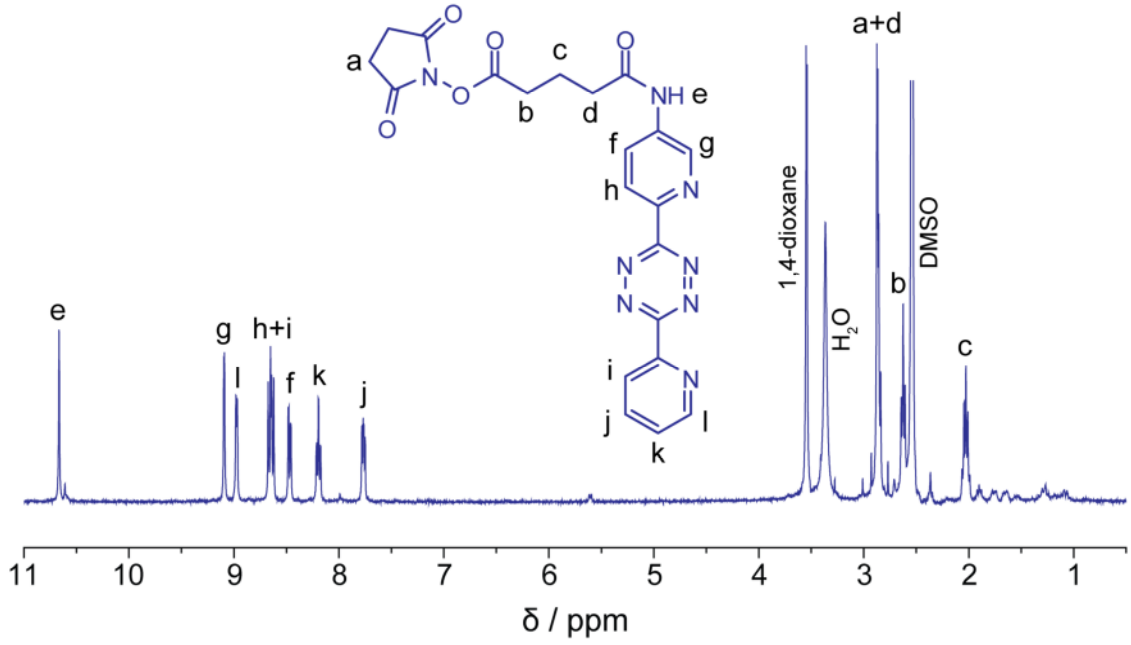

Figure 4.2 ^{1}H NMR spectrum of the Tz-containing activated ester, **11**. Solvent: d_6-DMSO.

Next, **11** was reacted with s0–NH_2 in DMF/PBS solution at 40°C, with a DNA concentration of 100 μM and a one thousand-fold excess of the small molecule. Analysis of the reaction mixture by HPLC showed that a number of products were formed (Figure 4.3). It was thought that many of these were likely to be formed as a result of the degradation of the Tz group. One peak was isolated, however, which exhibited the characteristic Tz UV-vis absorbance at around 330 nm (see inset to Figure 4.3). The mass of the isolated peak also corresponded with the expected mass of the product: 7 223.9 Da (Figure 4.4). These data confirmed the successful synthesis of the s0–Tz DNA species.

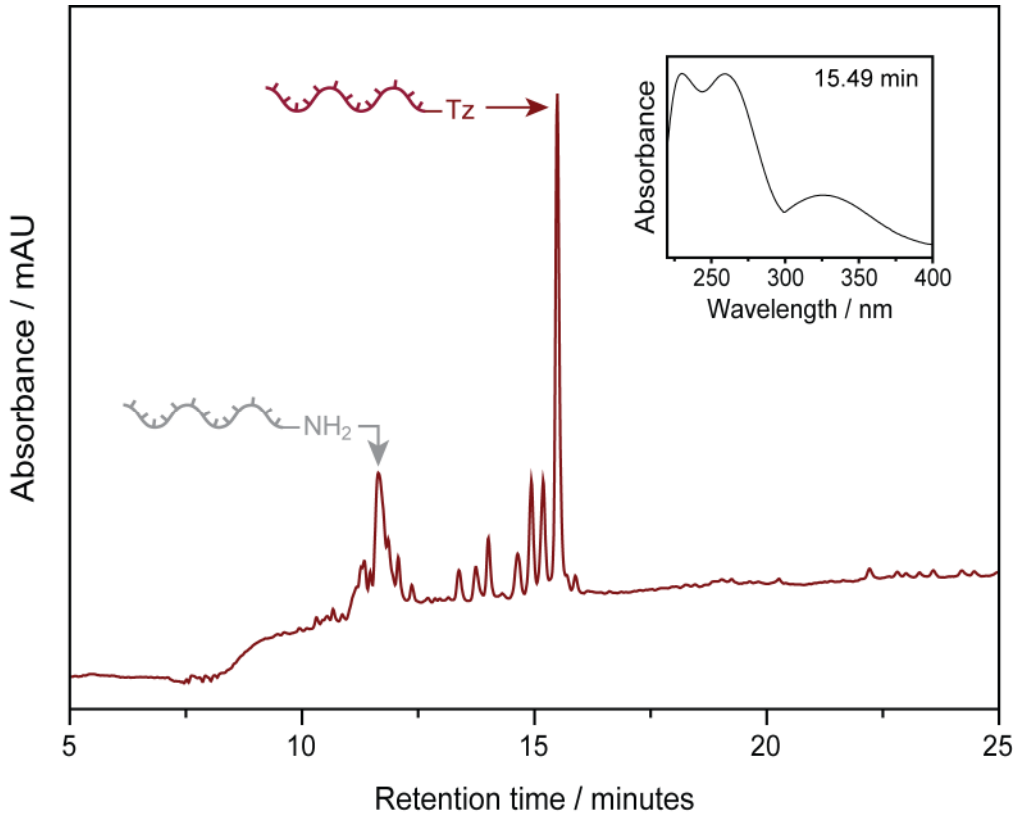

Figure 4.3 HPLC chromatogram showing the formation of s0–Tz. The UV-vis spectrum (inset) of the indicated peak exhibits a maximum at around 330 nm – this is characteristic of the Tz group.

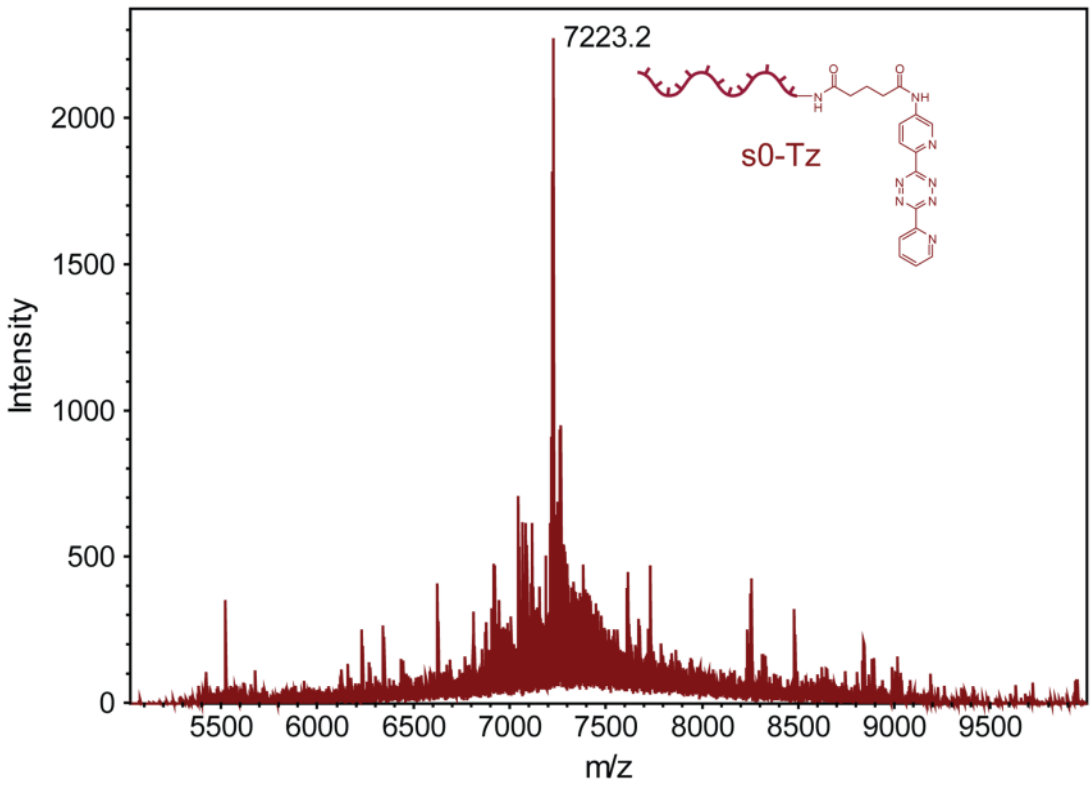

Figure 4.4 ESI MS spectrum of the s0–Tz molecule. The expected mass was 7 223.9 Da.

4.2.ii Control experiments with s0–Tz

To confirm the reactivity of s0–Tz, a small molecule test reaction was carried out in both water and DMF. Commercially available 5-norbornene-2-*exo*,3-*exo*-dimethanol was mixed with s0–Tz at a concentration of 50 μM and the reaction followed by HPLC. A clear peak shift was observed in both solvents (Figure 4.5), confirming that the tetrazine retained its reactivity once conjugated to the DNA strand. The yield of the reaction was estimated by comparison of the areas under the peaks due to the Tz–Nb coupling product and unreacted DNA and found to be approximately 70 % and 40 % in water and DMF respectively. The difference in yield can possibly be attributed to degradation of the Tz group by free amines present in the DMF used.††

†† Unpublished results from the O'Reilly research group.

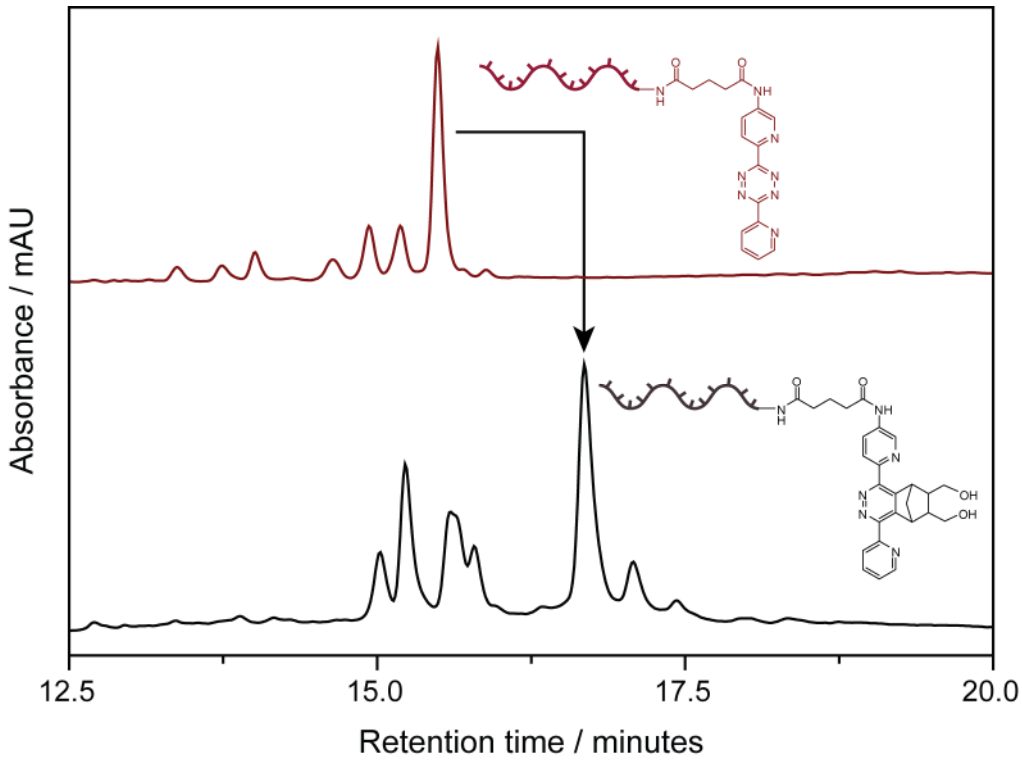

Figure 4.5 HPLC chromatograms showing the shift in retention time that occurred for the principal peak when a small molecule norbornene alcohol was added to s0–Tz.

4.2.iii Conjugation of polymers to s0–Tz

Next, DNA–polymer conjugation was attempted using poly(NIPAM) end-capped with a norbornene group (M_n 16.4 kDa, Đ 1.12), kindly provided by Prof. Filip du Prez.[16] After reacting with 10 μM s0–Tz DNA overnight at room temperature in DMF, DMAc or NMP, 15 % native PAGE analysis revealed that the conjugate had been formed in up to 50 % yield (by densitometry) – see Table 4.1 and Figure 4.6. Although the small molecule reaction had proceeded less efficiently in organic solvents (see above), they were used for the polymer conjugation reaction because one of the aims of this work was to find a robust, solution-phase method for DNA–polymer conjugation that could be used with organic solvents. The reaction was, however, also repeated in water and gave the conjugate in 30 % yield. Interestingly, increasing the equivalents of polymer used beyond 10 (relative to the DNA) had little effect on the yield; however, one equivalent alone was not sufficient to achieve good yields. The presence of other, unexplained bands in the PAGE analysis (see Figure 4.6) may point to degradation of the Tz group as the reason that these reactions

cannot go above approximately 50 % yield.

Table 4.1 Reaction conditions trialled for the synthesis of DNA–polymer conjugates from s0–Tz and poly(NIPAM)–Nb. * With respect to s0–Tz.

Reaction #	Equivalents of polymer*	Solvent	Coupling efficiency / %
5a	1		~0
5b	10	DMF	36
5c	100		50
5d	1		15
5e	10	DMAc	38
5f	100		35
5g	1		11
5h	10	NMP	38
5i	100		31

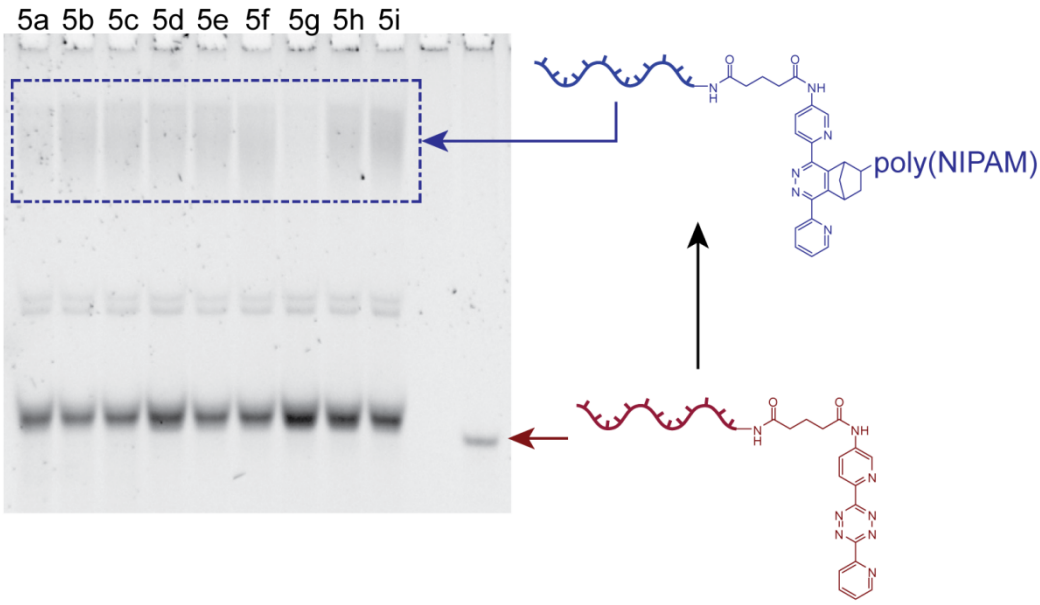

Figure 4.6 15 % native PAGE analysis showing the formation of a DNA–polymer conjugate using the Tz–Nb DA_{inv} reaction. Reaction conditions and coupling efficiencies (as estimated by densitometry) can be found in Table 4.1.

Although the conjugation reaction had proceeded in acceptable yield, it was decided to attempt to switch the positions of the Tz and Nb groups, in an effort to make the synthesis

of the DNA precursor more straightforward. The norbornene group is much less prone to degradation in water (if extremes of acidic and basic pH are avoided), so it was envisaged that this may prove easier to attach to a DNA strand.

4.2.iv Synthesis of s0–Nb

Norbornene-functionalised DNA (s0–Nb) was synthesised using an acid-containing norbornene and s0–NH_2 under standard EDCI/HOBt coupling conditions (Scheme 4.4). After one hour, HPLC analysis indicated the formation of two products (at 14.3 and 14.9 minutes retention time, see Figure 4.7). The yield was close to quantitative. After removal of the small molecules using a sephadex column, the two peaks were separated by HPLC, collected and analysed by MALDI-ToF MS (Figure 4.8).

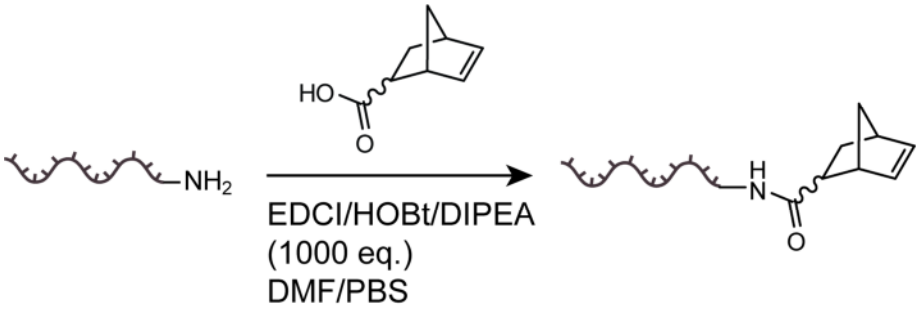

Scheme 4.4 Synthesis of s0–Nb from s0–NH_2 and a commercially available Nb acid using standard amide coupling conditions.

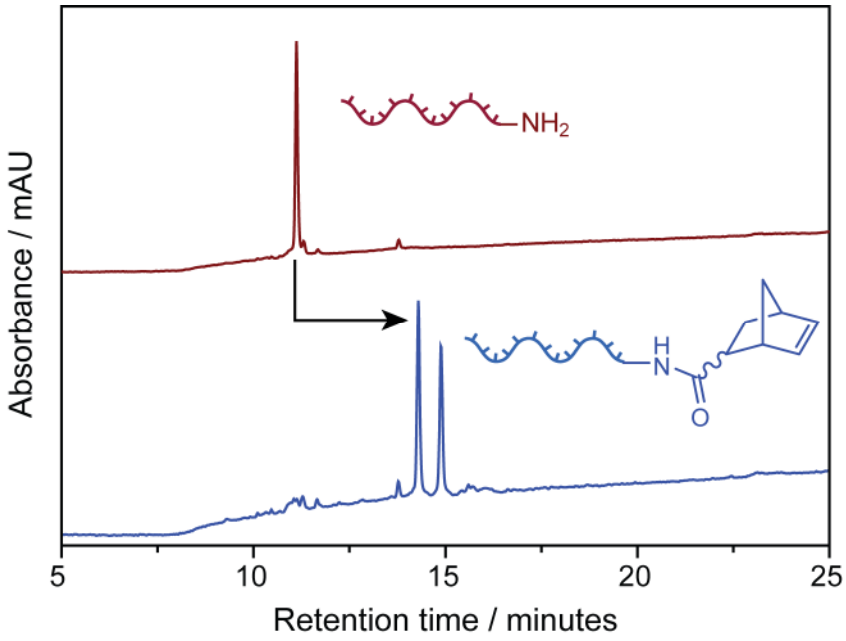

Figure 4.7 HPLC chromatograms showing the formation of s0–Nb (bottom) from s0–NH_2 (top) and a Nb acid.

Both had the same mass of 6 996 Da, which was the expected mass of s0–Nb; it was therefore concluded that the two products corresponded to the *endo*- and *exo*-Nb adducts (the Nb acid starting material was a mixture of the two isomers).

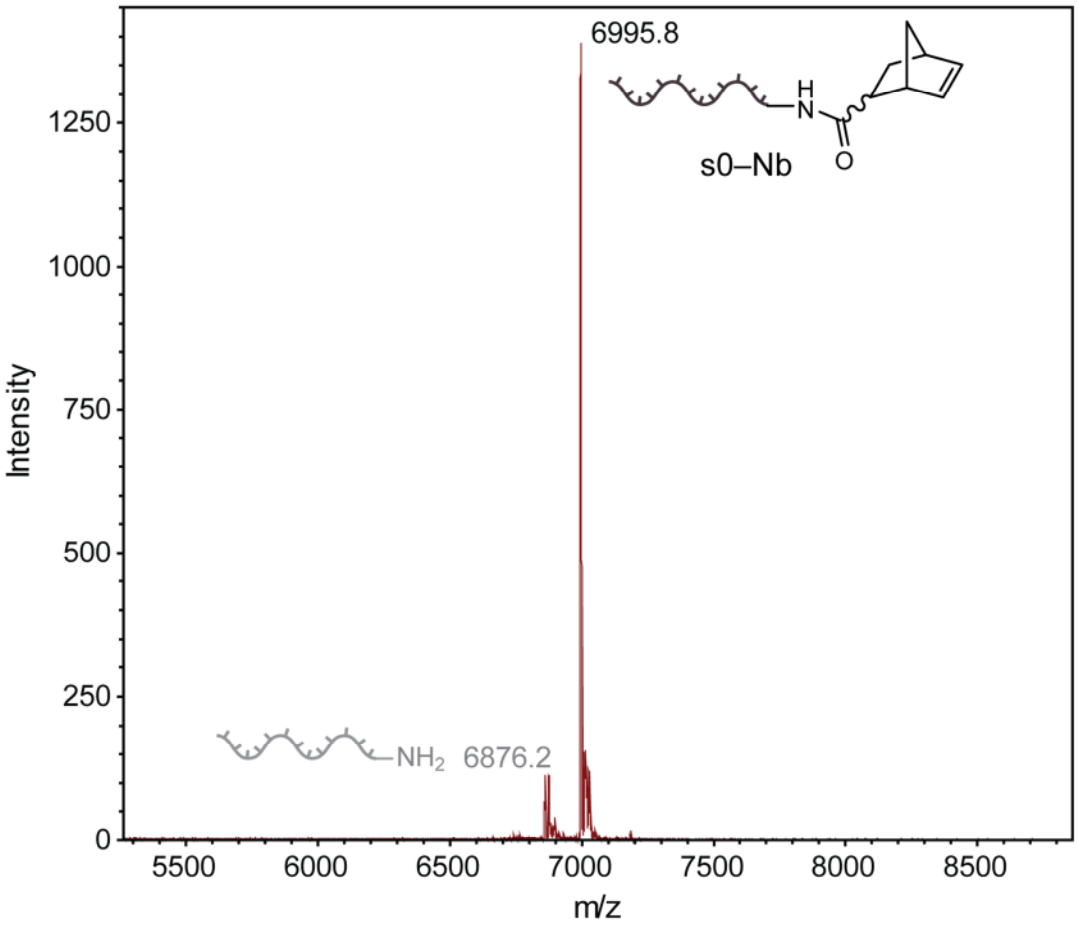

Figure 4.8 MALDI-ToF mass spectrum of s0–Nb using 3-Hydroxypicolinic acid (3-HPA) as matrix. A small amount of the s0–NH_2 starting material was observed. The expected peak molecular weight of the product was 6996.3 Da.

The reactivity of the Nb group on the DNA was tested by mixing each of the s0–Nb isomers (*endo* and *exo*) with an alcohol-functionalised Tz (**12**) under conditions analogous to those to be used for the DNA–polymer conjugation. Analysis of the DNA by HPLC before and after addition of **12** revealed a clear peak shift for both isomers (Figure 4.9), indicating that both retained an intact Nb group and that this group was reactive towards Tz.

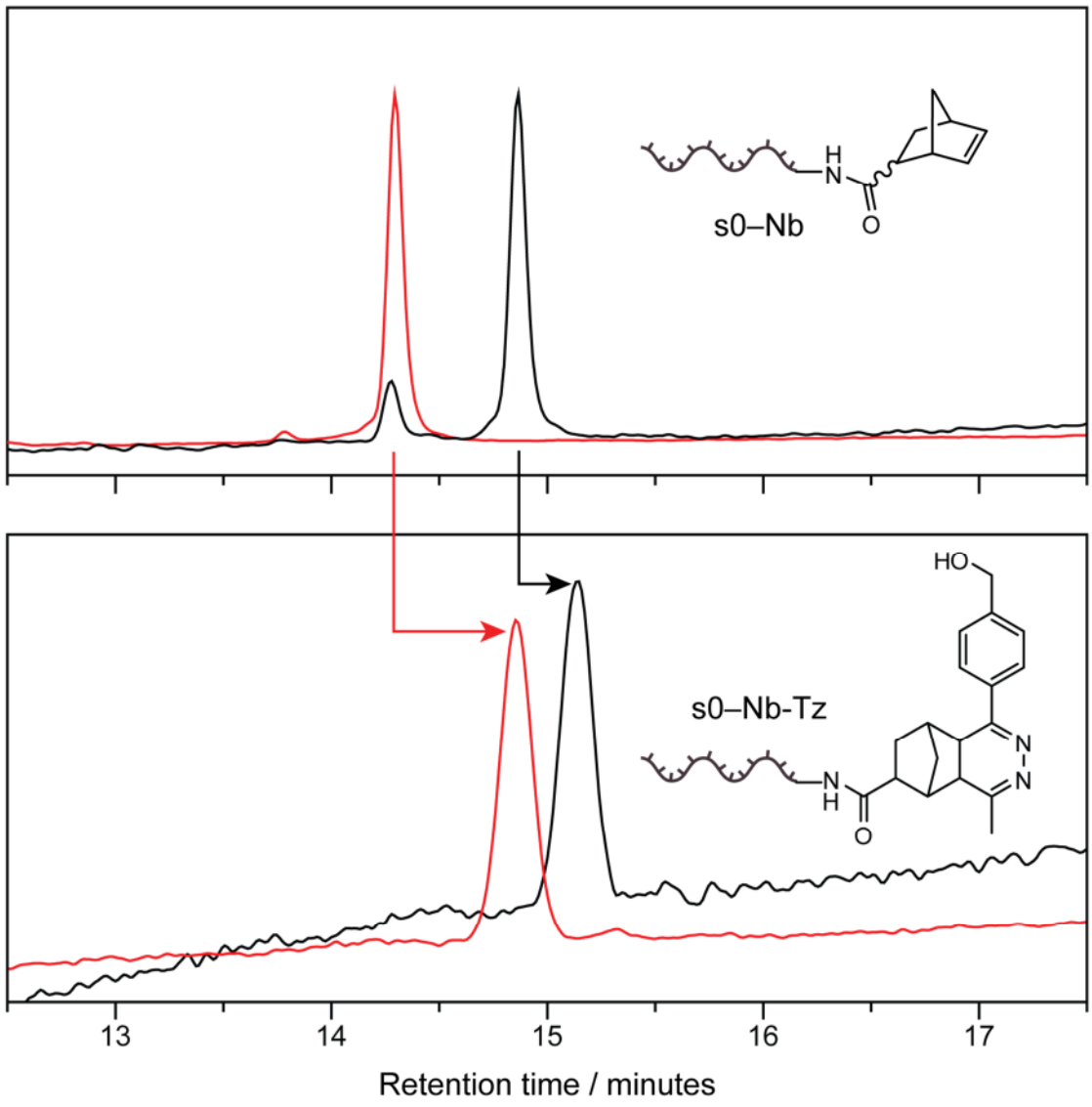

Figure 4.9 HPLC analysis of the reaction of s0–Nb with the small molecule Tz **12**. A clear peak shift was observed for both the *endo* and *exo* isomers, indicative of a successful reaction. Reaction conditions: s0–Nb (10 μM), **12** (1 mM), HPLC buffer (100 mM TEAA, 70 % MeCN), room temperature, 24 hours.

To further confirm that the observed peak shift was due to the reaction with the Tz molecule, the UV-vis spectra were examined before and after addition (Figure 4.10). This showed that there was a shift in the principal peak from 260 nm to 265 nm and the appearance of a shoulder around 310 nm, both characteristic of the addition of a tetrazine to the norbornene group (both absorbances can be seen below in Figure 4.18). 15 % native PAGE was also used to prove that the observed peak contained DNA and not just the Tz small molecule (right of Figure 4.10). The gel was stained with a nucleic acid specific stain

(which does not bind the Tz) and a clear band was observed.

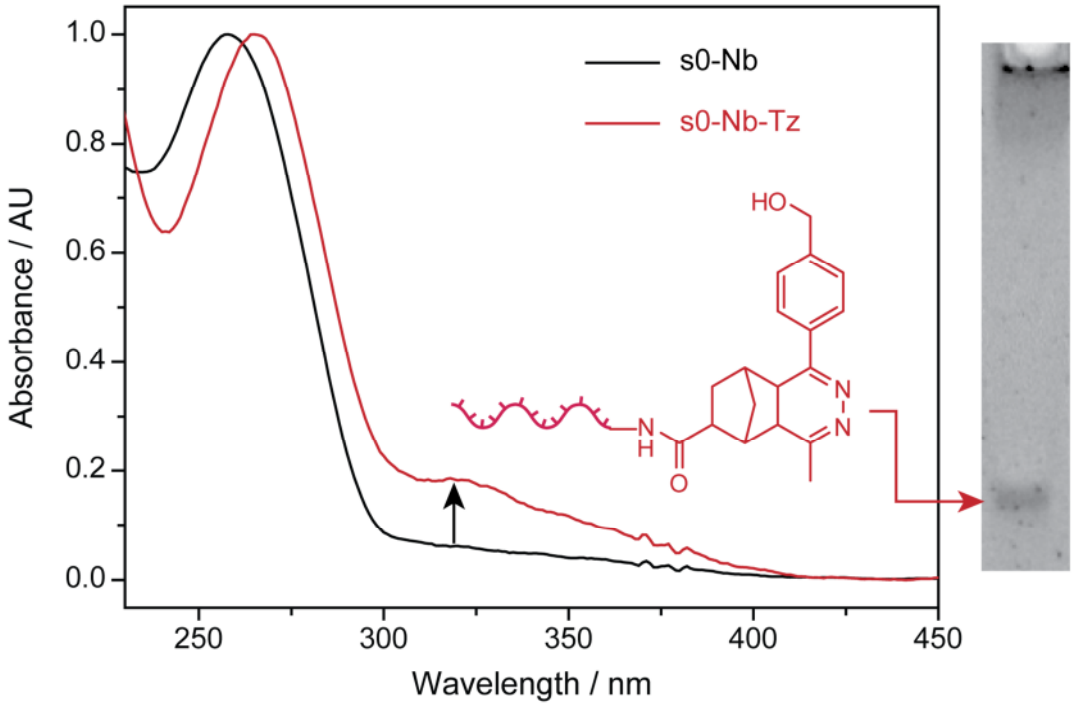

Figure 4.10 UV-vis spectra showing the change in absorbance maxima when the Tz-containing alcohol **12** was added to s0–Nb DNA. Addition of the Tz caused a shift in the principal peak from 260 nm to 265 nm, and a new peak was observed at around 310 nm. 15 % native PAGE (right), stained with a nucleic acid-specific dye, was used to confirm the presence of DNA in the sample.

4.2.v Synthesis of Tz-functionalised polymers

The Tz group is not stable towards radical polymerisation conditions as it reacts with monomers bearing vinyl functionality.[6] Incorporation of this group into an appropriate CTA was therefore not a viable option for the production of Tz-functionalised polymers by RAFT polymerisation. The logical choice, then, was to pursue a post-polymerisation modification strategy. Since it had already been shown in the work discussed in Chapter 2 that activated ester-containing polymers are straightforward to prepare using RAFT and appropriately-functionalised CTAs, it seemed logical to exploit this reactivity. However, amine-containing Tz compounds are difficult to synthesise – low yields are often reported because in solution the amine group can attack the tetrazole ring, causing its degradation – so it was necessary to utilise the alcohol-containing Tz, **12** (see Figure 4.11).

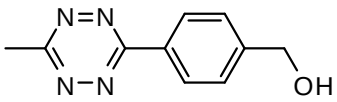

12

Figure 4.11 The tetrazine compound used for post-polymerisation modification.

The formation of esters from alcohols and PFP esters is documented in the literature, although not extensively.[17-19] Typically, this reaction is slower than the corresponding amide formation, and always requires an auxiliary base to serve as a catalyst. Heat is also occasionally employed to promote the process.

Initially, functionalisation of the PFP-containing polymers from Chapter 2 was attempted (Scheme 4.5). However, after three days stirring at room temperature in the presence of TEA (acting as an auxiliary base) no reaction was observed by ^{1}H NMR (the product would be expected to exhibit a peak around 5.2 ppm due to the $CO_2C\underline{H}_2$ group) or DMF SEC (the product should have an absorbance at 540 nm due to the Tz group, but no peak was observed at this wavelength).

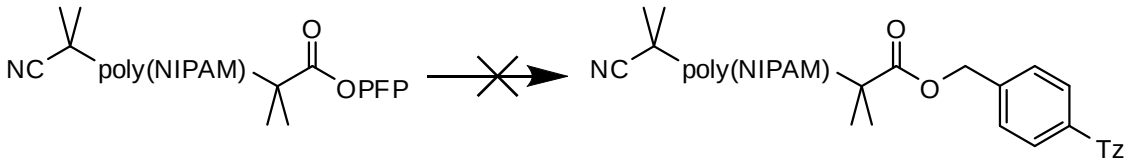

Scheme 4.5 Attempted modification of PFP-functionalised poly(NIPAM) using **12**. Reaction conditions: **12** (10 eq. w.r.t. polymer PFP group), TEA (1 eq.), THF, N_2, room temperature, 3 days.

It was hypothesised that the two methyl groups α to the PFP ester were hindering the attack of the alcohol – indeed, PFP-methacrylate has been observed to react with alcohols much more slowly (if at all) than the acrylate analogue.[20] An alternative PFP-containing CTA, **14**, was therefore synthesised wherein the PFP group was held at the end of an ethyl linker, minimising steric blocking (see Scheme 4.6). **14** has been reported previously by addition of pentafluorophenyl alcohol to **13** under amide coupling conditions using 1,1'-carbonyldiimidazole,[21] but a long reaction time was required and the yield was low (20 %).

By using pentafluorophenyl trifluoroacetate as the source of the PFP group, the yield was dramatically improved (80 %), with the reaction complete in just one hour

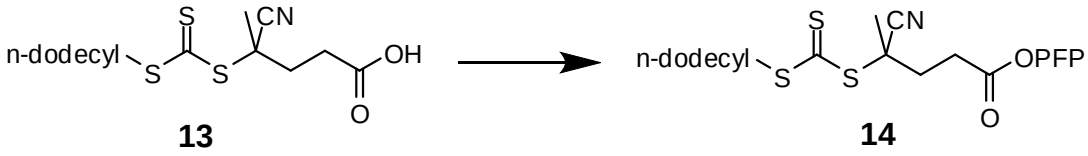

Scheme 4.6 Synthesis of the PFP-functionalised CTA, **14**. Reaction conditions: pentafluorophenyl trifluoroacetate (1.2 eq.), DIPEA (2.0 eq.), DMF, 0°C, N_2, 1 hour. Yield: 80 %.

Next, the CTA **14** was used to control the RAFT polymerisation of NIPAM. Good control was achieved over molecular weight and dispersity (see Table 4.2). ^{1}H NMR spectroscopy confirmed the presence of the end groups in the product: the peaks due to the SC$\underline{H}_2$ (3.31 ppm) and C$\underline{H}_2$CO$_2$PFP (2.84 ppm) groups were both visible (Figure 4.12). ^{19}F NMR spectroscopy showed that the PFP group remained intact following the polymerisation (Figure 4.13). Inclusion of trifluorotoluene as an external standard allowed quantification of the degree of PFP incorporation following the polymerisation (see Chapter 2).

Table 4.2 Properties of the polymers synthesised using PFP-containing CTA **14**.

Polymer	DP^{NMR}	M_n^{NMR} / kDa	M_n^{SEC} / kDa	Đ	PFP incorporation
P10	80	9.6	13.0	1.06	90 %
P11	105	12.5	11.5	1.05	98 %

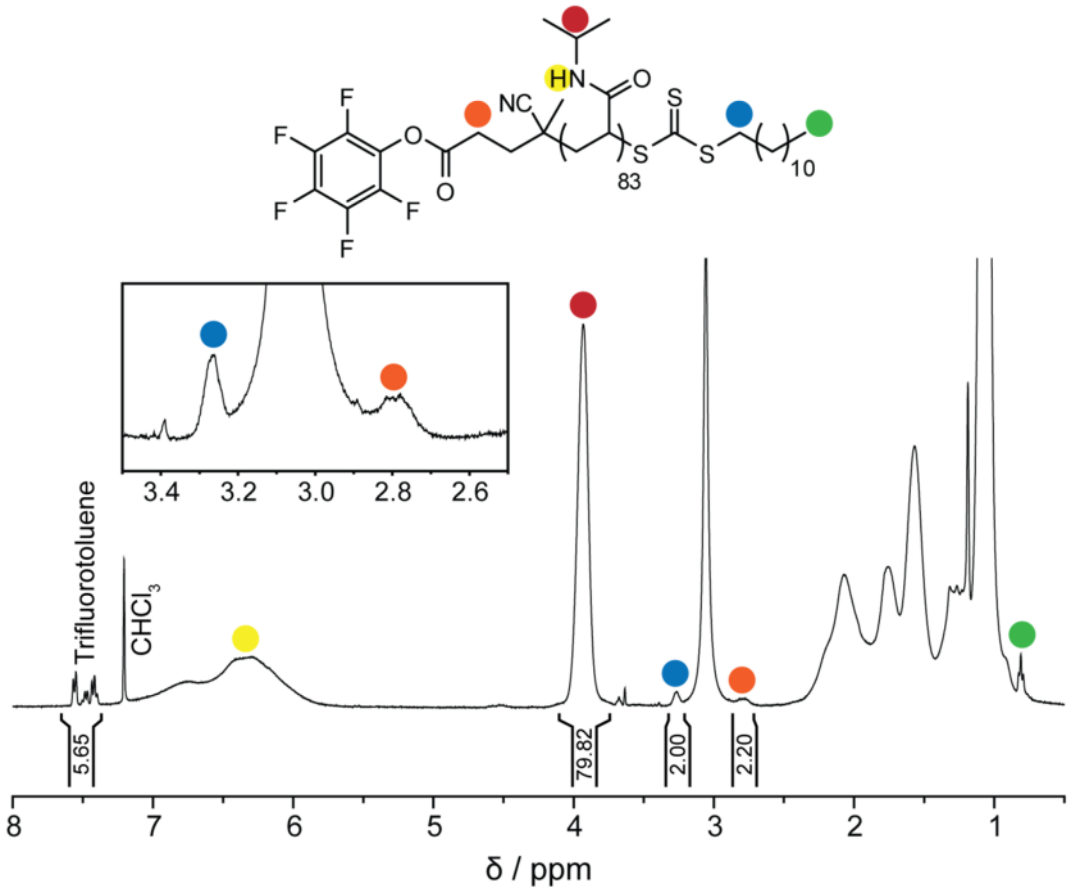

Figure 4.12 ^{1}H NMR spectrum of **P10** showing the presence of the key peaks due to the polymer end groups. Trifluorotoluene was included as an external standard to assess the degree of incorporation of the PFP activated ester group. Solvent: $CDCl_3$.

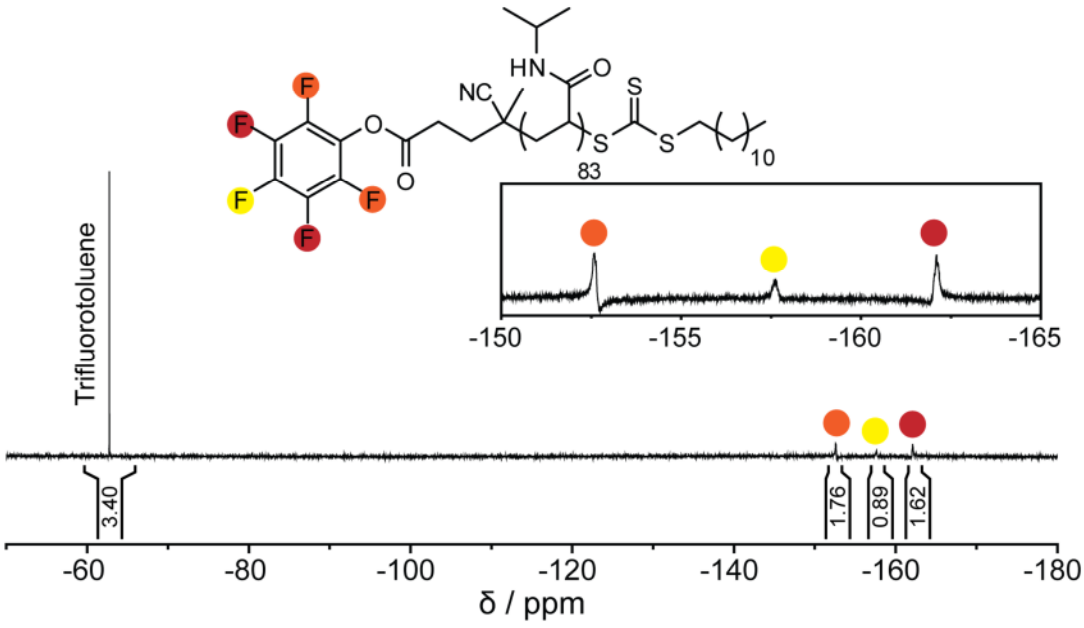

Figure 4.13 ^{19}F NMR spectrum of **P10** showing the presence of the PFP activated ester peaks. Trifluorotoluene was included as an external standard to assess the degree of incorporation of the PFP activated ester group. Solvent: $CDCl_3$.

Modification of **P10** and **P11** was then attempted using either propargyl alcohol or benzyl alcohol – these molecules have a characteristic signal in ^{1}H NMR spectroscopy due to the CH_2 group adjacent to the alcohol, making it easy to assess the degree of incorporation, even at low concentrations. Either cesium fluoride or 4-(dimethylamino)pyridine (DMAP) was used as the catalyst to enhance the nucleophilicity of the alcohol group. The PFP-capped polymer was mixed with the catalyst and propargyl alcohol in tetrahydrofuran (THF) and stirred for twenty-four hours at room temperature. Various equivalents of DMAP were tested to ascertain whether this would have an effect on the efficiency of the reaction. The percentage incorporation of the alcohol was measured by ^{1}H NMR spectroscopy. First, the integral of the poly(NIPAM) NHC*H* peak was fixed at the degree of polymerisation for the polymer (for example, 83 for **P10**). The peak due to the CH_2 group adjacent to the newly-formed ester was then integrated. The percentage incorporation was calculated by dividing this value by two (the expected value if complete conversion of the PFP ester had occurred). An example is shown in Figure 4.14, and the results are given in Table 4.3.

Table 4.3 Details of the catalyst conditions tested for the addition of propargyl (*) or benzyl (†) alcohol to poly(NIPAM) containing a PFP activated ester (**P10** and **P11**). Reaction conditions: alcohol (10 equivalents), polymer (1 eq.), catalyst, THF, N_2, room temperature, 24 hours.

Catalyst	Equivalents	Incorporation of alcohol	Retention of trithiocarbonate
CsF	0.2*	0 %	100 %
DMAP	1*	65 %	65 %
	0.5†	38 %	90 %
	0.1*	29 %	100 %

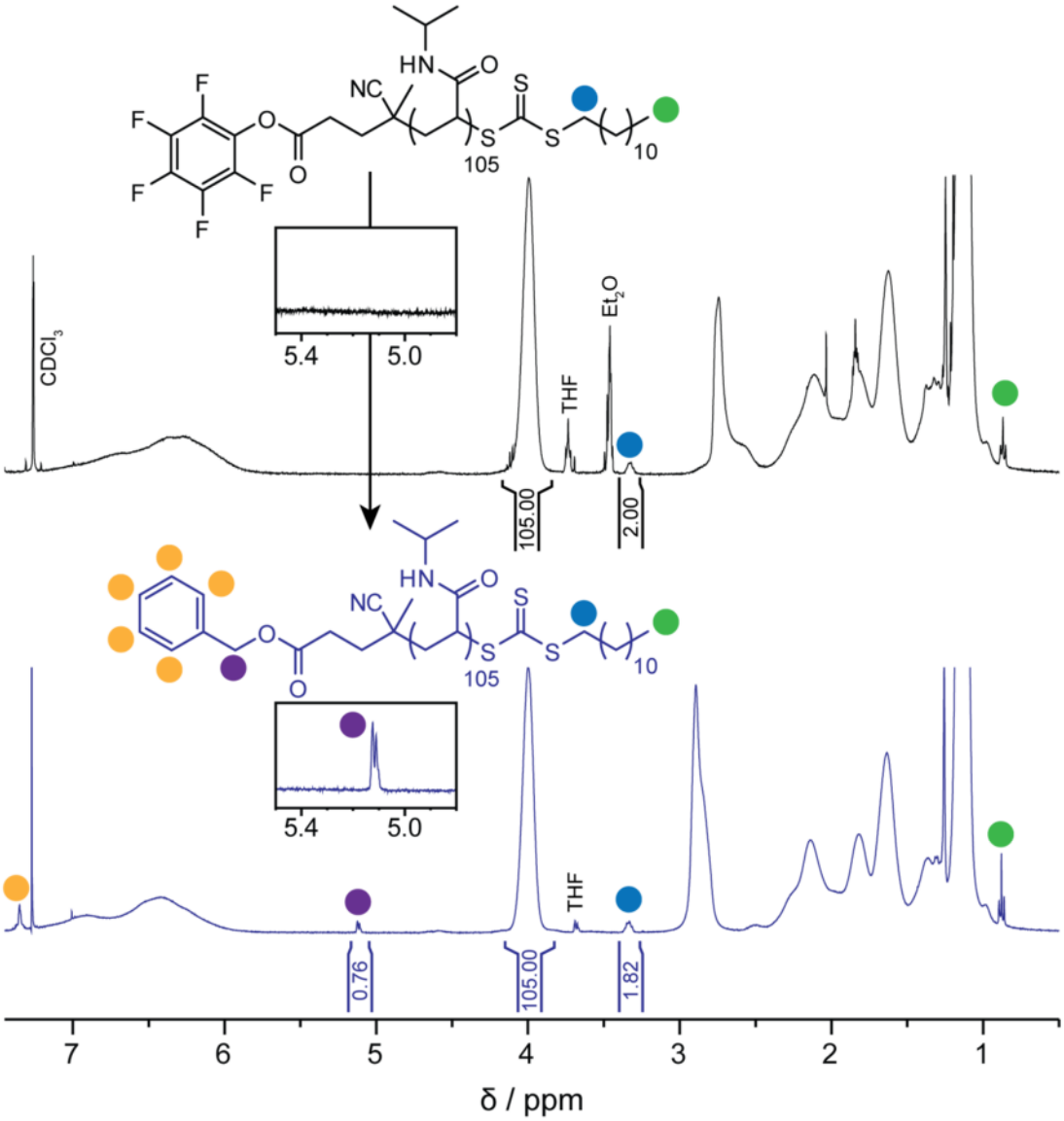

Figure 4.14 ^{1}H NMR spectra of **P11** before (top) and after (bottom) addition of benzyl alcohol. Reaction conditions: Benzyl alcohol (10 eq. w.r.t PFP ester), DMAP (0.5 eq.), THF, N_2, room temperature, 24 hours. NMR solvent: $CDCl_3$.

The retention of the trithiocarbonate group was also measured by ^{1}H NMR spectroscopy, by comparing the integral of the SC*H*$_2$ group to the poly(NIPAM) NHC*H* group before and after the reaction with the alcohol, to see whether any degradation was occurring.

No reaction was observed when cesium fluoride was used as the catalyst, which was ascribed to the insolubility of this compound in THF. Varying degrees of incorporation were observed when DMAP was used. At low concentrations of DMAP, the trithiocarbonate group was retained but the conversion to the ester was low. Increasing the

concentration of DMAP improved the conversion. However, this also resulted in degradation of the trithiocarbonate group.

In an attempt to increase the degree of alcohol incorporation, the trithiocarbonate end group was removed from the poly(NIPAM) with AIBN and lauroyl peroxide (LPO) as described in Chapter 2. This had previously been shown to be effective when amines were used as the nucleophile in the substitution reaction. The end group removal proceeded as expected and analysis by ^{19}F and ^{1}H NMR spectroscopy (Figure 4.15 and Figure 4.16) revealed the successful removal of the trithiocarbonate group and 99 % retention of the PFP activated ester (as quantified by inclusion of trifluorotoluene as an external standard – see Chapter 2). Analysis of the polymer by DMF SEC using a UV-vis detector also confirmed the loss of the trithiocarbonate by the disappearance of a peak at 309 nm (Figure 4.17).

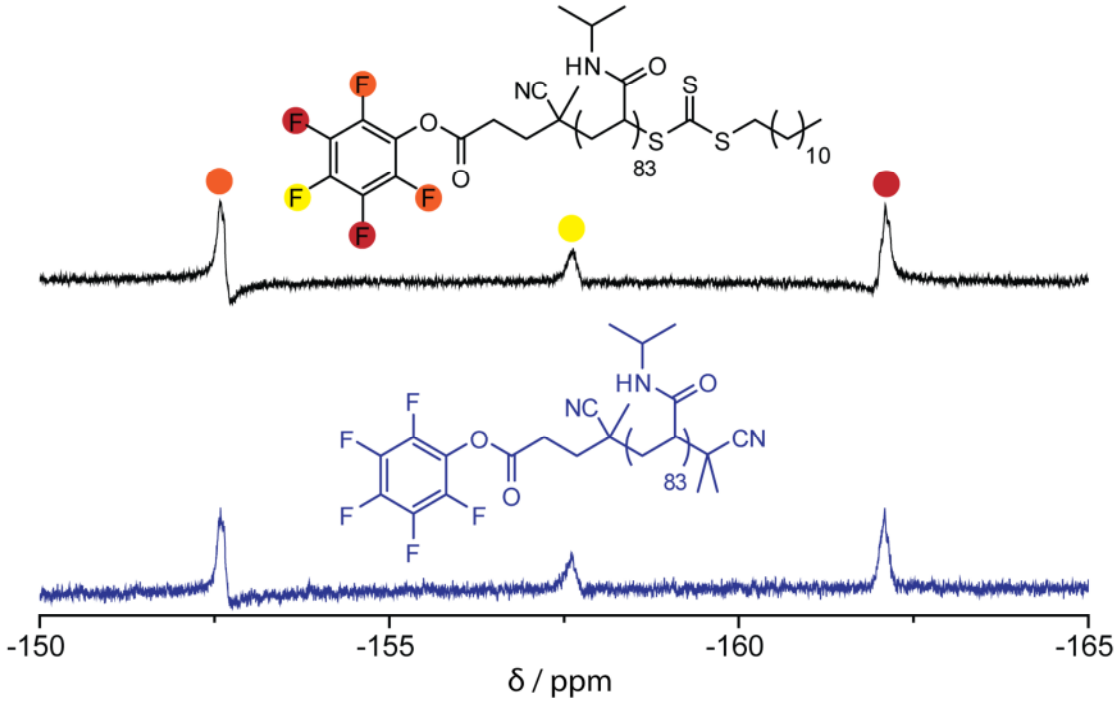

Figure 4.15 ^{19}F NMR spectra of **P10** before (top) and after (bottom) removal of the trithiocarbonate group using AIBN and LPO. Inclusion of an external standard containing both hydrogen and fluorine groups allowed quantification of the retention of the PFP group. Solvent: $CDCl_3$.

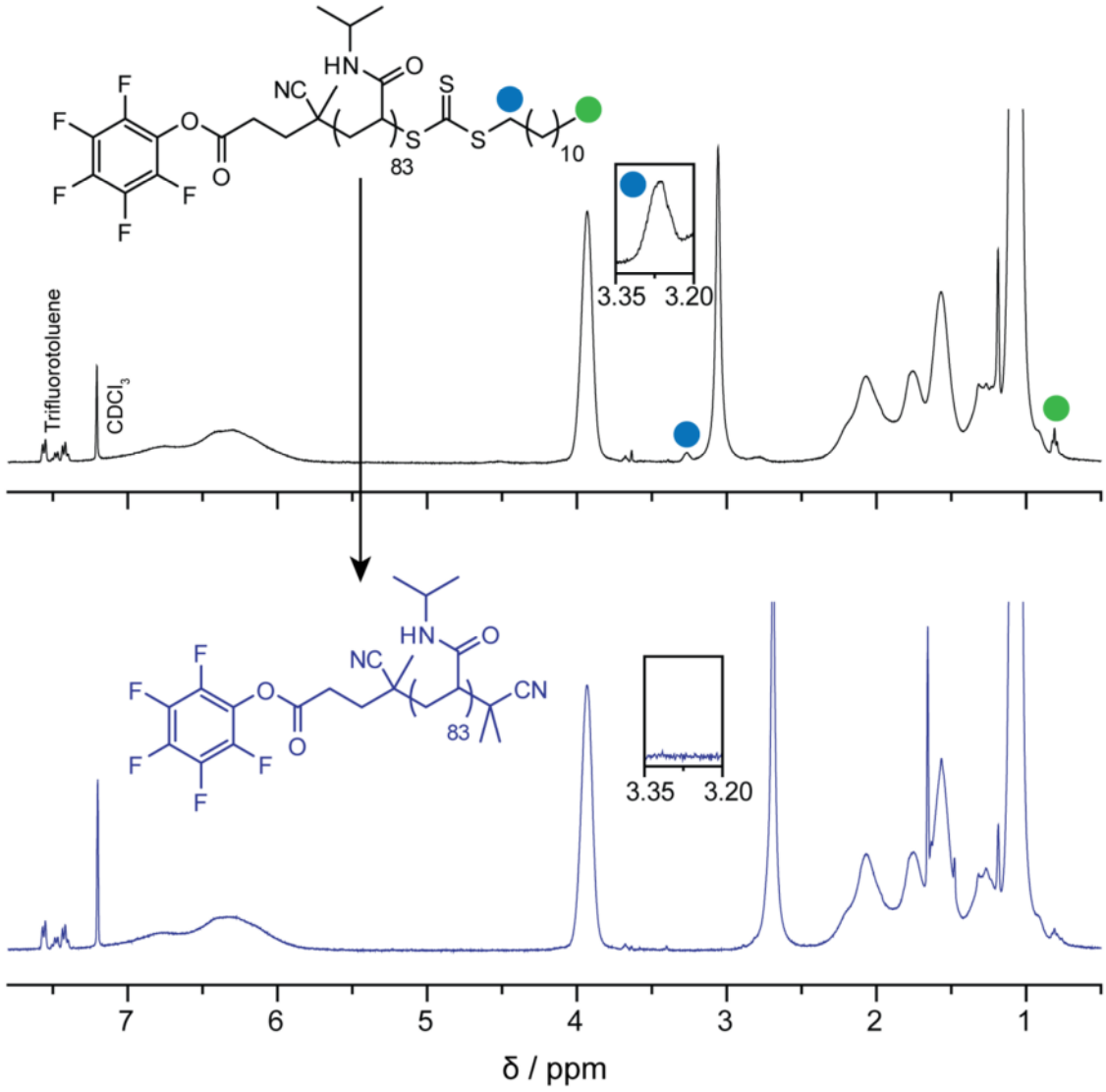

Figure 4.16 ^{1}H NMR spectra showing the successful removal of the trithiocarbonate group from **P10** using AIBN and LPO by the disappearance of the signal due to the adjacent CH_2 group. Reaction conditions: AIBN (100 eq.), LPO (4 eq.), THF, N_2, 65°C, 6 hours. NMR solvent: $CDCl_3$.

The coupling was then attempted again using propargyl alcohol and DMAP (one equivalent relative to the PFP group). The conversion to the ester was measured after twenty-four hours and found to be 53 %. Removal of the trithiocarbonate group had therefore not improved the yield of this reaction. This result suggested that increased concentrations of DMAP not only degraded the trithiocarbonate group but also led to degradation of the PFP activated ester before it could react with the alcohol.

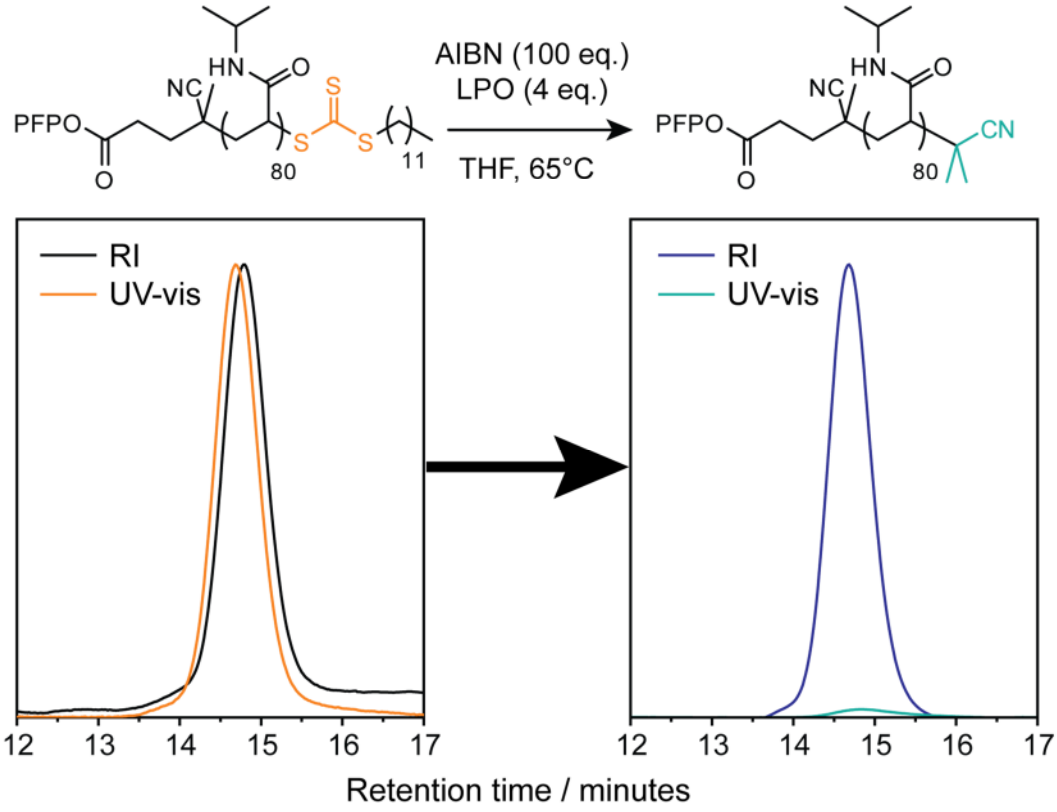

Figure 4.17 DMF SEC chromatograms showing the successful removal of the trithiocarbonate group from **P10**. The refractive index (RI) trace remains unchanged, but a very large decrease in the UV-vis trace recorded at 309 nm, which is characteristic of the trithiocarbonate group, was observed, indicating that this group had been successfully removed.

The reaction conditions that resulted in the highest conversion of the alcohol without significant degradation of the trithiocarbonate (0.5 equivalents of DMAP relative to PFP, 10 equivalents of alcohol) were then used to produce Tz-functionalised poly(NIPAM). Alcohol **12** was mixed with **P11** and DMAP and stirred for twenty-four hours in anhydrous THF under an atmosphere of nitrogen. The polymer was then separated from the excess alcohol by preparatory SEC in DMF. Removal of the solvent under high vacuum yielded a pink solid which was studied by UV-vis spectroscopy and found to have the same peaks as the starting material, suggesting that the Tz group had been incorporated successfully (Figure 4.18).

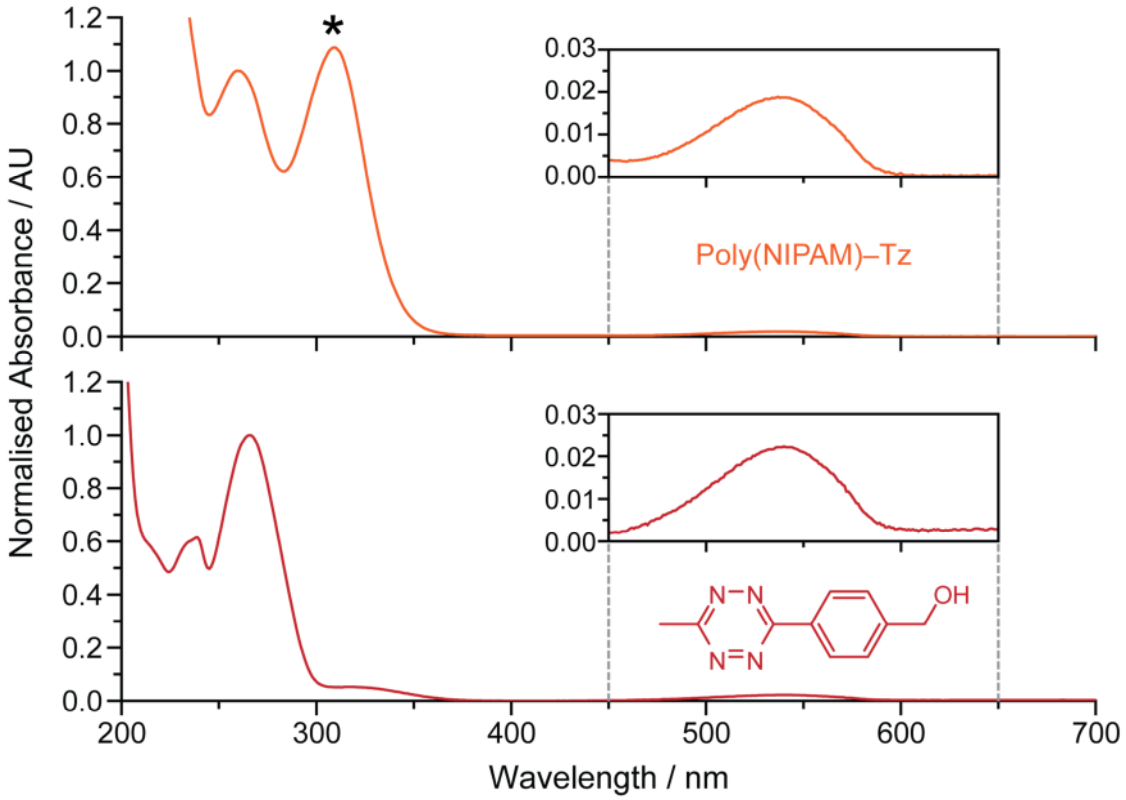

Figure 4.18 UV-vis spectrum of the tetrazine alcohol **12** (bottom, red) and Tz-functionalised poly(NIPAM) (top, orange). The polymer exhibited the characteristic Tz absorbances at 265 nm and 540 nm (insets), as well as a peak at 309 nm due to the trithiocarbonate group at the opposite end of the polymer chain (*).

The poly(NIPAM)–Tz was analysed by ^{1}H NMR spectroscopy, which showed the presence of new peaks due to the Tz group and the CH_2 group adjacent to the newly-formed ester (Figure 4.19), confirming the incorporation of the Tz group in approximately 50 % yield. Full retention of the trithiocarbonate group was also confirmed by this method. The polymer was also analysed by DMF SEC with an in-line UV-vis detector set to 540 nm (the wavelength of one of the characteristic peaks of the Tz group). The results (Figure 4.20) showed both that the molecular weight and dispersity of the polymer remained unchanged, and that the Tz group had been successfully incorporated at the polymer chain end, by the appearance of a peak at 540 nm.

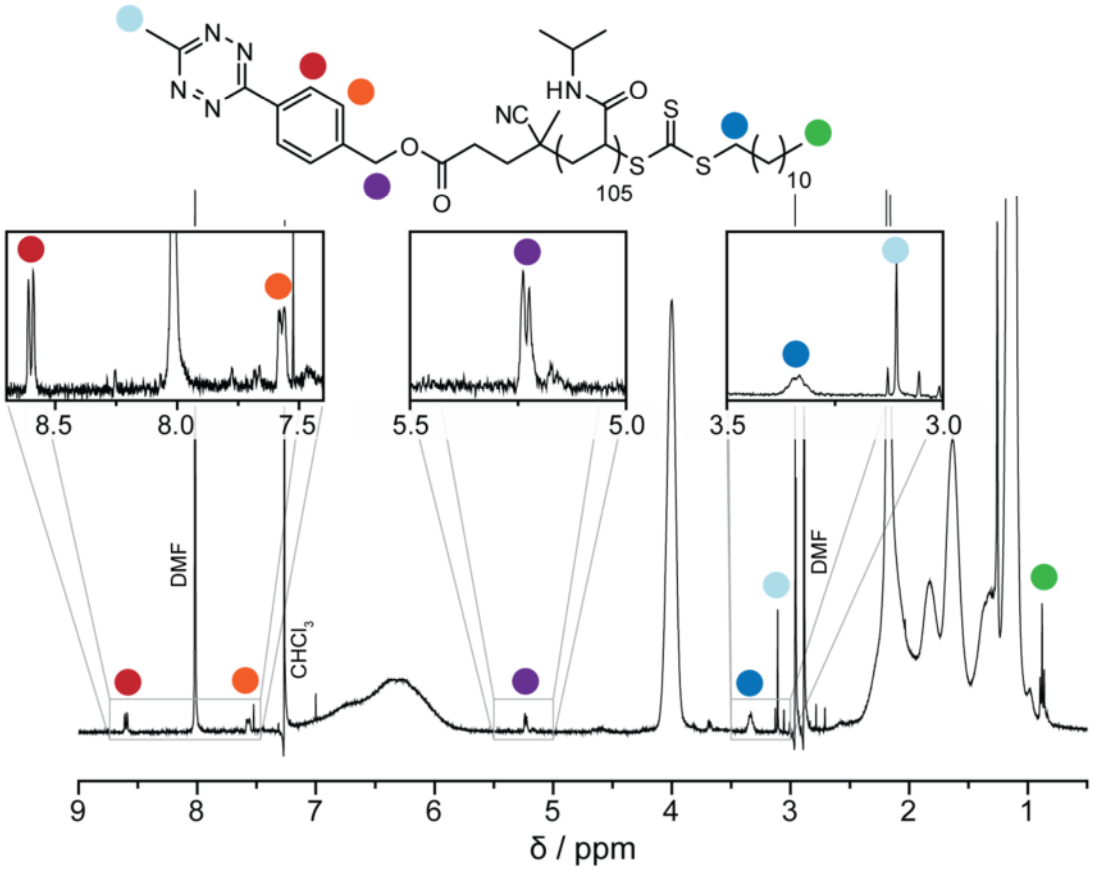

Figure 4.19 ^{1}H NMR spectrum of Tz-functionalised poly(NIPAM). The peaks due to both end groups are clearly visible, and all the peaks due to the Tz group are accounted for. Integration of the Tz signals to the poly(NIPAM) NHC*H* peak at 4.00 ppm revealed that this group had been incorporated with an efficiency of 53 %. Solvent: $CDCl_3$.

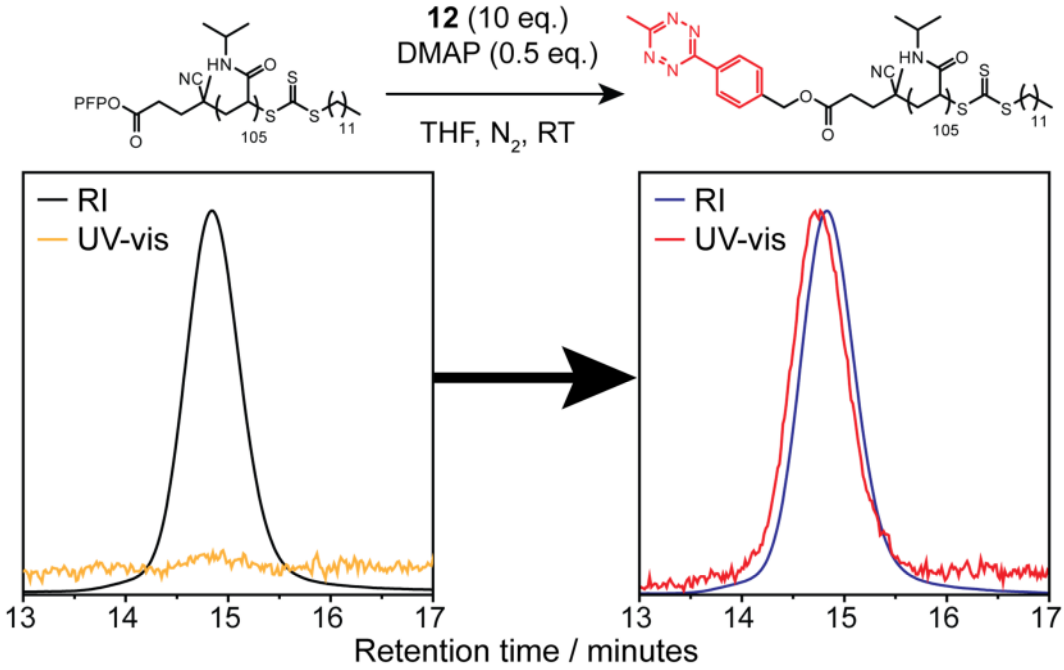

Figure 4.20 DMF SEC chromatograms showing the incorporation of the Tz group at the chain end of poly(NIPAM). There is the clear appearance of a peak in the UV-vis trace collected at 540 nm (characteristic of the Tz group).

Further confirmation was provided by running THF SEC analysis using a photodiode array (PDA) detector. This collected a full UV-vis spectrum for every retention time point. The result is shown in Figure 4.21, and shows the full Tz peak at 540 nm eluting at the same time as the main polymer peak. Importantly, both ^{1}H NMR spectroscopy and SEC indicated that no small molecule Tz was present in the sample.

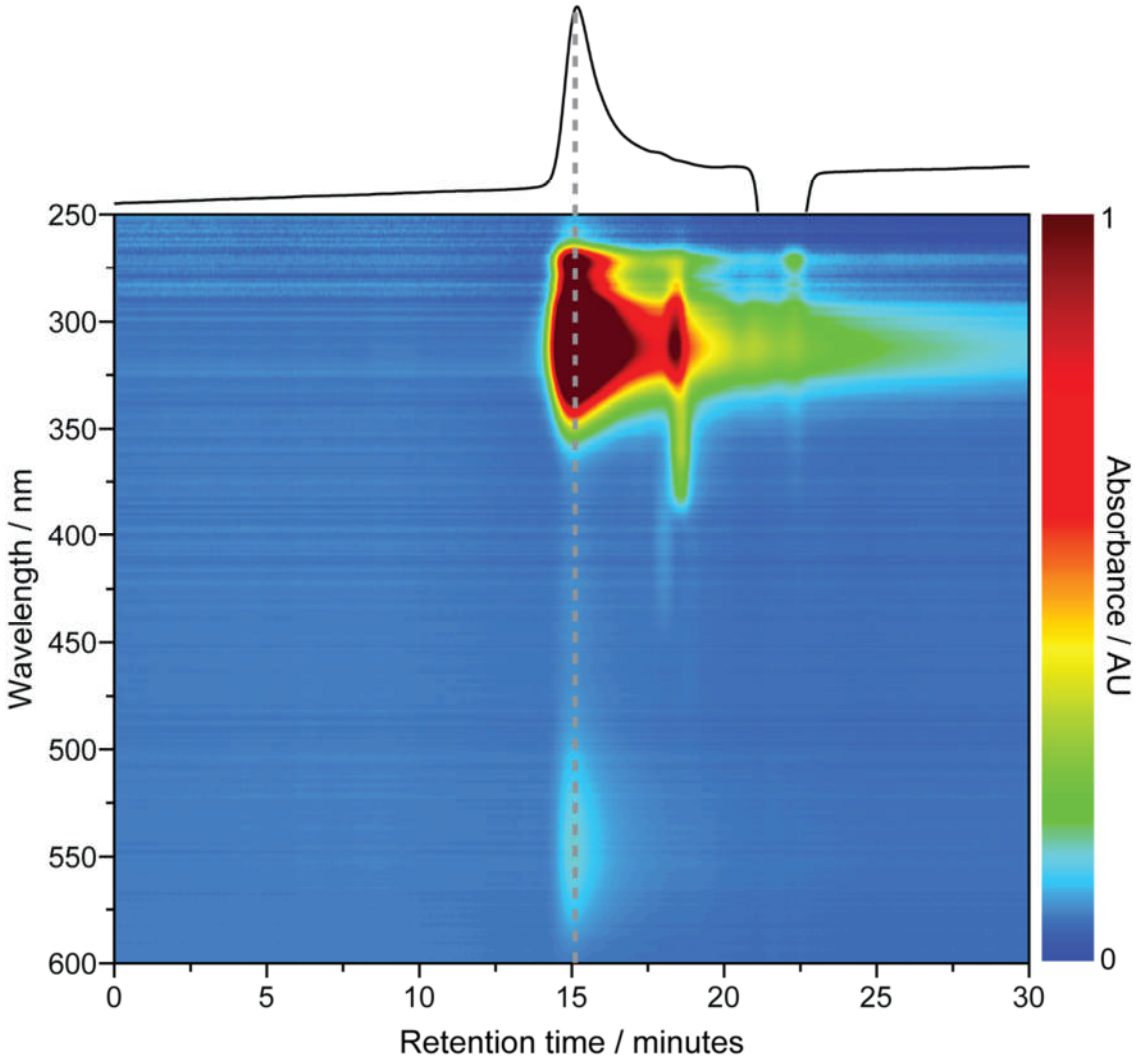

Figure 4.21 THF SEC refractive index chromatogram (top) and UV-vis 2D colour map (bottom) of Tz-functionalised poly(NIPAM). The colour map clearly shows that the characteristic Tz peak at 540 nm is only associated with the polymer, confirming its successful incorporation at the chain end.

4.2.vi Conjugation of polymers to s0–Nb

With the Tz-functionalised polymer in hand, coupling to s0–Nb was attempted in the same solvents trialled for conjugation of s0–Tz to poly(NIPAM)–Nb. The reaction conditions

tested are summarised in Table 4.4.

Table 4.4 Reaction conditions tested for the conjugation of poly(NIPAM)–Tz to s0–Nb. The DNA and polymer concentrations were kept constant at 10 μM and 1 mM respectively. All reactions were conducted at room temperature for 48 hours.

Reaction #	Solvent	Coupling efficiency / %
2a	Water	45
2b	DMF	7
2c	DMAc	7
2d	NMP	0
2e	DMSO	0

The reaction mixtures were analysed by 15 % native PAGE (Figure 4.22), which showed that the conjugate was formed in moderate yield in water by the clear appearance of a low-mobility band attributed to the product. When DMF or DMAc was used as the reaction solvent, yields were below 10 %, and in NMP and DMSO no reaction was observed.

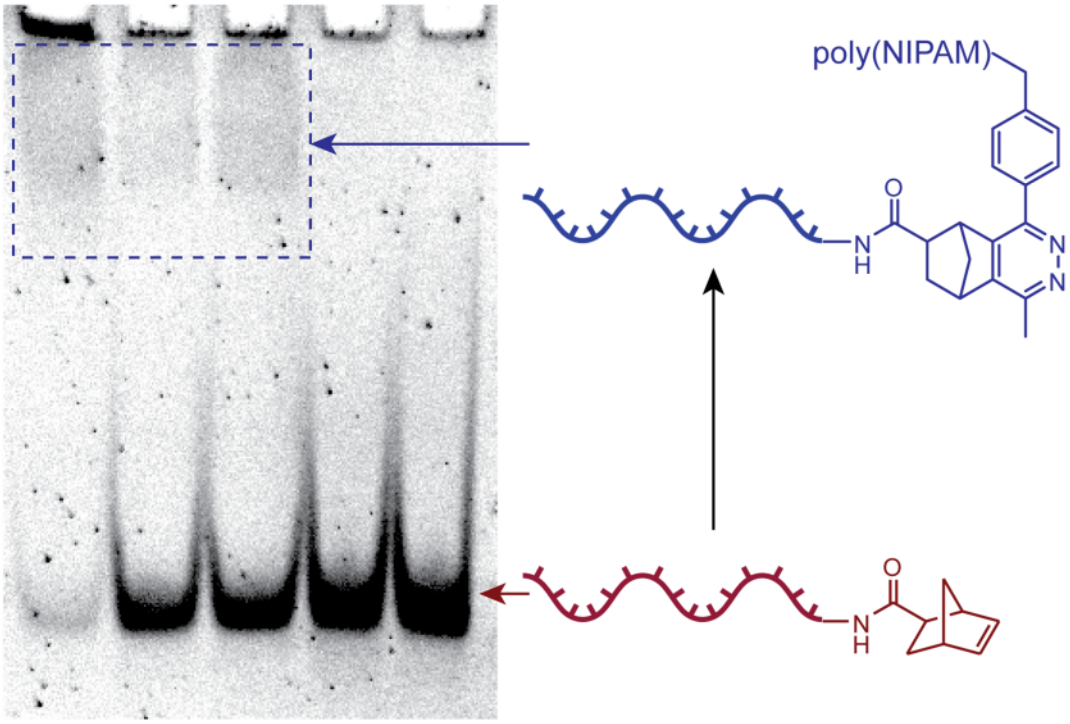

Figure 4.22 15 % native PAGE analysis of the reactions detailed in Table 4.4. The DNA–polymer conjugate was visible as a slow-migrating band (blue box) when water, DMF or DMAc were used as the reaction solvent.

The yields were much lower than for the reactions in which the functional groups were the opposite way around (Section 4.2.iii). This was attributed to the lower reactivity of **12** compared to **11** with respect to norbornene.[7] The difference in yield between solvents was attributed to the differences in solubility of the s0–Nb DNA strand, although it may also have been due to the polarity and chemical structure of the solvent, as this has been demonstrated to affect the rate of Tz–Nb reactions.[6]

4.3 Conclusions

Tetrazine (Tz)-functionalised DNA was synthesised from a commercially available amine-functionalised DNA strand and an activated ester Tz. The Tz-functionalised DNA strand was found to react with a norbornene (Nb)-containing small molecule in both aqueous and organic solutions. The Tz-functionalised DNA strand was then conjugated to poly(NIPAM) containing a terminal Nb group. Yields of the conjugate varied according to the solvent used but reached as high as 50 %.

The positions of the Tz and Nb groups were then switched to see whether this would affect the efficiency of the reaction and make synthesis of the precursors more straightforward. Nb-functionalised DNA was synthesised from commercially available starting materials in excellent yield, and the *exo* and *endo* isomers were separated. The availability of the Nb functionality was checked by reaction with a small molecule Tz. HPLC showed a clear peak shift for both isomers, indicating that there was no difference in reactivity between the two. Tz-functionalised poly(NIPAM) was synthesised by post-polymerisation modification of an activated ester-containing precursor with an alcohol-containing Tz. The efficiency of the reaction was found to be sensitive to the type and amount of catalyst used, and the presence of bulky groups close to the activated ester. Removal of the trithiocarbonate group from the polymer had no effect on the efficiency of the reaction. Incorporation of the Tz group at the polymer chain end was confirmed by ^{1}H NMR spectroscopy, UV-vis spectroscopy and SEC. Finally, conjugation of the Tz-functionalised polymer to the Nb-functionalised DNA was attempted. The reaction proceeded with moderate yield in water and a number of organic solvents. However, yields were lower than observed for Tz-functionalised DNA reacting with Nb-functionalised polymer. Overall, the difficulties with the synthesis of the precursor materials may mean that this method is not very attractive to the materials science community for the purposes of DNA–polymer conjugation.

4.4 Experimental

4.4.i Materials & Methods

For general materials and methods details, see the Appendix. 5-oxo-5-(6-(6-(pyridin-2-yl)-1,2,4,5-tetrazin-3-yl)pyridin-3-ylamino)pentanoic acid (**10**) and (4-(6-methyl-1,2,4,5-tetrazin-3-yl)phenyl)methanol (**12**) were synthesised according to previously published procedures.[12,15] Silica gel was treated with $EtSiCl_3$ according to a published procedure.[22] The DNA strand s0–NH_2 was purchased from Integrated DNA Technologies Ltd. And resuspended in 18 MΩ water to a concentration of 200 μM prior to use. NAP-5 sephadex purification columns were purchased from GE Healthcare. Poly(NIPAM) containing a terminal norbornene group (M_n 16.4 kDa, Đ 1.12) was synthesised according to a previously published procedure.[15] ZipTip® pipette tips were purchased from Merck Millipore. 4-Cyano-4-(dodecylthiocarbonothioylthio)pentanoic acid (**13**) was purchased from Sigma-Aldrich and used as received. Bio-Beads S-X1 for preparatory size exclusion chromatography were purchased from Bio-Rad Laboratories Inc.

4.4.ii 2,5-dioxopyrrolidin-1-yl 5-oxo-5-(6-(6-(pyridin-2-yl)-1,2,4,5-tetrazin-3-yl)pyridin-3-ylamino)pentanoate, 11

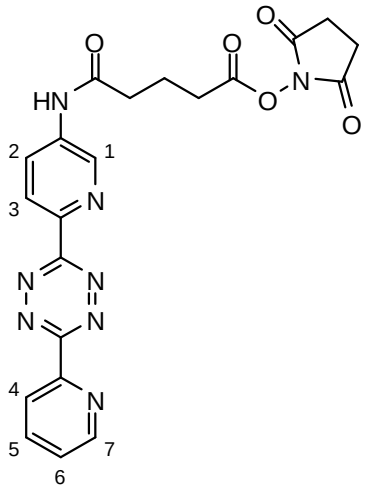

The tetrazine DNA adaptor was synthesised as follows. Tetrazine **10** (0.100 g, 0.27 mmol) and NHS (0.032 g, 0.27 mmol) were dissolved in DMF (4 mL) and the solution bubbled with nitrogen for 30 minutes. The mixture was then cooled using an ice bath and DCC

(0.057 g, 0.27 mmol) dissolved in DMF (1 mL) was added via syringe. After 30 minutes stirring the ice bath was removed and the reaction stirred under nitrogen for 16 hours. The reaction mixture was adsorbed onto silica which had been previously treated with $EtSiCl_3$. $EtSiCl_3$-treated silica gel column chromatography was then performed, eluting first with DMF, then acetone. The pure fractions were collected and combined, then dried *in vacuo* to afford the product **11** as a deep red powder (0.048 g, 38 %). ^{1}H NMR (400 MHz, d_6-DMSO) δ 10.67 (br s, 1H, N*H*C=O), 9.10 (d, *J* = 2 Hz, 1H, Tz *H*1), 8.97 (d, *J* = 4 Hz, 1H, Tz *H*7), 8.66 (d, *J* = 9 Hz, 1H, Tz *H*4), 8.63 (d, *J* = 8 Hz, 1H, Tz *H*3), 8.47 (dd, *J* = 2, 9 Hz, 1H Tz *H*2), 8.19 (td, *J* = 1, 4 Hz, 1H, Tz *H*6), 7.76 (dd, *J* = 5, 7 Hz, 1H, Tz *H*5), 2.87 (m, 6H, CH_2(C=O)N and CH_2(C=O)NH), 2.63 (t, *J* = 7 Hz, 2H, CH_2(C=O)OSu), 2.03 (quint, *J* = 7 Hz, 2H, CH_2CH$_2$(C=O)NH) ppm. ^{13}C NMR (125 MHz, d_6-DMSO) δ 172.5 (*C*=ONH), 170.7 (NHS *C*=O), 169.3 (*C*=OO), 163.5 (Tz N-*C*=N), 163.2 (Tz N-*C*=N), 151.1 (Tz *C*7), 150.7 (Tz C-*C*=N), 144.3 (Tz C-*C*=N), 141.8 (Tz *C*1), 138.9 (Tz *C*-NHC=O), 138.3 (Tz *C*5), 127.0, 126.7, 125.4, 124.7 (Tz *C*2/3/4/6), 35.1 (*C*H$_2$C=ONH), 30.0 (*C*H$_2$C=OO), 25.9 (NHS *C*H$_2$), 20.2 (*C*H$_2$CH$_2$C=O) ppm. IR (ν_{max} / cm^{-1}): 2895, 1732, 1714, 1543, 1392, 1061. ESI HR MS calcd. for $C_{21}H_{18}N_8O_5$ $[M+Na]^+$ 485.1298; observed 485.1293.

4.4.iii Synthesis of s0–Tz

300 mM solutions of EDCI, HOBt and **11** were prepared in DMF and then mixed in equal proportions. 100 μL of s0–NH_2 (200 μM in water) were added to a 1 mL centrifuge tube and the solvent removed *in vacuo*. 100 μL of the EDCI/HOBt/**11** mixture were added, followed by 100 μL of potassium phosphate buffer (100 mM, pH 8.0). The solution was vortexed to mix and then heated at 40°C for four hours, after which time small molecules were removed by passing the solution through a NAP-5 sephadex column, eluting with water. The sample was concentrated *in vacuo* and then purified by HPLC. The product was isolated as a single peak (6 %) and analysed by LC-MS. Expected mass 7 223.9 Da;

observed 7 223.2 Da.

4.4.iv Reaction of s0–Tz with 5-Norbornene-2-*exo*,3-*exo*-dimethanol

To a 0.2 mL centrifuge tube were added 2.5 μL of s0–Tz (200 μM in water). The solvent was removed *in vacuo* and then 10 μL of 5-Norbornene-2-*exo*,3-*exo*-dimethanol (1 mM in water) were added. The mixture was left to react for 16 hours at room temperature and then purified by HPLC.

4.4.v Conjugation of s0–Tz to poly(NIPAM)–Nb

The polymer (5 μL, 20/200/2 000 μM in the reaction solvent) was mixed with s0–Tz (3.18 μL, 31.4 μM in water) and the reaction solvent (1.82 μL). After 48 hours, the mixture was diluted with 5 × glycerol loading buffer and analysed by 15 % native PAGE. The conjugate was observed as a broad low mobility band in up to 50 % yield (calculated by densitometry).

4.4.vi Synthesis of s0–Nb

EDCI (100 μL, 300 mM in DMF) was mixed with HOBt (100 μL, 300 mM in DMF), 5-norbornene-2-carboxylic acid (100 μL, 300 mM in DMF) and PBS (150 μL) and thoroughly mixed. 75 μL of this solution was mixed with s0–NH_2 (25 μL, 200 μM in water) and DIPEA (0.87 μL). After one hour shaking the flask at room temperature the mixture was purified by HPLC and the product isolated as two separate peaks. Both were analysed by MALDI-ToF MS. Expected mass 6 996.3 Da; observed 6 995.8.

4.4.vii Reaction of s0–Nb with 12

The DNA strand s0–Nb (14.3 μL, 7 μM in water) was added to a centrifuge tube and the solvent removed *in vacuo*. HPLC buffer (9 μl, 100 mM TEAA, 70 % MeCN) was added and then **12** (1 μL, 10 mM in DMSO). After twenty-four hours the mixture was purified by ZipTip to remove excess small molecules, and analysed by HPLC, which revealed a significant peak shift from the starting material.

4.4.viii Attempted modification of PFP-containing poly(NIPAM) with 12

Post-polymerisation modification of a polymer synthesised using CTA **7** (see Chapter 6) was attempted as follows. Poly(NIPAM) (M_n 19.9 kDa, Đ 1.12 – **P17c**) (20 mg, 1 μmol), **12** (2 mg, 10 μmol) and TEA (0.5 mg, 5 μmol) were dissolved in anhydrous THF (0.25 mL) and stirred under nitrogen at 35°C for two hours, then for a further fifteen hours at room temperature. The solution was purified by preparatory SEC (Bio-Beads S-X1) and the polymer isolated, dried and analysed by ^{1}H NMR spectroscopy and DMF SEC. Both indicated that no reaction had taken place.

4.4.ix Perfluorophenyl 4-cyano-4-(dodecylthiocarbonothioylthio)-pentanoate, 14

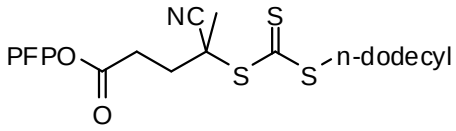

Perfluorophenyl 4-cyano-4-(dodecylthiocarbonothioylthio)pentanoate (**14**) was synthesised as follows.[21] **13** (0.5 g, 1.24 mmol) was added to an oven-dried flask under nitrogen. Anhydrous DMF (9 mL) was added followed by DIPEA (431 μL, 2.48 mmol). The mixture was cooled using an ice bath and pentafluorophenyl trifluoroacetate (255 μL, 1.49 mmol) was added dropwise with vigorous stirring. The reaction was allowed to proceed for one hour, then diethyl ether (40 mL) was added followed by 1 M HCl (40 mL). The organic layer was separated and washed with water (2 × 40 mL) and brine (40 mL). The solvent was then removed *in vacuo* and the residue purified by silica gel column chromatography, eluting with a mixture of hexane and diethyl ether (10:1). The product (R_f 0.21) was isolated as an orange viscous liquid (0.563 g, 80 %). ^{1}H NMR (300 MHz, $CDCl_3$) δ 3.34 (t, J = 7 Hz, 2H, SCH_2), 3.01 (m, 2H, CH_2CO_2PFP), 2.60 (m, 2H, $CH_2CH_2CO_2PFP$), 1.93 (s, 3H, $SCCH_3$), 1.70 (quint, J = 7 Hz, 2H, SCH_2CH_2), 1.40 (m, 2H, $SCH_2CH_2CH_2$), 1.26 (br s, 16H, $S(CH_2)_3(CH_2)_8CH_3$), 0.88 (t, J = 7 Hz, 3H, $S(CH_2)_{11}CH_3$) ppm. IR (ν_{max} / cm^{-1}) 2918, 2850, 1797, 1517, 1094, 990, 803. (These values compare well with the literature values

above, but are given because a significantly different method was used for the synthesis.)

4.4.x RAFT polymerisation of NIPAM using CTA 14

NIPAM (1 g, 8.84 mmol), **14** (50.3 mg, 0.09 mmol) and AIBN (1.5 mg, 0.01 mmol) were dissolved in 1,4-dioxane (2 mL) and the mixture degassed by three successive freeze-pump-thaw cycles. After warming to room temperature, the reaction vessel was sealed under nitrogen and placed in an oil bath heated to 65°C for four hours. The solution was diluted with THF (1 mL) and the polymer precipitated into diethyl ether (300 mL) cooled with an external dry ice bath. The solvent was decanted and the solid re-dissolved in THF (2 mL) and precipitated into cold diethyl ether once more. The product was isolated by filtration and drying as a pale yellow solid (841 mg, 84 %[#]), which was analysed by DMF SEC using PMMA calibration standards (M_n 13.0 kDa, Đ 1.05). ^{1}H NMR ($CDCl_3$, 400 MHz) δ 7.40-5.50 (br m, PNIPAM N*H*), 3.93 (br s, PNIPAM NHC*H*), 3.26 (br m, 2H, SCH_2), 2.80 (br m, 2H, CH_2CO$_2$PFP), 2.50-0.50 (br m, PNIPAM backbone *H* and NCH(CH_3)$_2$), 0.81 (t, *J* = 6 Hz, 3H, S(CH$_2$)$_{11}$CH_3) ppm. ^{19}F NMR ($CDCl_3$, 375 MHz) δ −152.6 (br s, 2F, ortho *F*), −157.6 (br s, 1F, para *F*), −162.1 (br s, 2F, meta *F*) ppm.

4.4.xi Modification of poly(NIPAM)–PFP with propargyl or benzyl alcohol

Either propargyl or benzyl alcohol was used, with cesium fluoride or DMAP as the catalyst. An example procedure follows. PFP-terminated poly(NIPAM) (M_n 10.0 kDa, **P10**) (50.0 mg, 5 μmol), benzyl alcohol (4.3 mg, 40 μmol) and DMAP (0.2 mg, 2 μmol) were dissolved in anhydrous THF (0.25 mL) and stirred under an atmosphere of nitrogen at room temperature for twenty-four hours. 18 MΩ water (10 mL) was added and the mixture dialysed against DI water (MWCO 1 kDa) incorporating five water changes. The product was isolated by freeze-drying as a white solid (34.0 mg, 68 %). The incorporation of the benzyl group was calculated to be 38 % by comparison of the PhCH_2O peak to the polymer NHC*H* peak in the ^{1}H NMR spectrum. ^{1}H NMR ($CDCl_3$, 400 MHz) δ 7.35 (br m,

[#] Based on 99 % monomer conversion as assessed by ^{1}H NMR spectroscopy at the end of the polymerisation.

1.9H, benzyl group *H*), 7.20-5.70 (br m, PNIPAM N*H*), 5.12 (br m, 0.76H, CO_2CH_2Ph), 4.00 (br s, PNIPAM NHC*H*), 3.34 (br m, 2H, SCH_2), 2.51 (br m, 2H, CH_2CO_2), 2.40-0.60 (br m, PNIPAM backbone *H*), 0.88 (t, J = 7 Hz, 3H, $S(CH_2)_{11}CH_3$) ppm.

4.4.xii Removal of the trithiocarbonate group from poly(NIPAM)–PFP

P10 (400 mg, 0.04 mmol), AIBN (657 mg, 4.00 mmol) and LPO (64 mg, 0.16 mmol) were dissolved in anhydrous THF (110 mL) and the solution degassed by bubbling with nitrogen for thirty minutes. The mixture was then heated to 65°C for six hours then allowed to cool and the solvent removed *in vacuo*. THF (1 mL) was added and the polymer precipitated into diethyl ether (300 mL) cooled with an external dry ice bath. The product was isolated by filtration and drying as a white solid (304 mg, 76 %), which was analysed by DMF SEC using PMMA calibration standards (M_n 13.8 kDa, Đ 1.07). ^{1}H NMR ($CDCl_3$, 400 MHz) δ 7.30-5.60 (br m, PNIPAM N*H*), 3.93 (br s, PNIPAM NHC*H*), 2.50-0.50 (br m, PNIPAM backbone *H* and $NHCH(CH_3)_2$) ppm. ^{19}F NMR ($CDCl_3$, 375 MHz) δ −152.6 (br s, 2F, ortho *F*), −157.6 (br s, 1F, para *F*), −162.1 (br s, 2F, meta *F*) ppm.

4.4.xiii Modification of poly(NIPAM)–PFP with 12

P11 (50.0 mg, 4 μmol), **12** (8.1 mg, 40 μmol) and DMAP (0.2 mg, 2 μmol) were dissolved in THF (0.25 mL) and the solution stirred under an atmosphere of nitrogen for twenty-four hours at room temperature. The solvent was then removed by blowing with compressed air and DMF (0.5 mL) was added. The polymer was then purified from excess small molecules by preparatory SEC (Bio-Beads S-X1) using DMF as the eluent. The fastest-eluting pink band was collected and dried down to yield the product as a light pink solid (41 mg, 82 %), which was analysed by DMF SEC using PMMA calibration standards (M_n 13.1 kDa, Đ 1.04). The incorporation of the Tz group was calculated to be 53 % by comparison of the $ArCH_2O$ peak to the polymer NHC*H* peak in the ^{1}H NMR spectrum. ^{1}H NMR ($CDCl_3$, 400 MHz) δ 8.60 (d, J = 8 Hz, 0.95H, Tz aromatic *H*), 7.57 (d, J = 7 Hz, 1.19H, Tz aromatic *H*), 7.20-5.60 (br m, PNIPAM N*H*), 5.23 (d, J = 6 Hz, 1.09H, CO_2CH_2Ar), 4.00

(br s, PNIPAM NHC*H*), 3.34 (br m, 2H, SCH_2), 3.11 (s, 1.60H, Tz-CH_3), 2.65-0.55 (br m, PNIPAM backbone *H* and NHCH(CH_3)$_2$), 0.88 (t, J = 7 Hz, 3H, S(CH$_2$)$_{11}$CH_3) ppm.

4.4.xiv Conjugation of s0–Nb to poly(NIPAM)–Tz

s0–Nb (0.5 μL, 70 μM in water) was mixed with the reaction solvent (5.0 μL) and poly(NIPAM)–Tz (0.5 μL, 14 mM in DMF) and left at room temperature for forty-eight hours. The mixture was diluted with water (35 μL) and 5 × glycerol loading buffer (10 μL) and analysed by 15 % native PAGE. The yield was calculated by densitometry after staining with SYBR Gold and visualisation under UV transillumination.

4.5 References

(1) Nicolaou, K. C.; Snyder, S. A.; Montagnon, T.; Vassilikogiannakis, G. *Angew. Chem., Int. Ed.* **2002**, *41*, 1668.

(2) Durmaz, H.; Colakoglu, B.; Tunca, U.; Hizal, G. *J. Polym. Sci., Part A: Polym. Chem.* **2006**, *44*, 1667.

(3) Dag, A.; Durmaz, H.; Tunca, U.; Hizal, G. *J. Polym. Sci., Part A: Polym. Chem.* **2009**, *47*, 178.

(4) Durmaz, H.; Dag, A.; Altintas, O.; Erdogan, T.; Hizal, G.; Tunca, U. *Macromolecules* **2006**, *40*, 191.

(5) Carboni, R. A.; Lindsey, R. V. *J. Am. Chem. Soc.* **1959**, *81*, 4342.

(6) Wijnen, J. W.; Zavarise, S.; Engberts, J. B. F. N.; Charton, M. *J. Org. Chem.* **1996**, *61*, 2001.

(7) Karver, M. R.; Weissleder, R.; Hilderbrand, S. A. *Bioconjugate Chem.* **2011**, *22*, 2263.

(8) Blackman, M. L.; Royzen, M.; Fox, J. M. *J. Am. Chem. Soc.* **2008**, *130*, 13518.

(9) Devaraj, N. K.; Weissleder, R.; Hilderbrand, S. A. *Bioconjugate Chem.* **2008**, *19*, 2297.

(10) Devaraj, N. K.; Upadhyay, R.; Haun, J. B.; Hilderbrand, S. A.; Weissleder, R. *Angew. Chem., Int. Ed.* **2009**, *48*, 7013.

(11) Devaraj, N. K.; Hilderbrand, S.; Upadhyay, R.; Mazitschek, R.; Weissleder, R. *Angew. Chem., Int. Ed.* **2010**, *49*, 2869.

(12) Hansell, C. F.; O'Reilly, R. K. *ACS Macro Lett.* **2012**, *1*, 896.

(13) Han, H.-S.; Devaraj, N. K.; Lee, J.; Hilderbrand, S. A.; Weissleder, R.; Bawendi, M. G. *J. Am. Chem. Soc.* **2010**, *132*, 7838.

(14) Schoch, J.; Wiessler, M.; Jäschke, A. *J. Am. Chem. Soc.* **2010**, *132*, 8846.

(15) Hansell, C. F.; Espeel, P.; Stamenović, M. M.; Barker, I. A.; Dove, A. P.; Du Prez, F. E.; O'Reilly, R. K. *J. Am. Chem. Soc.* **2011**, *133*, 13828.

(16) Stamenović, M. M.; Espeel, P.; Camp, W. V.; Du Prez, F. E. *Macromolecules* **2011**, *44*, 5619.

(17) Sanders, D. P.; Fukushima, K.; Coady, D. J.; Nelson, A.; Fujiwara, M.; Yasumoto, M.; Hedrick, J. L. *J. Am. Chem. Soc.* **2010**, *132*, 14724.

(18) Sanders, D. P.; Hedrick, J. L.; Yasumoto, M.; Fujiwara, M. (International Business Machines Corporation, USA; IBM United Kingdom Limited; Central Glass Co., Ltd.). Cyclic carbonyl compounds with pendant carbonate groups, preparations thereof, and polymers therefrom. Patent No.: WO2011135046A1, 2011.

(19) Fujiwara, M.; Hedrick, J.; Sanders, D.; Terui, Y.; Yasumoto, M. (International Business Machines Corp., USA; Central Glass Co., Ltd.). Cyclic carbonyl compounds bearing pendant pentafluorophenyl ester groups, their functionalization and ring-opening polymerization. Patent No.: WO2011136872A1, 2011.

(20) Eberhardt, M.; Mruk, R.; Zentel, R.; Théato, P. *Eur. Polym. J.* **2005**, *41*, 1569.

(21) Pötzsch, R.; Fleischmann, S.; Tock, C.; Komber, H.; Voit, B. I. *Macromolecules* **2011**, *44*,

3260.

(22) Panne, P.; Fox, J. M. *J. Am. Chem. Soc.* **2006**, *129*, 22.

Chapter 5

DNA–polymer conjugation using the CuAAC reaction

5.1 Introduction

The copper-catalysed azide–alkyne cycloaddition (CuAAC) reaction has been known for more than a decade, and it remains one of the most popular methods of chemical ligation.[1,2] Its popularity stems from several key properties: it can be performed under mild conditions (room temperature), using water as the solvent; conversion is very high (often quantitative); the reaction is very fast (typically taking under a hour to reach completion); a wide range of functional groups are tolerated; and the process is highly atom efficient. All of these mean it qualifies as one of Sharpless *et al.*'s 'Click' reactions,[3] and, perhaps because of this tag, has found a wide array of applications from small molecule synthesis to polymerisation to protein modification.[4] The mechanism (Scheme 5.1) relies on the use of a terminal alkyne, and the 1,4-regioisomer is selectively produced over the 1,3 version.[5-7]

Recently, there has also been a lot of interest in the use of the CuAAC reaction for the modification of polymers,[8,9] to introduce side chains or terminal groups that would otherwise be incompatible with radical polymerisation techniques, to attach the polymer to a surface for microarray applications,[10,11] or achieve efficient macromolecular coupling of polymers.[7] There has also been a great deal of interest in the modification of DNA strands using this chemistry,[12-15] and alkyne- and azide-functionalised oligonucleotides are now widely commercially available. Using a single DNA scaffold, a multitude of functional structures can be synthesised by employing the CuAAC reaction post-assembly. Mirkin *et al.* have used the CuAAC reaction to synthesise 'programmable atom equivalents' – nanoparticles bearing a corona of single stranded DNA.[16] DNA has also been used to template the azide–alkyne cycloaddition.[17]

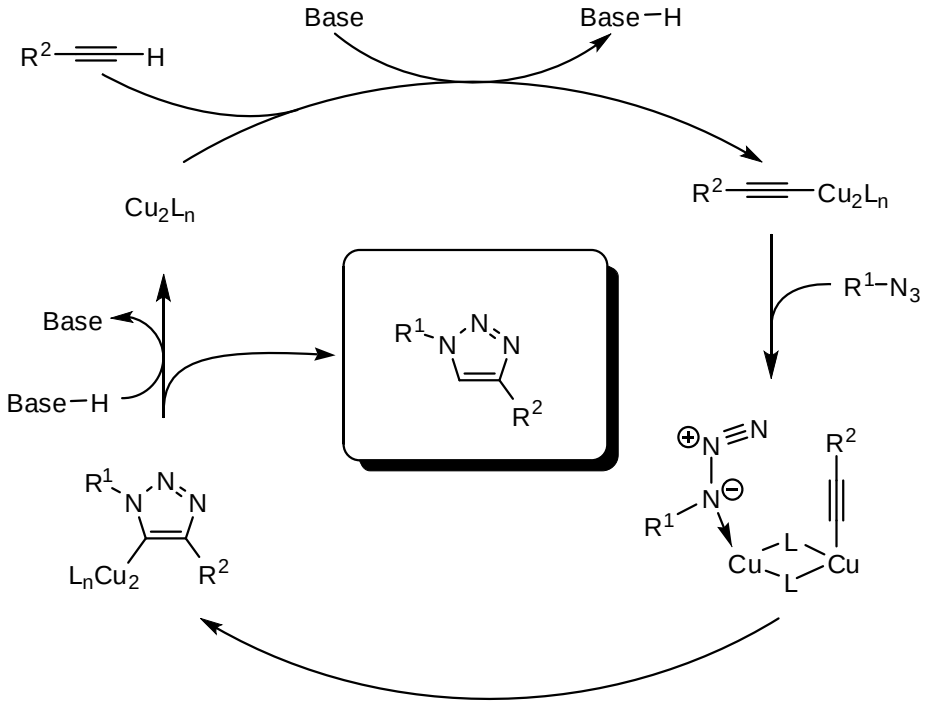

Scheme 5.1 Simplified catalytic cycle for the copper-catalysed azide–alkyne cycloaddition (CuAAC) reaction. The 1,4-regioisomer (outlined) is produced selectively.

Of particular interest to the present work is the conjugation of polymers to proteins using CuAAC.[18-20] The principle of combining the structural and functional precision of the latter with the diverse physical and chemical properties of the former is very attractive. However, while proteins are undoubtedly more interesting to chemists in terms of their potential properties (catalysis, signalling, energy storage and so on) than is DNA, the scientific community currently lacks the ability to programme protein–protein interactions and thus design higher order assemblies of these conjugates. DNA, by contrast, is straightforward to control in this manner.[21] Given the popularity of CuAAC for protein–polymer conjugation, it is, then, surprising to find so few examples of the use of this chemistry for DNA–polymer conjugation. Indeed, yields for the DNA conjugation were excellent (almost quantitative) but the chemistry was limited to use in an aqueous environment.[22] It was decided that the CuAAC reaction may provide an extremely efficient route to DNA–polymer conjugates, particularly if the use of organic solvent systems was explored, since this would enable the conjugation of hydrophobic polymers – a previously unrealised goal

using this chemistry. A thorough study of the effects of ligand, copper source, solvent and the locations of the functional groups (i.e. on the polymer or on the DNA strand) was therefore undertaken, as described below.

5.2 Results & Discussion

5.2.i Synthesis of alkyne-containing polymers

The alkyne group is stable towards RAFT polymerisation conditions,[23-25] so a suitable CTA (Figure 5.1, **15**) was identified that contained the group and would result in its insertion into the R group of the polymeric product.

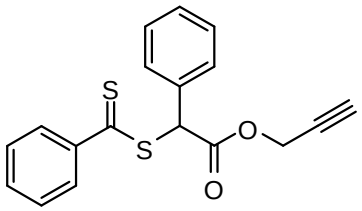

15

Figure 5.1 Structure of the CTA used to produce polymers containing an alkyne group.

Table 5.1 summarises the properties of the polymers synthesised using CTA **15**. Both polymers were of controlled molecular weight and dispersity.

Table 5.1 Properties of polymers synthesised using the alkyne-containing CTA, **15**. DPs were determined by ^{1}H NMR by comparison of the integrals of the alkyne C≡C–H peak with signals due to the Hs in the polymer backbone. * Determined using THF SEC with PS calibration standards. † Determined using DMF SEC with PMMA calibration standards.

Polymer	Type	DP^{NMR}	M_n^{NMR} / kDa	M_n^{SEC} / kDa	Đ
P12	poly(styrene)	39	4.4	3.6*	1.12*
P13	poly(NIPAM)	61	7.3	6.9†	1.16†

The presence of the alkyne group in the final polymer products was confirmed using ^{1}H NMR spectroscopy. The alkyne proton displayed a characteristic signal at 2.34 ppm and the CH_2 group next to the ester group was also visible as part of a broad multiplet between 4.3-4.7 ppm – see Figure 5.2.

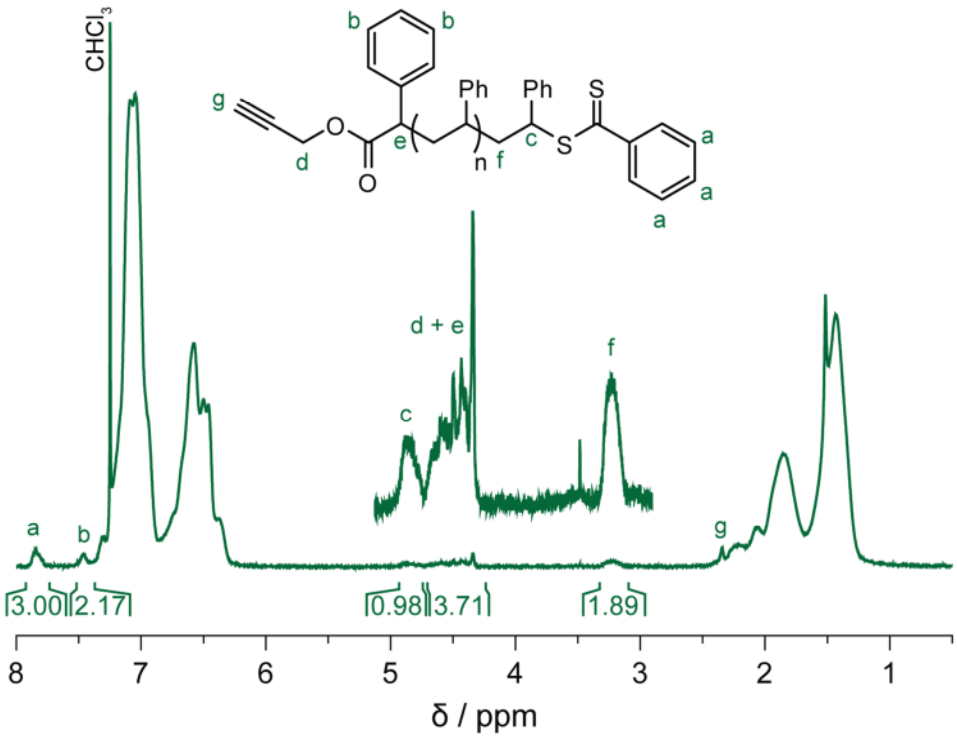

Figure 5.2 ^{1}H NMR spectrum of alkyne-functionalised poly(styrene) (**P12**) synthesised using CTA **15**. All the expected peaks due to the polymer end groups were observable except for some of the aromatic signals, which were obscured by those from the polymer. Solvent: $CDCl_3$.

5.2.ii Synthesis of azide-containing polymers

Initially, the synthesis of azide-containing polymers was approached in the same way as that used above: the azide group was incorporated into a trithiocarbonate CTA (Figure 5.3, **16**), which was then used to control the RAFT polymerisation of dimethylacrylamide (DMA), NIPAM and styrene.

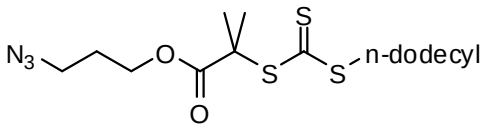

16

Figure 5.3 Structure of the CTA used to produce polymers containing an azide group.

The CTA **16** was obtained by esterification of DDMAT with 3-azidopropan-1-ol. FTIR spectroscopy confirmed the presence of the azide as this group exhibits a characteristic stretch at 2 100 cm^{-1} (see Figure 5.4).[10] Conveniently, this region of the IR spectrum is

usually free of other peaks, so the presence or absence of an azide in even a high molecular weight polymer could quickly be confirmed.

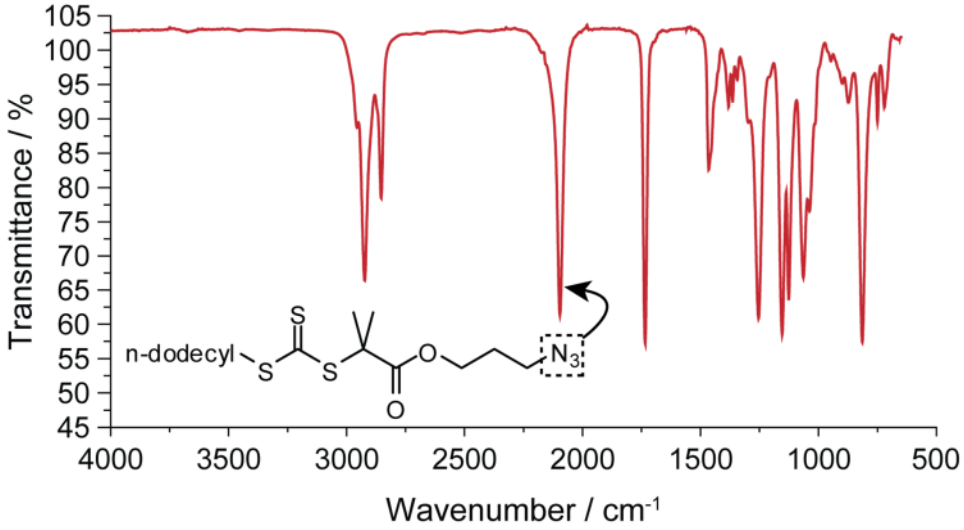

Figure 5.4 FTIR spectrum of CTA **16**, showing the prominent azide N–N stretch at 2 100 cm^{-1}.

Table 5.2 summarises the properties of the polymers synthesised using CTA **16**. Good control was achieved over molecular weight and dispersity.

Table 5.2 Properties of polymers synthesised using the azide-containing CTA, **16**. DPs were determined by ^{1}H NMR by comparison of the integrals of the CH_2 groups at the chain ends with signals due to the Hs in the polymer backbone. * Determined using THF SEC with PS calibration standards. † Determined using DMF SEC with PMMA calibration standards.

Polymer	Type	DP^{NMR}	M_n^{NMR} / kDa	M_n^{SEC} / kDa	Đ
P14	poly(DMA)	90	9.4	7.8†	1.13†
P15	poly(NIPAM)	90	10.6	8.5†	1.16†
P16	poly(styrene)	117	12.6	13.3*	1.09*

FTIR showed small azide peaks for all of the polymers synthesised above (see Figure 5.5). However, since neither this technique nor ^{1}H NMR spectroscopy could quantify the degree of azide functionalisation, the stability of the azide CTA towards RAFT polymerisation conditions was tested. CTA **16** was mixed with AIBN in 1,4-dioxane and heated to 65°C under a nitrogen atmosphere for six hours. The CTA was then re-isolated from the

solution and the ^{1}H NMR spectra compared from before and after the reaction (see Figure 5.6).

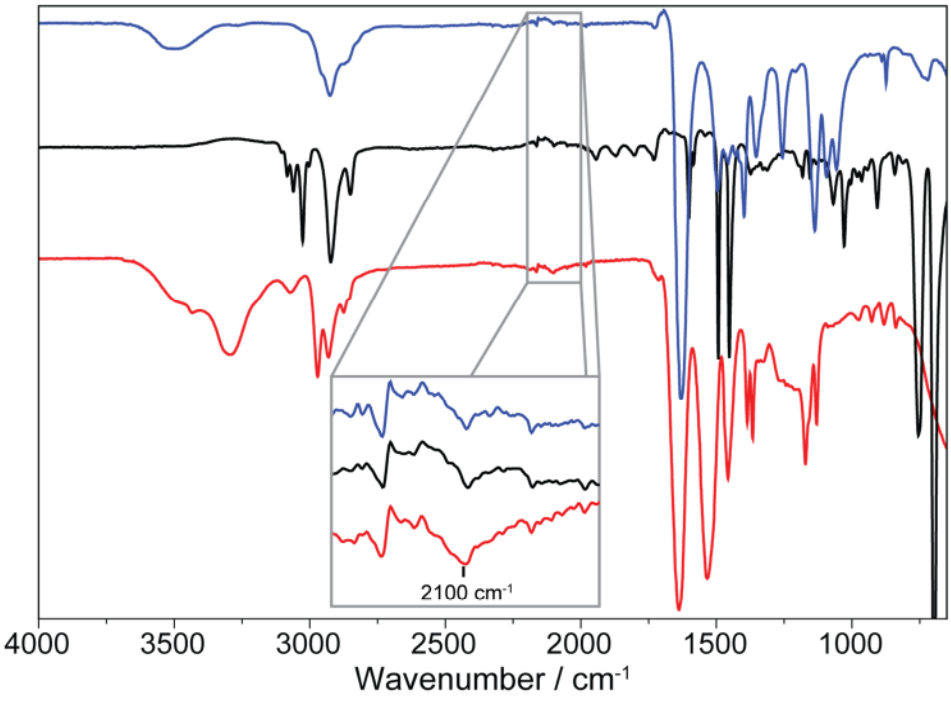

Figure 5.5 FTIR spectrum showing the presence of the azide group in the polymers synthesised using CTA **16** detailed in Table 5.2. Blue trace: **P14**, poly(DMA). Black trace: **P16**, poly(styrene). Red trace: **P15**, poly(NIPAM).

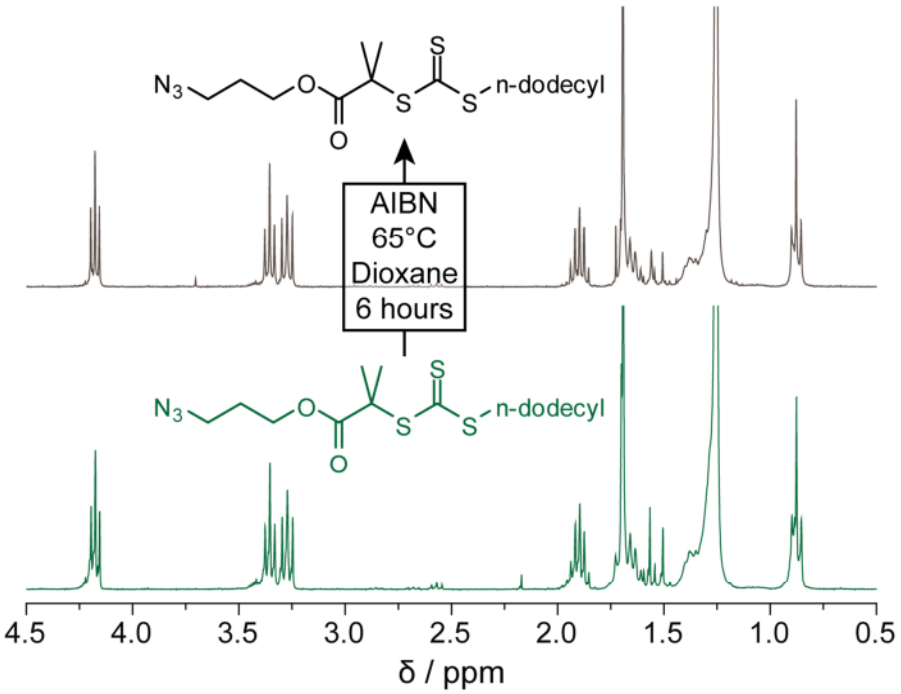

Figure 5.6 ^{1}H NMR spectra showing that there is no noticeable degradation of CTA **16** upon exposure to RAFT polymerisation conditions in the absence of monomer.

The CTA does not appear to degrade under the polymerisation conditions (degradation would have been expected to cause the signal due to the CH_2 group adjacent to the azide to shift and/or change shape); however, the reaction of the azide group with various common monomers has been reported,[26] and so an alternative route to azide-functionalised polymers was sought in order that the degree of azide incorporation could be better quantified. In order to avoid potential monomer–azide interactions, a post-polymerisation modification strategy was adopted utilising the PFP-functionalised CTA (**7**) synthesised in Chapter 2, as outlined in Scheme 5.2.

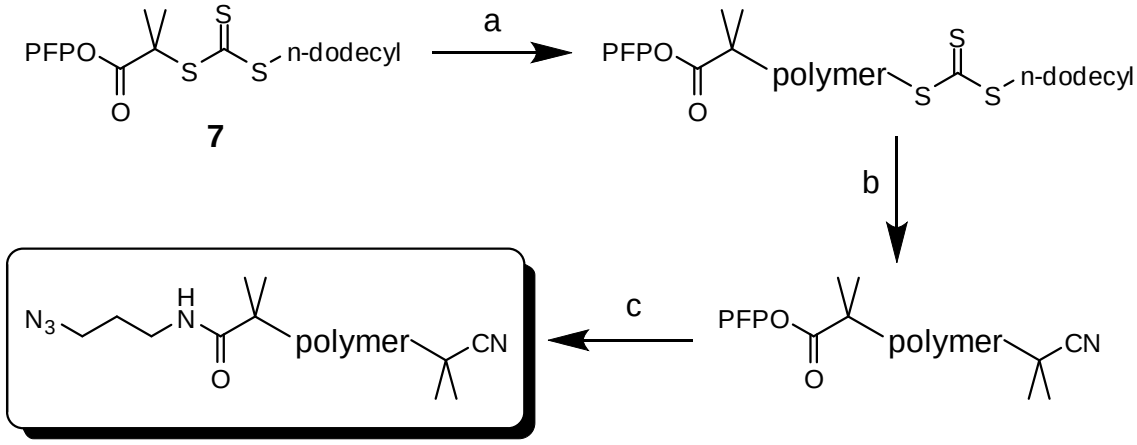

Scheme 5.2 Procedure for the synthesis of azide-containing polymers by post-polymerisation modification. Step a) RAFT polymerisation using a PFP-containing CTA; b) removal of the trithiocarbonate group; c) substitution of the PFP group with a primary amine containing the azide functionality.

Six polymers were synthesised (see Table 5.3) using the route above, all of which exhibited near quantitative conversion to the amide, as assessed by ^{1}H NMR spectroscopy. The water soluble polymers were purified by extensive dialysis against 18 MΩ water to remove the excess small molecule azide; the poly(styrene) was repeatedly precipitated from cold methanol to the same end. Figure 5.7 shows ^{1}H NMR analyses demonstrating the steps in Scheme 5.2. Removal of the trithiocarbonate group is evidenced by the disappearance of the triplet at 3.35 ppm. The appearance of new signals in this region after the introduction of 3-azido-1-aminopropane proves that the substitution of the PFP group had been successful.

Table 5.3 Properties of the polymers synthesised containing an azide end group. All polymers were analysed using DMF SEC with PMMA calibration standards, except for **P20**, which was analysed using THF SEC with PS standards. DPs were estimated by ^{1}H NMR by comparing the integral of the SCH_2 group in the starting polymer with that of the following groups: NIPAM – C*H*$(CH_3)_2$; DMA – N(C*H*$_3)_2$; 4-acryloyl morpholine (4-AM) – NC*H*$_2$C*H*$_2$O; styrene – Ph group. * It was not possible to quantify the degree of azide incorporation for **P19** since the end group signals lie underneath those due to the polymer side chain; however, the group was observed by FTIR.

Polymer	Type	DP^{NMR}	M_n^{NMR} / kDa	M_n^{SEC} / kDa	Đ	Azide incorporation
P17a	poly(NIPAM)	45	5.6	5.6	1.07	97 %
P17b	poly(NIPAM)	84	10.0	8.0	1.09	95 %
P17c	poly(NIPAM)	148	17.3	15.3	1.09	92 %
P18	poly(DMA)	67	7.2	11.1	1.09	94 %
P19	poly(4-AM)	94	13.8	9.3	1.11	N/A*
P20	poly(styrene)	87	9.6	8.1	1.08	89 %

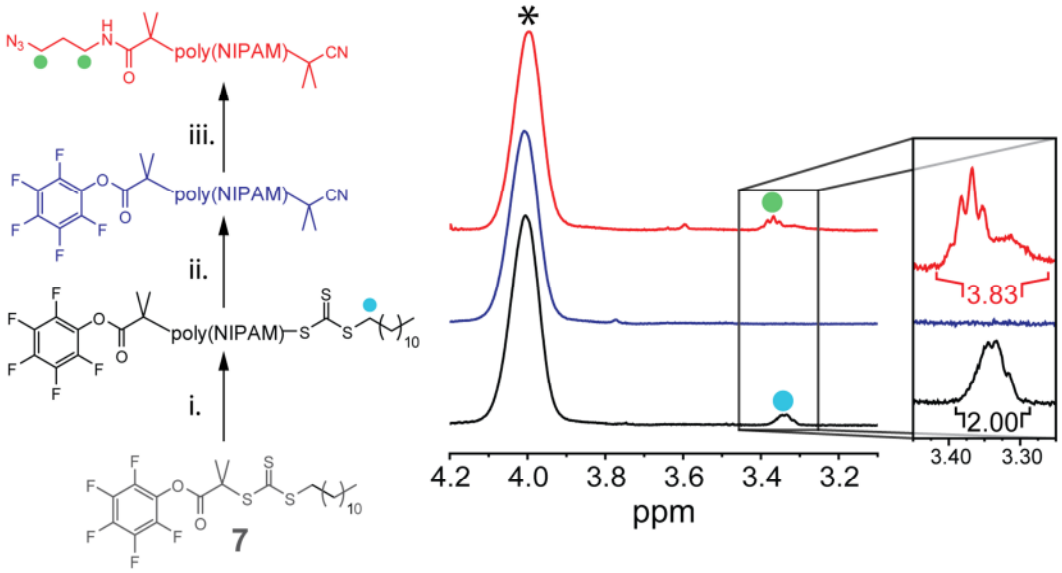

Figure 5.7 ^{1}H NMR spectra showing the synthesis of azide-capped poly(NIPAM) from a PFP-containing CTA (**7**) (Solvent: $CDCl_3$). NIPAM is first polymerised using **7**; the trithiocarbonate group is then removed; finally, the PFP activated ester is substituted with an azide-containing amine. The peak labelled * corresponds to the C*H*$(CH_3)_2$ group in poly(NIPAM). Reaction conditions: i) NIPAM (100 eq. w.r.t. **7**), AIBN (0.1 eq.), 1,4-dioxane (1.5 mL per gram of monomer), N_2, 65°C, 2 hours; ii) AIBN (100 eq.), LPO (4 eq.), toluene, N_2, 80°C, 5 hours; iii) 3-azido-1-aminopropane (5 eq.), TEA (2.5 eq.), THF, 35°C to RT, 17 hours.

Comparing the IR traces of a polymer synthesised using CTA **16** and *via* the PFP ester using CTA **7** revealed the enhanced incorporation of this group – Figure 5.8 shows that the azide stretch at 2 100 cm^{-1} was much stronger in the latter case (the polymers compared were of similar molecular weight). This confirmed that the azide group was indeed being degraded during RAFT polymerisation and provided further vindication for adopting the post-polymerisation modification route.

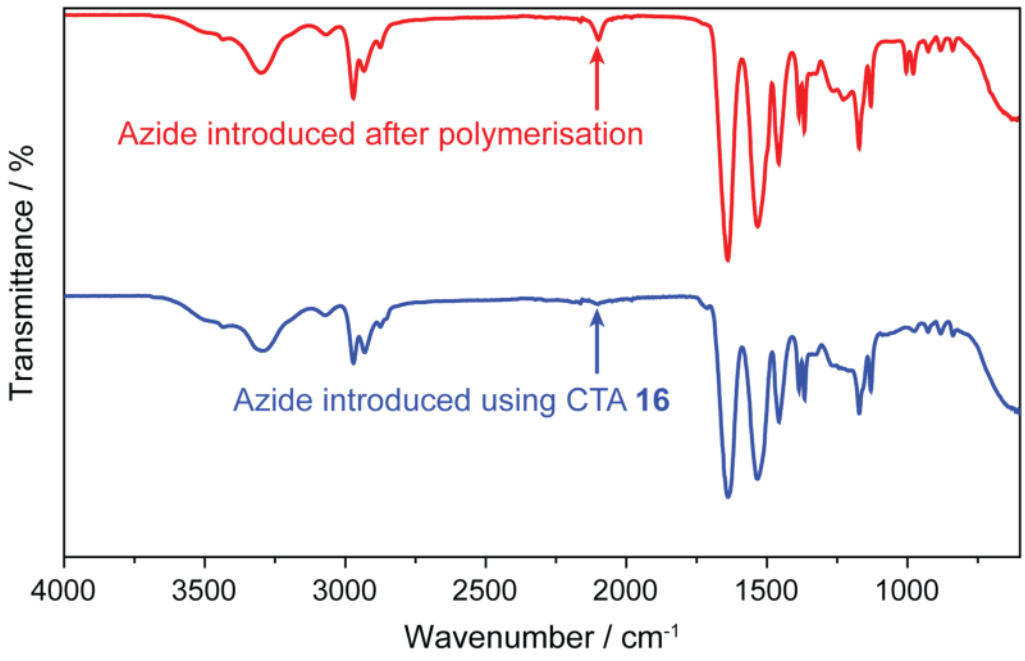

Figure 5.8 Comparison of the IR spectra of poly(NIPAM)–N_3 synthesised using CTA **16** (**P15**, blue) and *via* the PFP ester using CTA **7** (**P17b**, red). The azide stretching mode (2 100 cm^{-1}) was much stronger when the group was introduced post-polymerisation.

5.2.iii Catalyst testing

The CuAAC reaction has been extensively used in aqueous media to achieve efficient macro-molecular coupling[7] – including DNA–DNA coupling and nucleotide modification (as exemplified by the work of Brown *et al.*[12,13]) – but has been less successful in organic solvents. It has been suggested that the formation of the active copper species is much more difficult in these systems due to the strongly coordinating nature of the solvent,[27] so with this is in mind a variety of catalyst combinations were tested in the hope of identifying one that would be effective for DNA–polymer conjugation.

N,*N*-dimethylformamide (DMF), dimethylsulfoxide (DMSO) and tetrahydrofuran (THF) were all tested as the reaction solvent. A strand of 22 nucleotides in length with a 5' azide modification (s0–azide – base sequence given in Figure 5.9) and alkyne-functionalised poly(NIPAM) (see Table 5.1, **P13**) were used for all initial catalyst testing.

s0-azide = 5'- N_3-GCC CGA AAT ACC CCG TTA GAA A -3'

Figure 5.9 Base sequence of the DNA strand s0–azide used in this work.

Of the catalysts tested (Table 5.4), only one was found to be effective in producing the desired product: copper iodide triethyl phosphite ($CuI \cdot P(OEt)_3$).

Table 5.4 Catalyst combinations tested for the CuAAC reaction between azide-functionalised DNA (s0–azide) and alkyne-functionalised poly(NIPAM) (**P13**). NHPMI = *N*-(*n*-hexyl)-2-pyridylmethanimine. THPTA = *tris*-(hydroxypropyltriazolylmethyl)amine. PMDETA = *N*,*N*,*N*',*N*',*N*''-pentamethyldiethylenetriamine. BiPy = 2,2'-bipyridine.

Reaction #	Catalyst	Solvent
1a		DMF
1b	Cu(I)Br/THPTA	THF
1c		DMSO
1d		DMF
1e	Cu(I)Br/PMDETA	THF
1f		DMSO
1g		DMF
1h	Cu(I)Br/NHPMI/TEA	THF
1i		DMSO
1j		DMF
1k	$CuI \cdot P(OEt)_3$	THF
1l		DMSO
1m		DMF
1n	Cu(I)Br/BiPy/TEA	THF
1o		DMSO

Unlike the other combinations trialled, this species contained a pre-complexed copper (I) centre, so the active catalyst was already formed when the solution was added to the reaction mixture.In the case of every other catalyst system investigated, the active species needed to be formed *in situ*, and it is believed that it was this step that was slow and causing the reaction to become inefficient. Figure 5.10 shows the 15 % native PAGE analysis of reactions 1a-o.

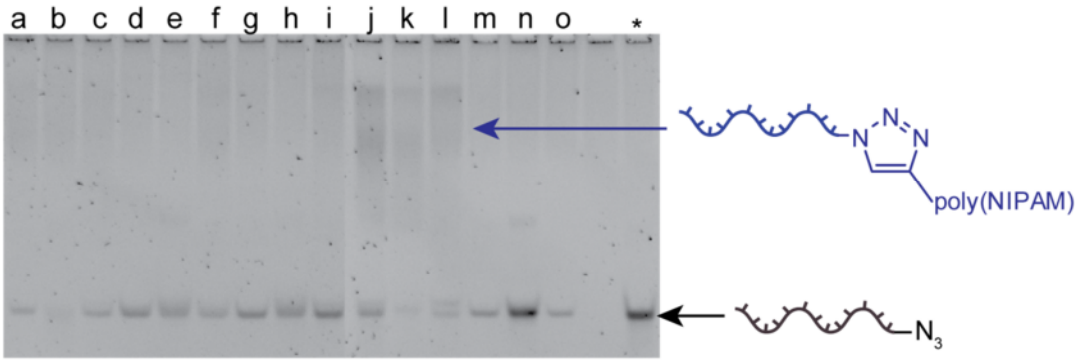

Figure 5.10 15 % native PAGE analysis of the CuAAC reactions detailed in Table 5.4 (lane a corresponds to reaction 1a and so on). The DNA–polymer conjugate manifests itself as a broad, low-mobility band. Lane * contains s0–azide DNA as a negative control.

The DNA–polymer conjugate was clearly visible in lanes j-l as a broad, low-mobility band (which is in line with the results from Chapter 2).

5.2.iv Catalyst optimisation

Having identified a suitable catalyst for the CuAAC reaction, further optimisation of the reaction conditions was then carried out by testing more solvents and varying the number of equivalents of polymer and catalyst used – see Table 5.5. 15 % native PAGE analysis of the reactions mixtures is shown in Figure 5.11. The reaction works extremely well (up to 90 % yield according to densitometry) in DMF, DMSO and NMP. Some product is observed in MeCN, but the yields are very much lower. No product is observed when THF is used; the volatility of this solvent also makes working on small reaction scales (i.e. 10 μL or less) extremely difficult. The overall trend indicates that more polar solvents increase the efficiency of the reaction. Whilst it would be useful for the reaction to proceed in THF

(since this is generally a good solvent for most polymers), the fact that it does not should have little impact on the general applicability of this chemistry: it will almost always be the case that at least one of the three high-yielding solvents will dissolve the polymer of interest.

Table 5.5 Reactions conditions used in catalyst optimisation for DNA–polymer conjugation *via* CuAAC.

Reaction #	[Polymer] / μM	[CuI · P(OEt)$_3$] / μM	Solvent
2a	1000	1000	DMF
2b	5000		
2c	1000	5000	
2d	5000		
2e	1000	1000	DMSO
2f	5000		
2g	1000	5000	
2h	5000		
2i	1000	1000	MeCN
2j	5000		
2k	1000	5000	
2l	5000		
2m	1000	1000	NMP
2n	5000		
2o	1000	5000	
2p	5000		
2q	1000	1000	THF
2r	5000		
2s	1000	5000	
2t	5000		

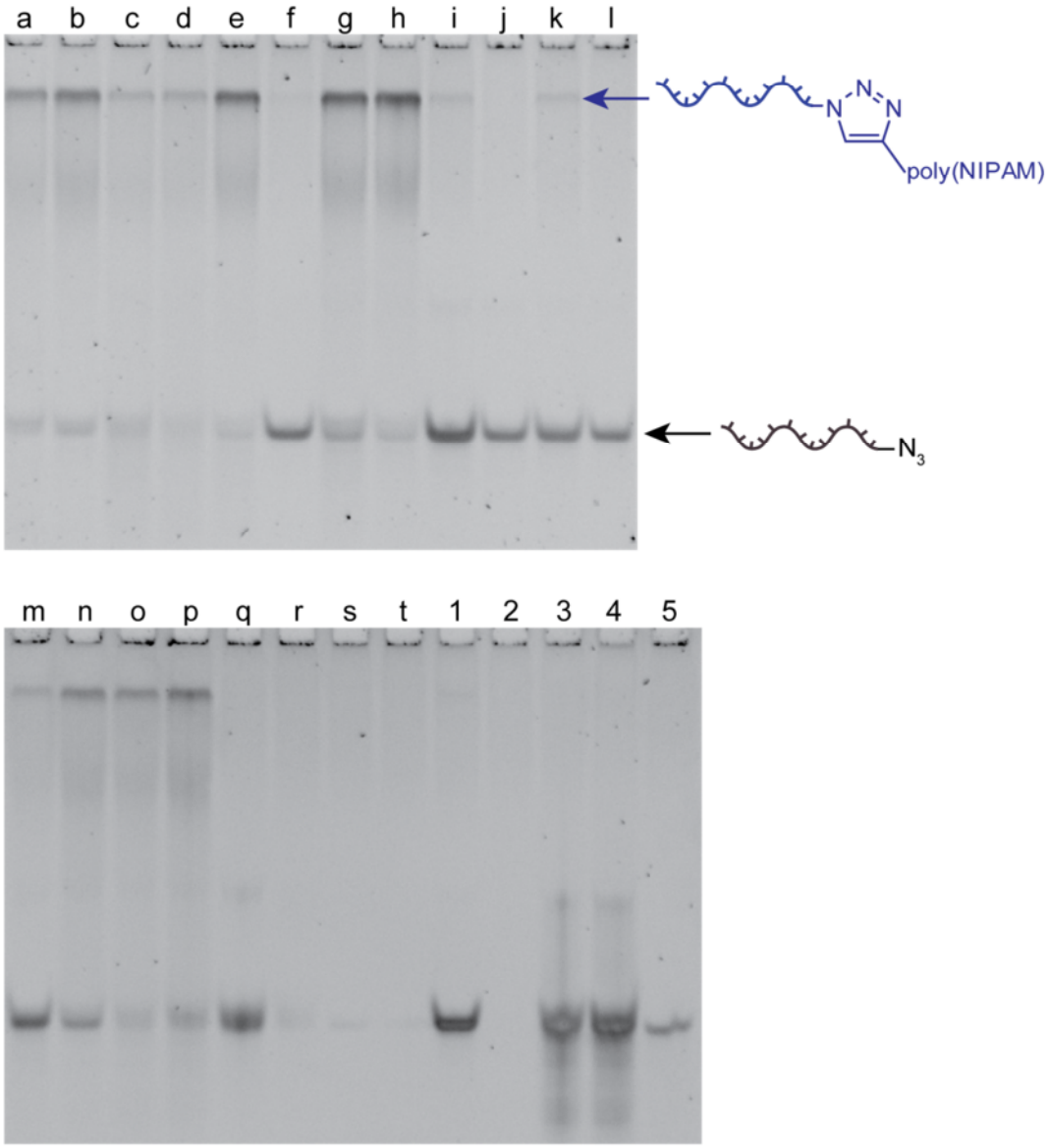

Figure 5.11 15 % native PAGE analysis showing the optimization of catalyst conditions for the synthesis of DNA–polymer conjugates via CuAAC. Lanes a-t: reaction mixtures as detailed in Table 5.5 (lane a corresponds to reaction 2a and so on); lane 1: s0–azide DNA + P13 (no catalyst); lane 2: alkyne poly(NIPAM); lane 3: s0–azide DNA + CuI · $P(OEt)_3$; lane 4: s0–NH_2 DNA + P13 + CuI · $P(OEt)_3$; lane 5: s0–azide DNA.

Lanes one to five in Figure 5.11 also provide confirmation that the band due to the DNA–polymer conjugate has been correctly identified. Lane one shows that no conjugate is formed in the absence of the CuAAC catalyst. Lane two confirms that the free polymer does not bind the dye used for visualisation of the PAGE gel (SYBR Gold). Lane three shows that the catalyst does not cause degradation or oligomerisation of the azide DNA. Lane four contains a mixture of all the normal CuAAC reaction components, except that

the azide DNA has been replaced with amine DNA – this proves that the CuAAC reaction is responsible for the product. Lane five contains only azide DNA. Taken together, these results lead to the conclusion that the new, low-mobility band on the PAGE gel must be due to the DNA–polymer conjugate.

5.2.v Effect of the position of the azide group

To ascertain whether the position of the azide group (i.e. at the polymer chain end or on the DNA strand) had any effect on the efficiency of the reaction, the coupling was repeated in DMF under identical conditions to those above, but using alkyne-functionalised DNA (s0–alkyne – see Figure 5.12 for base sequence) and azide-functionalised poly(NIPAM).

```
s0-alkyne =  5'- alkyne-GCC CGA AAT ACC CCG TTA GAA A -3'
```

Figure 5.12 Base sequence of the DNA strand s0–alkyne used in this work.

Native PAGE (see Figure 5.13) revealed that there was (within experimental error) no difference in the coupling efficiency – that is, the reaction was independent of the locations of the two functional groups.

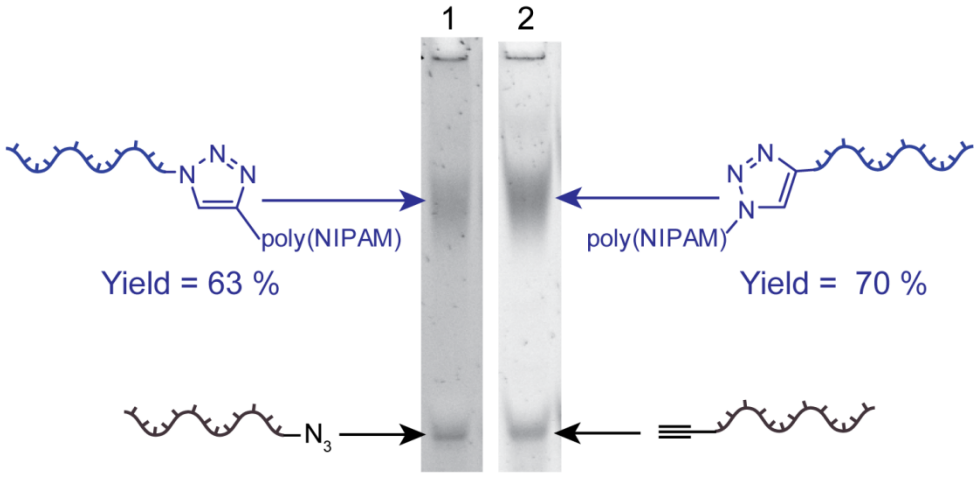

Figure 5.13 15 % native PAGE analyses of the synthesis of DNA–poly(NIPAM) conjugates by CuAAC in DMF. Both polymers were of approximately the same molecular weight (7 kDa) and functionalised with either an alkyne (**P13**, lane one) or azide (**P17a**, lane two) group. All other experimental conditions (catalyst, equivalents and concentrations of reagents) were identical. Yields were estimated by densitometry.

These results confirm the versatility of the CuAAC reaction in this context – in contrast to the amide coupling chemistries employed in Chapter 2, this chemistry gives reproducible results and is not sensitive to small variations in the experimental conditions. In terms of accessibility, it is also useful that the reaction works so well with alkyne-functionalised DNA, since this is much less expensive than its azide counterpart.

During initial experiments using azide-functionalised polymers and alkyne DNA low yields were encountered. It was noticed that the band due to the starting material DNA was in these cases slightly retarded or even visibly split in two (see Figure 5.14). It was hypothesised that this was due to the presence of trace amounts of the small molecule azide in the polymer samples (which were not, however, visible by NMR spectroscopy), which reacted much more quickly with the alkyne DNA than the bulky polymer chain end. Further purification was, therefore, carried out. Both dialysis and repeat precipitation of the polymers were explored; the former was found to be far more effective in removing trace impurities and also gave higher recoveries.

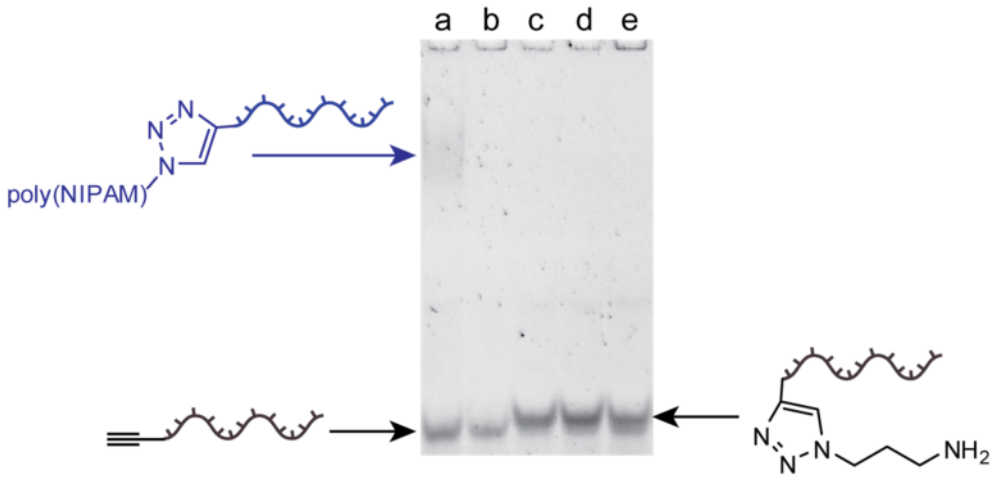

Figure 5.14 15 % native PAGE gel showing a successful DNA–polymer conjugation reaction (lane a), starting material s0–NH_2 DNA (lane b) and three failed coupling reactions (lanes c, d and e). Failed couplings exhibit a second, slightly retarded band, which is attributed to the reaction product of the alkyne DNA with the small molecule azide used to perform the polymer end group modification reaction.

5.2.vi Glaser homocoupling of alkyne DNA

Whilst the synthesis of DNA–polymer conjugates using s0–alkyne was being investigated, it was noticed that a new, unidentified band was present during PAGE analysis (see Figure 5.15 B). This band migrated more slowly than the starting material DNA, but was narrow, suggesting that it was not due to a polymer-coupled product.

To ascertain whether the emergence of the unknown product was dependent on the type of polymer used in the coupling reaction, several reactions were set up using different azide-functionalised polymers (see Table 5.6). The reaction mixtures were then analysed by HPLC. As shown in Figure 5.15 A the same impurity was observed for all reactions, regardless of the polymer used.

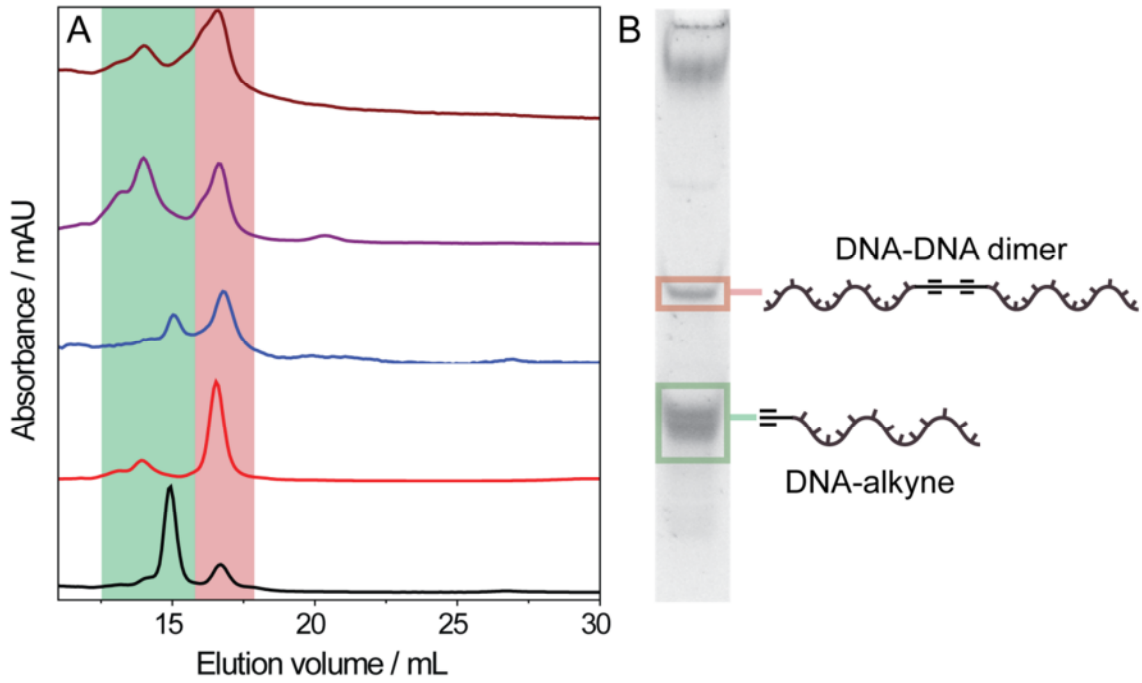

Figure 5.15 A: HPLC analyses of the reaction mixtures detailed in Table 5.6 – The material within the green band is starting material DNA and that within the red band the Glaser homocoupling product. **B**: 15 % native PAGE analysis showing the presence of the DNA–DNA dimer.

Table 5.6 Polymers used in the reactions analysed by HPLC as shown in Figure 5.15. All reactions contained 10 μM s0–alkyne DNA, 1 mM polymer, and 1 mM CuI · $P(OEt)_3$ in DMF. * Synthesised using CTA **16**. † Synthesised by post-polymerisation modification of polymers made using CTA **7**.

Reaction #	Polymer	Type
3a	**P16**	poly(styrene)*
3b	**P15**	poly(NIPAM)*
3c	**P20**	poly(styrene)†
3d	**P18**	poly(DMA)†
3e	**P17a**	poly(NIPAM)†

Since the only other components present in the reaction was the DNA and the copper catalyst, it was concluded that Glaser coupling must have been occurring between the alkynes attached to the DNA. The DNA dimerisation explains the presence of the new, higher molecular weight band in the PAGE analysis. The Glaser reaction occurs when two terminal alkynes are mixed with a copper (I) salt in the presence of an oxidant (in this case molecular oxygen) and results in the formation of an alkyne dimer as shown in Figure 5.16.[28] Copper iodide triethyl phosphite has never, to the author's knowledge, been reported as a catalyst of the Glaser reaction, but its efficacy is not surprising given that it contains a copper (I) salt.

The Glaser coupling does not occur in the absence of oxygen, so to test the hypothesis s0–alkyne DNA was mixed in DMF either with or without initial degassing of the solvent (by bubbling with compressed air or nitrogen, respectively, for 30 minutes). As Figure 5.16 demonstrates, the new band was much more prominent when oxygen was present in the system. DNA–DNA dimerisation by the Glaser oxidation therefore seems a robust explanation for the new band in PAGE analysis. Further, indirect, confirmation of this theory arises from the fact that this band was never observed when s0–azide DNA was used (it is highly probable that polymer–polymer coupling was occurring in this case,

however).

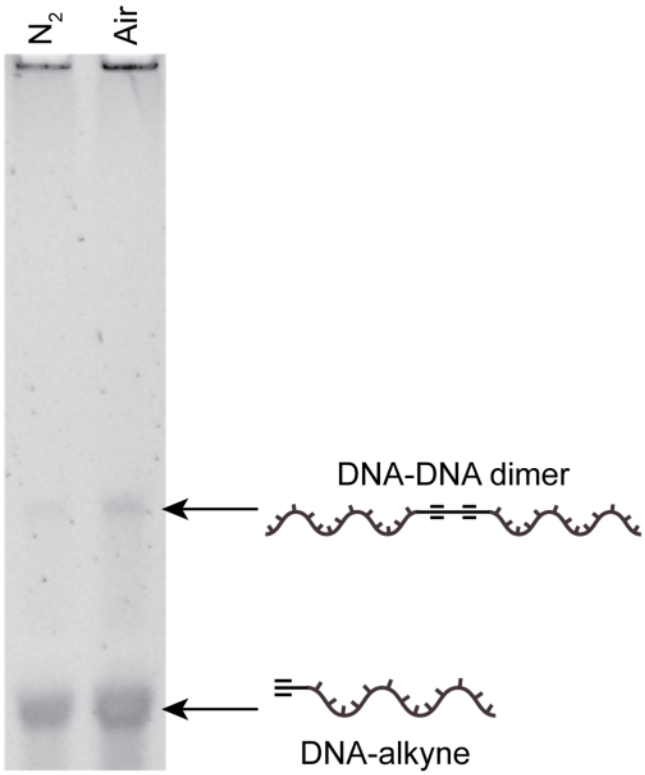

Figure 5.16 15 % native PAGE analysis of mixtures of s0–alkyne DNA with CuI · $P(OEt)_3$ in DMF bubbled with either nitrogen (left hand lane) or compressed air (right hand lane) for 30 minutes. A much larger degree of DNA–DNA coupling was observed in the presence of oxygen, providing strong support for the theory that the Glaser oxidation was occurring.

5.2.vii Coupling of other polymers to DNA using CuAAC

To test the versatility of the chemistry, the conjugation of three further polymers was attempted. First, poly(DMA) and poly(4-AM) were synthesised as described in Section 5.2.ii containing a terminal azide group. Both of these polymers are permanently hydrophilic (i.e. they exhibit no temperature responsive behaviour) and there is some evidence that they may be useful for the synthesis of biocompatible coatings.[29] Other hydrophilic polymers, most notably poly(ethylene oxide) (commonly referred to as PEO or PEG) have been used extensively in the literature to protect DNA from degradation *in vivo*, and also to impart so-called stealth properties to polymer nanoparticles intended for use as drug delivery agents.[30-35] It was therefore thought that the efficient conjugation of these polymers to DNA may prove to be useful.

Figure 5.17 shows PAGE analyses of the conjugation reactions between s0–alkyne and azide-functionalised poly(DMA) and poly(4-AM). The reactions proceeded efficiently, with yields of around 50 % estimated by densitometry. These results proved that the CuAAC reaction is generally applicable to the synthesis of hydrophilic DNA–polymer conjugates.

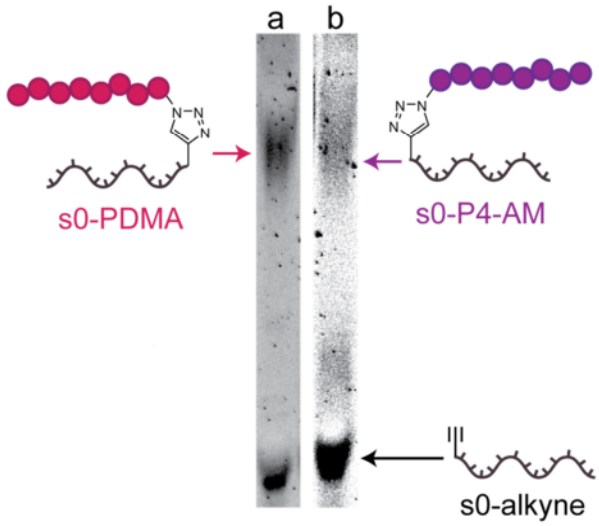

Figure 5.17 15 % native PAGE analyses of the poly(DMA) (**P18**, left) and poly(4-AM) (**P19**, right) DNA–polymer conjugates. Yields were around 50 % in both cases, as assessed by densitometry.

Next, the synthesis of DNA–poly(styrene) conjugates was attempted using the poly(styrene)–alkyne synthesised in Section 5.2.i (**P12**). Poly(styrene) has practically no solubility in water, so the synthesis of these conjugates has always proved to be very difficult, with yields typically below 5 %, even when solid phase synthesis techniques are employed.[36] Since the CuAAC system used in this work employs 5 % water as a DNA solubiliser, there was some concern that the polymer would become insoluble. However, it was found that the poly(styrene) used could tolerate a small amount of water, and was fully solubilised in the 95 % DMF solution used as the reaction solvent.

Despite the incompatibility of the polymer and DNA species, the conjugate was still observed in approximately 74 % yield by 2 % agarose gel electrophoresis (see Figure 5.18). Agarose was used instead of polyacrylamide for these analyses because its wider pores allow the migration of even relatively large aggregates.

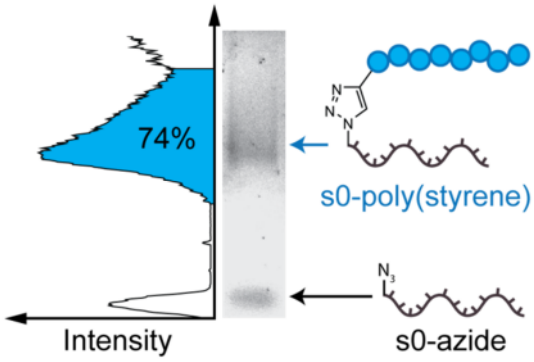

Figure 5.18 2 % agarose gel analysis showing the successful synthesis of a poly(styrene)–DNA conjugate using CuAAC. The yield by densitometry (left) was estimated to be 74 %.

It was hypothesised that, upon transfer of the conjugate into the aqueous loading buffer used for electrophoresis, the poly(styrene) segments would aggregate to form large, micellar structures and it is these that were observed in the gel and not the free conjugate itself. To test this hypothesis, the solution was analysed by dynamic light scattering (DLS). The results are shown in Figure 5.19 and revealed the presence of a significant population of particles around 50 nm in diameter.

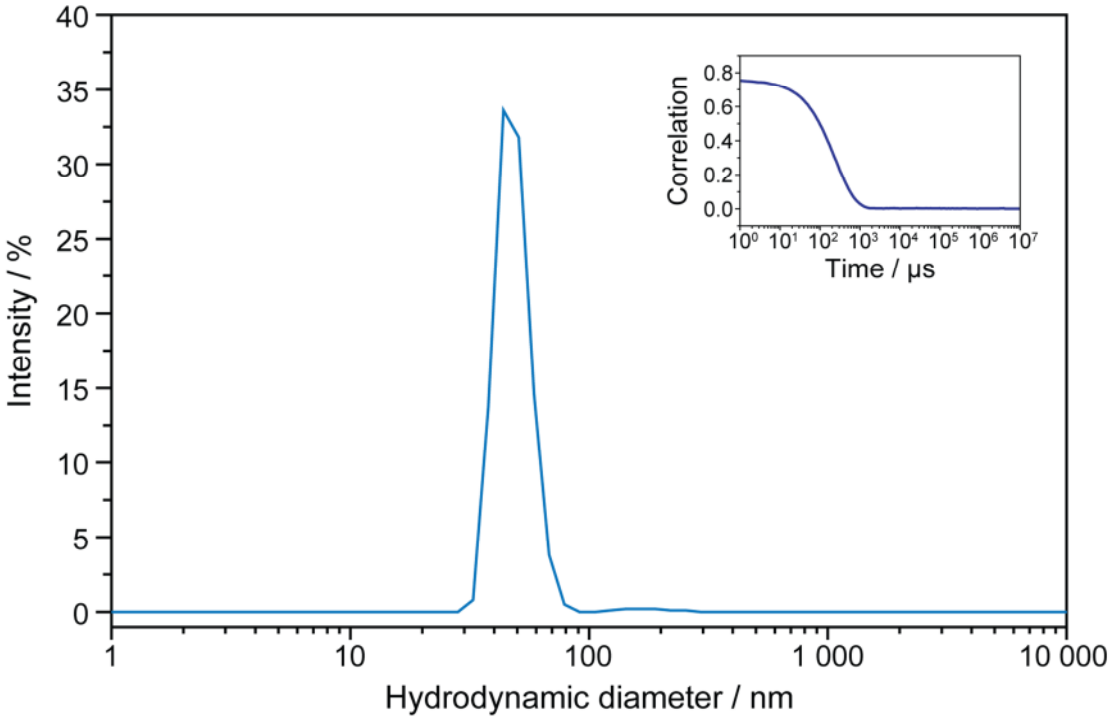

Figure 5.19 DLS analysis by number of a solution of the s0–poly(styrene) conjugate in water (correlation function inset). The main population had a hydrodynamic diameter of 48 nm and a dispersity of 0.24.

These particles were imaged by TEM, dry on a graphene oxide support, without staining.[37] Well-defined nanoparticles with diameters around 20 nm were observed (Figure 5.20 and Figure 5.21), confirming the amphiphilic nature of the DNA–poly(styrene) conjugate.

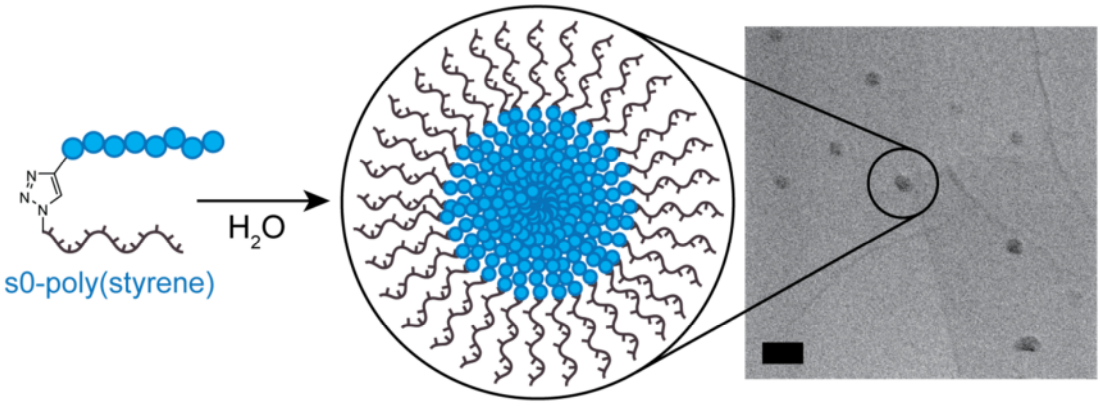

Figure 5.20 TEM micrograph of the nanoparticles formed when the s0–poly(styrene) conjugate was transferred from DMF (a good solvent for both blocks) to water (a poor solvent for poly(styrene)). The sample was dried directly onto the graphene oxide-coated TEM grid without staining. Scale bar: 50 nm.

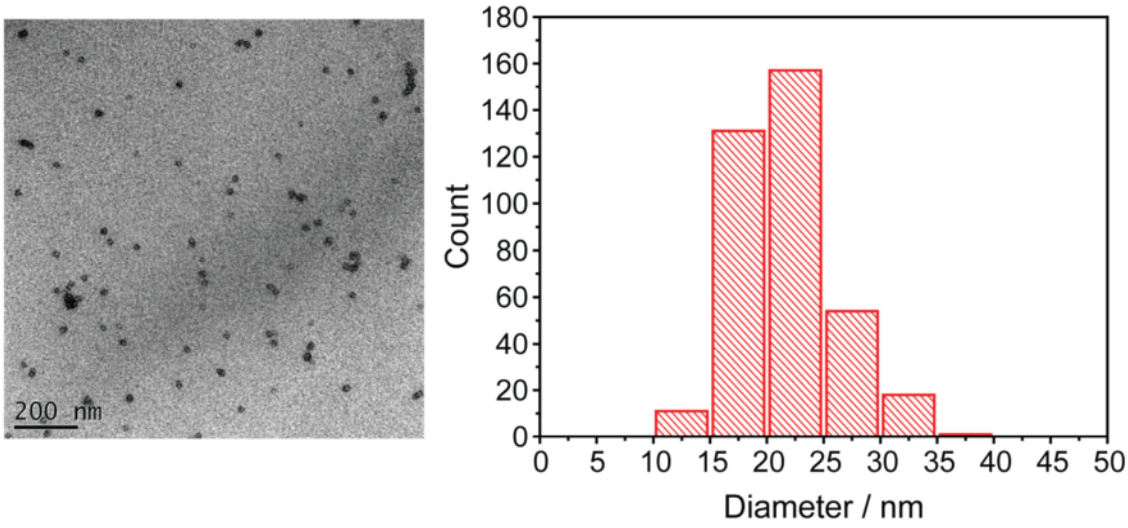

Figure 5.21 TEM micrograph (left) and particle size analysis (right) of the s0–poly(styrene) nanoparticles. Particle analysis of 372 nanoparticles.

The CuAAC reaction was thus shown to be an excellent chemistry for the conjugation of DNA to a wide range of functional polymers, including hydrophilic, temperature-responsive and hydrophobic.

5.3 Conclusions

The copper catalysed azide–alkyne cycloaddition (CuAAC) reaction was shown to be an excellent technique for the synthesis of DNA–polymer conjugates. An alkyne dithioester CTA was used to successfully polymerise styrene and NIPAM with good control over molecular weights and dispersity. NMR spectroscopy confirmed the presence of the alkyne functional group at the polymer chain termini. An azide-functionalised CTA was synthesised by esterification of the common trithiocarbonate CTA DDMAT, and was used to polymerise DMA, NIPAM and styrene with control. Whilst the CTA itself was observed to be stable under RAFT polymerisation conditions in the absence of monomer, FTIR studies of the polymers revealed only low incorporation of the azide group. A different route was therefore adopted, whereby azide-terminated polymers were synthesised by post-polymerisation modification of a PFP activated ester located at the polymer chain terminus. Using this method, azide-functionalised polymers of NIPAM, DMA, 4-AM and styrene were all synthesised. NMR spectroscopy revealed efficient substitution of the PFP ester, and FTIR confirmed an increase in incorporation of the azide group compared to polymers synthesised using the azide-functionalised CTA.

A large number of catalyst and solvent combinations were then tested for the DNA–polymer conjugation reaction. Only one – copper iodide triethylphosphite – was found to be effective in organic solvents. The reaction conditions were optimised and used to conjugate polymers of NIPAM, DMA, 4-AM and styrene to azide- and alkyne-functionalised DNA in up to 90 % yield. Coupling of poly(styrene) to azide DNA led to the formation of self-assembled hybrid DNA–polymer micelles, which were observed by agarose gel electrophoresis, DLS and TEM.

5.4 Experimental

5.4.i Materials & methods

For general materials and methods details, see the Appendix. 2-(Dodecylthiocarbonothioylthio)-2-methylpropionic acid (DDMAT), 3-azido-1-propanol, *N*-(*n*-hexyl)pyridylmethan-imine (NHPMI), *S*-Propargyloxycarbonylphenylmethyl dithiobenzoate (**15**) and copper iodide triethylphosphite (CuI · $P(OEt)_3$) were synthesized according to previously published procedures. [23,38-41] NIPAM was recrystallised from toluene before use. AIBN was recrystallised twice from methanol before use. 4-Acryloyl morpholine (4-AM) was distilled before use to remove the radical inhibitor. Azide- and alkyne-functionalised DNA strands (s0–azide and s0–alkyne) were purchased from Integrated DNA Technologies Ltd. and resuspended in 18 MΩ water to a final concentration of 200 μM before use.

5.4.ii RAFT polymerisation using CTA 15

NIPAM was polymerised using the alkyne-functionalised CTA, **15**, as follows. NIPAM (1 g, 8.84 mmol), **15** (29 mg, 0.09 mmol) and AIBN (3 mg, 0.02 mmol) were dissolved in DMF (2 mL) and the mixture transferred to an oven-dried ampoule under nitrogen. The solution was degassed by four successive freeze-pump-thaw cycles, then sealed under nitrogen and heated to 65°C for 23 hours. The solution was concentrated *in vacuo* and then poured into diethyl ether (300 mL). The precipitated product was isolated by filtration as a light pink solid (0.32 g, 51 %), and analysed by DMF SEC using PMMA calibration standards (M_n 6.9 kDa, Đ 1.16). ^{1}H NMR (400 MHz, $CDCl_3$) δ 7.94 (t, 2H, polymer end group Ar*H*), 7.54 (t, 1H, polymer end group Ar*H*), 7.37 (t, 2H, polymer end group Ar*H*), 7.32-7.14 (br m, polymer end group Ar*H*), 7.10-5.40 (br s, PNIPAM N*H*), 4.82-4.44 (br m, 2H, polymer end group CH_2C≡CH), 4.25-3.70 (br s, PNIPAM C*H*$(CH_3)_2$), 3.59 (br s, 1H, polymer end group C≡C*H*), 2.60-0.80 (br m, PNIPAM backbone *H*) ppm.

The polymerisation of styrene was conducted as follows. CTA **15** (0.063 g, 0.19 mmol) was

dissolved in styrene (1.1 mL, 9.60 mmol). The solution was transferred to an oven-dried ampoule which had been purged with nitrogen for 30 minutes. The mixture was subjected to five freeze-pump-thaw cycles and sealed under an atmosphere of nitrogen. It was then placed in an oil bath preheated to 110°C and stirred for 28 hours, after which time the reaction was allowed to cool to room temperature and poured into methanol (400 mL) cooled with dry ice. The product precipitated out and was collected by filtration, dissolved in a small amount of THF and re-precipitated into cold methanol (200 mL), and finally collected by filtration as a pink solid (0.371 g, 48 %), and analysed by $CHCl_3$ SEC using PS standards (M_n 3 600, Đ 1.12). ^{1}H NMR (400 MHz, $CDCl_3$) δ 7.84 (br m, 2H, S=CAr*H*), 7.46 (br m, 1H, S=CAr*H*), 7.41-6.08 (br m, PS Ar*H*), 5.02-4.26 (br m, 3H, OCH_2C≡CH and SC*H*Ph), 3.23 (br s, 1H, C≡C*H*), 2.66-0.51 (br m, PS backbone *H*) ppm.

5.4.iii 3-Azido-1-propanol

3-Bromo-1-propanol (5.00 g, 36 mmol) and sodium azide (4.68 g, 72 mmol) were dissolved in acetone (75 mL) and water (25 mL) and heated to reflux for 18 hours. The acetone was then removed *in vacuo*. Water (75 mL) was added and the product extracted with diethyl ether (3 × 100 mL). The combined organic layers were dried ($MgSO_4$) and the solvent removed to afford the product as a colourless oil (3.25 g, 90 %). ^{1}H NMR (400 MHz, $CDCl_3$) δ 3.76 (t, *J* = 6 Hz, 2H, CH_2N$_3$), 3.45 (t, *J* = 7 Hz, 2H, CH_2OH), 1.83 (quint, *J* = 6 Hz, 2H, CH_2CH$_2$OH), 1.64 (br s, 1H, O*H*) ppm. ^{13}C NMR (75 MHz, $CDCl_3$) δ 59.3 (*C*H$_2$OH), 47.9 (*C*H$_2$N$_3$), 30.8 (*C*H$_2$CH$_2$OH) ppm. IR (ν_{max} / cm^{-1}): 3348 (OH), 2947, 2881, 2090 (N$_3$ stretch), 1258, 1046. These values compare well with those from the literature.[42]

5.4.iv 3-Azidopropyl 2-(dodecylthiocarbonothioylthio)-2-methylpropanoate, 16

The azide-containing CTA **16** was synthesized as follows. DDMAT (0.2 g, 0.55 mmol), EDCI·HCl (0.105 g, 0.55 mmol) and DMAP (0.006 g, 0.05 mmol) were dissolved in dichloromethane (2 mL) and stirred for one hour at room temperature. 3-azido-1-propanol

(0.050 g, 0.50 mmol) was then added and the mixture stirred for one week at room temperature. The solvent was then removed *in vacuo*, water (20 mL) was added and the product extracted into ethyl acetate (3 × 20 mL). The combined organic layers were washed with water (2 × 20 mL) and brine (20 mL) and finally dried with $MgSO_4$, which was then removed by filtration. The solvent was removed *in vacuo* and the residue purified by silica gel column chromatography, eluting with a mixture of pet. ether 40-60 and ethyl acetate (9:1). The pure fractions (R_f 0.57) were combined and the solvent removed to afford the product as a yellow oil (0.116 g, 52 %). ^{1}H NMR (400 MHz, $CDCl_3$) δ 4.18 (t, *J* = 6 Hz, 2H, C*H*$_2$O), 3.36 (t, *J* = 7 Hz, 2H, C*H*$_2$N$_3$), 3.27 (t, *J* = 7 Hz, 2H, SC*H*$_2$), 1.90 (quint, *J* = 6 Hz, 2H, C*H*$_2$CH$_2$N$_3$), 1.69 (s, 6H, C(C*H*$_3$)$_2$), 1.66 (m, 2H, SCH$_2$C*H*$_2$), 1.38 (m, 2H, SCH$_2$CH$_2$C*H*$_2$), 1.34-1.21 (br m, 16H, SCH$_2$CH$_2$CH$_2$(C*H*$_2$)$_8$CH$_3$), 0.88 (t, *J* = 7 Hz, 3H, S(CH$_2$)$_{11}$C*H*$_3$) ppm. ^{13}C NMR (150 MHz, $CDCl_3$) δ 221.6 (*C*=S), 172.8 (*C*=O), 62.7 (O*C*H$_2$), 55.9 (*C*(CH$_3$)$_2$), 48.2 (*C*H$_2$N$_3$), 37.0 (S*C*H$_2$), 31.9, 29.6, 29.5, 29.4, 29.3, 29.1, 28.9, 28.0, 27.9, 25.4 (C(*C*H$_3$)$_2$), 22.7, 14.1 (S(CH$_2$)$_{11}$*C*H$_3$) ppm [Fewer signals are observed than expected because of overlap]. IR (ν_{max} / cm^{-1}): 2923, 2853, 2096 (N_3 stretch), 1734, 1254, 1154, 1126, 1064, 814. ESI HR MS calcd. for $C_{20}H_{37}N_3O_2S_3$ $[M+Na]^+$ 470.1946; observed 470.1942.

5.4.v RAFT polymerisation using CTA 16

NIPAM was polymerised as follows. CTA **16** (0.020 g, 0.04 mmol), NIPAM (0.500 g, 4.42 mmol) and AIBN (0.4 mg, 2 μmol) were dissolved in anhydrous DMF (0.75 mL), then transferred to an oven-dried ampoule which had been purged with nitrogen for 30 minutes. The solution was subjected to three freeze-pump-thaw cycles and sealed under an atmosphere of nitrogen. The ampoule was then placed in an oil bath preheated to 65°C and stirred for two hours. After cooling to room temperature, the reaction mixture was poured into diethyl ether (75 mL), which had been cooled to 0°C with an ice bath. The precipitated product was isolated by centrifugation followed by drying *in vacuo* at 40°C as a pale yellow

solid (0.248 g, 55 %), and analysed by DMF SEC using PMMA calibration standards (M_n 8 540 Da, Đ 1.16). ^{1}H NMR (400 MHz, $CDCl_3$) δ 7.20-5.64 (br m, PNIPAM N*H*), 4.00 (br s, PNIPAM C*H*$(CH_3)_2$), 3.40 (br m, 2H, PNIPAM end group CH_2N_3), 3.33 (br m, 2H PNIPAM end group SCH_2), 2.63-0.79 (br m, PNIPAM backbone *H*) ppm.

Styrene was polymerised as follows. CTA **16** (22 mg, 0.05 mmol), styrene (0.5 g, 4.80 mmol) and AIBN (0.8 mg, 0.01 mmol) were mixed and the solution transferred to an oven dried ampoule under nitrogen. The mixture was degassed by three successive freeze-pump-thaw cycles, sealed under nitrogen and then heated to 65°C for 46 hours. The highly viscous mass was dissolved in THF (2 mL) and poured into methanol (200 mL) that had been cooled with dry ice. The product was isolated, by filtration and drying, as a pale yellow solid (0.31 g, 62 %) and analysed by THF SEC using PS calibration standards (M_n 13.3 kDa, Đ 1.09). ^{1}H NMR (400 MHz, $CDCl_3$) δ 7.40-6.20 (br m, PS Ar*H*), 5.04-4.59 (br m, 1H, SC*H*(Ph)CH_2), 3.69-3.35 (br m, 2H, CH_2N_3), 3.27 (br t, 2H, SCH_2), 3.17 (br t, 2H, CO_2CH_2), 2.50-1.00 (br m, PS backbone *H*), 0.89 (br t, 3H, S$(CH_2)_{11}$CH_3) ppm.

5.4.vi Degradation of the azide group under RAFT conditions

To ascertain whether the azide group degraded under RAFT polymerisation conditions, the following experiment was carried out. **16** (10.0 mg, 20 μmol) and AIBN (0.4 mg, 2 μmol) were mixed in 1,4-dioxane (442 μL). The solution was degassed by three successive freeze-pump-thaw cycles, sealed under nitrogen and heated to 65°C for six hours. The solvent was then removed *in vacuo* and the residue analysed by ^{1}H NMR spectroscopy.

5.4.vii 1-Azido-3-aminopropane

Synthesised using a modified literature procedure.[43] 3-Chloropropylamine (4 g, 30.8 mmol) and sodium azide (6 g, 92.3 mmol) were mixed in water (30 mL) and heated to 80°C for 15 hours, after which most of the water was removed under vacuum. The reaction mixture was cooled in an ice bath and diethyl ether (50 mL) was added followed by potassium hydroxide, ensuring that the temperature stayed below 10°C at all times. After separation

of the organic phase, the aqueous layer was extracted again with diethyl ether (2 × 20 mL). The combined organic layers were dried (Na_2SO_4), the solvent removed *in vacuo* and the crude product purified by vacuum distillation (11 mbar, 303 K) to give a colourless oil (1.5 g, 49 %). ^{1}H NMR (300 MHz, $CDCl_3$) δ 3.36 (t, J = 7 Hz, 2H, CH_2N_3), 2.79 (t, J = 7 Hz, 2H, CH_2NH_2), 1.72 (quint, J = 7 Hz, 2H, $CH_2CH_2NH_2$), 1.12 (br s, 2H, NH_2) ppm. ^{13}C NMR (75 MHz, $CDCl_3$) δ 49.3 (CH_2N_3), 39.5 (CH_2NH_2), 32.6 ($CH_2CH_2NH_2$) ppm. These values agree well with those from the literature.

5.4.viii Azide modification of PFP-capped polymers

PFP-capped poly(NIPAM) was synthesised and the trithiocarbonate groups removed using AIBN and LPO, as described in Chapter 2.

The polymerisation of dimethylacrylamide (DMA) was conducted as follows. CTA **7** (53.5 mg, 0.10 mmol), DMA (1 g, 10.09 mmol) and AIBN (1.7 mg, 0.01 mmol) were dissolved in 1,4-dioxane (2 mL) and the mixture degassed by three successive freeze-pump-thaw cycles. The solution was sealed under a nitrogen atmosphere and placed in an oil bath preheated to 65°C for four hours. After rapid cooling with liquid nitrogen to quench the polymerisation, the flask was opened to the air and the solution added dropwise to a large volume of pet. ether 40-60 (300 mL). The precipitated product was collected by filtration as a yellow solid (0.871 g, 87 %), and analysed by DMF SEC using PMMA calibration standards (M_n 11.1 kDa, Đ 1.09). ^{1}H NMR (400 MHz, $CDCl_3$) δ 5.18 (m, 1H, $SCHC{=}ONMe_2$), 3.31 (m, 2H, SCH_2), 3.40-2.00 (br m, PDMA $N(CH_3)_2$ and $CHC{=}ONMe_2$), 2.00-1.00 (br m, PDMA backbone CH_2) ppm. ^{19}F NMR (375 MHz, $CDCl_3$) δ −153.0 (br m, 2F, PFP end group ortho *F*), −158.1 (br m, 1F, PFP end group para *F*), −162.3 (br m, PFP end group meta *F*) ppm.

The polymerisation of 4-acryloyl morpholine (4-AM) was conducted as follows. CTA **7** (37.6 mg, 0.07 mmol), 4-AM (1 g, 7.08 mmol) and AIBN (1.2 mg, 0.01 mmol) were dissolved in 1,4-dioxane (3 mL) and the solution degassed by three successive freeze-

pump-thaw cycles. The reaction mixture was sealed under a nitrogen atmosphere and placed in an oil bath preheated to 65°C for four hours. After rapid cooling with liquid nitrogen to quench the polymerization, the flask was opened to the air and the solution added dropwise to a large volume of diethyl ether (200 mL) cooled in an ice bath. The precipitated product was collected by filtration and drying as a yellow solid (0.793 g, 82 %), and analysed by DMF SEC using PMMA calibration standards (M_n 9.3 kDa, Đ 1.11). ^{1}H NMR (400 MHz, $CDCl_3$) δ 5.16 (m, 1H, SC*H*C=ON), 4.00-3.00 (br m, P4-AM NCH_2CH_2), 2.90-1.00 (br m, P4-AM backbone *H*), 0.87 (t, 3H, S$(CH_2)_{11}$CH_3) ppm. ^{19}F NMR (375 MHz, $CDCl_3$) δ −153.3 (br m, 2F, PFP end group ortho *F*), −157.6 (br m, 1F, PFP end group para *F*), −161.9 (br m, PFP end group meta *F*) ppm.

The PFP end group was then substituted with 3-azido-1-aminopropane as follows, using a modified literature procedure.[44] Poly(NIPAM) (M_n 8.2 kDa, Đ 1.11) (40.0 mg, 5 μmol), 3-azido-1-aminopropane (2.4 mg, 24 μmol) and TEA (1.2 mg, 12 μmol) were dissolved in anhydrous THF (0.5 mL) under nitrogen in an oven-dried ampoule. The solution was degassed by three successive freeze-pump-thaw cycles, and then heated to 35°C for two hours, then for a further 15 hours at room temperature. Water (10 mL) was added and the mixture dialysed against 18 MΩ water (MWCO 1 kDa), with six water changes, to remove excess small molecules. The product was isolated by freeze-drying as a white solid (21 mg, 53 %) and analysed by DMF SEC using PMMA calibration standards (M_n 8.0 kDa, Đ 1.09). ^{1}H NMR (400 MHz, $CDCl_3$) δ 7.20-5.50 (br m, PNIPAM N*H*), 4.00 (br s, PNIPAM C*H*$(CH_3)_2$), 3.42-3.21 (br m, 4H, CONHCH_2 and CH_2N_3), 2.80-0.5 (br m, PNIPAM backbone *H*) ppm. IR (ν_{max} / cm^{-1}): 3296, 2971, 2100 (N_3 stretch), 1639, 1535, 1458.

5.4.ix CuAAC catalyst testing

All solvents were degassed by bubbling with N_2 for 30 minutes prior to use. The catalyst/ligand (1.0 μL, 2 mM in the reaction solvent), polymer (1.0 μL, 2 mM in the reaction solvent) and DNA (0.5 μL, 200 μM in water) solutions were mixed in a centrifuge

tube, and the volume topped up to 10 μL with the reaction solvent. The tube was closed, briefly vortexed and then left overnight. The yield of the DNA–polymer conjugate was assessed by 15 % native PAGE analysis using densitometry.

5.4.x CuAAC catalyst optimisation

Optimisation of the CuAAC reaction conditions was carried out as above, varying the equivalents of polymer and catalyst, and exploring further solvent systems.

5.4.xi Glaser homocoupling of alkyne DNA

DMF was bubbled with either compressed air or nitrogen for 30 minutes. CuI · $P(OEt)_3$ (3.6 mg, 1 mmol) was then dissolved in this DMF (1 mL). The resultant solution (8.5 μL) was mixed with s0–alkyne DNA (0.5 μL, 200 μM in water) and left at room temperature for 48 hours, then analysed by 15 % native PAGE.

5.4.xii DNA–PS conjugates

Alkyne-functionalised poly(styrene) (1 μL, 10 mM in DMF) was mixed with CuI · $P(OEt)_3$ (1 μL, 10 mM in DMF), s0–azide DNA (0.5 μL, 200 μM in water) and DMF (7.5 μL) and left for 16 hours at room temperature. Native loading buffer (see Appendix) (40 μL) was added and the mixture analysed by 2 % agarose electrophoresis and DLS, and dry by TEM on a graphene oxide support.

5.5 References

(1) Rostovtsev, V. V.; Green, L. G.; Fokin, V. V.; Sharpless, K. B. *Angew. Chem., Int. Ed.* **2002**, *41*, 2596.

(2) Tornøe, C. W.; Christensen, C.; Meldal, M. *J. Org. Chem.* **2002**, *67*, 3057.

(3) Kolb, H. C.; Finn, M. G.; Sharpless, K. B. *Angew. Chem., Int. Ed.* **2001**, *40*, 2004.

(4) Meldal, M.; Tornøe, C. W. *Chem. Rev. (Washington, DC, U. S.)* **2008**, *108*, 2952.

(5) Rodionov, V. O.; Fokin, V. V.; Finn, M. G. *Angew. Chem., Int. Ed.* **2005**, *44*, 2210.

(6) Himo, F.; Lovell, T.; Hilgraf, R.; Rostovtsev, V. V.; Noodleman, L.; Sharpless, K. B.; Fokin, V. V. *J. Am. Chem. Soc.* **2004**, *127*, 210.

(7) Bock, V. D.; Hiemstra, H.; van Maarseveen, J. H. *Eur. J. Org. Chem.* **2006**, 51.

(8) Fournier, D.; Hoogenboom, R.; Schubert, U. S. *Chem. Soc. Rev.* **2007**, *36*, 1369.

(9) Kempe, K.; Krieg, A.; Becer, C. R.; Schubert, U. S. *Chem. Soc. Rev.* **2012**, *41*, 176.

(10) Godula, K.; Rabuka, D.; Nam, K. T.; Bertozzi, C. R. *Angew. Chem., Int. Ed.* **2009**, *48*, 4973.

(11) Li, Y.; Wang, J.; Cai, C. *Langmuir* **2011**, *27*, 2437.

(12) El-Sagheer, A. H.; Brown, T. *Chem. Soc. Rev.* **2010**, *39*, 1388.

(13) Dallmann, A.; El-Sagheer, A. H.; Dehmel, L.; Mügge, C.; Griesinger, C.; Ernsting, N. P.; Brown, T. *Chem. A Eur. J.* **2011**, *17*, 14714.

(14) Alvira, M.; Eritja, R. *Chem. Biodiversity* **2007**, *4*, 2798.

(15) Hong, V.; Presolski, S. I.; Ma, C.; Finn, M. G. *Angew. Chem., Int. Ed.* **2009**, *48*, 9879.

(16) Cutler, J. I.; Zheng, D.; Xu, X.; Giljohann, D. A.; Mirkin, C. A. *Nano Lett.* **2010**, *10*, 1477.

(17) Imoto, S.; Hirohama, T.; Nagatsugi, F. *Bioorg. Med. Chem. Lett.* **2008**, *18*, 5660.

(18) Averick, S. E.; Paredes, E.; Grahacharya, D.; Woodman, B. F.; Miyake-Stoner, S. J.; Mehl, R. A.; Matyjaszewski, K.; Das, S. R. *Langmuir* **2012**, *28*, 1954.

(19) Le Droumaguet, B.; Velonia, K. *Macromol. Rapid Commun.* **2008**, *29*, 1073.

(20) Li, M.; De, P.; Gondi, S. R.; Sumerlin, B. S. *Macromol. Rapid Commun.* **2008**, *29*, 1172.

(21) Rothemund, P. W. K. *Nature* **2006**, *440*, 297.

(22) Averick, S.; Paredes, E.; Li, W.; Matyjaszewski, K.; Das, S. R. *Bioconjugate Chem.* **2011**, *22*, 2030.

(23) O'Reilly, R. K.; Joralemon, M. J.; Hawker, C. J.; Wooley, K. L. *J. Polym. Sci., Part A: Polym. Chem.* **2006**, *44*, 5203.

(24) Lim, J.; Yang, H.; Paek, K.; Cho, C.-H.; Kim, S.; Bang, J.; Kim, B. J. *J. Polym. Sci., Part A: Polym. Chem.* **2011**, *49*, 3464.

(25) Schmidt, B. V. K. J.; Hetzer, M.; Ritter, H.; Barner-Kowollik, C. *Polym. Chem.* **2012**, *3*, 3064.

(26) Ladmiral, V.; Legge, T. M.; Zhao, Y.; Perrier, S. b. *Macromolecules* **2008**, *41*, 6728.

(27) Presolski, S. I.; Hong, V.; Cho, S.-H.; Finn, M. G. *J. Am. Chem. Soc.* **2010**, *132*, 14570.

(28) Glaser, C. *Justus Liebigs Annalen der Chemie* **1870**, *154*, 137.

(29) Torchilin, V. P.; Trubetskoy, V. S.; Whiteman, K. R.; Caliceti, P.; Ferruti, P.; Veronese, F. M. *J. Pharm. Sci.* **1995**, *84*, 1049.

(30) Jeong, J. H.; Kim, S. W.; Park, T. G. *Bioconjugate Chem.* **2003**, *14*, 473.

(31) Jeong, J. H.; Kim, S. H.; Kim, S. W.; Park, T. G. *J. Biomater. Sci., Polym. Ed.* **2005**, *16*, 1409.

(32) Jeong, J. H.; Kim, S. H.; Kim, S. W.; Park, T. G. *Bioconjugate Chem.* **2005**, *16*, 1034.

(33) Oishi, M.; Sasaki, S.; Nagasaki, Y.; Kataoka, K. *Biomacromolecules* **2003**, *4*, 1426.

(34) Oishi, M.; Nagatsugi, F.; Sasaki, S.; Nagasaki, Y.; Kataoka, K. *ChemBioChem* **2005**, *6*, 718.

(35) Oishi, M.; Nagasaki, Y.; Itaka, K.; Nishiyama, N.; Kataoka, K. *J. Am. Chem. Soc.* **2005**, *127*, 1624.

(36) Li, Z.; Zhang, Y.; Fullhart, P.; Mirkin, C. A. *Nano Lett.* **2004**, *4*, 1055.

(37) Patterson, J. P.; Sanchez, A. M.; Petzetakis, N.; Smart, T. P.; Epps, T. H.; Portman, I.; Wilson, N. R.; O'Reilly, R. K. *Soft Matter* **2012**, *8*, 3322.

(38) Skey, J.; O'Reilly, R. K. *Chem. Commun.* **2008**, 4183.

(39) Scheel, A. J.; Komber, H.; Voit, B. I. *Macromol. Rapid Commun.* **2004**, *25*, 1175.

(40) Haddleton, D. M.; Crossman, M. C.; Dana, B. H.; Duncalf, D. J.; Heming, A. M.; Kukulj, D.; Shooter, A. J. *Macromolecules* **1999**, *32*, 2110.

(41) Ziegler, F. E.; Fowler, K. W.; Rodgers, W. B.; Wester, R. T. *Org. Synth.* **1987**, *65*, 108.

(42) Munuera, L.; O'Reilly, R. K. *Dalton Trans.* **2010**, *39*, 388.

(43) Agut, W.; Agnaou, R.; Lecommandoux, S.; Taton, D. *Macromol. Rapid Commun.* **2008**, *29*, 1147.

(44) Wiss, K. T.; Theato, P. *J. Polym. Sci., Part A: Polym. Chem.* **2010**, *48*, 4758.

Chapter 6

Construction of a DNA tetrahedron–polymer conjugate

6.1 Introduction

Having identified a number of chemistries for the efficient conjugation of polymers to DNA, the next step was to use the DNA segment to assemble a complex 3D architecture that would be inaccessible using block copolymers alone. A further goal was to use the attached polymer to cause additional hierarchical assembly of the DNA–polymer conjugate. The DNA tetrahedron (Figure 6.1, A), as first reported by Goodman *et al.*,[1] was chosen as it represents a small, highly compact and precisely defined nanostructure that is not accessible by any other means. It has also been very well characterised, even down to the chirality of the helices (Figure 6.1, B).[2] Furthermore, recent reports have indicated that the caged structure may be useful in encapsulating enzymes, and penetrating and delivering drug molecules to mammalian cells.[3-5]

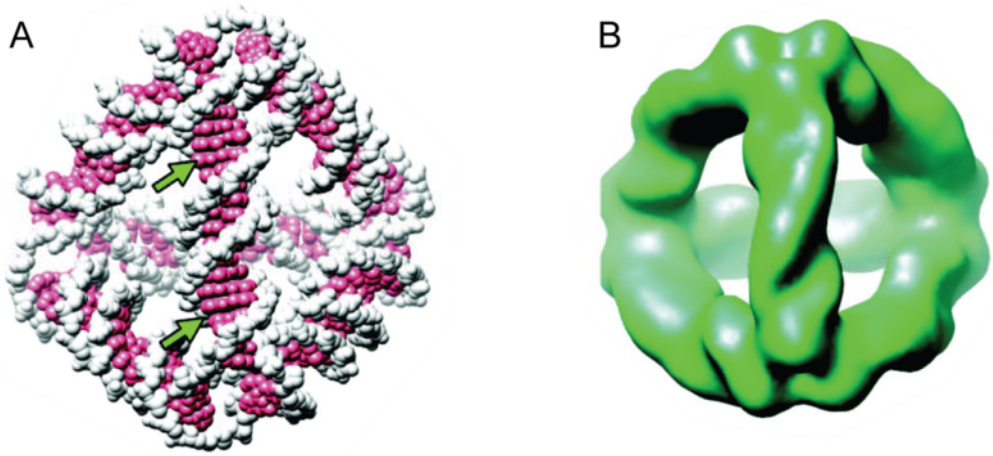

Figure 6.1 Structure of the DNA tetrahedron synthesised by Goodman *et al.* A: space-filling model of the DNA tetrahedron, with the locations of the major grooves indicated (green arrows). B: 3D density maps of the DNA tetrahedron calculated by cryoEM image reconstruction. Figure adapted from Goodman *et al.* and Kato *et al.*[1,2]

The tetrahedron (Figure 6.2 shows another 3D view of the structure, along with the

cartoon representation used for the bulk of this work) is assembled from four component strands (s1-4) by a very simple annealing process: heating to a high temperature for four minutes followed by rapid cooling. The structure is such that each strand forms a loop around one face of the tetrahedron, with an unpaired A residue forming a hinge at each corner. Each edge is 20 base pairs in length, with the full structure measuring approximately 7 nm across, and every strand contacts all others. Because of the loop structure, the 5' and 3' ends of the strands can be moved to any position on the edges of a given face, and, because of the helical structure of DNA, groups incorporated at these positions can be designed to face in or out of the central cavity.[6] Furthermore, the size and geometry of the cage can be altered simply by slightly altering the sequences of two or more of the component strands.[1]

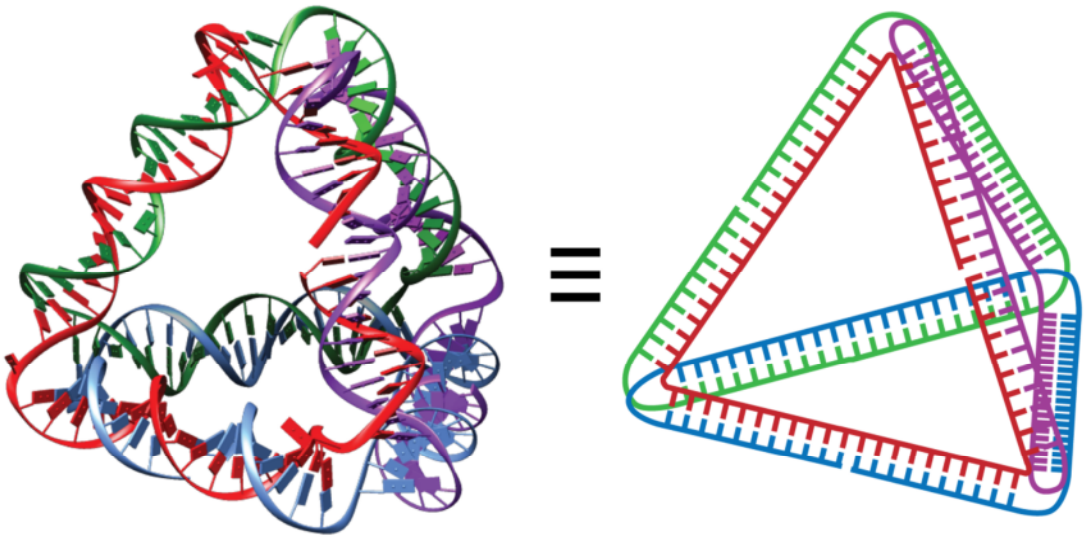

Figure 6.2 Left: 3D model of the DNA tetrahedron illustrating the helical nature of the structure; ribbon = phosphate backbone, and tube/slab = DNA base. Right: cartoon representation. The four component strands are s1 (red), s2 (green), s3 (blue) and s4 (purple).

For the polymer segment, poly(NIPAM) was chosen. Its temperature-responsive behaviour – hydrophobic at high temperatures and hydrophilic at low temperatures, with a cloud point typically around 32°C – made it an ideal candidate for this work, as it meant that the assembly of higher order structures could potentially be triggered by simply heating the solution.

6.2 Synthesis of DNA–polymer conjugates

6.2.i Conjugation chemistry & polymer syntheses

As discussed in Chapters 1-4 several conjugation chemistries had been found to be effective for the attachment of synthetic polymers to short oligonucleotides. Based on its high efficiency, and the ease of obtaining polymers and DNA bearing the appropriate functionalities, CuAAC was chosen for the work described below. As previously discussed, alkyne-functionalised DNA strands were used in conjunction with azide-functionalised polymers. The polymers used below were synthesised using the same method as that described in Chapter 5, employing a post-polymerisation modification route. Three different molecular weights of poly(NIPAM) were made (**P21**-**23**); their properties are outlined in Table 6.1. IR and ^{1}H NMR were used to confirm the successful incorporation of the azide group into these polymers (see Chapter 5 for a discussion of the analyses involved).

Table 6.1 Properties of the poly(NIPAM) samples synthesised for conjugation to a DNA tetrahedron. * Determined from the ratio of the integrated signal from the polymer end groups and the polymer NHC*H* signal in the ^{1}H NMR spectrum. † Determined by DMF SEC using PMMA calibration standards.

Polymer	M_n^{NMR} / kDa*	Đ†
P21	5.3	1.07
P22	10.4	1.09
P23	19.8	1.09

6.2.ii Conjugation of polymers to DNA tetrahedron oligonucleotides

In order to construct the polymer-functionalised DNA tetrahedron, it was first necessary to synthesise DNA–polymer conjugates containing the appropriate base sequence. The sequences of the four component strands of the tetrahedron (s1-4) are given in Figure 6.3. The s2 strand was purchased containing an alkyne-modified U in place of A12 (that is, the

12th nucleotide from the 5' end of the strand, which is an adenine residue that is incorporated at a vertex of the assembled tetrahedron) – this ensured that the polymer would be attached to one of the vertices of the tetrahedron once it was assembled.

```
        s1:  5'- AGG CAG TTG AGA CGA ACA TTC CTA AGT CTG AAA
             TTT ATC ACC CGC CAT AGT AGA CGT ATC ACC -3'

        s2:  5'- CTT GCT ACA CGA TTC AGA CTT AGG AAT GTT CGA
             CAT GCG AGG GTC CAA TAC CGA CGA TTA CAG -3'

 s2-alkyne:  5'- CTT GCT ACA CGU(alkyne) TTC AGA CTT AGG AAT
             GTT CGA CAT GCG AGG GTC CAA TAC CGA CGA TTA CAG
             -3'
        s3:  5'- GGT GAT AAA ACG TGT AGC AAG CTG TAA TCG ACG
             GGA AGA GCA TGC CCA TCC ACT ACT ATG GCG -3'

        s4:  5'- CCT CGC ATG ACT CAA CTG CCT GGT GAT ACG AGG
             ATG GGC ATG CTC TTC CCG ACG GTA TTG GAC -3'
```

Figure 6.3 Sequences of the DNA strands used to assemble the DNA tetrahedron. The colour coding corresponds to that used in the cartoon representation of the tetrahedron.

This internally modified strand (s2–alkyne), which was a synthetically more challenging structure to modify than the end-functionalised version (as used in Chapter 5), was conjugated to **P21**-**23** with efficiencies of up to 74 % as shown in Figure 6.4. The conjugates were purified by HPLC (see Figure 6.5), with a final isolated yield for the s2–**P21** conjugate of 50 %. This is almost ten times higher than the best reported yield for internal modification of DNA with poly(NIPAM).[7,8] The copper catalyst was capable of catalysing the homo-coupling of the DNA–alkyne in the presence of oxygen – *via* the Glaser oxidation – so it was essential that the reaction solvent was degassed prior to use (see Chapter 5).

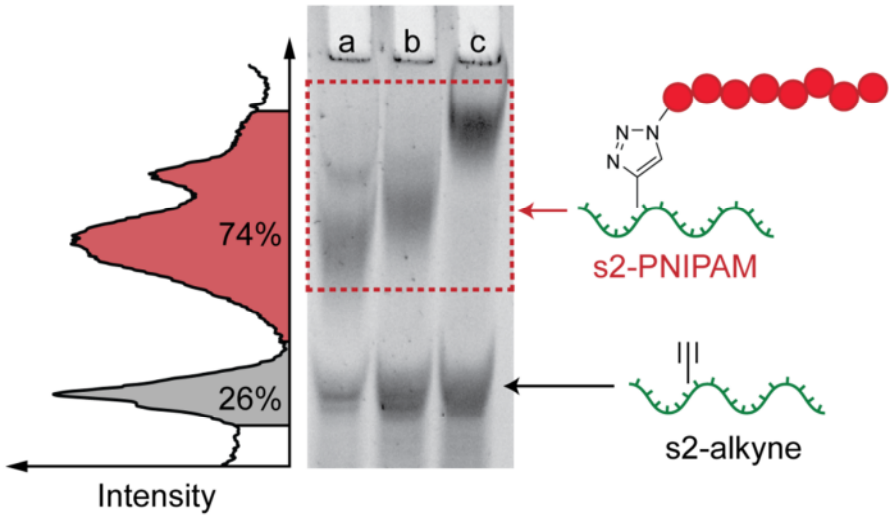

Figure 6.4 DNA–polymer conjugates containing the tetrahedron s2 strand. 15 % native PAGE analysis of crude reaction mixtures from the synthesis of: lane a – s2–**P21** (densitometry plot shown to left of gel); lane b – s2–**P21b**; lane c – s2–**P21c**.

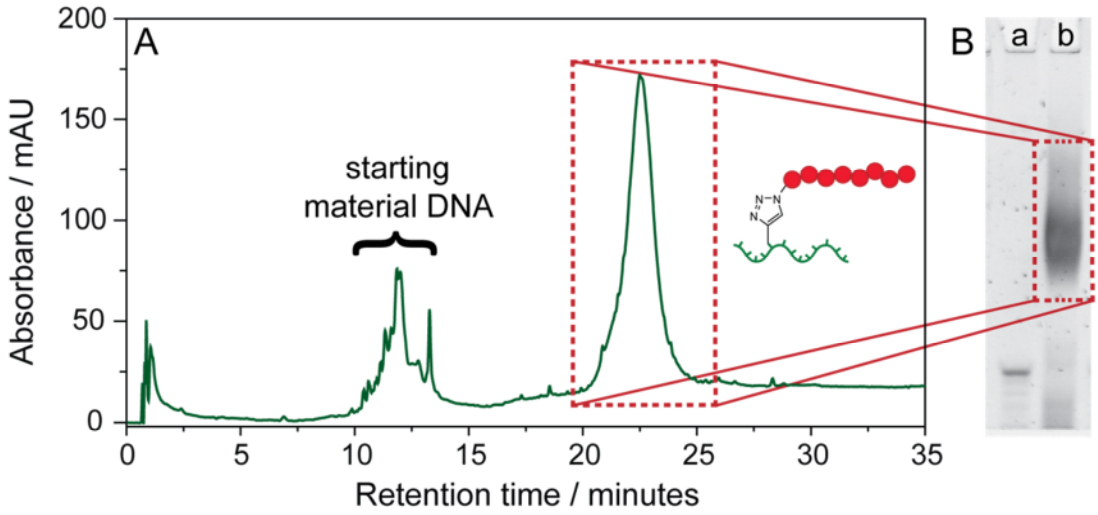

Figure 6.5 A: HPLC chromatogram of the crude reaction mixture in the synthesis of the s2–**P21** conjugate. B: PAGE analysis of the purified s2–**P21** conjugate. Lane a – s2 DNA. Lane b – s2–**P21** conjugate.

6.3 Assembly of polymer-functionalised DNA tetrahedra

6.3.i Assembly of tetrahedra

First, the plain tetrahedron was assembled from the component strands – s1-4 – by heating them to 95°C then cooling rapidly to 4°C.[1] Figure 6.6 shows a control experiment, demonstrating that the band attributed to the fully formed tetrahedron only appeared when

all four strands were present. It was possible to assign all other bands to particular DNA structures containing 3 or fewer of the component strands.

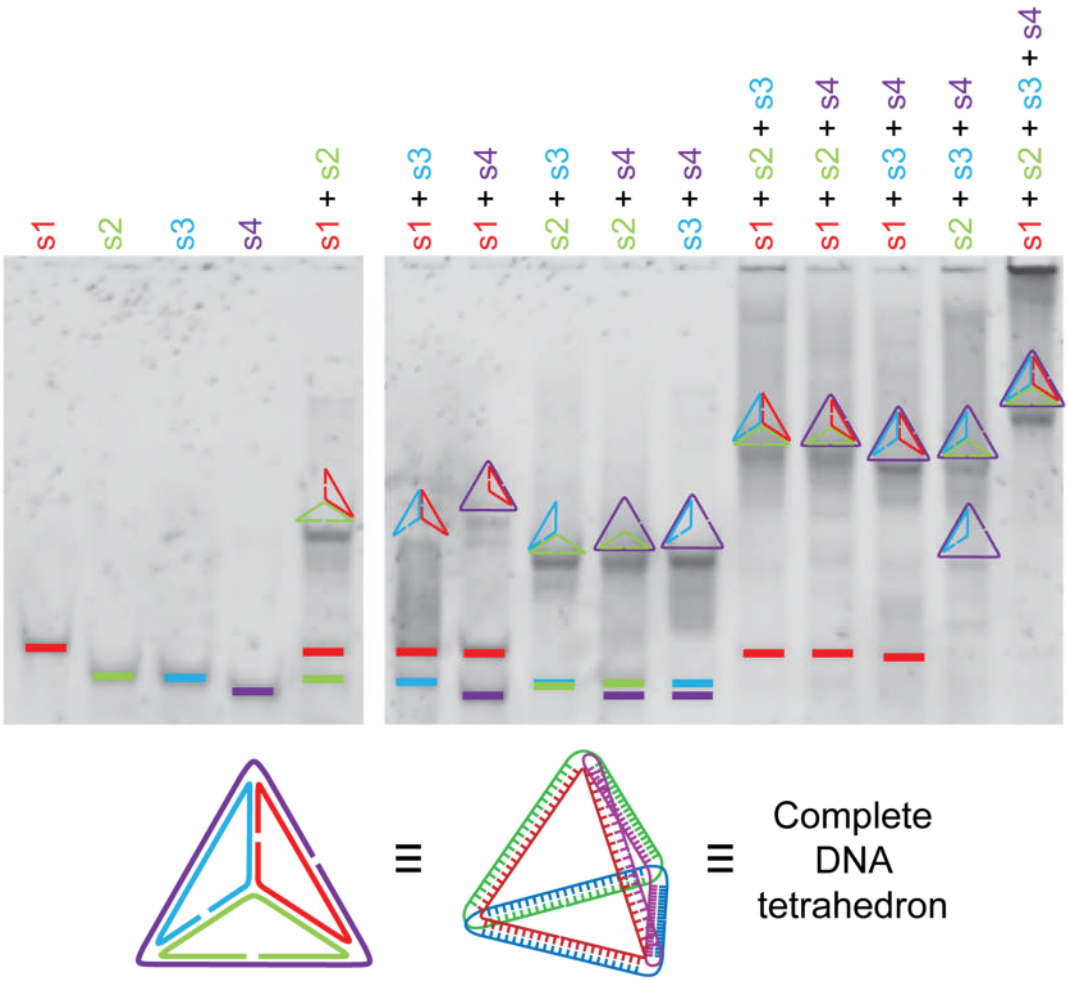

Figure 6.6 8 % native PAGE analysis of all possible combinations of the four component strands of the DNA tetrahedron (s1-4). The lowest mobility band (attributed to the complete DNA tetrahedron) was only visible when all four strands were present, and bands for all other possible structures could be identified, as shown (an unlabelled gel is presented in the Experimental Section).

The literature procedure used above for assembly of the DNA tetrahedra required that the four component strands (s1-4) be mixed and heated to 95°C. Since poly(NIPAM) has a lower critical solution temperature (LCST) (typically around 32°C, although as is discussed below this can vary widely depending on the molecular weight) it was desirable to avoid the use of heat as a denaturant. An isothermal assembly strategy was therefore adopted, as described previously by Simmel *et al.*[9] Equimolar amounts of s1, s2–**P21**, s3 and s4 were

mixed in formamide. This denatures all possible hydrogen-bonding interactions, meaning that tertiary structure formation is not possible. The solution was transferred to a microdialyser and stirred in a large volume of the assembly buffer overnight. The solution within the microdialyser was then removed and analysed by 8 % native PAGE (see Figure 6.7).

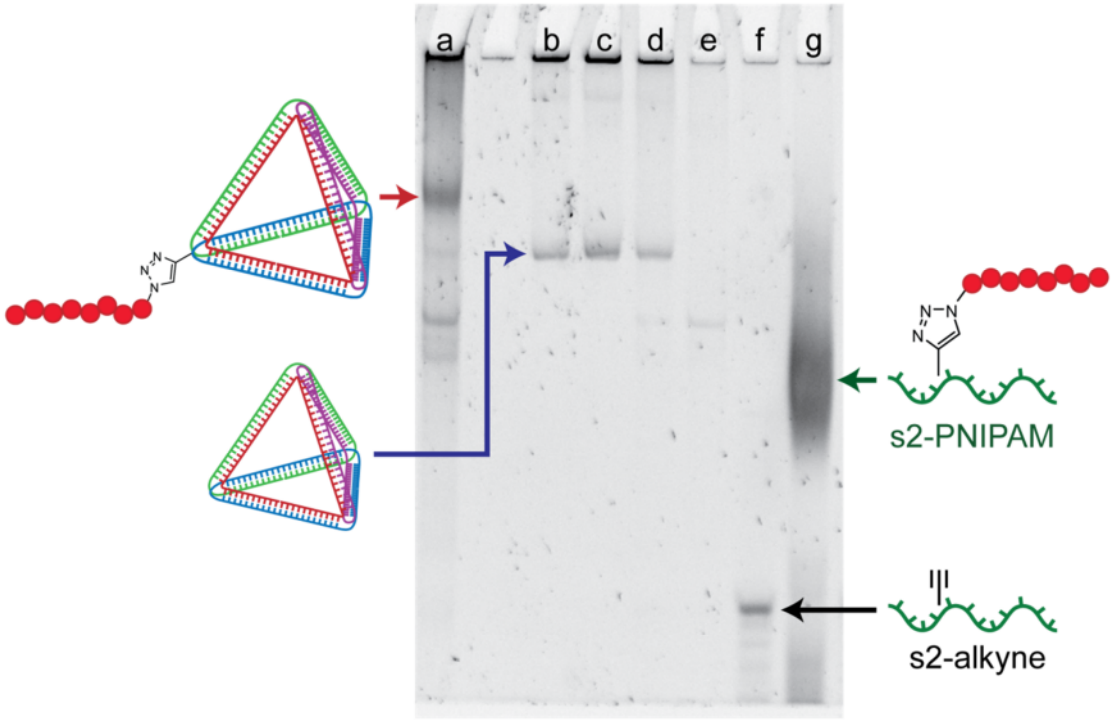

Figure 6.7 Tetrahedron–**P21** conjugate analysed by 8 % native PAGE. Lane a: Tetrahedron–**P21** conjugate; lane b, c, d: unfunctionalised DNA tetrahedra; lane e: s1 + s3 + s4; lane f: s2–alkyne; lane g: s2–**P21**.

A new, low-mobility band was clearly visible. To confirm that the polymer–tetrahedron conjugate was being formed and contained all four of the constituent DNA strands, control experiments were carried out in which one strand was systematically omitted from the mixture. Figure 6.8 shows the results – the lowest mobility band was only observed when all four DNA strands were present, confirming that the complete tetrahedron was being formed.

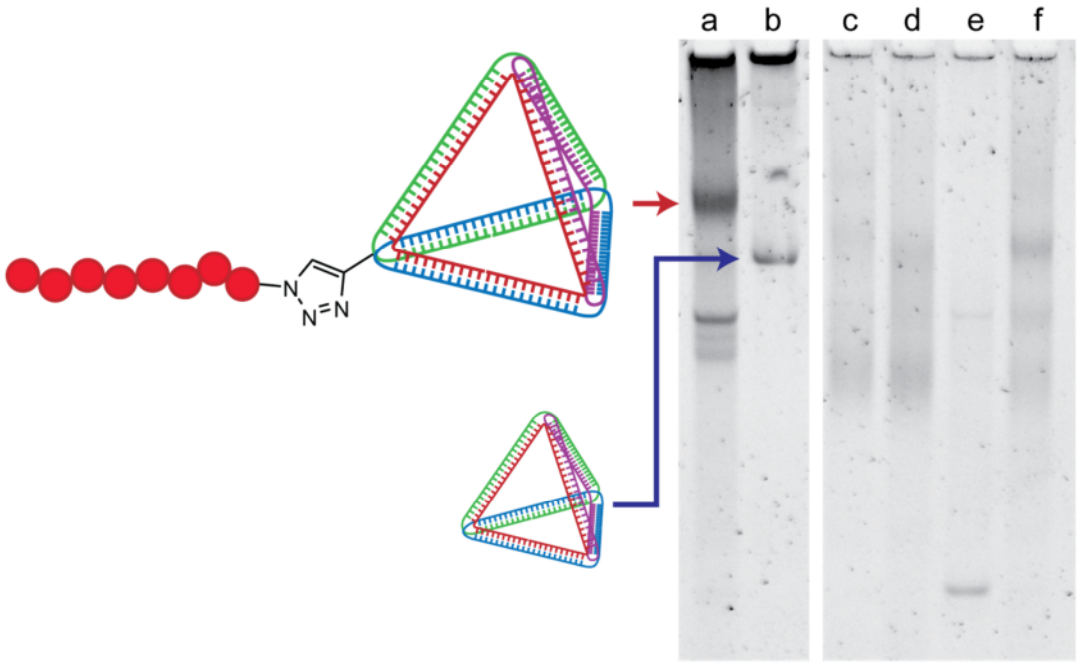

Figure 6.8 8 % native PAGE showing that the tetrahedron–polymer conjugate band is only formed when all four constituent DNA strands are present. Lane a: Tetrahedron–**P21** conjugate; lane b: plain tetrahedron; lane c: s1 + s2–**P21** + s3; lane d: s1 + s2–**P21** + s4; lane e: s1 + s3 + s4; lane f: s2–**P21** + s3 + s4.

6.3.ii Förster resonance energy transfer (FRET) studies of the assembled DNA tetrahedron–polymer conjugates

To confirm that the tetrahedral structure was maintained in the **P21** conjugate, fluorescence studies were carried out. First, the plain tetrahedron was assembled containing the fluorescent groups 6-carboxyfluorescein (FAM) and carboxytetramethylrhodamine (TAMRA) – Figure 6.9 is a schematic illustrating the relative positions of the fluorescent groups. This pair of fluorophores interacts by Förster resonance energy transfer (FRET) when brought into close proximity – the Förster distance for this pair of fluorophores is between 49 and 54 Å.[10] FAM and TAMRA were located on strands s1 and s3 respectively, so that upon assembly they would lie on adjacent edges of the tetrahedron, approximately 49 Å apart (as estimated using the 3D model depicted in Figure 6.9) – close enough for FRET to occur. If the structure was maintained then excitation of FAM should have caused energy transfer to the TAMRA group and consequent emission at a higher

wavelength, as well as a concomitant decrease in fluorescence intensity for the FAM group.

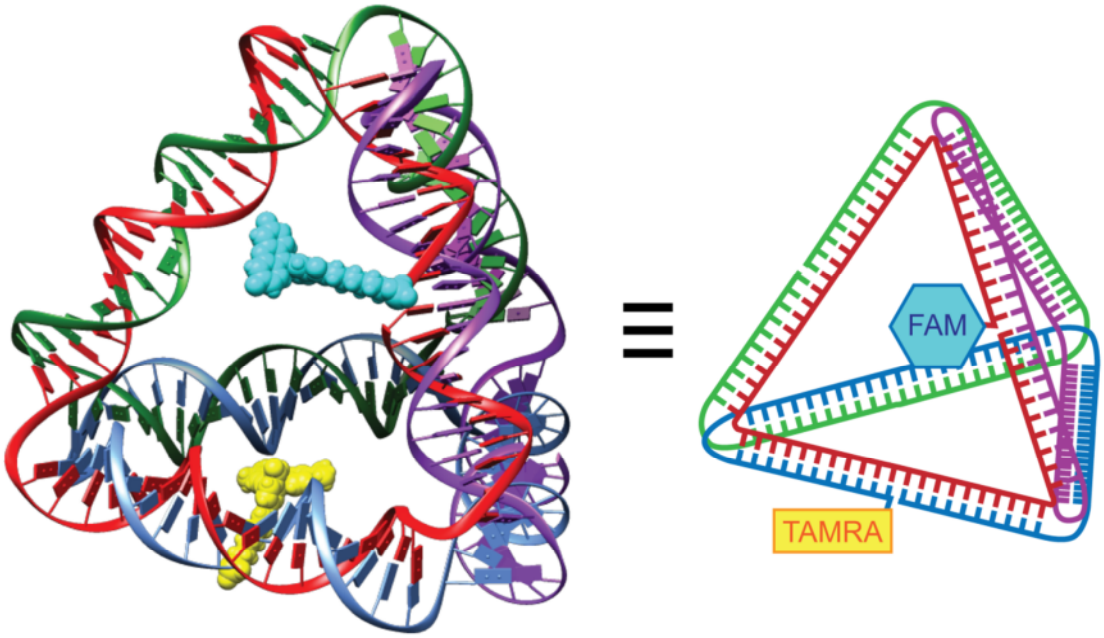

Figure 6.9 3D model (left) and cartoon (right) showing the positions of the FAM (light blue) and TAMRA (yellow) groups in the DNA tetrahedron. The spatial separation of the two groups was estimated by measuring the distance between the 5' ends of the s1 (red) and s3 (blue) DNA strands in the 3D model.

Figure 6.10 shows 8 % native PAGE analysis of the tetrahedra assembled containing FAM and TAMRA. In all cases the tetrahedra formed as expected.

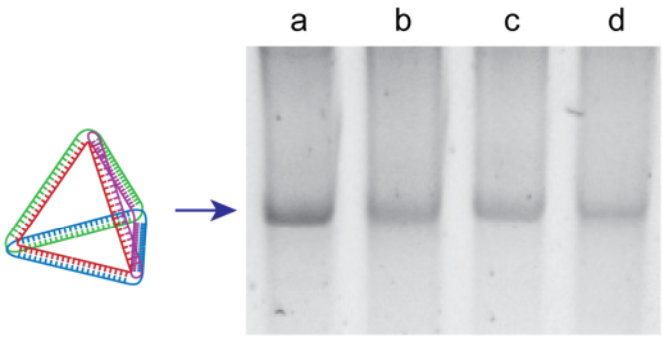

Figure 6.10 8 % native PAGE analysis of DNA tetrahedra assembled containing FAM and/or TAMRA. Lane: a – s1-4; b – s1–FAM, s2-4; c – s1, s2, s3–TAMRA, s4; d – s1–FAM, s2, s3–TAMRA, s4.

Figure 6.11 shows fluorescence spectroscopy data for each of the experiments in Figure 6.10. In all cases the excitation wavelength was the same – 495 nm, the excitation

maximum of the FAM group (the presence of the TAMRA group was confirmed by excitation at 559 nm – see inset to Figure 6.11).

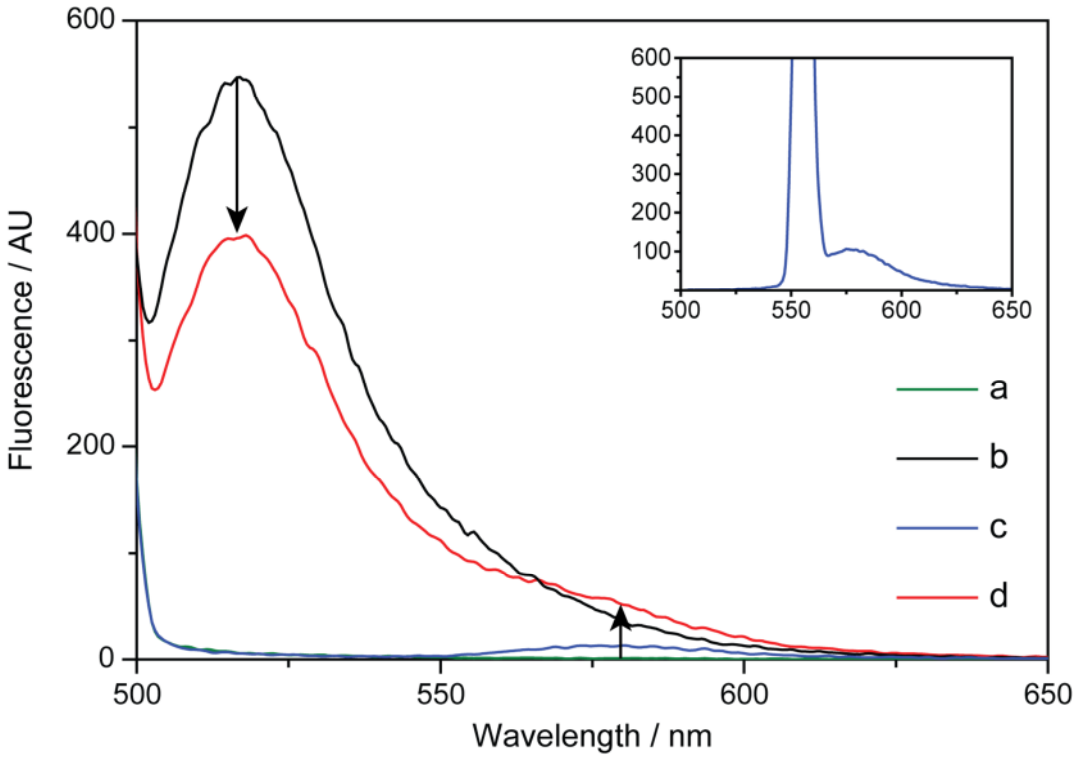

Figure 6.11 Fluorescence emission spectra of the fluorophore-functionalised tetrahedra, exciting at 495 nm. The experiment labels are the same as those used in Figure 6.10. Inset: fluorescence emission spectrum of experiment c, exciting at 559 nm to show the presence of the TAMRA group.

As expected, the non-fluorescent and TAMRA-functionalised tetrahedra exhibited almost no emission when excited at this wavelength. In the case of the FAM-functionalised tetrahedron, a large emission peak was observed at 520 nm, confirming incorporation of this group. When both FAM and TAMRA were included (Figure 6.11d), an extra peak was observed around 577 nm – characteristic of the TAMRA group – and a significant decrease in the emission of the FAM group occurred. These observations indicated that FRET was occurring and that these groups were therefore spatially close. A control experiment wherein the FAM and TAMRA strands were mixed without forming the tetrahedron confirmed that this extra peak was only observed in the presence of the DNA superstructure.

Having confirmed that FRET took place in the plain tetrahedron, the experiments were then repeated using the s2–**P21** conjugate. Figure 6.12 and Figure 6.13 show the results, and confirm that the tetrahedra were present on assembly with the polymer as FRET was observable when FAM and TAMRA were both included in the structure (Figure 6.13d).

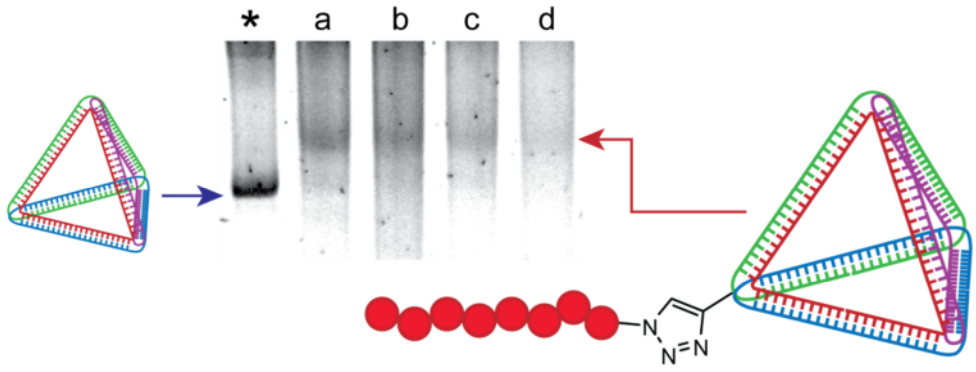

Figure 6.12 8 % native PAGE analysis of the tetrahedron–**P21** conjugate incorporating FAM and/or TAMRA. Lane: * – s1-4; a – s1, s2–**P21**, s3, s4; b – s1–FAM, s2–**P21**, s3, s4; c – s1, s2–**P21**, s3–TAMRA, s4; d – s1–FAM, s2–**P21**, s3–TAMRA, s4.

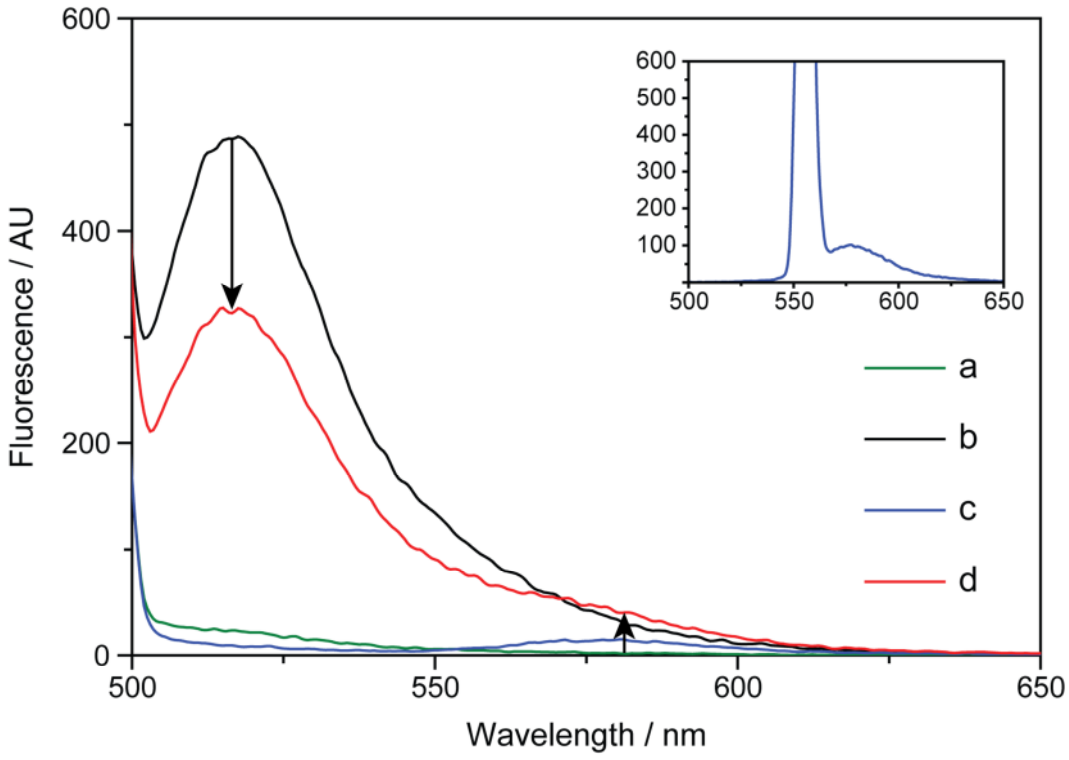

Figure 6.13 Fluorescence emission spectra of the fluorophore-functionalised **P21**–tetrahedron conjugates, exciting at 495 nm. The experiment labels are the same as those used in Figure 6.12. Inset: fluorescence emission spectrum of experiment c, exciting at 559 nm to show the presence of the TAMRA group.

6.3.iii Conjugation of polymers to a ligated DNA tetrahedron

To further confirm that the observed product was indeed the polymer–tetrahedron conjugate, the possibility of attaching the polymer to an already assembled DNA nanostructure was explored. Since concentration and/or the addition of organic solvents can cause the free tetrahedron to disassemble, it was desirable to lock the structure in place before manipulating it further. Since the tetrahedron structure forced the component strands to wrap around one another, this locking could be achieved by ligating the strands to form four interconnected loops – a catenane. Figure 6.14 shows a schematic representation of the ligated tetrahedron, illustrating the knotted nature of the structure.[1]

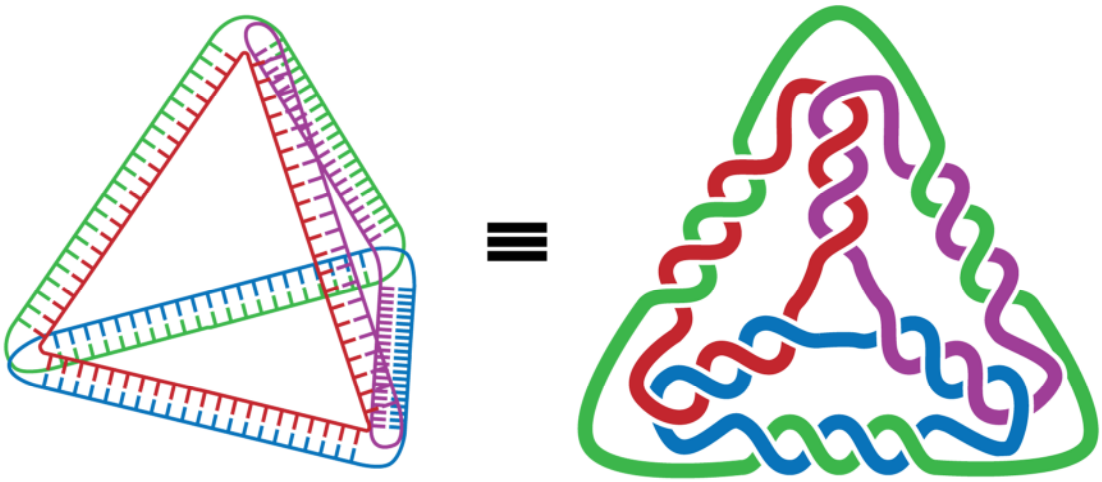

Figure 6.14 Schematic of a ligated tetrahedron, illustrating (right) the knotted catenane structure. Once ligated, the tetrahedron is topologically locked and it is impossible for it to disassemble.

The s1, s2–alkyne, s3 and s4 strands were first phosphorylated using T4 polynucleotide kinase – this enzyme adds a phosphate group to the 5' end of the DNA strands; the tetrahedron was then assembled using the normal thermal route (heating to 95°C for several minutes to completely melt any residual base pair interactions, followed by rapid cooling to 4°C). Phosphorylation was necessary to allow the ligation enzyme (T4 DNA ligase) to process the DNA strands – in the absence of a 5' phosphate group no linkage can occur. Scheme 6.1 outlines the transformations performed by each of the enzymes, for

clarity.

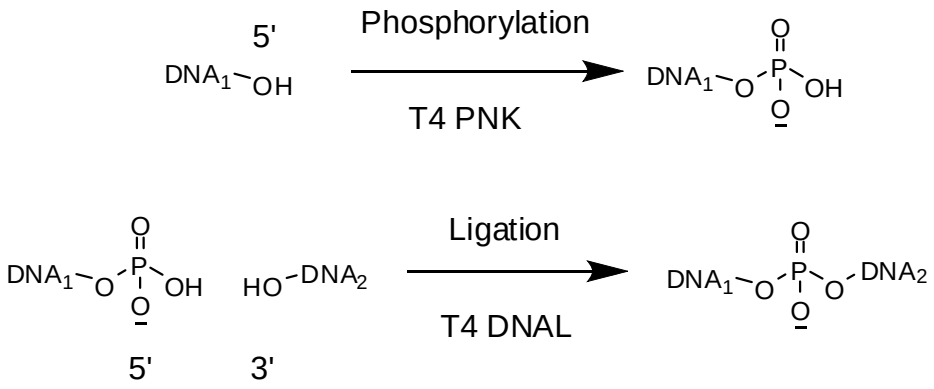

Scheme 6.1 Roles performed by the two enzymes – T4 polynucleotide kinase (T4 PNK) and T4 DNA ligase (T4 DNAL). T4 PNK converts the hydroxyl group at the 5' end of a DNA strand into a phosphate group. T4 DNAL joins a phosphate group at the 5' end of one DNA strand with a hydroxyl group at the 3' end of a second DNA strand to link the two strands *via* a new phosphate bridge.

Following incubation with the ligation enzyme, analysis by both native and denaturing PAGE confirmed the successful formation of the ligated tetrahedra (see Figure 6.15).

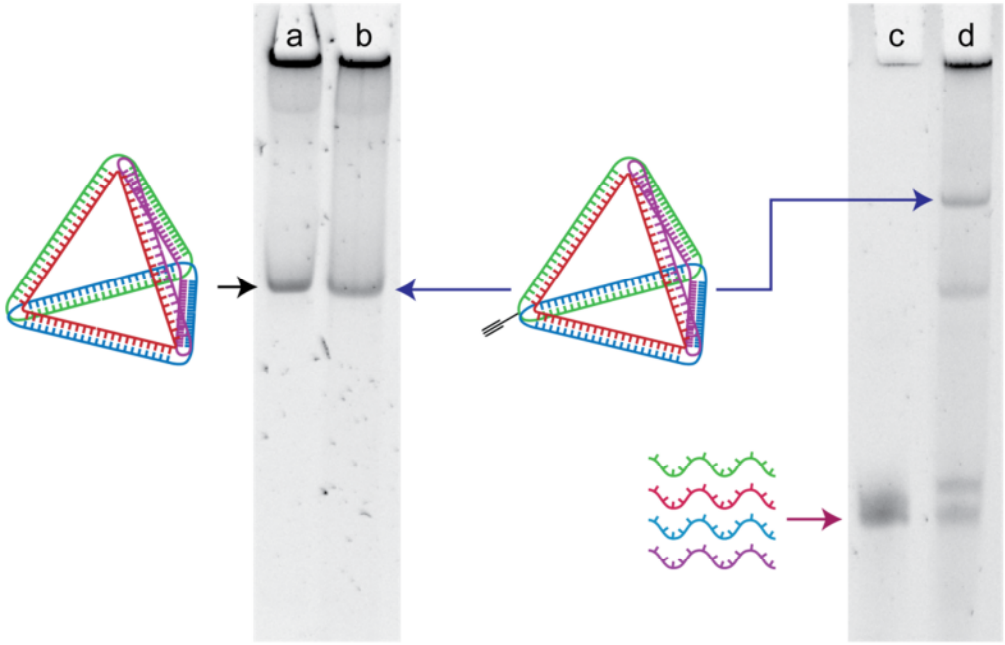

Figure 6.15 8 % native (left) and denaturing (right) PAGE analyses of ligated DNA tetrahedra. Lanes a and c contain unligated DNA tetrahedra and lanes b and d ligated tetrahedra. The ligated tetrahedra resisted degradation under denaturing conditions, while the unligated tetrahedra dissociated to the component DNA strands. Note that there is evidence of incomplete ligation (higher mobility bands) in the right-hand gel.

Conjugation of the polymer to the ligated tetrahedra was then performed using standard water-based CuAAC reaction conditions. The ligated tetrahedra were concentrated to approximately 1 μM and then mixed with **P21** (dissolved in degassed acetonitrile), $CuSO_4.5H_2O$, (+)-sodium L-ascorbate and tris-(hydroxypropyltriazolylmethyl)amine (THPTA) (all dissolved in degassed 18 MΩ water), and left overnight at 26°C. Analysis of the reaction mixture by 8 % native PAGE clearly showed the presence of a new band (Figure 6.16), which corresponded exactly with that attributed to the polymer–tetrahedron conjugate above. Since the ligated tetrahedron was incapable of disassembly (since it was topologically locked), this provided further strong evidence that this band had been correctly assigned, and that the conjugate had been successfully synthesised. It is worth noting that when the polymer was grafted to a pre-assembled tetrahedron the tetrahedron–polymer conjugate was only produced in around 40 % yield (relative to the plain tetrahedron by densitometry); by contrast, when the tetrahedron was assembled using the s2–**P21** species, almost no plain tetrahedron (i.e. without the polymer attached) was observed. The latter was clearly the superior of the two approaches.

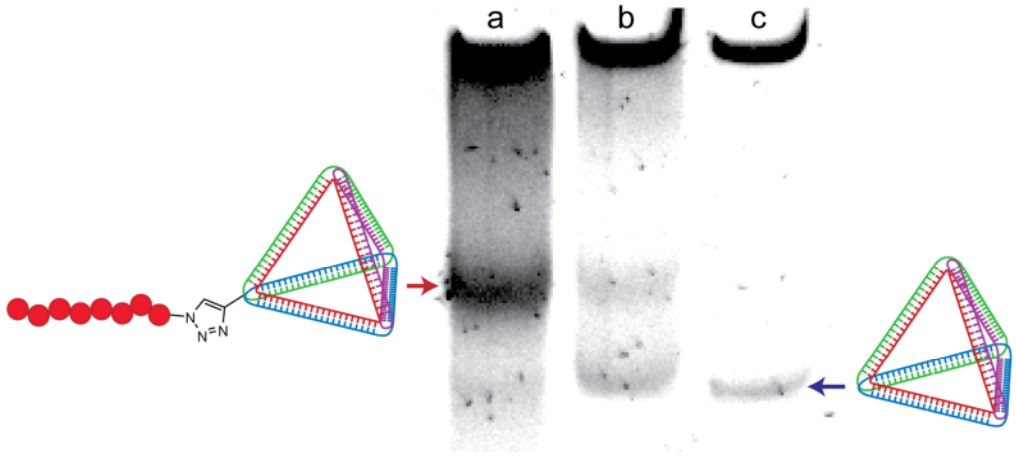

Figure 6.16 Tetrahedron–**P21** conjugate analysed by 8 % native PAGE. Lane a: Tetrahedron–**P21** conjugate synthesised by assembly using the s2–**P21** strand; lane b: Tetrahedron–**P21** conjugate synthesised by conjugation of **P21** to an alkyne-functionalised tetrahedron; lane c: plain DNA tetrahedron.

6.4 Thermally-induced self-assembly of the tetrahedron–polymer conjugate

6.4.i Measurement of the cloud point of poly(NIPAM)

Poly(NIPAM) is well-known for its temperature-responsive character, and typically exhibits a cloud point around 32°C in aqueous solution. It has previously been combined with oligonucleotides and the hybrids utilised for the thermally induced purification of plasmid DNA, PCR amplicons, genotoxins and DNA binding proteins.[8,11-14]

The cloud points of the poly(NIPAM) homopolymers (**P21**-**23**), under the conditions to be used for DNA self-assembly, were measured by following the UV-vis absorbance. A solution of the homopolymer (0.8 mg mL^{-1} in TEM buffer – 10 mM Tris HCl, 1 mM EDTA and 6 mM $MgCl_2$) was heated in a quartz cuvette within a UV-vis spectrometer, and the absorbance followed at 500 nm (Figure 6.17) from 20°C to 60°C. After normalization of the maximum absorbance to one, the cloud point was taken as the temperature at which the absorbance was 0.5.

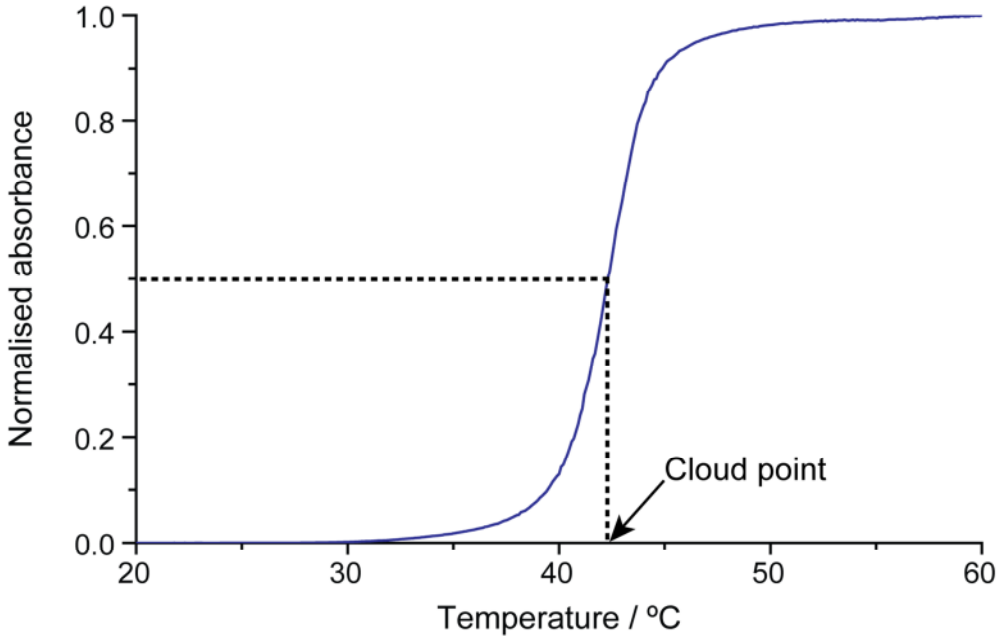

Figure 6.17 Determination of the cloud point of **P21** by UV-vis spectroscopy. The cloud point was taken as the temperature at which the normalised absorbance at 500 nm was equal to 0.5 (dotted line).

The cloud point of **P21** was measured to be 42°C (see Figure 6.17). This higher value can be attributed to the low molecular weight of the polymer and the relatively hydrophilic end groups. The cloud points of all the polymers synthesised for this work are given in Table 6.2.

Table 6.2 Cloud points of **P21-23** in 1 × TEM buffer at a concentration of 0.8 mg mL^{-1} as measured by UV-vis turbidimetry (heating cycle). The cloud point was taken as the temperature at which the normalised absorbance at 550 nm was equal to 0.5.

Polymer	Cloud point / °C
P21	42.0
P22	39.7
P23	36.3

By contrast, the s2**–P21** conjugate did not exhibit a cloud point at a concentration of 0.1 mg mL^{-1} . Dynamic light scattering (DLS) studies performed above the cloud point revealed the formation of very large aggregates (Figure 6.18), confirming that the poly(NIPAM) segment was collapsing as expected. Attempts to induce the formation of well-defined nanoparticles were, however, unsuccessful.

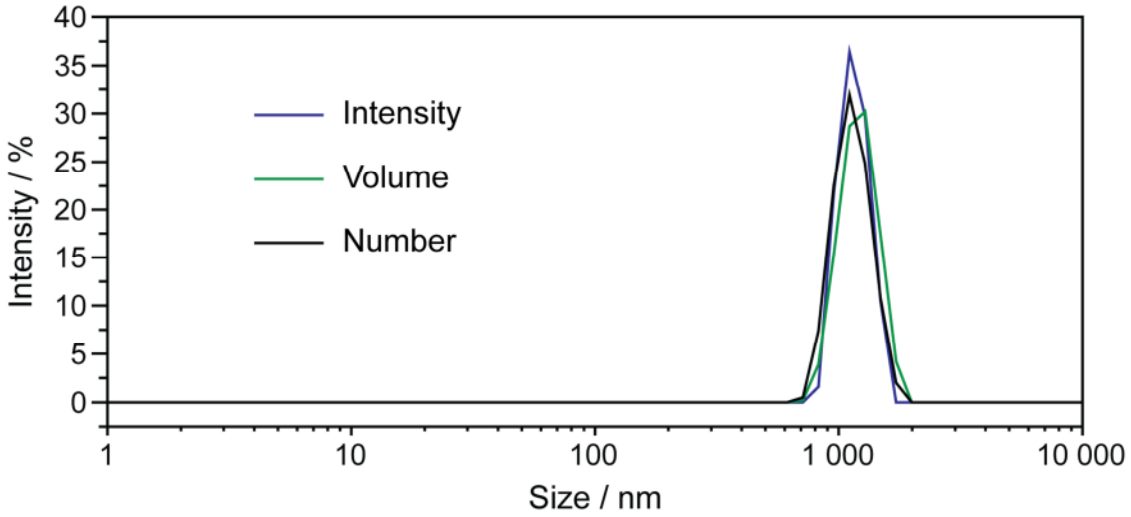

Figure 6.18 DLS intensity (blue), volume (green) and number (black) data for the s2–**P21** conjugate at a concentration of 0.1 mg mL^{-1} and a temperature of 45°C. Only very large aggregates were observed, suggesting that the poly(NIPAM) segment was collapsing as expected, but not to produce discrete micelles.

6.4.ii Self-assembly of the tetrahedron–poly(NIPAM) conjugate

It was similarly hypothesised that by heating the tetrahedron–**P21** conjugate to the polymer's cloud point, the collapse and aggregation of the polymer may drive the formation of micelle-like structures with a hydrophobic poly(NIPAM) core and a hydrophilic corona composed of DNA tetrahedra. However, the concentration of the conjugate after assembly was far below the critical micelle concentration (CMC) usually observed for poly(NIPAM) nanostructures, and – as mentioned above – no stable structures were observed at a concentration of 0.1 mg mL^{-1} (higher concentrations were not investigated as the synthesis of a large enough amount of material was not practical). It was reasoned that addition of free poly(NIPAM) homopolymer may ameliorate this by increasing the total polymer concentration, so an experiment was conducted as follows. A solution of the tetrahedron–**P21** or s2–**P21** conjugate was analysed by DLS, both at room temperature and at 40°C. As previously observed, the concentration of polymer was too low for any meaningful results to be extracted from the data. The solution was cooled to room temperature, an aliquot of poly(NIPAM) homopolymer solution was added and the measurements repeated; this process was iterated several times until ten equivalents (relative to the tetrahedron) of the homopolymer had been added. In the case of the s2–**P21** conjugate the DLS results did not indicate the presence of any stable structures.

By contrast, in the case of the tetrahedron–**P21** conjugate the DLS results showed the formation of stable nanoparticles with a hydrodynamic diameter of around 220 nm, see Figure 6.19.

These structures were not observed at room temperature, indicating that the temperature-responsive polymer was responsible for their formation. The solution of hybrid nanoparticles was studied further by increasing the temperature of the solution. This led to an increase in the particle size, as shown in Figure 6.21.

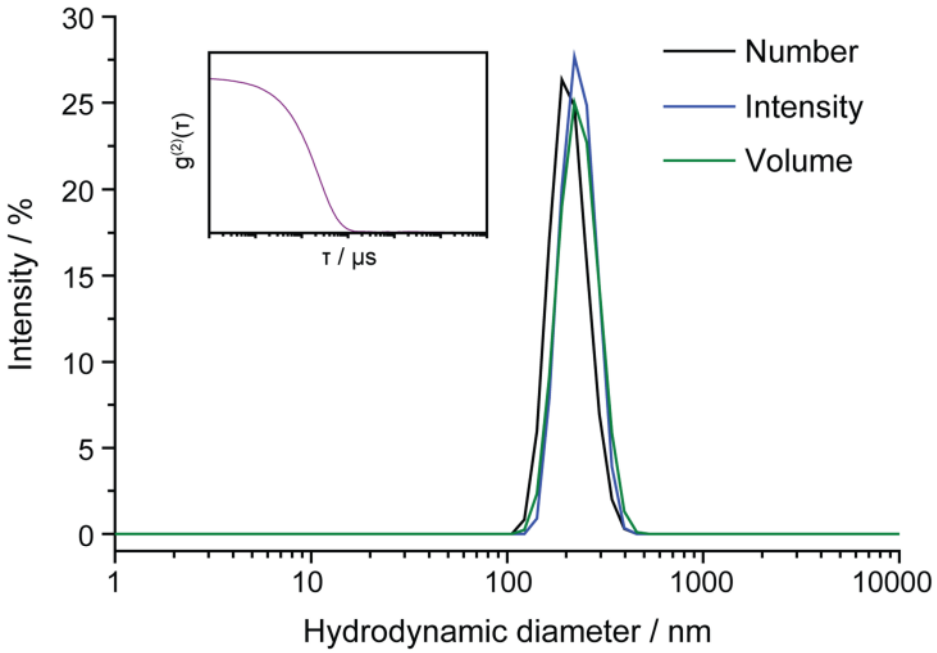

Figure 6.19 Temperature-induced formation of nanoparticles from **P21** in the presence of the tetrahedron–**P21** conjugate. DLS data for the nanoparticles at 40°C (correlation function inset) – there was good agreement between the analyses by scattering intensity (blue), particle volume (green) and number of particles (black). The hydrodynamic diameter of the particles was estimated to be 220 nm, with a dispersity of 0.13.

A possible cause of this phenomenon was the dynamic equilibrium between homopolymer free in solution and trapped in the core of the nanoparticles. As the temperature was increased, the equilibrium shifted to favour aggregation in the core, thus increasing the size of the particles.

The homopolymer alone exhibited none of these properties: upon heating it simply aggregated and precipitated (Figure 6.20 A). The s2–**P21** conjugate did exhibit the ability to form large structures under these conditions, but DLS indicated that they were unstable and the results were not reproducible (Figure 6.20 B) – interestingly, increasing the concentration of the s2–**P21** conjugate did not result in stabilisation, suggesting that the *structure* of the DNA plays an important role in the nanoparticle formation. As a final control, unconjugated tetrahedra were mixed with **P21** and studied by DLS at 40°C. Again, no stable structures were observed (Figure 6.20 C).

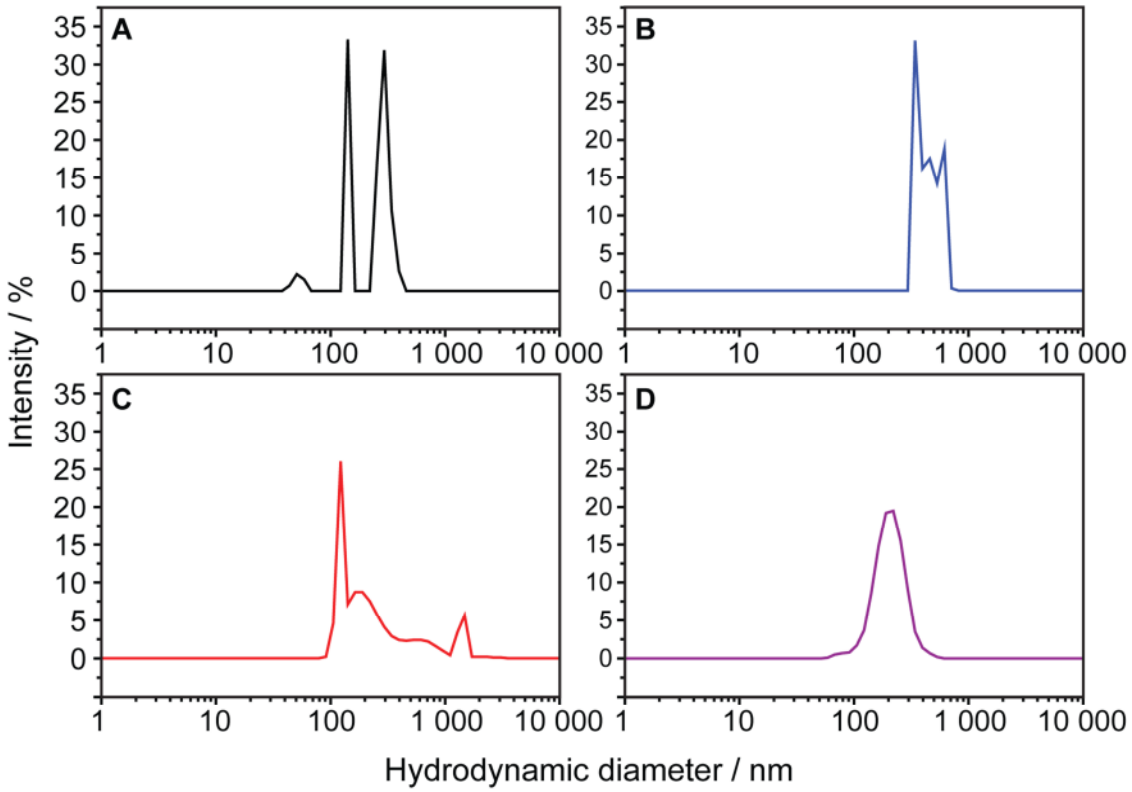

Figure 6.20 DLS analysis by intensity of solutions of the following in 1 × TEM buffer: A – **P21**; B – **P21** + s2–**P21**; C – **P21** + plain DNA tetrahedron; D – **P21** + DNA tetrahedron–**P21** conjugate. Stable nanoparticles were only observed in the presence of the DNA tetrahedron-polymer conjugate.

Based on these results, it was proposed that as **P21** approached its cloud point the tetrahedron–**P21** conjugate stabilised the formation of discreet nanoparticles (see Figure 6.22); the large volume occupied by the tetrahedron (relative to a single strand of DNA) meant that a relatively low concentration of the conjugate was needed for stabilisation to occur, and the high degree of negative charge present on the DNA nanostructure prevented aggregation of the nanoparticles.

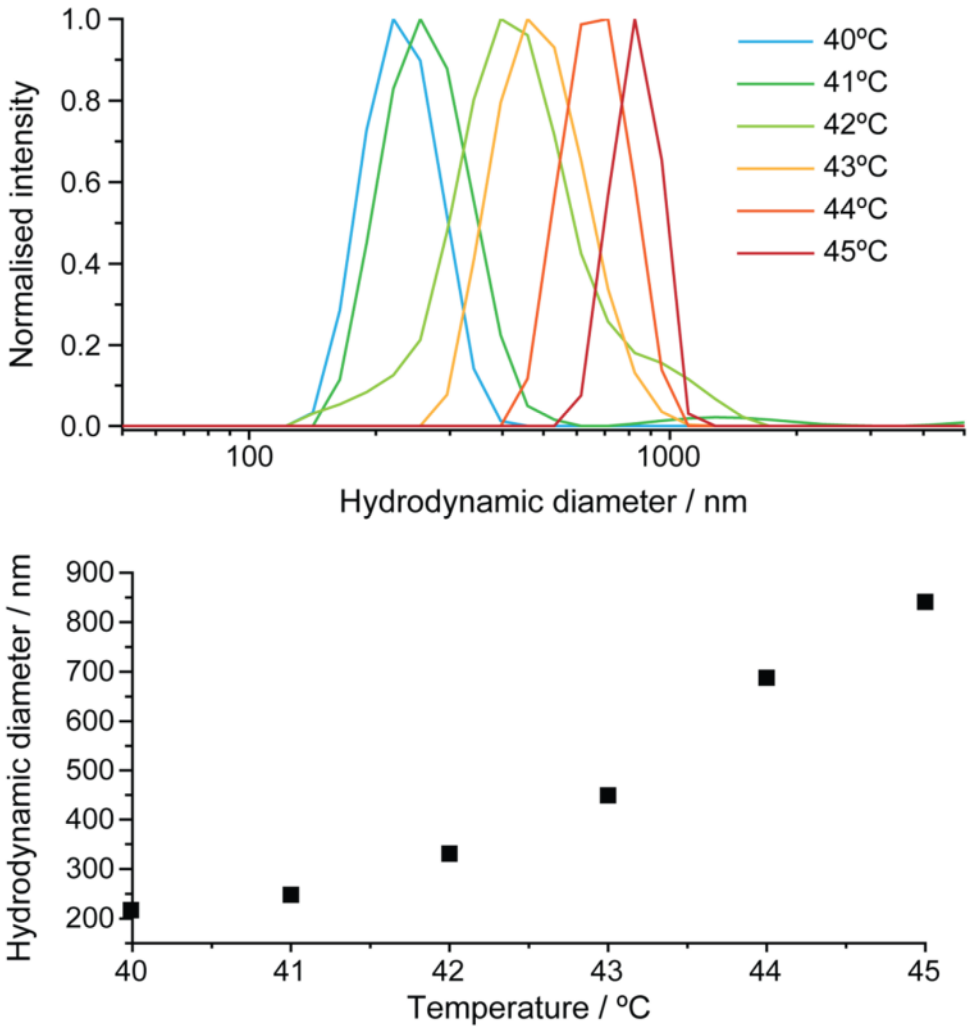

Figure 6.21 DLS studies of the dependence of the **P21**/tetrahedron–**P21** nanoparticle size on temperature. Top: DLS intensity traces. Bottom: plot of the average particle size by DLS versus temperature.

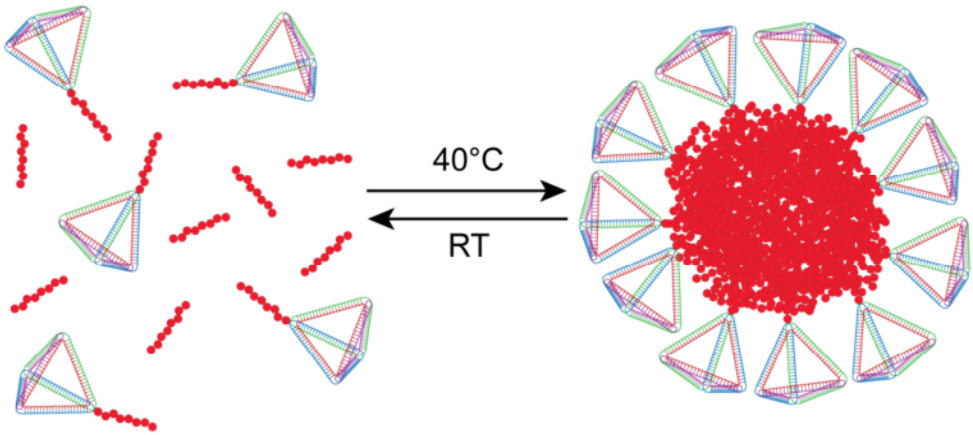

Figure 6.22 Cartoon of the proposed assembly process of the tetrahedron–**P21** nanoparticles. The DNA tetrahedra sit at the surface of a collapsed particle of poly(NIPAM) (red chains), acting like surfactants to stabilise the hydrophobic polymer.

To corroborate the light scattering data, the nanoparticles were studied by cryogenic transmission electron microscopy (cryoTEM). It proved difficult to ensure that the nanoparticle solution stayed above 40°C during preparation of the cryoTEM grid – this led to disassembly of the nanoparticles as the solution cooled down. A solution of the nanoparticles was studied by DLS immediately after it had been cooled to room temperature from 40°C. A plot of the correlograms revealed a steady decay over time (Figure 6.23).

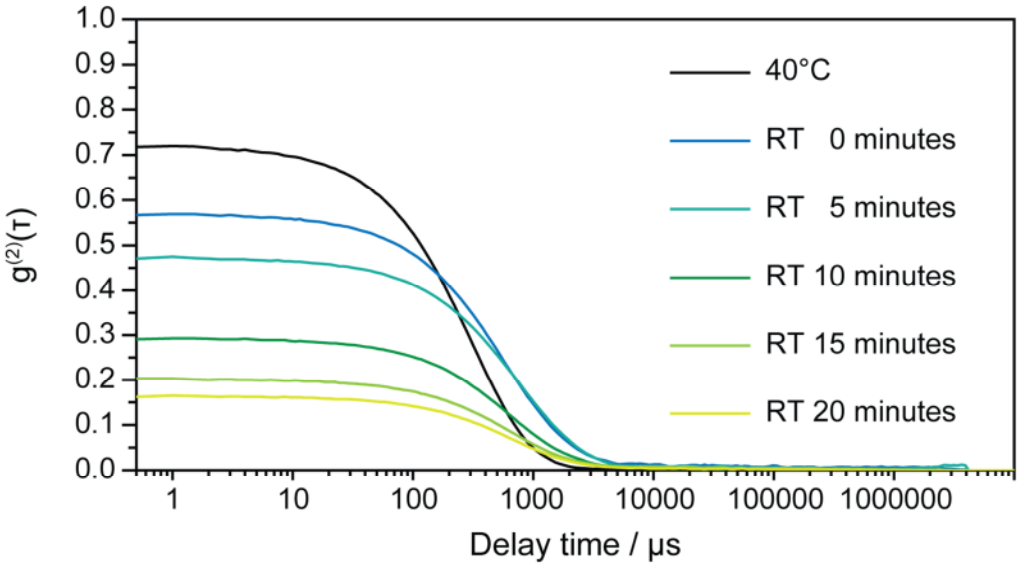

Figure 6.23 Correlograms from DLS analysis of a solution of the **P21**/tetrahedron–**P21** nanoparticles at 40°C (black trace) and at different times following rapid cooling to room temperature. The decay in the maximum value of the second order correlation function ($g^{(2)}(\tau)$) suggested the rapid disassembly of the nanoparticles.

The second order correlation function ($g^{(2)}(\tau)$) is related to the signal intensity by Equation 6.1. When the intensity of scattered light (I) is dominated by scattering from particles (that is, a large number are present in solution), the initial correlation (the intercept of the second order correlation function with the y axis) will be high. However, as the intensity becomes dominated by noise (because, for example, the concentration of particles has decreased) the initial correlation value will become lower. The intercept can therefore be regarded as a surrogate value for the concentration of particles in solution.

$$g^{(2)}(\tau) = \frac{\langle I(t)I(t+\tau)\rangle}{\langle I(t)\rangle^2}$$

Equation 6.1 Expression of the second order correlation curve ($g^{(2)}$) as a function of delay time (τ), showing the relation to the intensity (I) for all times t.

The decay in the correlation function intercept for the above experiment therefore indicated that the nanoparticles were indeed disassembling, and that the disassembly process had already begun by the time the solution reached room temperature.

A stabiliser was therefore sought that would make the sample preparation easier, but without altering the size or morphology of the nanoparticles too much. Citric acid (Figure 6.24) has been previously shown to stabilise nanostructures containing poly(NIPAM),[15] and so was tested as an additive to the **P21**/tetrahedron–**P21** nanoparticles. The multidentate structure of the acid means it is able to dehydrate and stabilise poly(NIPAM) nanostructures by forming multiple hydrogen bonds with the amide groups of the polymer.

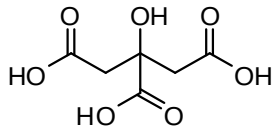

Figure 6.24 Citric acid.

To test the effect of the additive, the **P21**/tetrahedron–**P21** nanoparticles were assembled as normal at 40°C. DLS measurements were taken and revealed the formation of the expected structures (Figure 6.25, black trace). Citric acid was then added to give a final concentration of 12 mM and the DLS measurements repeated. As the red trace in Figure 6.25 shows, the main peak remained essentially unchanged, although there was some evidence of the formation of large aggregates. The solution was then cooled to room temperature and the measurements repeated once more after equilibration for five minutes (about the length of time required to make up a cryoTEM grid). The DLS results indicated that the nanoparticles persisted in solution (Figure 6.25, blue trace) even at this lower temperature, with no significant change in their size, suggesting that the citric acid was

having the desired stabilising effect; it was therefore used as an additive in the cryoTEM studies described below.

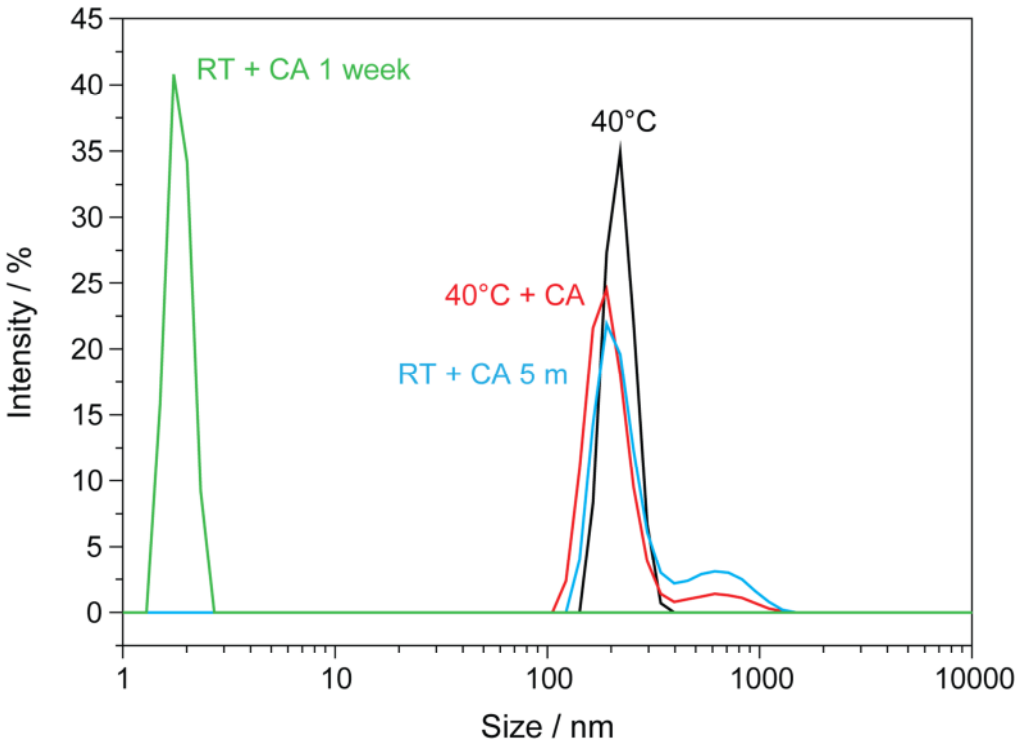

Figure 6.25 DLS analyses by number of a solution of the **P21**/tetrahedron–**P21** nanoparticles before and after the addition of citric acid (CA). Black: 40°C without CA. Red: 40°C with 12 mM CA. Blue: room temperature with 12 mM CA, 5 minutes after cooling from 40°C. Green: room temperature with 12 mM CA, 1 week after cooling from 40°C.

The citric acid-stabilised nanoparticles were analysed once more after being left for one week at room temperature. As the green trace in Figure 6.25 shows, the nanoparticles had completely disassembled to unimers – the crosslinking by citric acid was therefore reversible and short-lived.

Interestingly, upon reheating the solution to 40°C no stable nanoparticles were observed. This implied that the citric acid was interfering with the assembly process. Since formation of the nanoparticles relied on the controlled collapse of the polymer *via* hydrogen bonding interactions, it is perhaps unsurprising that the addition of a hydrogen bonding additive caused this mechanism to be disrupted. In all future work, therefore, the nanoparticles were pre-formed before addition of the citric acid stabiliser.

The nanoparticles were next studied by cryoTEM, using citric acid as an additive. Figure 6.26 shows a typical electron micrograph of one of the **P21**/tetrahedron–**P21** nanoparticles, and further images are shown in Figure 6.28.

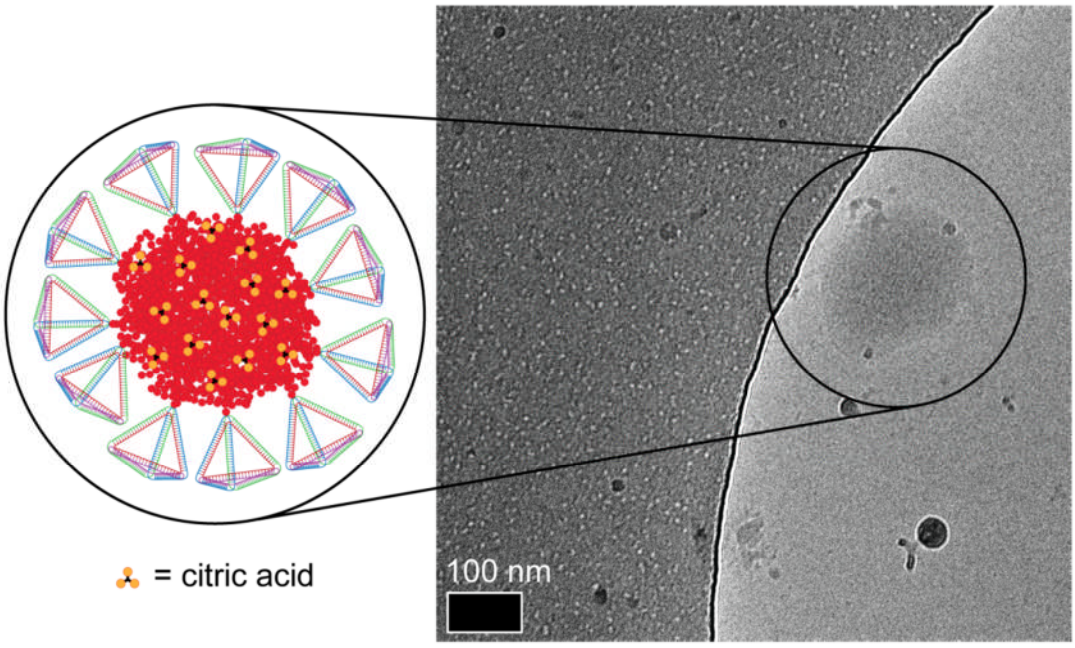

Figure 6.26 Representative cryoTEM micrograph of a DNA **P21**/tetrahedron–**P21** nanoparticle. Scale bar: 100 nm.

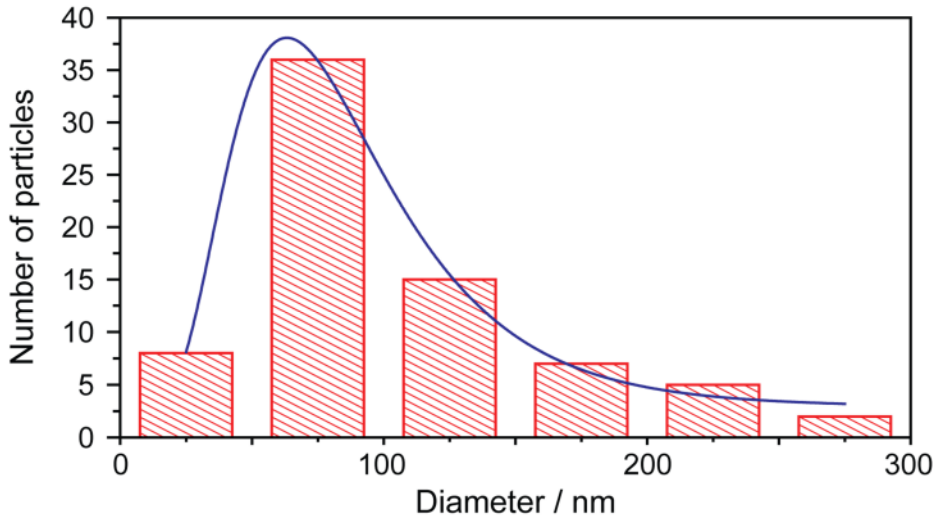

Figure 6.27 Particle size histogram (n = 73) for the **P21**/tetrahedron–**P21** nanoparticles imaged by cryoTEM; log-normal fit provided (blue trace).

A large number of particles (73) were measured and their sizes used to produce a particle size histogram (Figure 6.27). The average particle size (79 ± 3 nm) was estimated by fitting

a log-normal distribution to the data, and was smaller than that observed by DLS (220 nm). The discrepancy likely arose because the light scattering method gave undue weight to the small but significant population of particles above 200 nm in diameter.

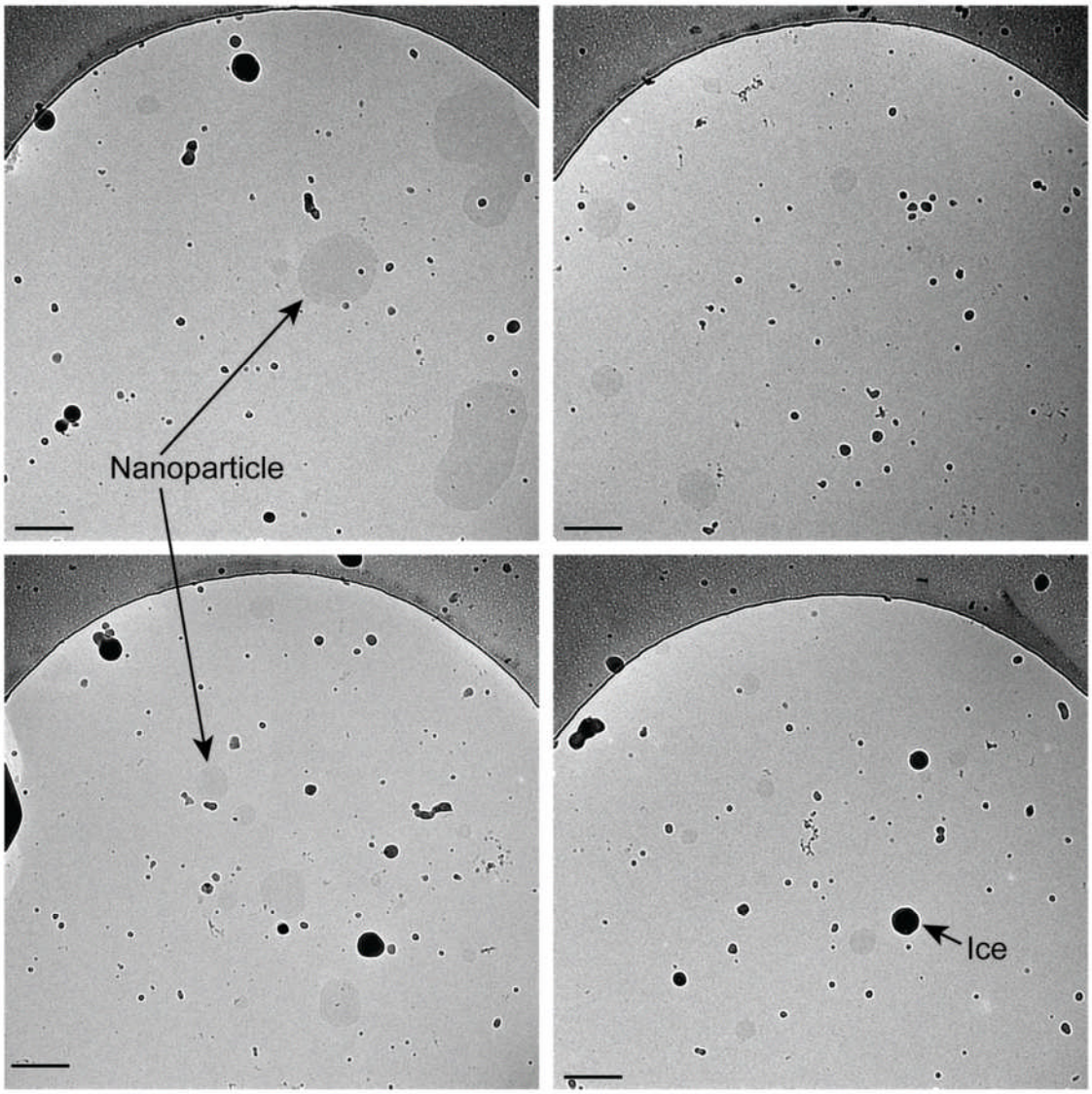

Figure 6.28 Additional cryoTEM images showing the **P21**/tetrahedron–**P21** nanoparticles. All scale bars are 200 nm.

The nanoparticles were studied by atomic force microscopy (AFM) by drying them onto either a mica or glass surface to assess retention of conjugate–polymer associations in the presence of both a high (mica) and low (glass) energy substrate. This was done in the absence of any additives as the AFM samples could be prepared at 40°C. On mica, DNA tetrahedron–polymer conjugates were observed both in isolation and in an aggregated state,

with polymer distributed intermittently over the surface (see bottom of Figure 6.29).

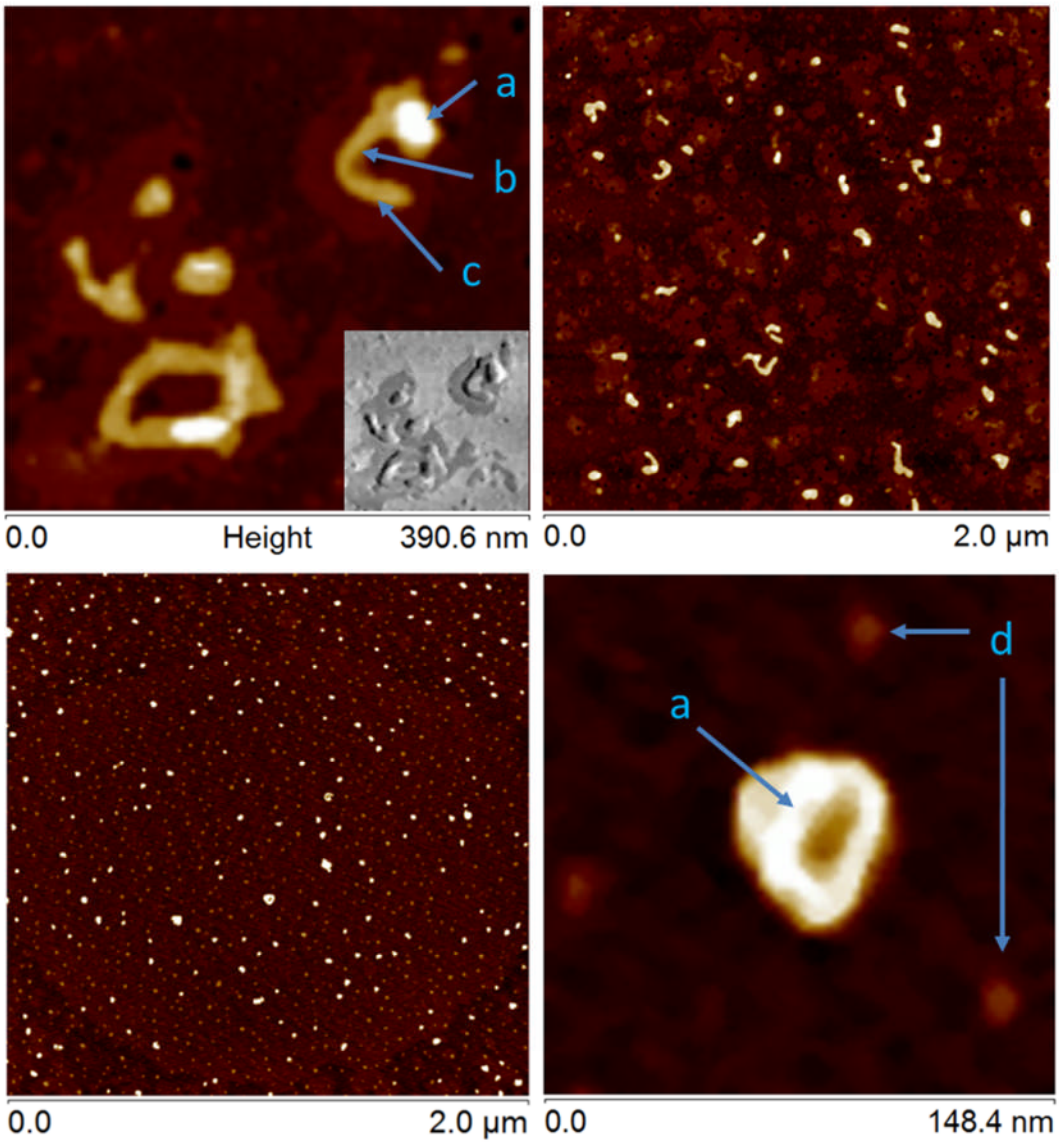

Figure 6.29 Representative AFM topography (tapping mode) micrographs of the **P21**/tetrahedron–**P21** nanoparticles. Top: spin coated on glass (phase contrast inset). Bottom: spin coated on mica. Structural assignments: (a) Tetrahedron–**P21** conjugate aggregate – tightly bound, (b) associated **P21**, (c) associated **P21** collapsed onto surface, and (d) individual tetrahedron–**P21** conjugates.

In all images, both the DNA tetrahedron–polymer conjugates and the aggregates were found primarily on areas of the substrate covered by polymer. These results suggested that the mica induced the large hybrid nanoparticles to partially disassemble upon drying and that the resultant material was more stable on polymer than on a high surface-energy substrate. On glass, a lower surface-energy substrate, the strong preference for free

polymer association to the DNA–polymer conjugates was more pronounced, with the polymer clustering around the DNA nanostructures (see top of Figure 6.29 and Figure 6.30) and overall diameters of the DNA nanostructures and associated polymer approaching those observed in cryoTEM (see Figure 6.31). The differences in diameter can be attributed to the effects of drying the sample to the AFM substrate.

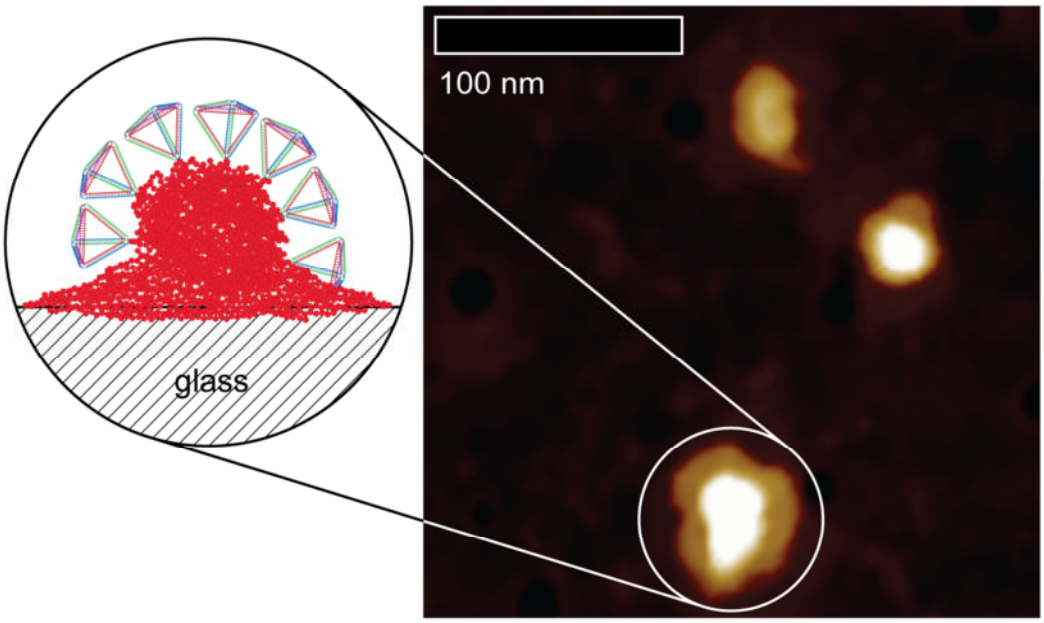

Figure 6.30 AFM micrograph of tetrahedron–**P21** nanoparticle and associated free polymer on glass.

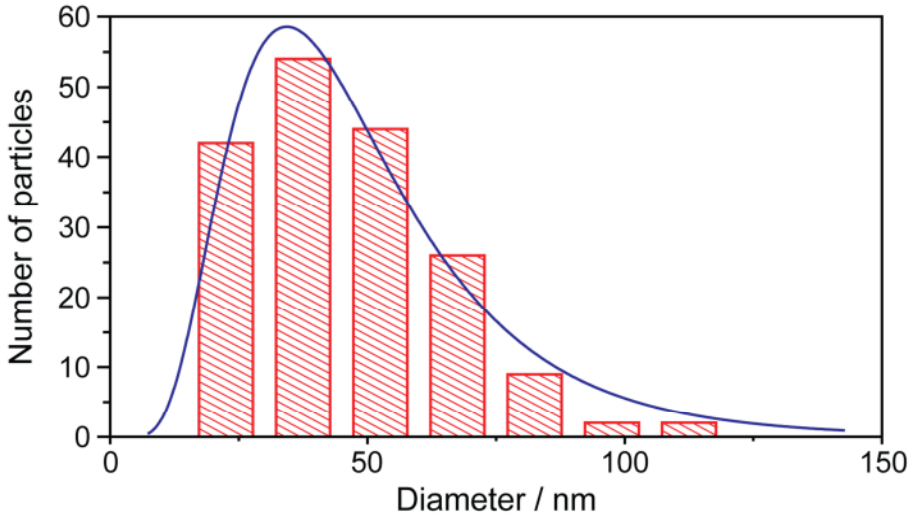

Figure 6.31 Particle diameter histogram (n = 178) of the **P21**/tetrahedron–**P21** nanoparticles imaged by AFM on glass; log-normal fit provided (blue trace).

Based on the data from DLS, cryoTEM and AFM, it is proposed that as **P21** approached its cloud point the formation of discrete nanoparticles (Figure 6.22) composed of a collapsed polymer core stabilised by DNA nanostructures anchored to its surface by a covalently attached polymer chain was favoured. As a result of the large volume occupied by the tetrahedron (relative to a single strand of DNA), only a low concentration of the conjugate was needed for stabilisation to occur. The high density of negative charge on the DNA nanostructure prevented aggregation of the nanoparticles. The DNA tetrahedron–**P21** species thus behaved like a 'giant surfactant'.

6.4.iii Shell crosslinking of DNA tetrahedron–poly(NIPAM) nanoparticles using a cationic polymer

Crosslinking of the shell of the nanoparticles was next attempted. To do this, an additive was required that would interact with the DNA and be able to span adjacent tetrahedra. Poly(ethyleneimine) (PEI, Figure 6.32) is a hydrophilic, positively charged, branched polymer capable of forming a charge complex with the negatively charged phosphate backbone of DNA, and was therefore selected as a potential shell-crosslinker.

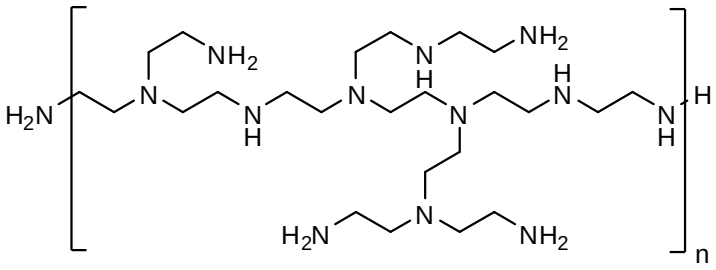

Figure 6.32 The structure of poly(ethyleneimine) (PEI) illustrating the branched nature of the polymer (note that this is an illustration only and does not describe the exact structure of the polymer). Although drawn as neutral here, in solution PEI carries multiple positive charges due to protonation of its amino groups.

The **P21**/tetrahedron–**P21** nanoparticles were assembled at 40°C as described above and the mixture analysed by DLS. Increasing equivalents of PEI (measured as the amine to phosphate group ratio) were then added as shown in Table 6.3.

Table 6.3 Conditions tested for the attempted shell crosslinking of **P21**/tetrahedron–**P21** nanoparticles using PEI. The reactions were carried out by addition of an aliquot of a concentrated solution of PEI to a much larger volume of the nanoparticles.

Reaction #	Amine/phosphate ratio
1a	0.005
1b	0.01
1c	0.05
1d	0.1
1e	0.5
1f	1

For each concentration the solution was analysed after the addition of PEI both at 40°C and then again at room temperature. Lower numbers of equivalents of PEI caused destabilisation of the nanoparticles both at high and low temperatures. However, at an amine to phosphate ratio of 0.5 the nanoparticles were observed to be stable both at 40°C and at room temperature, even after equilibration for 30 minutes (Figure 6.33).

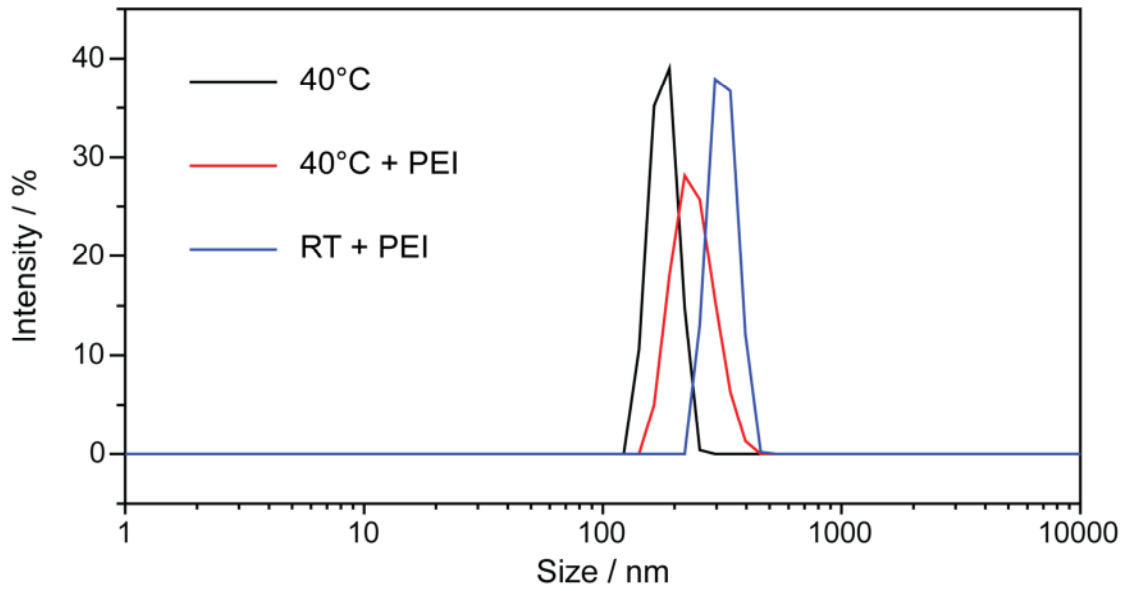

Figure 6.33 DLS analyses by number of a solution of the **P21**/tetrahedron–**P21** nanoparticles at 40°C before (black) and after (red) the addition of PEI (0.5 amines per DNA phosphate group), and at room temperature in the presence of PEI after 30 minutes equilibration time. The particles were observed to persist and swell upon cooling to room temperature.

Furthermore, at room temperature the nanoparticles were observed to swell, with the hydrodynamic diameter increasing from around 200 nm to nearly 400 nm. This can be explained by the changing hydrophilicity of the poly(NIPAM) trapped within the crosslinked nanoparticles. At lower temperatures, the poly(NIPAM) core became more hydrated, swelling the nanoparticles; the degree of crosslinking in the shell was enough to prevent the nanoparticles from disassembling, but low enough to allow this swelling to take place.

At an amine to phosphate ratio of one, the particles once more became destabilised and formed large aggregates both at 40°C and room temperature. Once a charge neutral complex was formed between the PEI and DNA backbone, the shell of the nanoparticles became hydrophobic, negating the surfactant-like properties of the tetrahedron–**P21** conjugate and causing disassembly of the nanoparticles. This mechanism of charge-neutralisation has been used many times in the literature to form so-called polyion complex micelles,[16,17] and so it is gratifying that a similar effect was observed here.

The ability of PEI to effectively crosslink the nanoparticles provided further strong evidence that the DNA tetrahedra resided in the shell of these structures. Figure 6.34 illustrates the proposed crosslinking process.

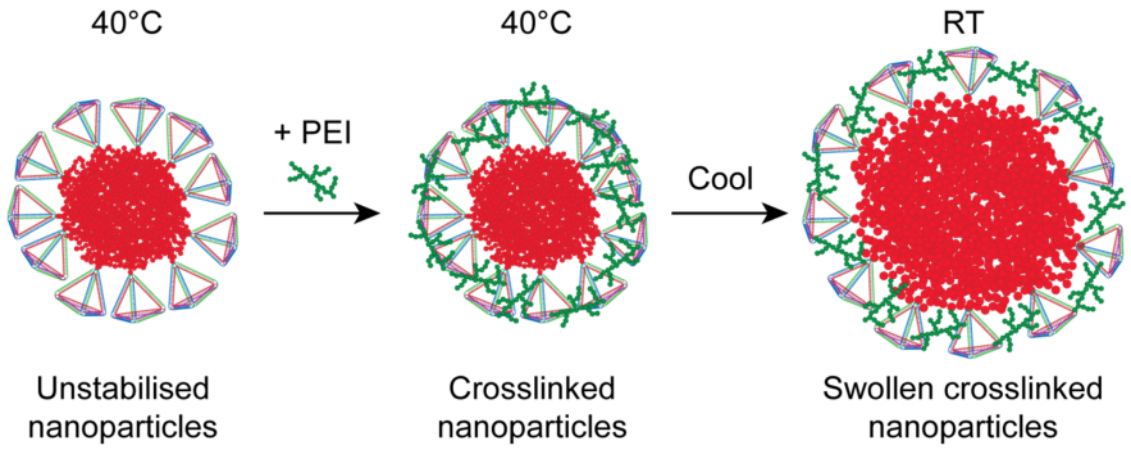

Figure 6.34 Cartoon of the proposed shell-crosslinking of the **P21**/tetrahedron–**P21** nanoparticles by PEI. PEI formed a charge complex with the phosphate groups of DNA, which caused the particles to maintain their shape upon cooling of the solution. Cooling also induced swelling of the cross-linked particles as the poly(NIPAM) core became hydrated.

6.4.iv Assembly using higher molecular weight poly(NIPAM)

Formation of polymer-functionalised tetrahedra from the s2–**P22** conjugate synthesised above was also attempted. The tetrahedron–**P22** conjugate was assembled using the same dialysis method as described above, by mixing the four component strands in formamide and then dialysing against the assembly buffer. Analysis by 4 % native PAGE (Figure 6.35) indicated that the tetrahedron had formed as expected, as a broad, low-mobility band had appeared and no other bands (due to incomplete tetrahedra or free s1, s3 or s4 – see Figure 6.6) were observed, except for some residual s2–**P22** conjugate, indicating that this component had been added in a slight excess.

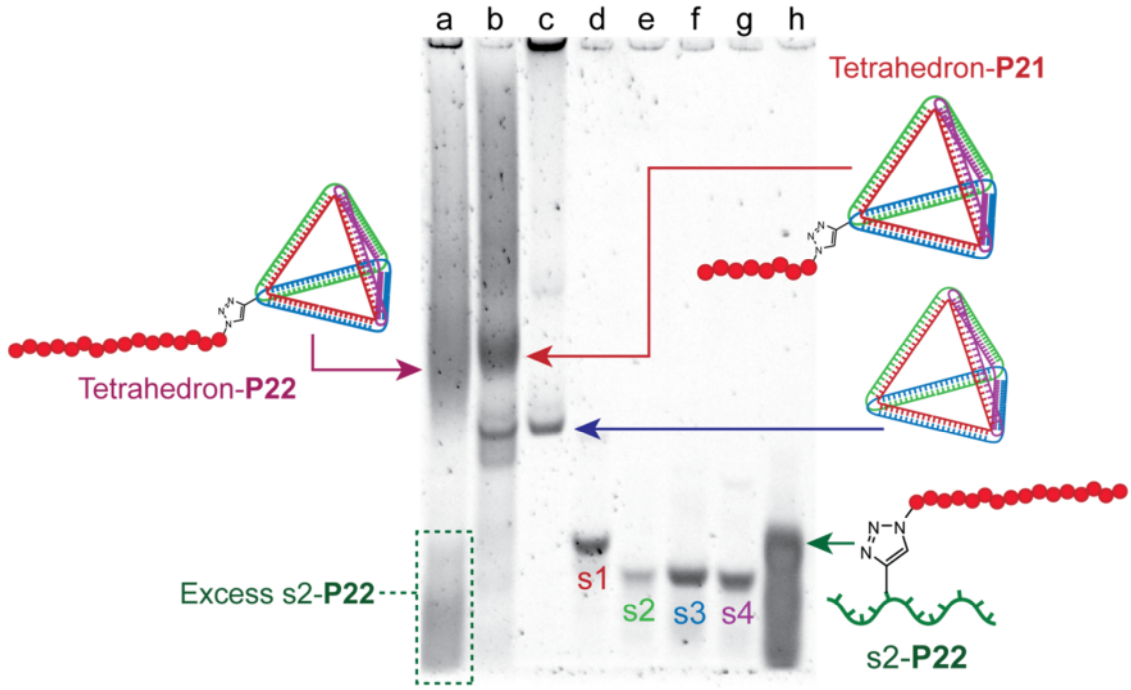

Figure 6.35 4 % native PAGE analysis showing the formation of the tetrahedron–**P22** conjugate. Some free s2–**P22** conjugate was observed, but no free s1, s3 or s4 or partially-assembled tetrahedra. Lane: a – tetrahedron–**P22** conjugate; b – tetrahedron–**P21** conjugate; c – plain tetrahedron; d – s1; e – s2; f – s3; g – s4; h – s2–**P22** conjugate.

Next, ten equivalents of free **P22** homopolymer were added to the tetrahedron–**P22** conjugates and their self-assembly studied at a range of temperatures from 35°C to 45°C. Below the cloud point of **P22** (39.7°C) no structures were observed; upon heating above this temperature, large, ill-defined particles were observed (Figure 6.36). However, at no

point were stable particles (analogous with those formed from the tetrahedron–**P21** conjugate above) observed. It is proposed that this arose from the higher molecular weight of **P22** compared to **P21**, which resulted in aggregation being favoured over the formation of discrete nanoparticles.

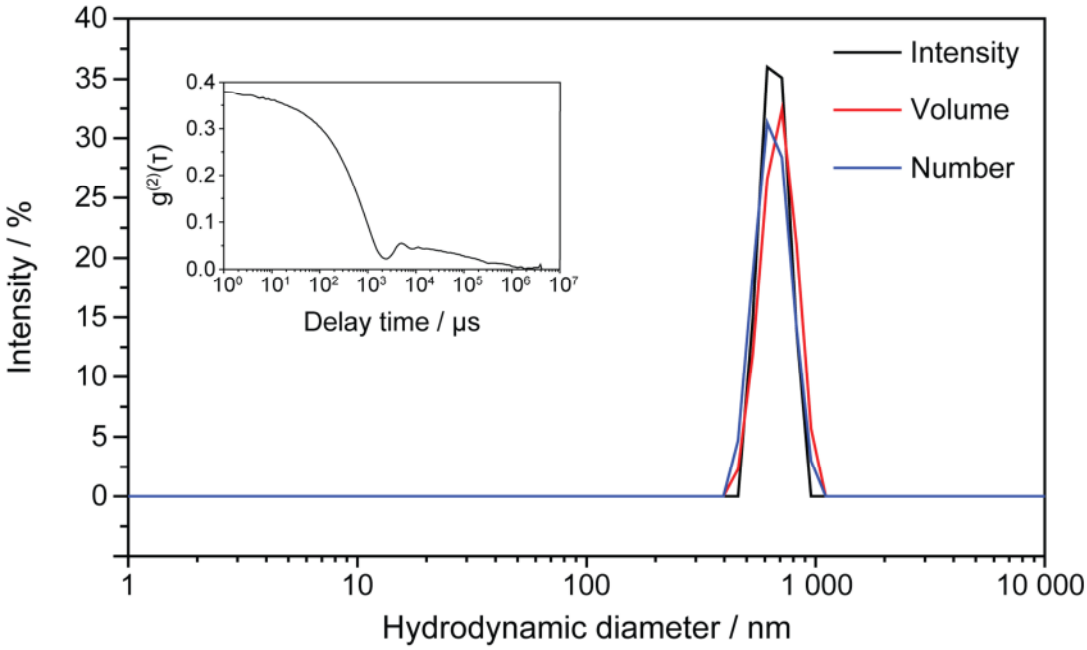

Figure 6.36 DLS analysis by intensity (black), volume (red) and number (blue) of a mixture of **P22** and DNA tetrahedron–**P22** conjugate in 1 × TEM buffer at 40°C. Only large aggregates were observed and the correlation function (inset) indicated poor data quality.

Finally, purification of the s2–**P23** conjugate was attempted, but insufficient material was recovered upon which to perform further assembly studies.

6.5 Conclusions

DNA–polymer conjugates were successfully synthesised incorporating poly(NIPAM) and the s2 component strand of a DNA tetrahedron. The DNA tetrahedron was successfully assembled from this conjugate and the three other component strands (s1, s3 and s4) using an isothermal strategy. Formation of the tetrahedron structure was proved by native PAGE analysis by a series of controls wherein one strand was systematically omitted from the structure. Incorporation of the fluorophores FAM and TAMRA on separate strands resulted in the observation of FRET in the assembled structures by fluorescence spectrometry, providing further strong evidence for the correct formation of the DNA nanostructure. The same polymer was also conjugated to a ligated, alkyne-functionalised tetrahedron; the product displayed identical migration behaviour under electrophoresis, strongly supporting the conclusion that the tetrahedron had been formed correctly.

The tetrahedron–poly(NIPAM) conjugates were found to stabilise the formation of large particles of poly(NIPAM) homopolymer upon heating close to the polymer's cloud point. These nanoparticles were observed to be highly dynamic in nature and increased in size as the temperature was raised from 40°C to 45°C. The particles were characterised by DLS, cryoTEM and AFM, all of which supported the hypothesis of a shell of tetrahedron–polymer conjugates surrounding a collapsed polymer core. Citric acid was found to be an effective temporary crosslinker of the core of the nanoparticles, which provided further evidence of a poly(NIPAM) core. Finally, PEI was employed to successfully crosslink the shells of the nanoparticles. Crosslinking provided evidence of the presence of DNA in the nanoparticles and resulted in their stabilisation at room temperature, with concomitant swelling due to the increased hydration of the core polymer domain.

6.7 Experimental section

6.7.i Materials & Methods

For general materials and methods details, see the Appendix. The component strands of the plain DNA tetrahedron (s1-4), two containing fluorescent groups (s1–FAM and s3–TAMRA), and one containing an internal alkyne modification (s2–alkyne) were purchased from Integrated DNA Technologies Ltd. and resuspended in 18 MΩ water to a final concentration of 200 μM prior to use. HPLC buffer A consisted of 0.1 M triethylammonium acetate (TEAA) containing 5 % acetonitrile. 10 × TEM buffer contained 10 mM Tris HCl, 1 mM EDTA and 6 mM $MgCl_2$. An Eppendorf Mastercycler® was used for assembly of plain DNA tetrahedra. T4 polynucelotide kinase (10 000 units mL^{-1}), T4 DNA ligase (400 000 cohesive end units mL^{-1}) and T4 DNA ligase buffer were purchased from New England Biolabs and used as received. All others materials were purchased from Sigma-Aldrich and used as received.

6.7.ii Synthesis of s2–poly(NIPAM) conjugates

DMF was degassed by bubbling with N_2 for 30 minutes prior to use. DMF (75 μL), poly(NIPAM)–N_3 (**P21**, **P22** or **P23**) (10 μL, 1 mM in DMF), CuI · $P(OEt)_3$ (10 μL, 1 mM in DMF) and s2–alkyne DNA (5 μL, 200 μM in water) were mixed in a centrifuge tube and left at room temperature overnight. The reaction mixture was then concentrated *in vacuo* to a final volume of approximately 10 μL. HPLC buffer A (90 μL) was added and the mixture vortexed then centrifuged. The s2–poly(NIPAM) conjugates were identified by 15 % native PAGE, and s2–**P21** and s2–**P22** isolated by HPLC. After resuspension of the dried fractions in 18 MΩ water, the yield was estimated to be 50 % by UV-vis spectroscopy in both cases.

6.7.iii Assembly of DNA tetrahedra

Equal volumes (10 μL) of 1 μM solutions of s1, s2, s3 and s4 were mixed with 10 × TEM buffer (10 μL) and 18 MΩ water (50 μL). The mixture was sealed inside a centrifuge tube

and heated in a PCR machine to 95°C for four minutes, then rapidly cooled to 4°C over the course of one minute. Finally, the solution was allowed to warm to room temperature.

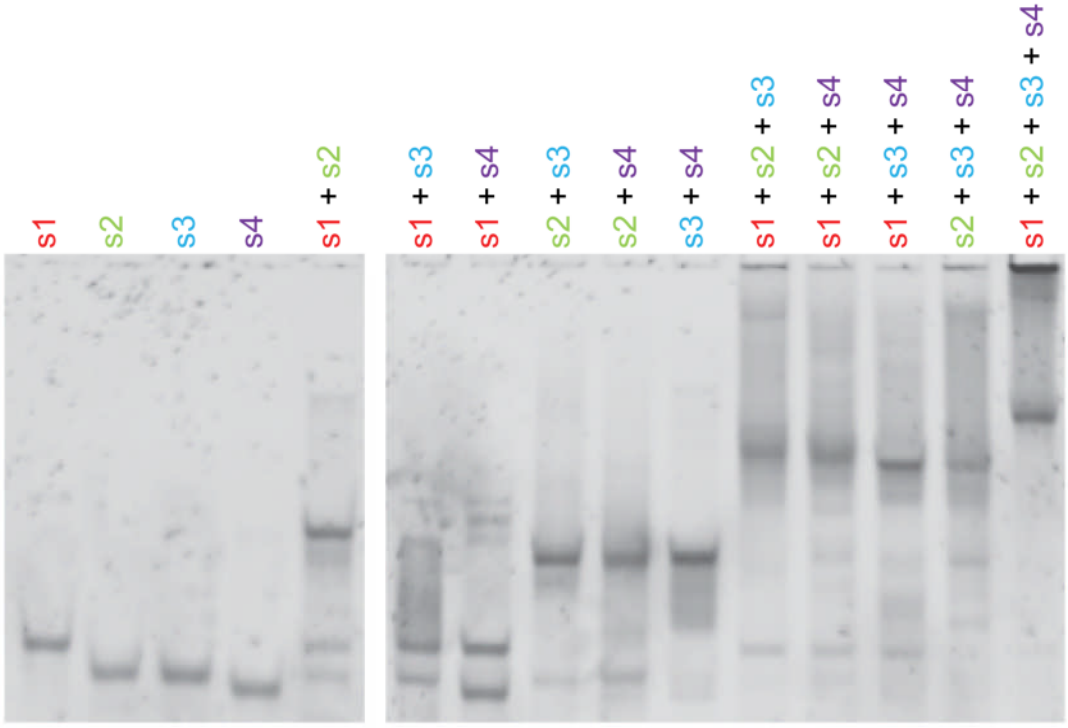

Figure 6.37 Unlabelled version of the gel presented above in Figure 6.6.

6.7.iv Assembly of tetrahedron–polymer conjugates

Equal volumes (20 μL) of 5 μM solutions of s1, s2–**P21**, s3 and s4 were mixed with formamide (850 μL) and 18 MΩ water (70 μL). The solution was transferred to a microdialyser fitted with a 1 000 Da MWCO membrane and stirred in a large volume of the assembly buffer (1 × TEM buffer) overnight.

6.7.v Fluorescence study of FAM- and TAMRA-labelled tetrahedra

FAM- and TAMRA- functionalised DNA tetrahedra and tetrahedron–**P21** conjugates were prepared as described above by employing the dye labelled strands s1–FAM and s3–TAMRA. The fluorescence spectra of the tetrahedra incorporating none, one or both of the dyes were then recorded by exciting at 495 nm. The presence of the TAMRA group was confirmed (where it was present) by excitation at 559 nm.

6.7.vi Ligation of an alkyne-functionalised tetrahedron

The alkyne-functionalized DNA tetrahedron was assembled and ligated as follows. DNA strands s1, s2–alkyne, s3 and s4 (1 μL of each, 10 μM in water) were mixed with 18 MΩ water (84 μL), 10 × T4 DNA ligase buffer (10 μL) and T4 polynucleotide kinase (2 μL, 10 000 units mL^{-1}) and the solution heated at 37°C for 30 minutes. The temperature was then increased to 65°C for 20 minutes to deactivate the enzyme.

The temperature was again increased, to 95°C, for 4 minutes, after which time the solution was cooled rapidly by submersing the reaction vessel in an ice bath. Once cool, T4 DNA ligase (5 μL, 400 000 cohesive end units mL^{-1}) was added and the mixture incubated at room temperature for one hour. Analysis by 8 % native PAGE confirmed the successful formation of the tetrahedron, and denaturing PAGE confirmed that the ligation procedure had been successful.

6.7.vii Conjugation of poly(NIPAM) to a ligated tetrahedron

All solutions were degassed by bubbling with nitrogen for 30 minutes prior to use. The ligated alkyne-functionalised tetrahedron (20 μL, 250 nM in 1 × TEM buffer), **P21** (10 μL, 10 mM in acetonitrile), copper sulfate pentahydrate (10 μL, 10 mM in water), (+)-sodium L-ascorbate (10 μL, 10 mM in water) and *tris*-(hydroxypropyltriazolylmethyl)amine (THPTA) (10 μL, 10 mM in water) were mixed and left overnight at 26°C. Analysis by 8 % native PAGE confirmed that the tetrahedron–polymer conjugate had been formed in approximately 40 % yield.

6.7.viii Measurement of cloud points

The cloud points of **P21**, **P22** and **P23** were measured by following the UV-vis absorbance. A solution of the homopolymer (0.8 mg mL^{-1} in 1 × TEM buffer) was heated in a quartz cuvette within a UV-vis spectrometer, and the absorbance followed at 500 nm from 20°C to 60°C. After normalisation of the maximum absorbance to one, the cloud point was taken as the temperature at which the absorbance was 0.5.

6.7.ix Formation of P21/tetrahedron–P21 nanoparticles

Hybrid nanoparticles were produced as follows. A solution of the tetrahedron–**P21** conjugate (60 μL, 100 nM in 1 × TEM buffer) was added to a DLS cuvette and the light scattering data recorded at 24°C. The temperature was then increased to 40°C and the measurement repeated. After cooling to 25°C, an aliquot of **P21** homopolymer (0.8 mg mL^{-1} in 1 × TEM buffer) was added, the sample was allowed to equilibrate for 2 minutes, and the DLS measurement taken. The temperature was then increased to 40°C and the measurement repeated. This process was iterated until data had been acquired for the addition of 0.1, 0.5, 1, 2, 5 and 10 equivalents of homopolymer (relative to the tetrahedron–**P21** conjugate).

To ascertain whether the tetrahedron structure was responsible for the stabilisation of the nanoparticles, the experiment was repeated using the s2–**P21** conjugate. In place of the DNA tetrahedron, the DNA component of this species was a single strand without designed secondary structure. DLS indicated the formation of large, unstable particles ranging in diameter from around 50 to 500 nm.

To check that the homopolymer did not form structures on its own, a solution of **P21** was heated to 40°C and a DLS measurement taken. Even after extended equilibration at this temperature, only macroscopic aggregates were observed.

Identical procedures were followed using the s2–**P22** conjugate.

6.7.x CryoTEM measurements

The **P21**/tetrahedron–**P21** nanoparticles were studies by cryogenic TEM (cryoTEM) by assembling at 40°C (with a final tetrahedron concentration of 100 nM in 50 μL 1 × TEM buffer), adding citric acid (2 μL, 0.25 M in water) and quickly transferring the solution to the TEM grid and vitrifying in liquid ethane.

6.7.xi AFM measurements

Samples of the **P21**/tetrahedron–**P21** were both spin cast and drop cast onto freshly cleaved mica and glass as follows. Steel-fixed AFM substrates (2 mica, 2 glass) were preheated to 45°C using a hotplate. The **P21**/tetrahedron–**P21** solution was heated with the vial in a water bath, in turn submerged in an oil bath. The oil bath was regulated to 55°C at a rate of 0.5°C min^{-1} from room temperature.The water bath was monitored until a temperature of 50°C was reached, with total sustained time over 40°C approximately 18 minutes. The water bath was taken directly to the AFM substrates and the mica was cleaved. Spin coated glass and mica samples were cast using ~20 μL of solution with a 10 s 500 rpm/50 s 3000 rpm cycle and then dried further under dry filtered nitrogen for 10 minutes at room temperature. Drop cast glass and mica samples were cast using ~20 μL of solution, placed back on the hot plate for 20 s, wicked dry and then dried further under dry filtered nitrogen for 10 minutes at room temperature. After casting the samples, the water bath was confirmed to still be above 42°C.

6.7.xii Shell crosslinking of P21/tetrahedron–P21 nanoparticles with PEI

The shell of the **P21**/tetrahedron–**P21** nanoparticles was crosslinked using poly(ethyleneimine) (PEI) as follows. The nanoparticles were assembled as normal at 40°C at a volume of 100 μL, and a DLS measurement taken. PEI (4.5 μL, 0.1 μM in water) was added and the solution allowed to equilibrate for one minute before repeating the DLS measurement. The solution was then cooled to room temperature and equilibrated for a further minute before repeating the DLS measurement again. Finally, the solution was reheated to 40°C, equilibrated for one minute and the DLS measurement repeated once more. This process was iterated several times, so that measurements were taken at the following amine/phosphate ratios: 0.005, 0.01, 0.05, 0.1, 0.5 and 1. The branched PEI used had a number average molecular weight of 1 200 Da and a dispersity of 1.1 and was supplied by Sigma Aldrich.

6.8 References

(1) Goodman, R. P.; Schaap, I. A. T.; Tardin, C. F.; Erben, C. M.; Berry, R. M.; Schmidt, C. F.; Turberfield, A. J. *Science* **2005**, *310*, 1661.

(2) Kato, T.; Goodman, R. P.; Erben, C. M.; Turberfield, A. J.; Namba, K. *Nano Lett.* **2009**, *9*, 2747.

(3) Erben, C. M.; Goodman, R. P.; Turberfield, A. J. *Angew. Chem., Int. Ed.* **2006**, *45*, 7414.

(4) Walsh, A. S.; Yin, H.; Erben, C. M.; Wood, M. J. A.; Turberfield, A. J. *ACS Nano* **2011**, *5*, 5427.

(5) Kim, K.-R.; Kim, D.-R.; Lee, T.; Yhee, J. Y.; Kim, B.-S.; Kwon, I. C.; Ahn, D.-R. *Chem. Commun.* **2013**, *49*, 2010.

(6) Crawford, R.; Erben, C. M.; Periz, J.; Hall, L. M.; Brown, T.; Turberfield, A. J.; Kapanidis, A. N. *Angew. Chem., Int. Ed.* **2013**, *52*, 2284.

(7) Safak, M.; Alemdaroglu, F. E.; Li, Y.; Ergen, E.; Herrmann, A. *Adv. Mater.* **2007**, *19*, 1499.

(8) Costioli, M. D.; Fisch, I.; Garret-Flaudy, F.; Hilbrig, F.; Freitag, R. *Biotechnol. Bioeng.* **2003**, *81*, 535.

(9) Jungmann, R.; Liedl, T.; Sobey, T. L.; Shih, W.; Simmel, F. C. *J. Am. Chem. Soc.* **2008**, *130*, 10062.

(10) Wu, P. G.; Brand, L. *Anal. Biochem.* **1994**, *218*, 1.

(11) Alemdaroglu, F. E.; Herrmann, A. *Org. Biomol. Chem.* **2007**, *5*, 1311.

(12) Umeno, D.; Maeda, M. *Anal. Sci.* **1997**, *13*, 553.

(13) Ayaz, M. S.; Kwak, M.; Alemdaroglu, F. E.; Wang, J.; Berger, R.; Herrmann, A. *Chem. Commun.* **2011**, *47*, 2243.

(14) Maeda, M.; Nishimura, C.; Inenaga, A.; Takagi, M. *React. Polym.* **1993**, *21*, 27.

(15) Moughton, A. O.; Patterson, J. P.; O'Reilly, R. K. *Chem. Commun.* **2011**, *47*, 355.

(16) Oishi, M.; Sasaki, S.; Nagasaki, Y.; Kataoka, K. *Biomacromolecules* **2003**, *4*, 1426.

(17) Wakebayashi, D.; Nishiyama, N.; Yamasaki, Y.; Itaka, K.; Kanayama, N.; Harada, A.; Nagasaki, Y.; Kataoka, K. *J. Control. Release* **2004**, *95*, 653.

Chapter 7

Design and synthesis of polymers capable of interacting non-covalently with DNA

7.1 Introduction

Whilst a reasonably large body of work exists covering the chemical attachment of polymers to DNA (as reviewed in Chapter 1), almost no attention has been paid to the exploitation of other interactions for the creation of DNA–polymer conjugates. The structure of double stranded DNA presents a number of possible binding sites, as shown in Figure 7.1. Firstly, there are the major and minor grooves, formed by the asymmetric positioning of the phosphate backbone on the DNA bases (right of Figure 7.1).

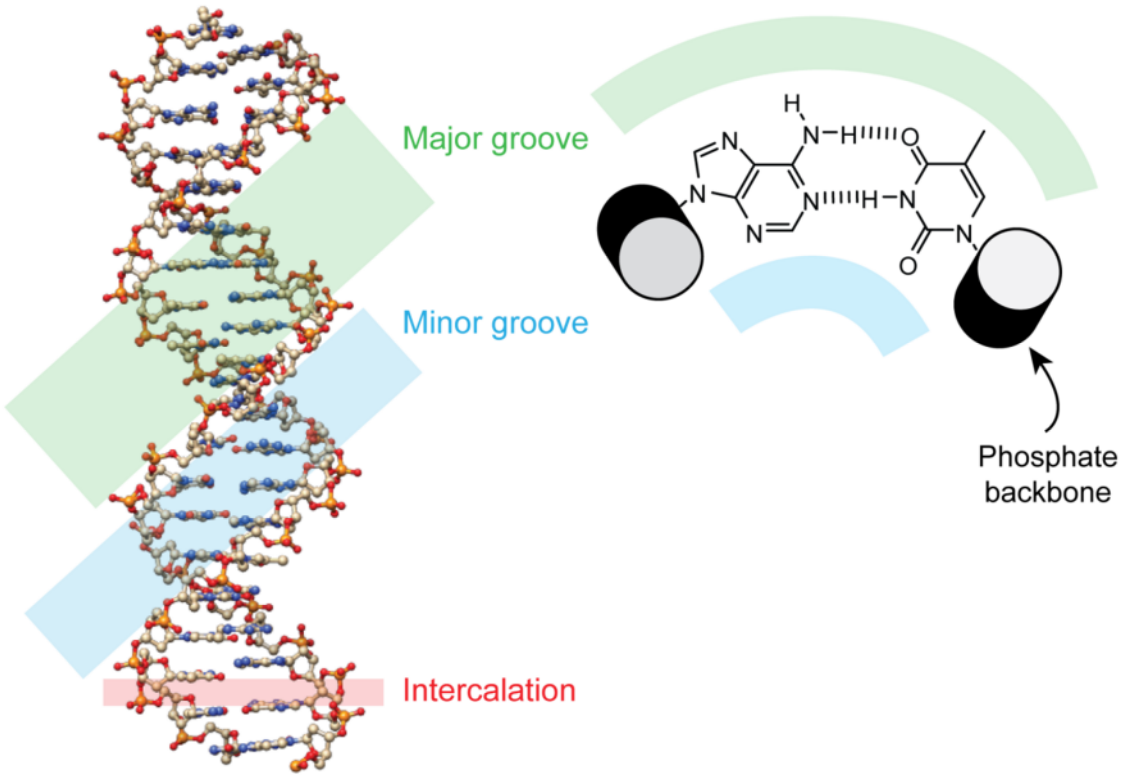

Figure 7.1 DNA double helix (left) with the positions of the major and minor grooves indicated. The grooves are formed by the asymmetric positioning of the phosphate backbone on the DNA bases (right). Intercalation may take place between any base pair.

Binding in the major groove of DNA is very common for proteins involved in DNA replication, handling and translation, which are able to use the large amount of exposed functionality to bind sequence-specifically to the DNA strand.[1] This high degree of functionality makes it more difficult to design small molecules that will bind in this region, but the minor groove provides a much easier target; Netropsin and Hoechst 33258 (Figure 7.2), which bind by a combination of hydrogen bonding and hydrophobic interactions, are typical examples.[2] Minor groove binding has been exploited to control the positioning of gold nanoparticles,[3] to make 'wires' capable of energy transfer along a DNA strand,[4,5] and to create microarrays for highly sequence-selective detection of double stranded DNA.[6] In fact, a binary system based on imidazole and pyrrole groups has been devised meaning that a molecule can be designed to target any given sequence of double stranded DNA.[7] To the author's knowledge, there have so far been no reports of DNA–polymer conjugation using groove binders to provide a reversible linkage. This is probably because the binders themselves are not easy to synthesise or modify (although the Burley group has made significant advances in the area of minor groove binders[4]), and so are unappealing to the majority of polymer synthesis groups. For the same reasons, the use of these molecules was not explored in the work described below.

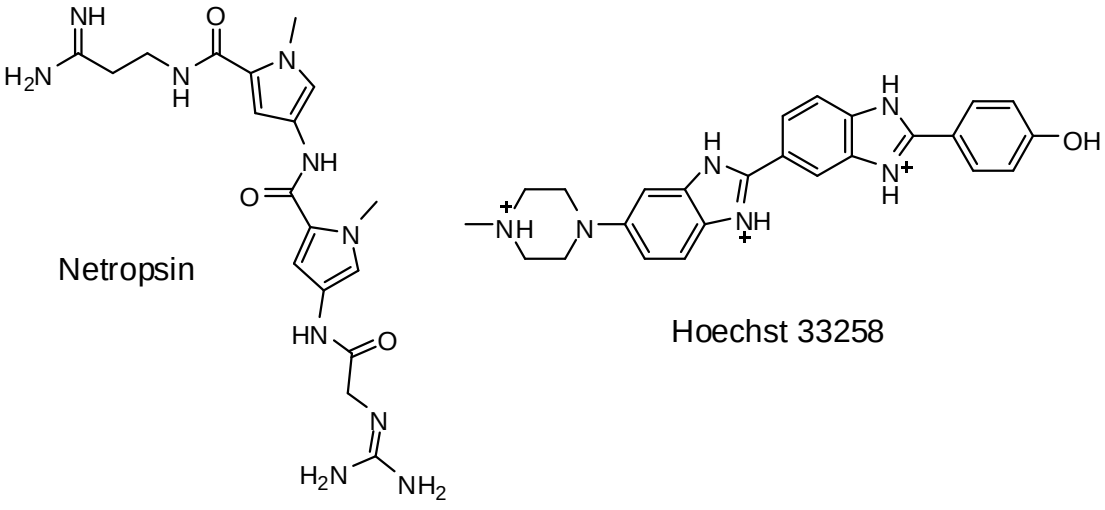

Figure 7.2 Structures of the DNA minor groove binders Netropsin and Hoechst 33258. The curved nature of the Netropsin molecule in particular enables strong binding to DNA.

Secondly, the space between the base pairs of DNA can also serve as a binding site for large, planar aromatic molecules such as acridine, Doxorubicin (a powerful anti-cancer drug) and ethidium bromide (a commonly used nucleic acid stain), the structures of which are shown in Figure 7.3.

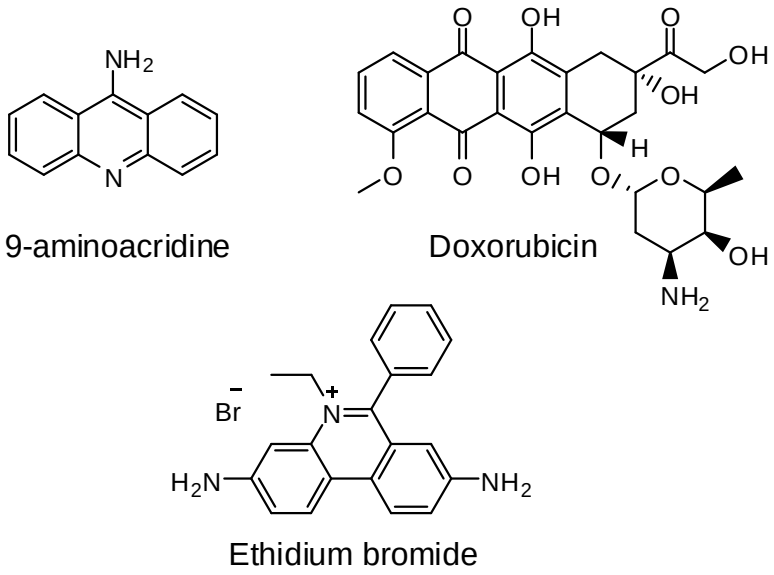

Figure 7.3 Structures of the DNA intercalators 9-aminoacridine, Doxorubicin and ethidium bromide. Intercalation is promoted by a large, planar aromatic system.

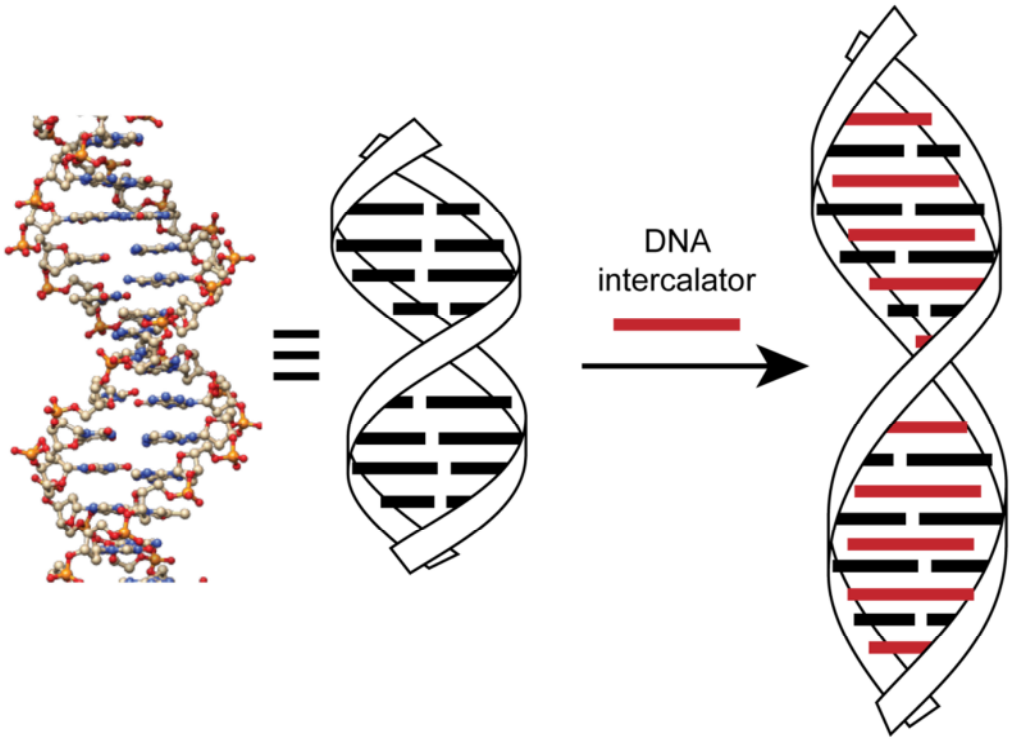

Figure 7.4 A schematic of the unwinding of the DNA double helix caused by intercalation.

The mechanism of binding involves unwinding of the DNA helix to create a sandwich complex with the intercalator (Figure 7.4). Molecules that bind to DNA in this manner are typically highly cytotoxic (but not always).[8] Aside from their use as drug molecules and dyes, DNA intercalators have also been used (in conjunction with a minor groove binder) to template the CuAAC reaction on a DNA strand.[9] There are a handful of reports of the use of DNA intercalation to facilitate DNA–polymer conjugation. One strategy has been to introduce a vinyl group into the DNA strand by using an appropriately-functionalised intercalator (in this case psoralen), which could then be permanently affixed by UV crosslinking with the base pairs; the 'DNA macromonomer' was then co-polymerised with acrylamide-type monomers to give a DNA–polymer hybrid material. However, the site of attachment and resultant polymers were poorly defined.[10] A similar strategy led to incorporation of salmon sperm DNA in acrylamide-based hydrogels (Figure 7.5).[11] Polymerisation of the DNA with NIPAM afforded conjugates that exhibited temperature-responsiveness and could be used to recover DNA-binding molecules such as ethidium bromide by simple heat-induced precipitation.[12]

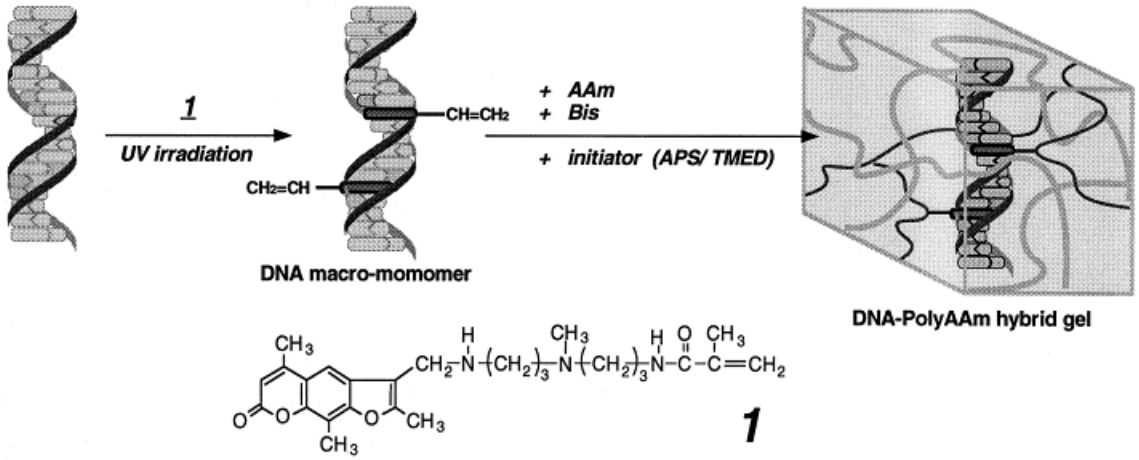

Figure 7.5 Synthesis of DNA-containing poly(acrylamide) hydrogels by use of a vinyl-functionalised DNA intercalator (psoralen), as described by Umeno and co-workers.[11]

The use of other intercalators for the purpose of DNA–polymer conjugation has not, to the author's knowledge, been explored, and no work has been done to quantify the effect of polymer size and structure on the strength of the intercalation interaction. The work that follows is an attempt to fill this gap.

7.2 Results & Discussion

7.2.i Synthesis of a RAFT CTA incorporating acridine

During the RAFT process, the R group of the CTA plays a key role. The R group radical must be stable enough to be a good leaving group during the pre-equilibrium step, but not so stable as to disfavour re-initiation. Aromatic groups such as benzene and pyrene are widely used and are effective at controlling the polymerisation of a wide range of monomers.[13]

The acridine group is a large, aromatic moiety and it was thought that it may be an effective R group for RAFT polymerisation. The CTA, **17**, was therefore synthesised as shown in Scheme 7.1.

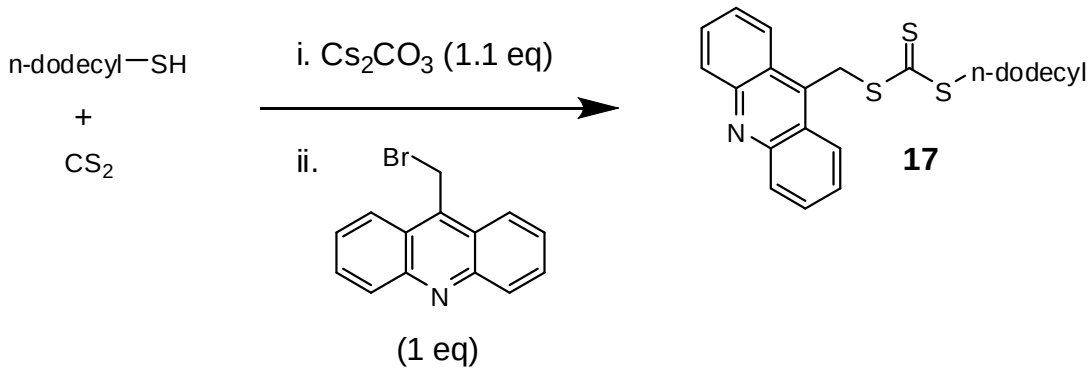

Scheme 7.1 Synthesis of a CTA containing the acridine group. The reaction was performed in acetone at room temperature; yield: 38 %.

Table 7.1 Details of the polymerisations attempted with CTA **17**. * Determined by integration of the SCH_2 group to the OCH_3 group. † Determined by THF SEC using PMMA calibration standards; two peaks were observed, which were analysed separately. ‡ Part of the distribution fell outside the calibration limits – these numbers are therefore likely to be inaccurate.

Monomer	Conversion after 24 h	M_n^{NMR} / Da*	M_n^{SEC} / Da†	Đ†
Styrene	0 %	-	-	-
NIPAM	0 %	-	-	-
MA	13 %	2 700	3 500	1.12
			163 000‡	1.39‡

17 was then used in the polymerisation of NIPAM, styrene and methyl acrylate (MA). The results are summarised in Table 7.1. For NIPAM and styrene, no monomer conversion was observed after 24 hours, and no polymer was detected by SEC analysis of the polymerisation reaction mixtures. In the case of MA, polymerisation was observed. However, SEC analysis showed a bimodal distribution for the sample, consisting of both very high and low molecular weight populations (see Figure 7.6).

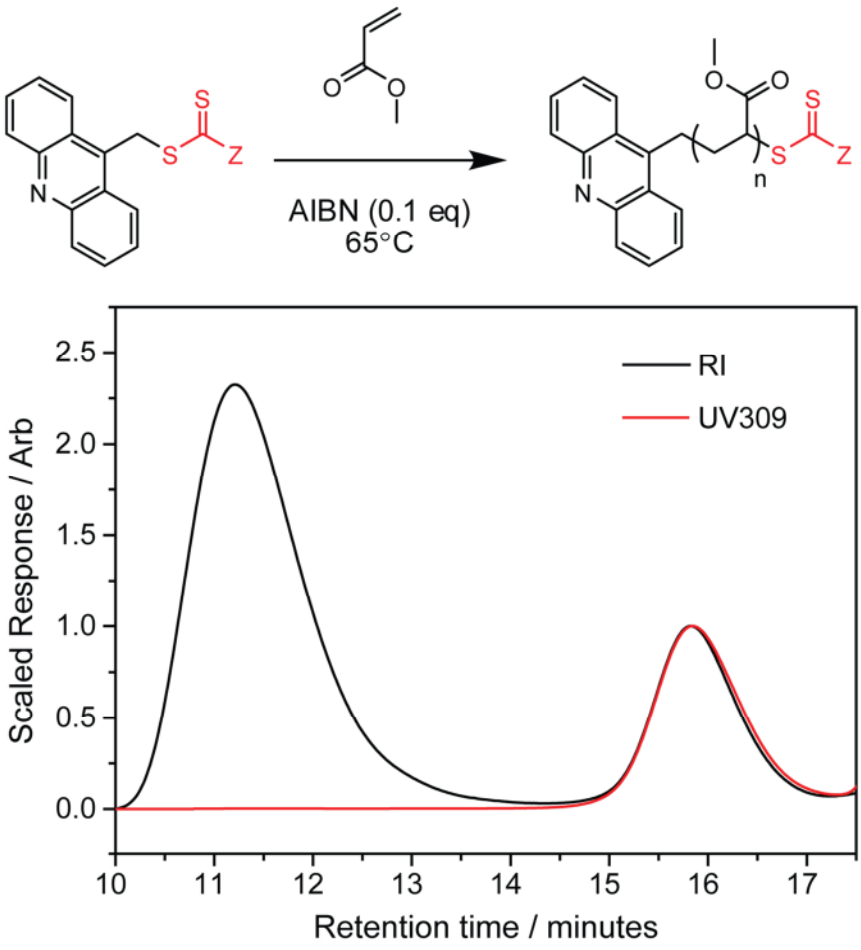

Figure 7.6 THF SEC chromatogram of the product of the attempted RAFT polymerisation of MA with CTA **17**. The refractive index (RI) trace showed two peaks: a broad, high molecular weight population (low retention time) and a narrow, low molecular weight population (high retention time). The UV trace recorded at 309 nm (UV309) shows only one peak. This implies that the trithiocarbonate group was only present in the lower molecular weight population, and subsequently that the high molecular weight population was not polymerised *via* the RAFT mechanism. The reaction was conducted for 24 hours under a nitrogen atmosphere.

Only the low molecular weight population exhibited a response at 309 nm (characteristic of the trithiocarbonate group in the CTA), implying that the high molecular weight population was formed by free radical polymerisation and not *via* the RAFT mechanism.

The poor performance of **17** as a CTA for the polymerisation of these monomers probably stemmed from the stability of the methyl acridine radical. One of the key steps in RAFT polymerisation is re-initiation (Scheme 7.2), wherein the R group radical ejected during the pre-equilibrium restarts the polymerisation of the monomer (M).

Initiation:

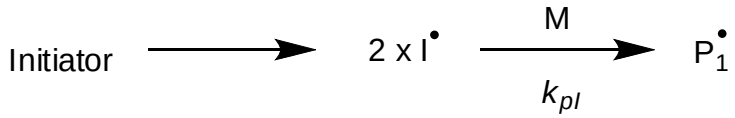

Propagation:

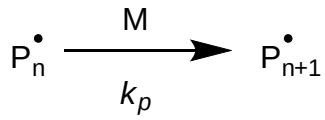

Pre-equilibrium:

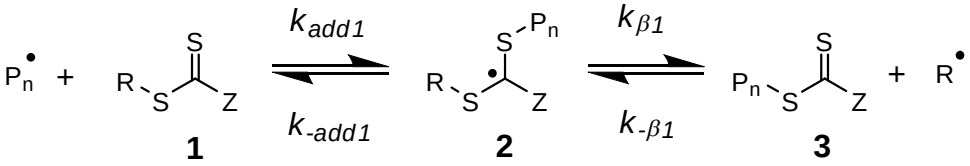

Re-initiation:

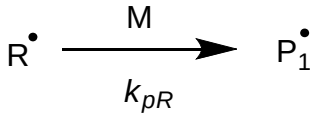

Main equilibrium:

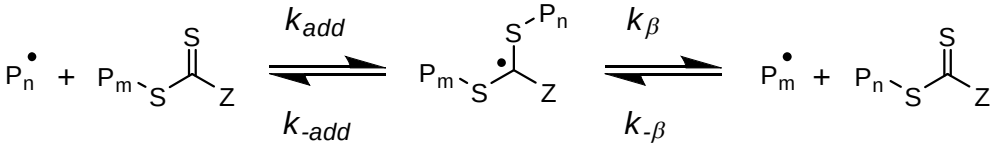

Scheme 7.2 The initiation period and main equilibrium from the proposed mechanism of RAFT polymerisation.

Re-initiation can only occur if the R group radical (methyl acridine in this case) is sufficiently reactive towards the monomer (M). It is proposed that the methyl acridine radical would be highly stabilised by the nitrogen atom (see Figure 7.7) and so be relatively unreactive. This group therefore acted as a radical trap to completely inhibit the polymerisation of styrene and NIPAM. In the case of MA, some re-initiation occurred, leading to the low molecular weight polymer distribution, but this was accompanied by uncontrolled free radical polymerisation, which gave rise to the high molecular weight distribution.

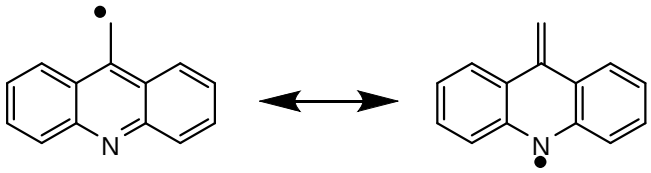

Figure 7.7 Resonance stabilisation of the methyl acridine radical by the nitrogen atom.

Given that the methyl acridine group seemed to be incapable of controlling the RAFT polymerisation of the monomers of interest, it was decided that the synthesis of an alternative CTA should be attempted.

7.2.ii Synthesis of an alternative acridine-containing CTA

In order to keep the acridine group away from the trithiocarbonate group – and therefore prevent it from interfering with the control of the polymerisation – a five carbon linker was first introduced by modification of 9-chloroacridine with 5-amino-1-pentanol to give **18** (step i, Scheme 7.3).[9] Next, **18** was coupled to the widely used CTA 2-(Dodecylthiocarbono-thioylthio)-2-methylpropionic acid (DDMAT) using standard esterification conditions (step ii, Scheme 7.3). UV-vis spectroscopy confirmed the presence of both the acridine (characteristic absorbance at 395 nm) and trithiocarbonate (309 nm) groups in the final product, **19** (see Figure 7.8). The extinction coefficient for **19** at 395 nm in acetonitrile was measured to be 787 ± 6 M^{-1}.

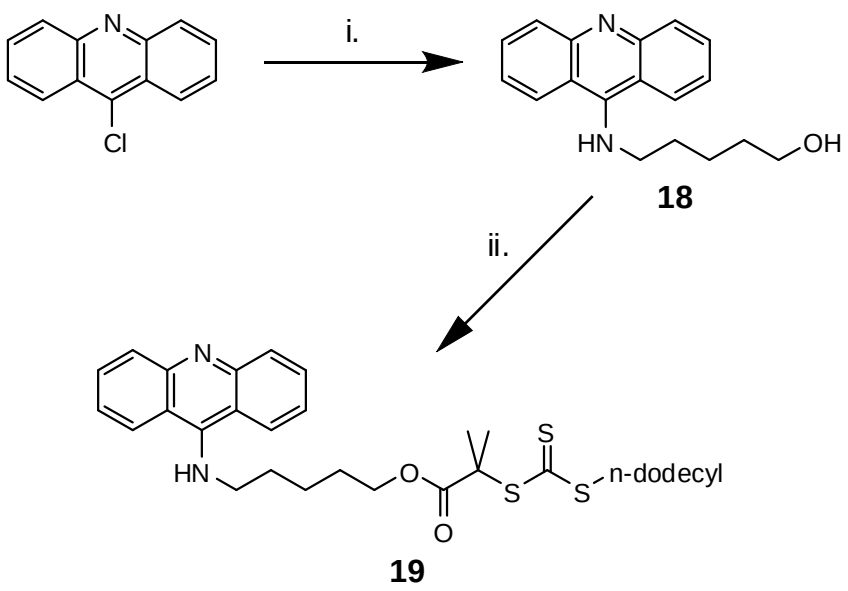

Scheme 7.3 Synthesis of the acridine-containing CTA **19**. Reaction conditions: i) 5-amino-1-pentanol (2.5 eq), DMF, N_2, 100°C, 5 hours, 85 %; ii) DDMAT (1 eq), EDCI (2 eq), DMAP (0.5 eq), $CHCl_3$/DCM, N_2, 48 hours, 53 %.

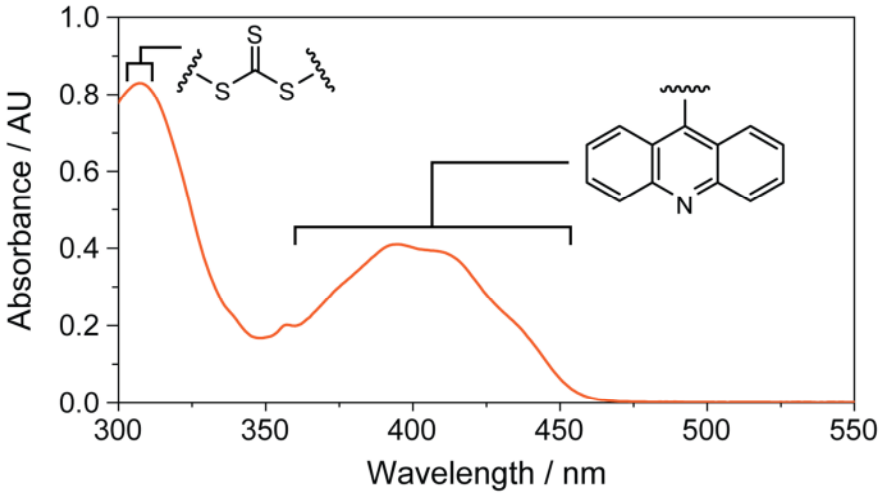

Figure 7.8 UV-vis spectrum of the acridine-containing CTA **19** in acetonitrile at 50 μM. The peaks due to the trithiocarbonate (309 nm) and acridine (distinctive pattern of several peaks with a maximum at 395 nm) groups were both clearly visible.

Interestingly, the acridine absorbance region for the CTA **19** differed significantly in peak shape and position from that in **18** (see Figure 7.9). This was attributed to the close proximity of the trithiocarbonate group in **19**, which probably had a significant effect on the energetics of the acridine group (particularly since their key transitions overlapped and were therefore of similar energy).[14] Given that, in the polymers that would be synthesised,

the acridine and trithiocarbonate groups would be separated by a long polymer chain (and therefore presumably not capable of interacting), it was decided that **18** should be used as the model small molecule compound for comparison with the polymers rather than **19**. Furthermore, whilst **18** was soluble in a wide range of polar solvents, **19** exhibited low solubility, particularly in the aqueous buffer systems in which DNA intercalation studies would be carried out.

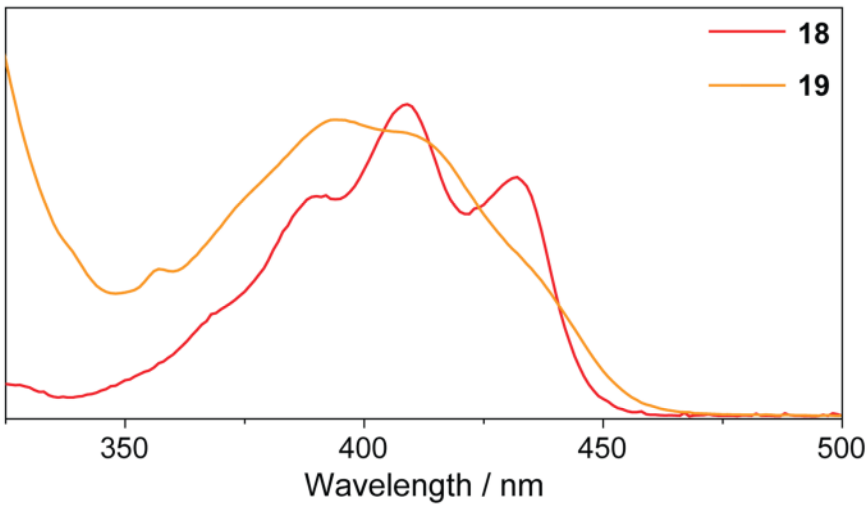

Figure 7.9 UV-vis spectrum showing the qualitative differences between the peaks in the acridine region from the acridine-containing CTA **19** (orange) and the precursor **18** (red) in acetonitrile. **18** exhibits a more defined peak shape and has absorbance maxima shifted relative to those of **19**.

7.2.iii RAFT polymerisation using CTA 19

Since the acridine-containing CTA **17** was found to inhibit the polymerisation of several monomers, **19** was tested to ascertain whether a similar effect would be produced when the acridine group was kept away from the trithiocarbonate group. The RAFT polymerisation of NIPAM with **19** was attempted and the reaction followed by ^{1}H NMR spectroscopy and SEC; in contrast to **17**, a controlled polymerisation was achieved. The dispersity (Đ) steadily decreased as the reaction proceeded and good control over molecular weight was achieved in the product (Đ < 1.2) (top of Figure 7.10). The data also showed a linear relationship between monomer conversion and number average molecular weight (M_n) (bottom of Figure 7.10).

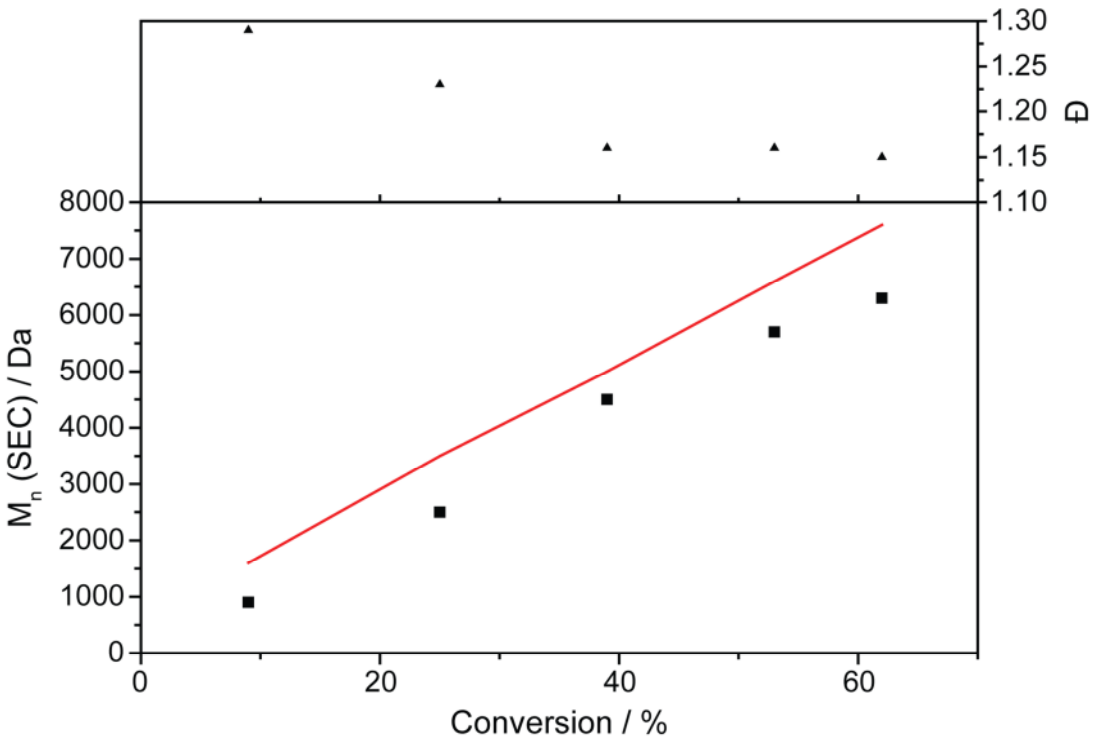

Figure 7.10 Plots of dispersity (Đ) and number average molecular weight (M_n) versus conversion for the polymerisation of NIPAM with CTA **19**. These data display two key characteristics of a pseudo-living polymerisation: M_n increased linearly with conversion (red line = theoretical M_n); Đ decreased with conversion and remained below 1.2.

Finally, the reaction displayed first order kinetics with respect to the monomer – that is, a plot of the natural logarithm of the ratio between the initial monomer concentration ($[M]_0$) and monomer concentration at a particular time point ([M]) versus time displayed a linear relationship (Figure 7.11).

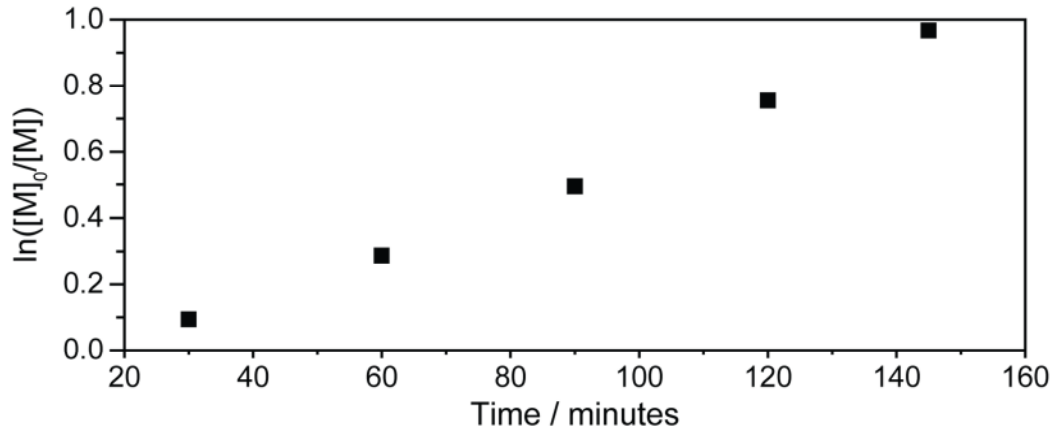

Figure 7.11 Plot of $\ln([M]_0/[M])$ versus time for the polymerisation of NIPAM with CTA **19**. $[M]_0$ is the initial monomer concentration and [M] is the concentration of monomer at a particular time point. These data display a further key characteristic of a pseudo-living polymerisation: first order kinetic behaviour i.e. a linear relationship between $\ln([M]_0/[M])$ and time.

These features are characteristic of a pseudo-living polymerisation, and furthermore no induction period was observed. It was therefore concluded that the acridine group did not have an adverse effect on the polymerisation when incorporated away from the trithiocarbonate group.

Having proven that **19** was an effective CTA for RAFT polymerisation, a number of different water soluble polymers were synthesised (see Table 7.2, **P24**-**28**). Figure 7.12 shows the structures of the monomers used.

Table 7.2 Properties of the polymers synthesized using CTA **19**. * Determined by ^{1}H NMR spectroscopy. † Determined by DMF SEC using PMMA calibration standards. ‡ Controlled polymerisation of HEA was not achieved § The large discrepancy between the SEC and NMR values arose because PMMA is not a good model for the solution-phase behaviour of PTEGA.

Sample	Monomer	M_n^{NMR} / kDa*	M_n^{SEC} / kDa†	Đ†
P24	NIPAM	5.7	6.3	1.15
P25a	DMA	10.2	6.7	1.13
P25b	DMA	26.0	24.2	1.16
P26	TEGA	22.5	10.1§	1.22
P27	4-AM	6.3	8.4	1.15
P28	HEA‡	-	22.9	1.89

Good control was achieved over the polymerisations of NIPAM (**P24**), dimethylacrylamide (DMA) (**P25a**-**b**), triethylene glycol methyl ether acrylate (TEGA) (**P26**) and 4-acryloyl morpholine (4-AM) (**P27**). However, the controlled polymerisation of hydroxyethyl acrylate (HEA) (**P28**) was unsuccessful, with SEC indicating a significant degree of crosslinking. The controlled polymerisation of this monomer was not further investigated. The other products included two polymers with full solubility in water (**P25** and **P27**), one with a low cloud point (**P24**) and one with a high cloud point (**P26**) – an interesting spread of properties for future studies.

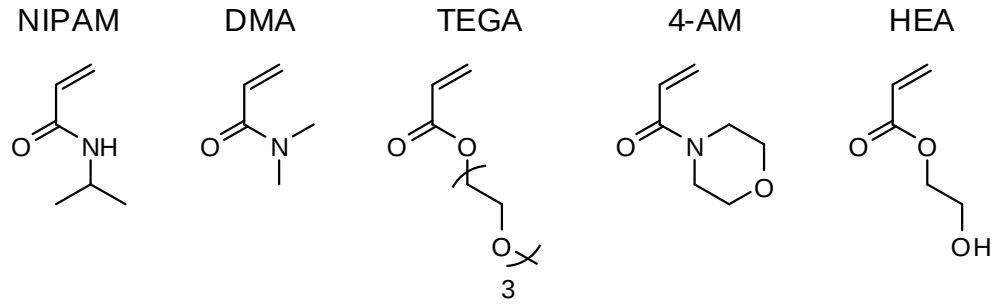

Figure 7.12 Structures of the monomers polymerised using the acridine CTA, **19**. NIPAM = *N*-isopropylacrylamide; DMA = dimethylacrylamide; TEGA = tri(ethyleneglycol) acrylate; 4-AM = 4-acryloyl morpholine; HEA = hydroxyethyl acrylate.

To confirm the presence of the acridine end group in the polymers they were analysed by SEC using both refractive index (RI) and UV-vis detectors. The UV detector was set to collect at 309 and 411 nm – the principal absorption maxima of the trithiocarbonate and acridine end-groups respectively. Figure 7.13 shows the trace for **P24**.

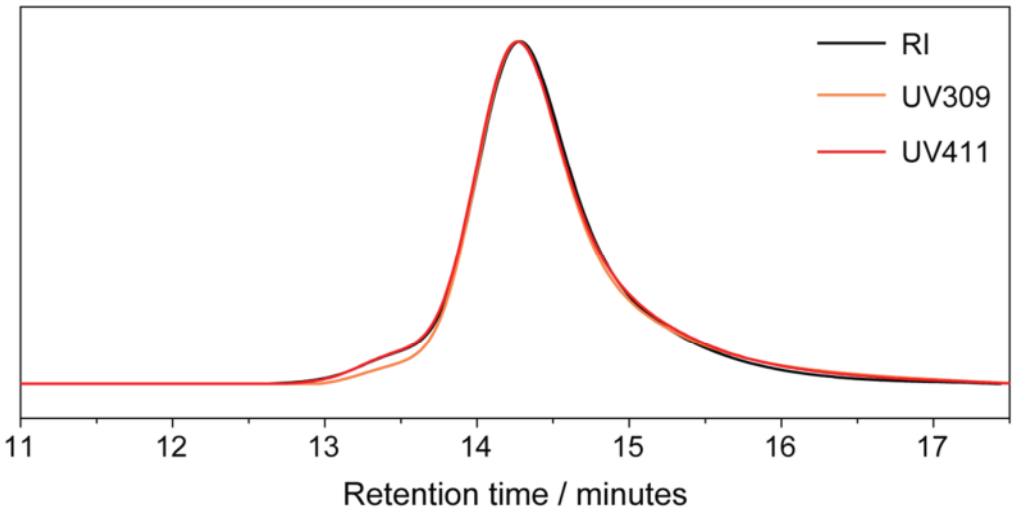

Figure 7.13 DMF SEC chromatogram of **P24**. The refractive index (RI – black) and UV-vis (orange and red) traces show excellent agreement, indicating that both the trithiocarbonate (λ_{max} 309 nm) and acridine (λ_{max} 411 nm) are retained in the product polymer.

All three traces clearly overlap; furthermore, there was no evidence of any acridine-containing small molecules, suggesting that this group was always to be found attached to a polymer chain. The presence of the acridine group was also confirmed by ^{1}H NMR spectroscopy. The aromatic protons display characteristic signals between 7.2 and 8.4 ppm

– Figure 7.14 shows an example spectrum for **P27** (data for the other polymers can be found in the Experimental Section).

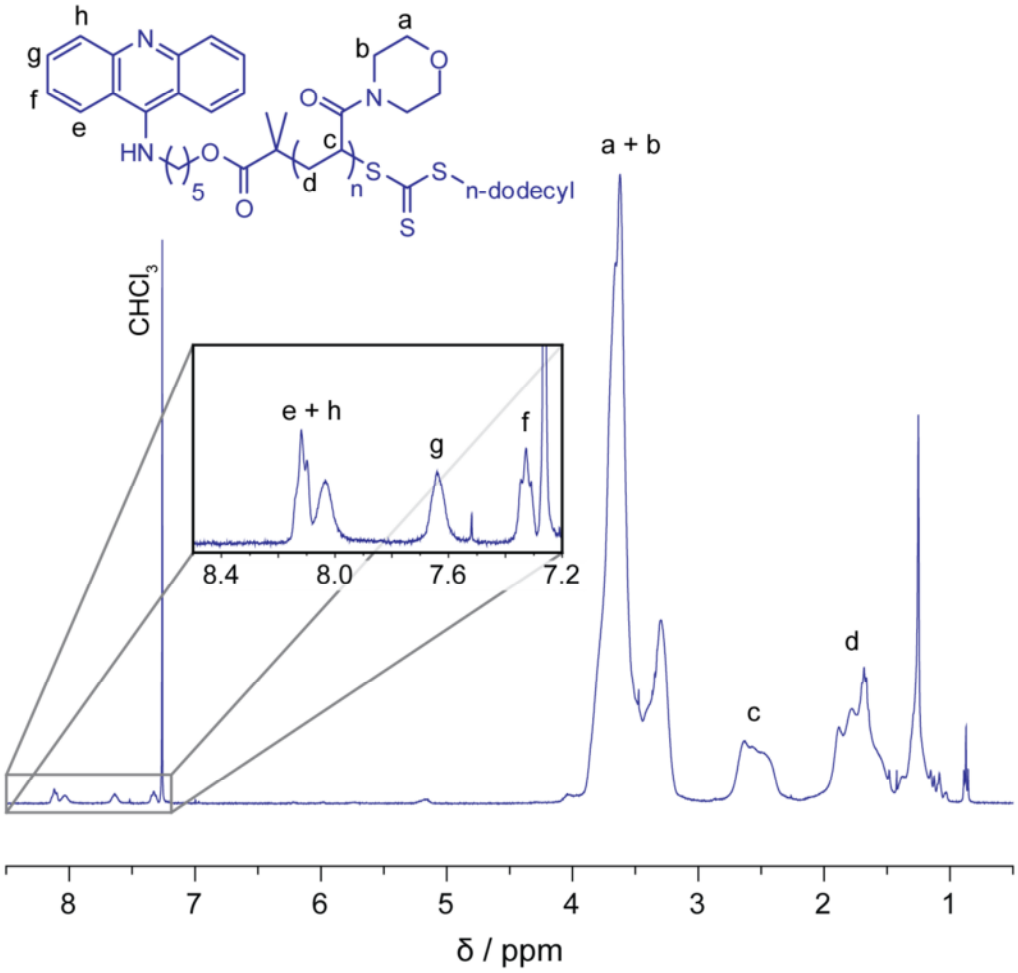

Figure 7.14 ^{1}H NMR spectrum of **P27**. The signals due to the acridine end group (e-h) are clearly visible. Solvent: $CDCl_3$.

7.2.iv Studies of DNA–polymer interactions

Having successfully synthesised a range of polymers containing the acridine end group, their interaction with double stranded DNA (dsDNA) was studied using UV-vis and linear dichroism (LD) spectroscopy. DNA isolated from calf thymus (ctDNA) was used as it is one of the standards in the literature, making comparison with previous studies more straightforward. Intercalation of the acridine group between the base pairs of this long, genomic DNA should result in both a red shift (bathochromicity) of the absorbance maxima and a decrease in the absorbance (hypochromicity) in the UV-vis spectrum, as the

energetics of the system are altered by the close proximity of the purine and pyrimidine groups of DNA. As described below, this method can be used to extract an equilibrium binding constant, K_a, for the process, allowing quantitative comparison of the strength of binding of an acridine group at the polymer chain end and free in solution.

LD spectroscopy is a useful technique for measuring interactions involving large biomolecules.[15] The molecule of interest (in this case a long DNA strand) is first oriented in a particular direction. This is achieved by spinning a cuvette containing the sample around a stationary rod (Figure 7.15).

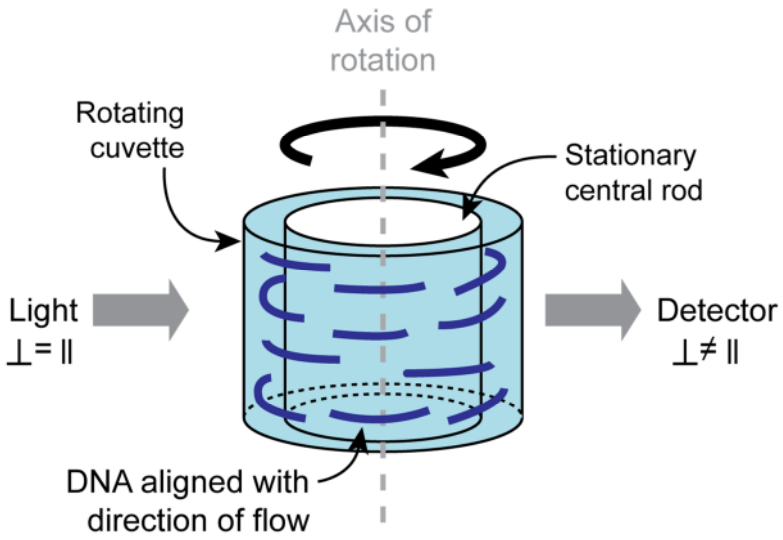

Figure 7.15 Diagram illustrating the experimental set-up for LD spectroscopy. The sample (in this case DNA) is placed within a cuvette and rapidly rotated around a central, stationary rod. Viscous drag then causes the sample to align with the direction of rotation. A light source is passed through the sample and the difference between the absorbance of perpendicular (⊥) and parallel (||) polarised light is measured.

The viscous drag created as a result aligns the DNA with the direction of flow. A beam is then shone on the sample consisting of light that is polarised either parallel (||) or perpendicular (⊥) to the direction of flow. Finally, a detector is used to measure the difference in the absorbance of parallel to perpendicular polarised light; this quantity (Equation 7.1) is known as the linear dichroism (LD).

$$\text{LD} = A_{\parallel} - A_{\perp}$$

Equation 7.1 Definition of the linear dichroism (LD) of an aligned molecule, where $A_{\parallel}$ is the absorbance of parallel polarised light and $A_{\perp}$ is the absorbance of perpendicularly polarised light.

Any molecules that do not interact with the DNA strand will not exhibit LD because they are oriented randomly in solution and therefore $A_{\perp} = A_{\parallel}$. Molecules that *do* interact with the DNA strand, but which can do so in any orientation will likewise exhibit no LD response. Any molecules that both interact with the DNA strand *and* must adopt a specific orientation to do this will have $A_{\perp} \neq A_{\parallel}$ and therefore a non-zero LD. For intercalation, a negative LD response should be observed as the interaction is taking place perpendicular to the direction of flow and therefore $A_{\perp} > A_{\parallel}$ – this is illustrated in Figure 7.16.

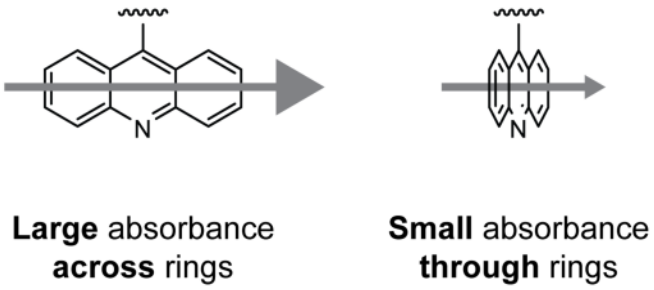

Figure 7.16 Illustration of the difference in absorbance of the acridine group when light passes across and through the ring system. This difference leads to the molecule's LD behaviour.

First, however, it was important to confirm that the acridine group was capable of intercalating into dsDNA under the conditions to be used for the polymer studies. The solubility of CTA **19** in water was very low, so the precursor **18** was used in its place. Since the acridine and trithiocarbonate groups were positioned at opposite ends of the product polymers (and not in close proximity as in the CTA), this may in fact be a better model for the interaction at the polymer chain end, as discussed above.

The absorbance spectrum was taken for **18** at a concentration of 20 μM. Calf thymus DNA (ctDNA) was then titrated into the cuvette, with the absorbance spectrum recorded after the addition of each aliquot (after equilibration for one minute). The results, shown in

Figure 7.17, confirmed that intercalation occurred. The UV-vis spectroscopy titration series exhibited clear batho- and hypochromicity, which was the expected effect of intercalation.

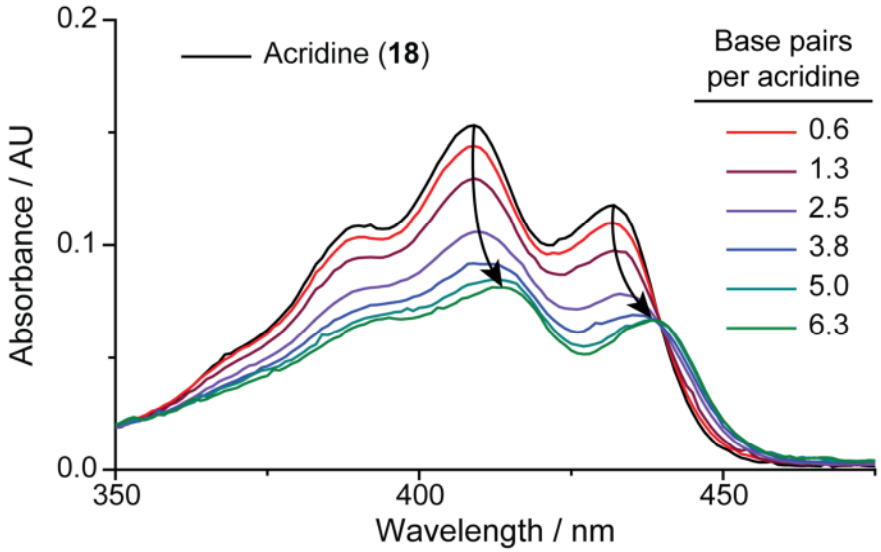

Figure 7.17 UV-vis spectroscopy titration series showing the effect of the addition of ctDNA to a solution of **18** in water. As expected, intercalation of the acridine group caused batho- and hypochromicity (indicated by the black arrows). Absorbance values were adjusted to take into account the change in concentration due to the added volume of the aliquot of ctDNA.

A similar titration in the LD machine led to the results shown in Figure 7.18.

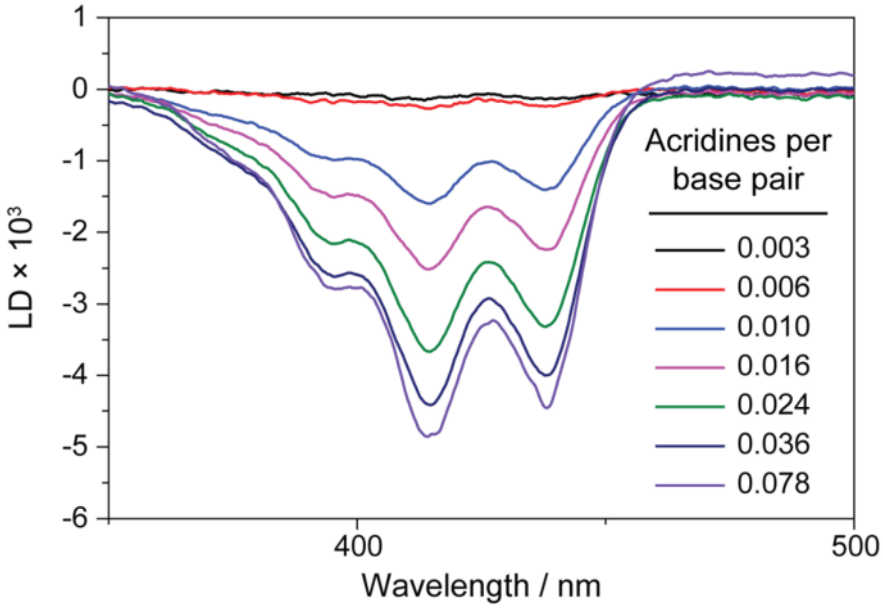

Figure 7.18 LD spectroscopy titration series showing the effect of adding **18** to ctDNA under Couette flow. A negative response indicates that the observed interaction was occurring perpendicular to the direction of flow – in this case this confirmed that intercalation was occurring.

A significant negative response quickly manifested itself, proving that the interaction observed in the UV-vis spectroscopy study was occurring perpendicular to the direction of flow; that is, intercalation was occurring as opposed to minor groove binding (which would have led to a positive response) or non-specific association (which would have given no response as the orientation of the acridine group would have been random).

Having confirmed intercalation of the small molecule acridine, the UV-vis spectroscopy studies were repeated using the poly(NIPAM) sample (**P24**) synthesised above. Initial results were promising, with similar batho- and hypochromicity effects observed (Figure 7.19) and a significant, if weaker, LD response (Figure 7.20).

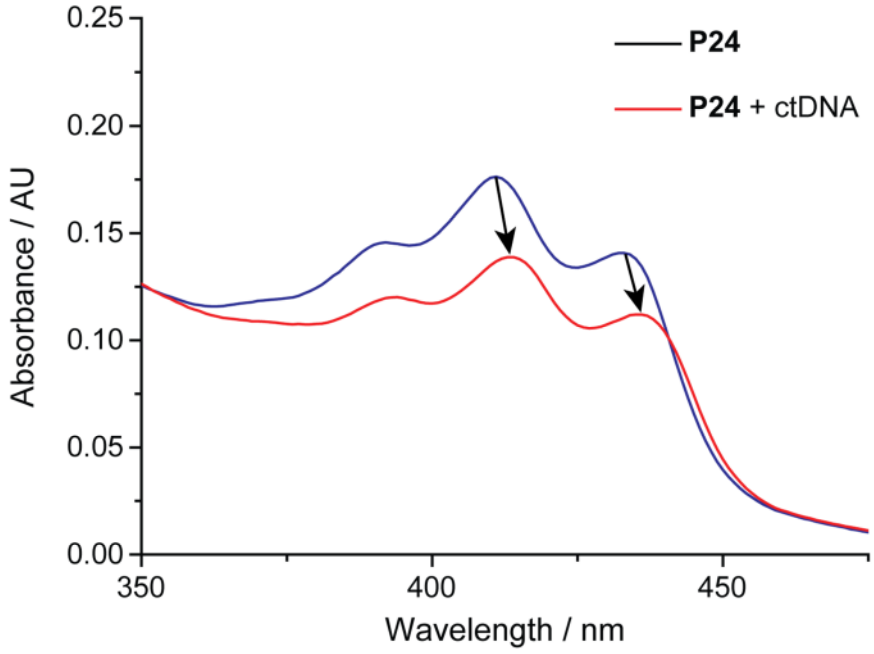

Figure 7.19 UV-vis spectra showing the effect of adding ctDNA (at a ratio of 0.24 base pairs per acridine) to an aqueous solution of P24. Clear batho- and hypochromicity was observed as a result of intercalation into DNA.

However, further studies revealed that addition of the ctDNA caused precipitation of the polymer, even at very low concentrations. Figure 7.21 is a plot of the absorbance at 550 nm (commonly used as a measure of precipitation when measuring cloud point temperatures) versus polymer concentration. In each case, 2 μL of a 4.2 mM solution of ctDNA was added to 2 mL of the **P24** solution and the mixture vigorously stirred for two minutes

before recording the absorbance value. Above a polymer concentration of around 10 μM significant precipitation was observed – at 25 μM the effect was even observable by eye – suggesting that the ctDNA was causing collapse of the polymer chains and the formation of mesoscopic aggregates.

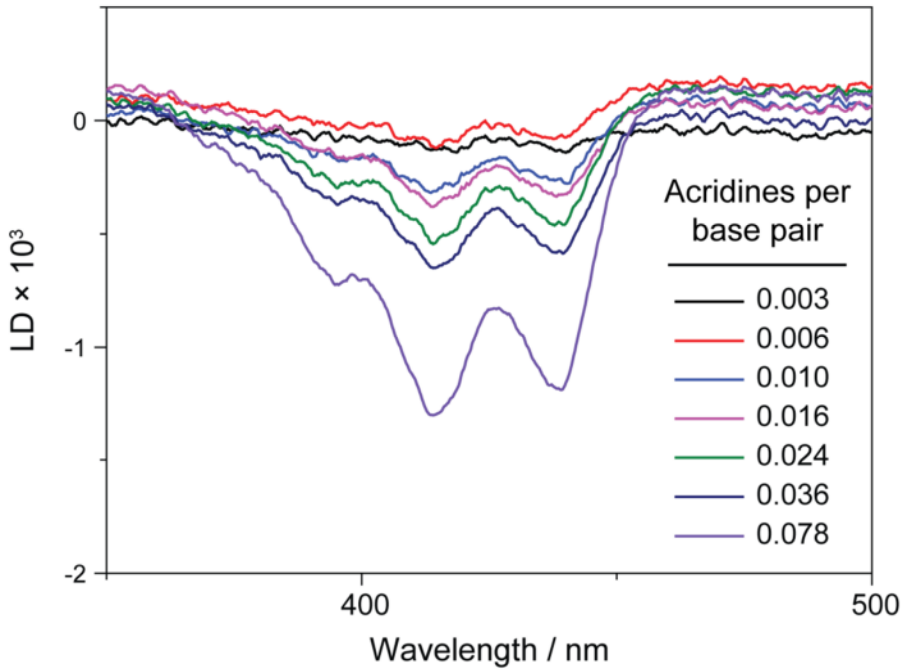

Figure 7.20 LD spectroscopy titration series showing the effect of adding a solution of **P24** to a solution of ctDNA under Couette flow.

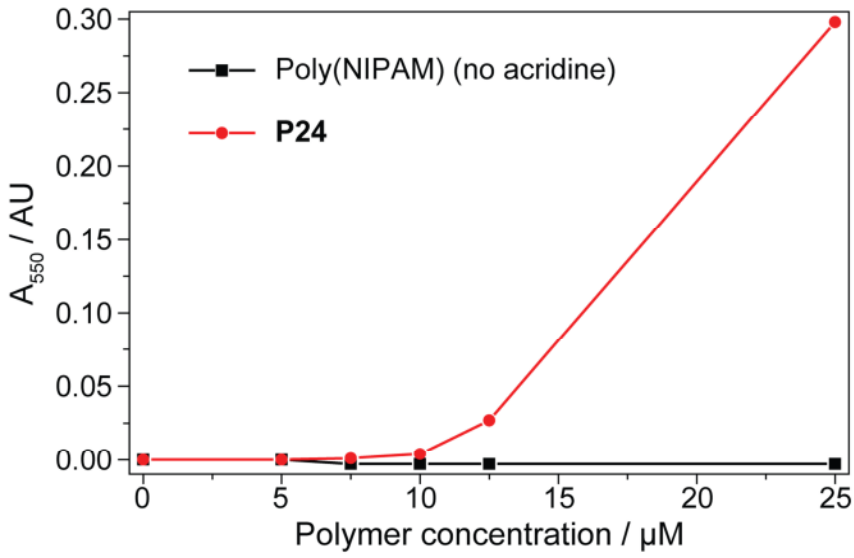

Figure 7.21 Plot of absorbance at 550 nm versus polymer concentration for a series of solutions containing **P24** (red) or poly(NIPAM) containing no acridine group (black), and ctDNA (4.2 μM). Significant precipitation was observed above 10 μM.

DNA collapse and precipitation – commonly known as compaction – induced by neutral polymers is a known phenomenon, but few studies exist exploring the reasons behind it.[16-19] To our knowledge, no study of DNA compaction induced by poly(NIPAM) or any of the other polymers listed in Table 7.2 has been performed. For other neutral polymers, such as PEG, the mechanism of DNA collapse is proposed to be 'all-or-none', wherein the elongated coil state coexists with the compact state and no intermediate states exist. This intuitively makes sense since polymers are long, flexible molecules capable of inducing unfavourable contacts between DNA monomers and excluding solvent over a large area – once binding has occurred compaction would then be expected to be rapid.

It was proposed that the temperature-responsive nature of poly(NIPAM) may have been responsible for its ability to compact DNA. The lower critical solution temperature (LCST) behaviour of poly(NIPAM) arises because, as the temperature is increased, hydrogen bonding between polymer side chains becomes favoured over hydrogen bonding to water, thus causing chain collapse and aggregation. DNA presents many hydrogen bonding sites in both the minor and major grooves and could therefore interact with the polymer, lowering the LCST. However, this hypothesis was not supported when it was found that poly(NIPAM) of a similar molecular weight but containing no acridine group caused no compaction of ctDNA at identical concentrations to those used for **P24** above (Figure 7.21).

It was thought that a permanently hydrophilic polymer might present fewer problems with regard to DNA compaction, so acridine-capped poly(DMA) (see Table 7.2, **P25a**) was investigated for its interaction with ctDNA. Initial results were disappointing: a high degree of DNA precipitation was observed with no apparent hypo- or bathochromicity in the UV-vis spectra. A detailed study was then conducted to test the effect of various conditions on the amount of DNA compaction observed, as shown in Table 7.3.

Table 7.3 Experimental conditions tested for the promotion of intercalation of **P25a** into ctDNA. TE = Tris HCl/EDTA (10:1) buffer solution; the concentration given is that of the Tris HCl component. * Indicates that precipitation was observed by eye. † 18 MΩ water.

Experiment #	pH	Temperature / °C	[$MgCl_2$] / mM	[TE] / mM
1a*	4.0			
1b*	5.5			
1c*	7.0	20	0	0
1d	9.0			
1e*	10.0			
1f		10		
1g		20		
1h	~5.8†	30	0	0
1i		40		
1j		50		
1k			0	
1l			1	
1m	~5.8†	20	10	0
1n			100	
1o*			1000	
1p				0.1
1q				1
1r	8.0	20	0	10
1s				100
1t				1000

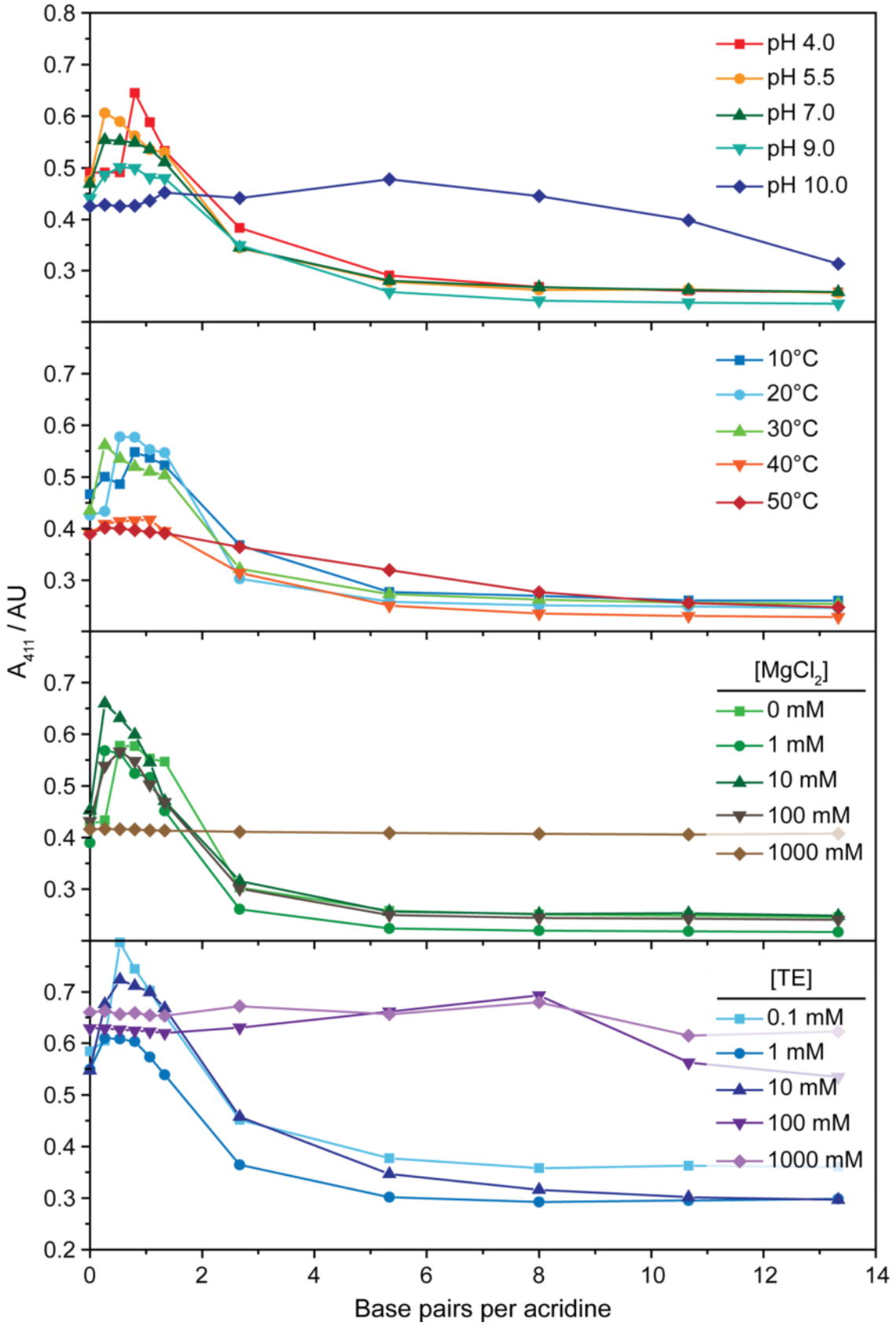

Figure 7.22 Progression of absorbance at 411 nm (A_{411}) with base pair/acridine ratio for **P25a** interacting with ctDNA under a variety of conditions. Top: pH variation; pH was adjusted using concentrated HCl or NaOH, 20°C. Middle-top: temperature variation; pH ~5.8 (18 MΩ water). Middle-bottom: salt concentration variation; pH ~5.8 (18 MΩ water), 20°C. Bottom: buffer concentration variation; pH ~5.8 (18 MΩ water), 20°C.

The procedure followed for all experiments was identical: aliquots of ctDNA (20 mM) were added successively to a solution of **P25a** (50 μM in water) and the UV-vis spectrum recorded after each addition. Figure 7.22 show the trends in the absorbance at 411 nm (λ_{max} for the acridine group) as the concentration of ctDNA was increased. The first point to note is that high pH and concentrations of salt or buffer led to blocking of the intercalation interaction, as evidenced by the fact that there was little to no change in the absorbance of the acridine group as more ctDNA was added. Below pH 10, however, it appeared that there was no dependence of the efficiency of intercalation on pH. Similarly, below 1 M $MgCl_2$ and 100 mM TE, there was no clear trend relating the concentrations of these components to intercalation efficiency.

A notable feature of all experiments in which intercalation successfully occurred (that is, A_{411} had decreased by the end of the titration series) was that the first few aliquots of ctDNA caused an *increase* in A_{411}, followed by a rapid decrease before plateauing to a lower value. Inspection of the entire UV-vis spectrum for these early aliquots revealed that the absorbance was increased across the range of the scan, indicating that clouding of the solution was taking place due to polymer/DNA aggregation. Increasing the temperature appeared to eliminate this effect.

The changing ratio of polymer to DNA as the experiment progressed may explain this phenomenon. At the start of the titration, no DNA was present and the polymer remained soluble. After the first aliquot, a low concentration of DNA existed and therefore a high ratio of polymer to DNA. The DNA was thus completely saturated with polymer, creating a very high local polymer concentration, which in turn favoured aggregation and clouding of the solution. As more DNA was added the ratio of polymer to DNA decreased and at some point the DNA strands became desaturated. After this point had been reached, addition of more DNA led to a decrease in the number of polymer chains per DNA strand – effectively, the polymer strands became more widely spaced and so their local

concentration decreased – and aggregation became disfavoured. At this point the effects of intercalation – hypo- and bathochromicity – became apparent in the UV-vis spectrum. Figure 7.23 shows a cartoon of the proposed process. Effectively, what was being observed was a change in cloud point behaviour due to the confinement of polymer chains by the DNA intercalation interaction, an effect that has been well documented for polymers arrayed on flat surfaces and nanoparticles.[20]

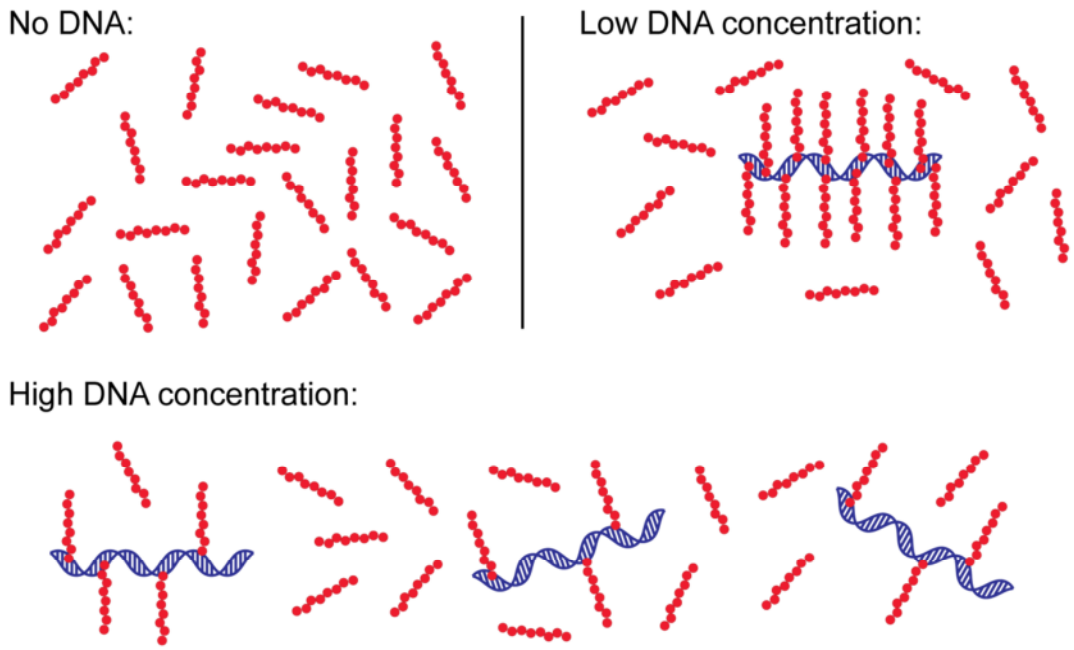

Figure 7.23 Cartoon of the proposed process occurring when ctDNA is added to a solution of acridine-capped poly(DMA) in water. Top: With no DNA present, polymer chains are free in solution. Middle: At a low DNA concentration, the DNA strand (blue) is saturated with polymer; the densely packed structure is prone to aggregation. Bottom: At higher DNA concentrations, fewer polymer chains per DNA strand leads to a more loosely packed structure less likely to aggregate.

The saturation point of the DNA can be estimated from the data in Figure 7.22 as, according to the above model, it must lie at the peak of the titration curve. The data points either side of the peak thus provide a range within which the saturation point must lie. These are shown in Table 7.4. The saturation point always lay below one base pair per acridine unit. This implies that every base pair could accommodate an acridine group, even in the presence of the bulky polymer chains, which might have been expected to block

intercalation to a certain extent.

Table 7.4 Saturation points for **P25a** interacting with ctDNA under a range of conditions. The saturation point is the maximum number of polymer chains that can be accommodated per base pair. A - indicates that no intercalation was observed.

Experiment #	Saturation point / base pairs per acridine
1a	0.5-1.1
1b	0.0-0.5
1c	0.0-0.5
1d	0.3-0.8
1e	-
1f	0.5-1.1
1g	0.3-0.8
1h	0.0-0.5
1i	0.8-1.3
1j	0.0-0.5
1k	0.3-0.8
1l	0.0-0.5
1m	0.0-0.5
1n	0.3-0.8
1o	-
1p	0.3-0.8
1q	0.0-0.5
1r	0.3-0.8
1s	-
1t	-

In all cases where intercalation was observed, the A_{411} values only fell back below their initial values when there was more than one base pair per acridine unit – this is the point at which the density of polymer chains on the DNA strands would have begun to decrease. This observation supported the conclusion that the dense packing of polymer chains along the DNA strand caused the aggregation observed at low DNA concentrations. The earlier observation that **P24** caused significant DNA compaction, whereas poly(NIPAM) of a

similar molecular weight (but lacking the acridine group) did not, could also be explained by this model – in the absence of an intercalation interaction the dense packing did not occur and therefore aggregation was avoided.

Having identified a number of experimental conditions under which intercalation could be reliably measured by UV-vis spectroscopy, extraction of the equilibrium binding constant, K_a, was next attempted.

Because the aggregation that occurred in the early stages of the titration would interfere with the calculations, only data collected after this phase had passed was used. The experiment was conducted by measuring the UV-vis spectrum of a 20 μM solution of **P25a** at 30°C in 18 MΩ water. An aliquot of ctDNA (20 mM in 1 × TE buffer) was then added and the solution allowed to equilibrate for one minute before repeating the UV-vis measurement. This process was repeated several times to obtain a concentration series as depicted in Figure 7.24. Next, the difference – or 'delta' – plots for the titration series were obtained by subtracting the UV-vis spectrum at a particular point from the spectrum of free **P25a**. The delta plots are depicted in Figure 7.25 and were used to identify the wavelength at which the greatest change in absorbance values occurred – in this case 409 nm.

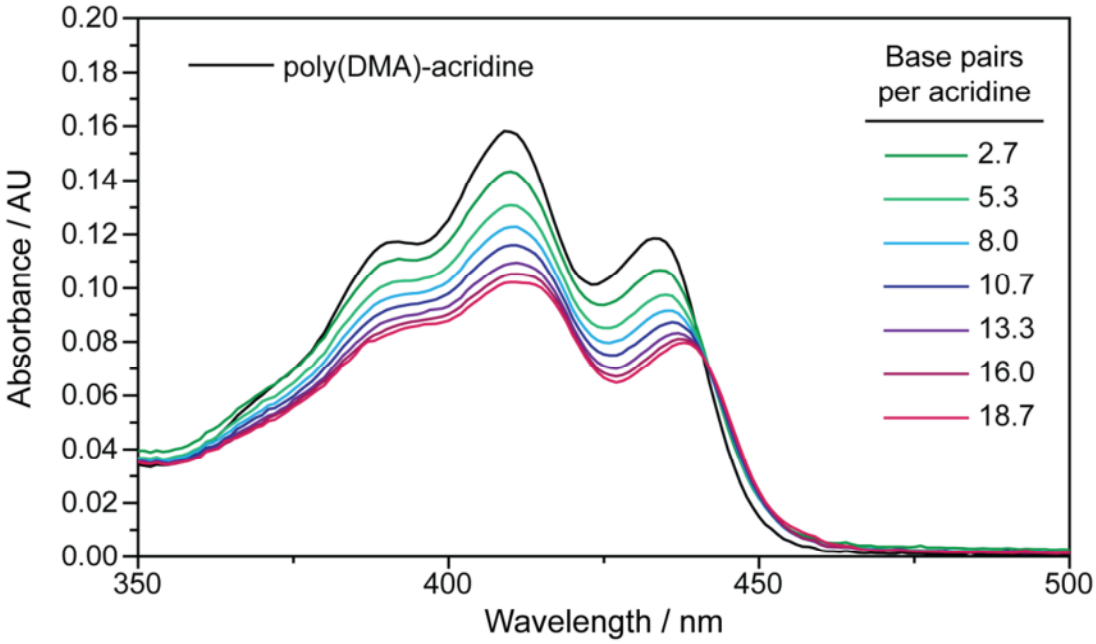

Figure 7.24 UV-vis spectroscopy titration series showing the effect of the addition of increasing amounts of ctDNA to a solution of **P25a** at 20 μM in water. As expected, intercalation of the acridine group caused batho- and hypochromicity. Absorbance values were adjusted to take into account the added volume of the aliquot of ctDNA.

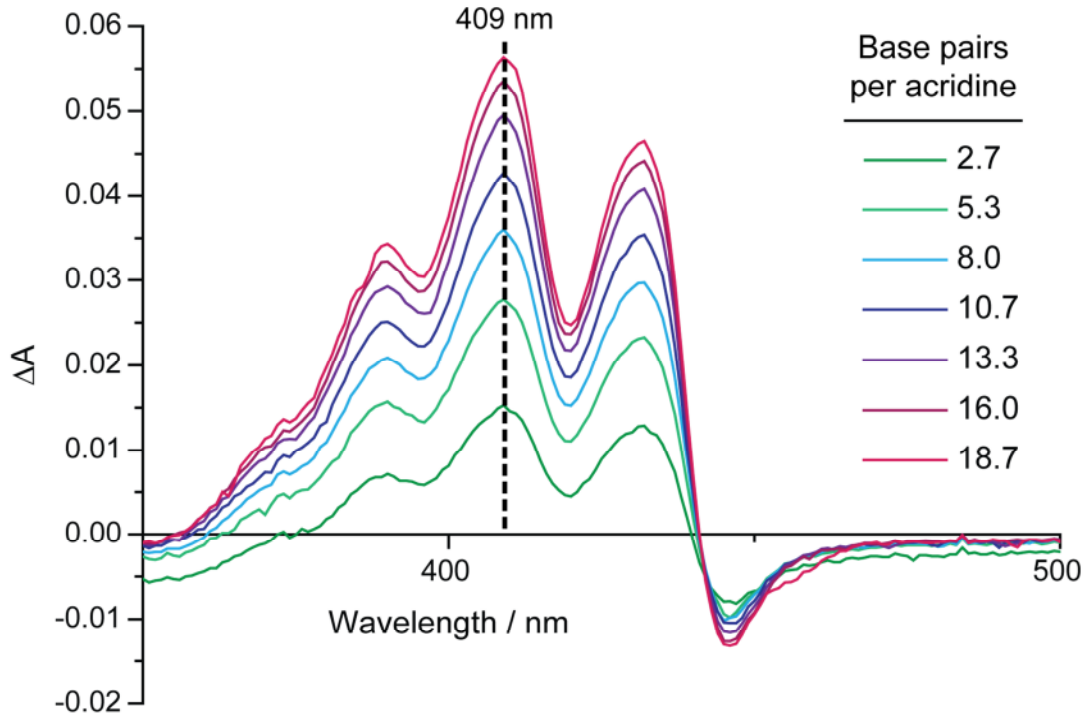

Figure 7.25 Delta plots for the interaction of **P25a** with ctDNA. Each spectrum was obtained by subtracting the UV-vis spectrum at that point during the titration from the original spectrum of free **P25a**. The greatest change in absorbance was observed at 409 nm, as indicated.

The determination of the association constant, K_a, was conducted as follows. It was

assumed that the complex formed according to the equilibrium in Scheme 7.4. It is important to remember that 'BP' in this scheme actually represents the gap between two adjacent base pairs, and that a single strand of the ctDNA used for the titration has many of these binding sites.

Scheme 7.4 The equilibrium formed between a free DNA base pair (BP), free acridine (Acr) and the base pair–acridine complex (BP–Acr) formed by intercalation.

The association constant is then defined as shown in Equation 7.2. This then leads to an equation for the observed change in UV-vis absorbance in terms of the concentration of base pairs, as shown in Equation 7.3. Details of the full derivation of this equation can be found in the Experimental Section.

$$K_a = \frac{[\mathrm{BP{-}Acr}]}{[\mathrm{BP}][\mathrm{Acr}]}$$

Equation 7.2 Definition of the equilibrium association constant, K_a.

$$\Delta A = \frac{\Delta A_{max} K_a [\mathrm{BP}]}{1 + K_a [\mathrm{BP}]}$$

Equation 7.3 The relation between ΔA and free base pair concentration used to extract the association constant, K_a, for the interaction between ctDNA and **P25a** from UV-vis spectroscopy data.

In this case, three key assumptions were made about the system. Firstly, to simplify the calculations, the following approximation was made: $[\mathrm{BP}] \approx [\mathrm{BP}]_0$. That is, the concentration of free base pairs ([BP]) was approximately equal to the initial concentration of base pairs ($[\mathrm{BP}]_0$). This is reasonable because the DNA is added in excess from the first point of the titration.[21] Secondly, it was assumed that there was no co-operativity (positive or negative) between adjacent binding sites on the DNA. Finally, it was assumed that the

concentration of intercalator remained constant throughout the titration, although in fact it dropped slightly due to dilution by the added aliquots of DNA (the effect of dilution was removed by rescaling the data accordingly). Given these assumptions, the calculated values of K_a given below should be viewed as estimates only. They are, however, useful for comparison between different polymer structures.

The change in absorbance at 409 nm was plotted against the concentration of ctDNA and a non-linear least squares method used to fit a curve to the data in accordance with Equation 7.3 – see Figure 7.26. ΔA_{max} is the maximum change in absorbance that can be observed for the interaction, and was iterated manually, taking the original A_{409} value from the UV-vis spectrum of the free polymer–acridine species as an upper bound. The best fit to the data occurred with a ΔA_{max} value of 0.11. The association constant for the ctDNA/**P25a** interaction was found to be 7 700 ± 80 M^{-1}. The association constant for the ctDNA/**18** interaction was calculated in a similar manner and found to be 8 600 ± 440 M^{-1} (with a ΔA_{max} value of 0.15). The values of K_a are given as the mean plus or minus two standard deviations, with the errors calculated by the fitting program. The presence of the polymer can therefore be said to have had a minimal effect on the association constant of the DNA/acridine interaction, although interestingly a significant difference in the ΔA_{max} values was observed. This indicated that the polymer was having an effect on the structure of the BP–acridine complex.

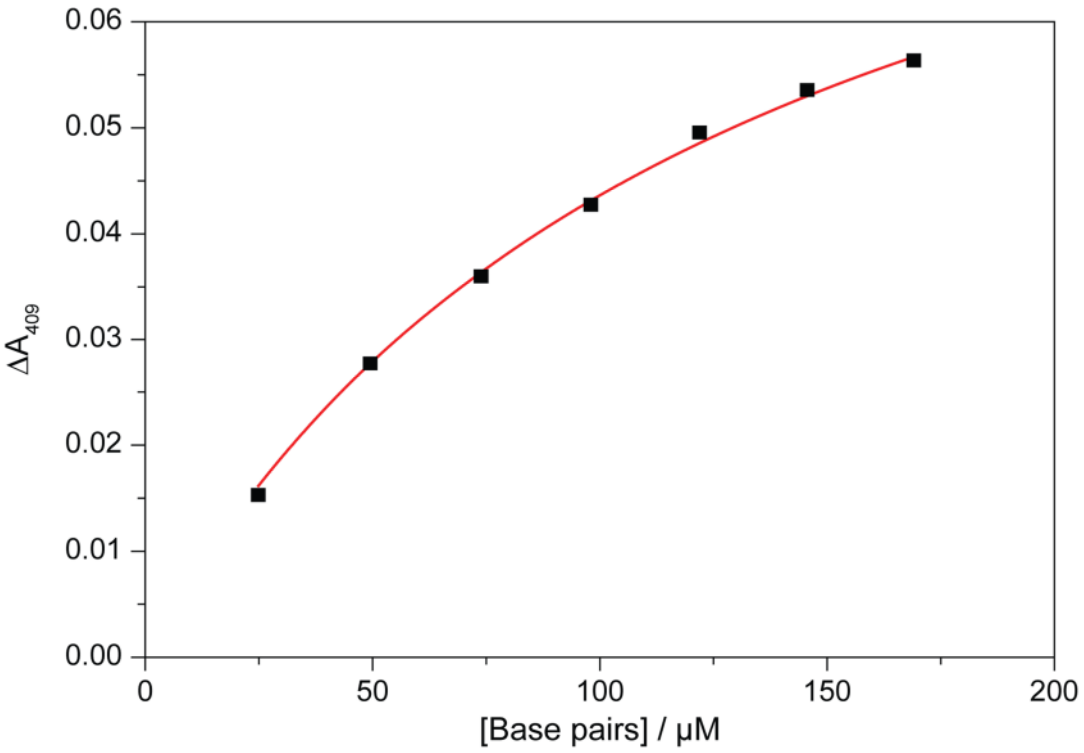

Figure 7.26 Plot of base pair concentration versus change in absorbance at 409 nm for **P25a** interacting with ctDNA. The red line is from the fitted equation used to determine the equilibrium binding constant, K_a.

LD spectroscopy was also used to confirm that the interaction observed was indeed intercalation. Figure 7.27 shows a titration series in which **P25a** was added to a solution of ctDNA under Couette flow. A significant negative response was recorded, proving that the observed interaction was taking place perpendicular to the direction of flow – that is, intercalation was occurring.

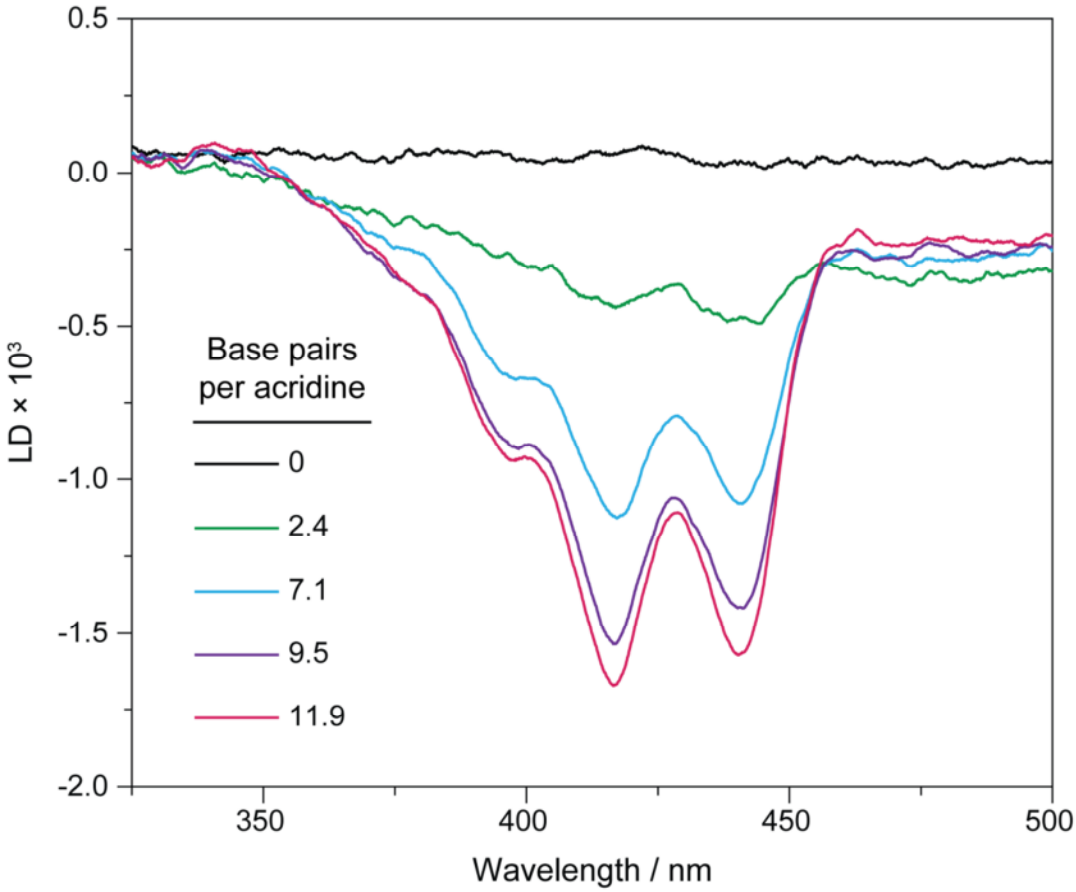

Figure 7.27 LD spectroscopy titration series measuring the interaction between **P25a** and ctDNA under Couette flow. The characteristic acridine peak shape emerged over the course of the titration and displayed a negative response, indicating that the measured interaction was taking place perpendicular to the direction of flow.

Having shown that DNA intercalation occurred for poly(DMA)–acridine, poly(TEGA)–acridine (**P26**) was investigated. An identical UV-vis spectroscopy titration series showed that, whilst there was evidence of some intercalation occurring, the interaction was much weaker. Figure 7.28 compares the UV-vis spectra at the same point in the titration series for **P25a** and **P26** – much less hypo- and bathochromicity was observed for the latter. Another notable feature of the **P26** UV-vis spectra was the difference in the shape of the acridine peak (Figure 7.28). This suggested a difference in the environment surrounding this group. The equilibrium binding constant was measured for the interaction using the method described above (see Figure 7.29) and found to be 1 030 ± 20 M^{-1} – an eight-fold decrease in binding strength compared to **P25a**. However, it should be noted that the fit to

the data was not good, possibly suggesting that intercalation was not in fact occurring.

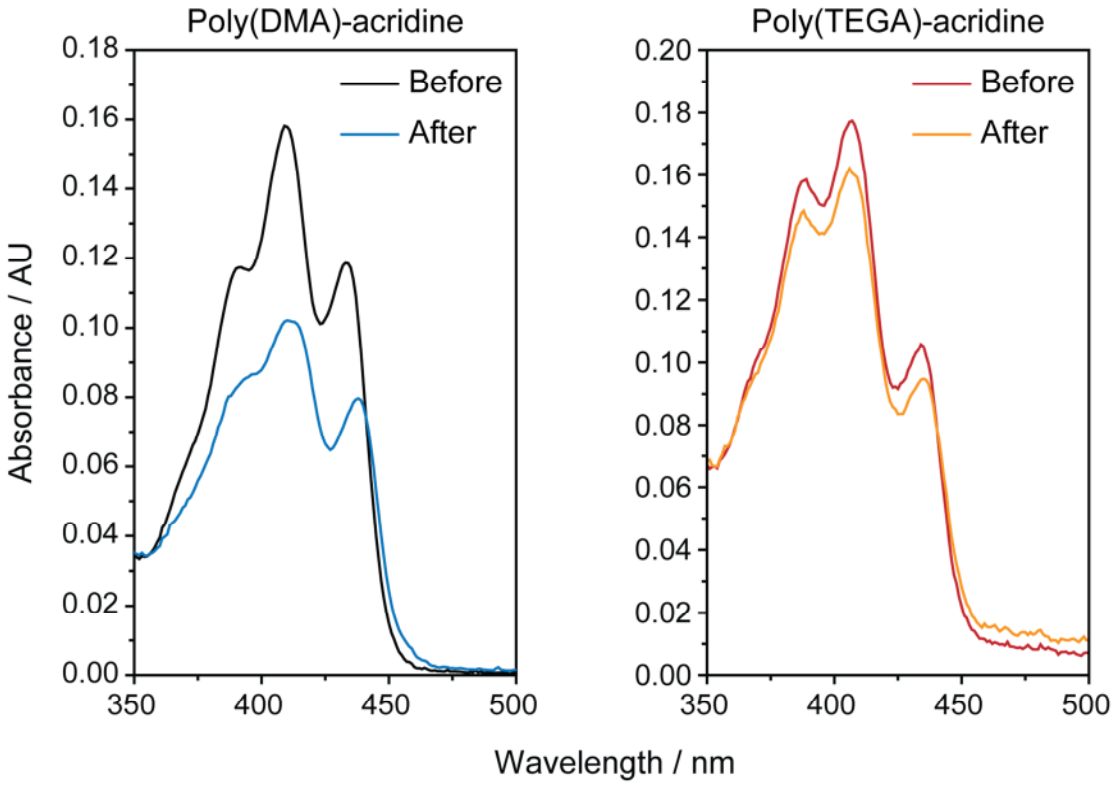

Figure 7.28 UV-vis spectra of **P25a** (left) and **P26** (right) before and after the addition of ctDNA (18.7 base pairs per acridine). A much smaller effect was observed for **P26**, as well as a difference in peak shape.

It was reasoned that the decrease in binding strength could be attributed to one of two factors: the higher molecular weight of **P26**, or the chemical structure of the polymer (in particular, the brush-like nature of poly(TEGA)). To ascertain which, poly(DMA)–acridine was synthesised with a much higher molecular weight (26.0 kDa, Table 7.2 **P25b**). The equilibrium binding constant was calculated using the UV-vis titration described above and found to be 4 030 ± 350 M^{-1} – half that of **P25a**. The decrease, however, was not as large as that observed for **P26**, which had a similar molecular weight. Furthermore, the titration data for **P25b** fitted Equation 7.2 much better. The chemical structure of the polymer must, therefore, have played an important role in determining the strength of the intercalation interaction. Based on these results, it is proposed that poly(TEGA) inhibited the intercalation interaction because its brush-like structure made it difficult for the acridine

group to get close enough to the DNA. Increasing the molecular weight of the polymer decreased the strength of the intercalation interaction because, for the same concentration of acridine, there was a higher mass of polymer in solution – this led to an increase in non-specific interactions between the polymer and DNA, which blocked the intercalation sites.

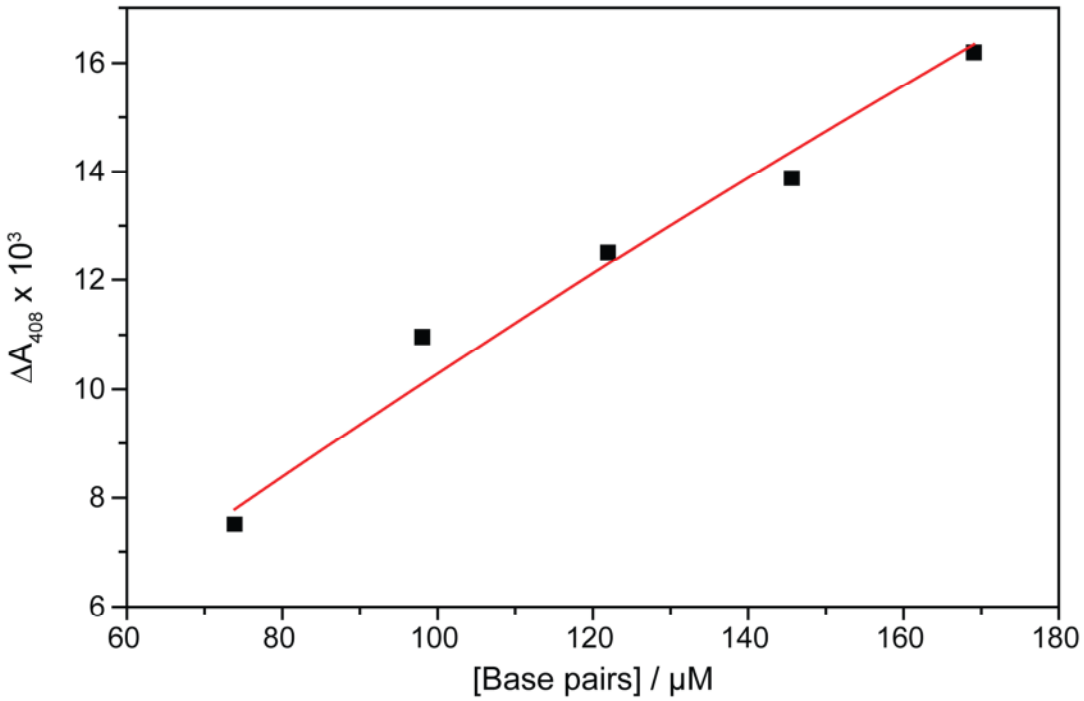

Figure 7.29 Plot of base pair concentration versus change in absorbance at 408 nm for **P26** interacting with ctDNA. The red line is from the fitted equation used to determine the equilibrium binding constant, K_a.

Poly(4-AM)–acridine (**P27**) was also tested for its interaction with ctDNA. An interaction was observed, as shown in Figure 7.30, but it proved impossible to extract a binding constant for this polymer due to the extent of aggregation in the early stages of the titration. This is highlighted in Figure 7.31, which plots the absorbance at 411 nm versus the base pair/acridine ratio.

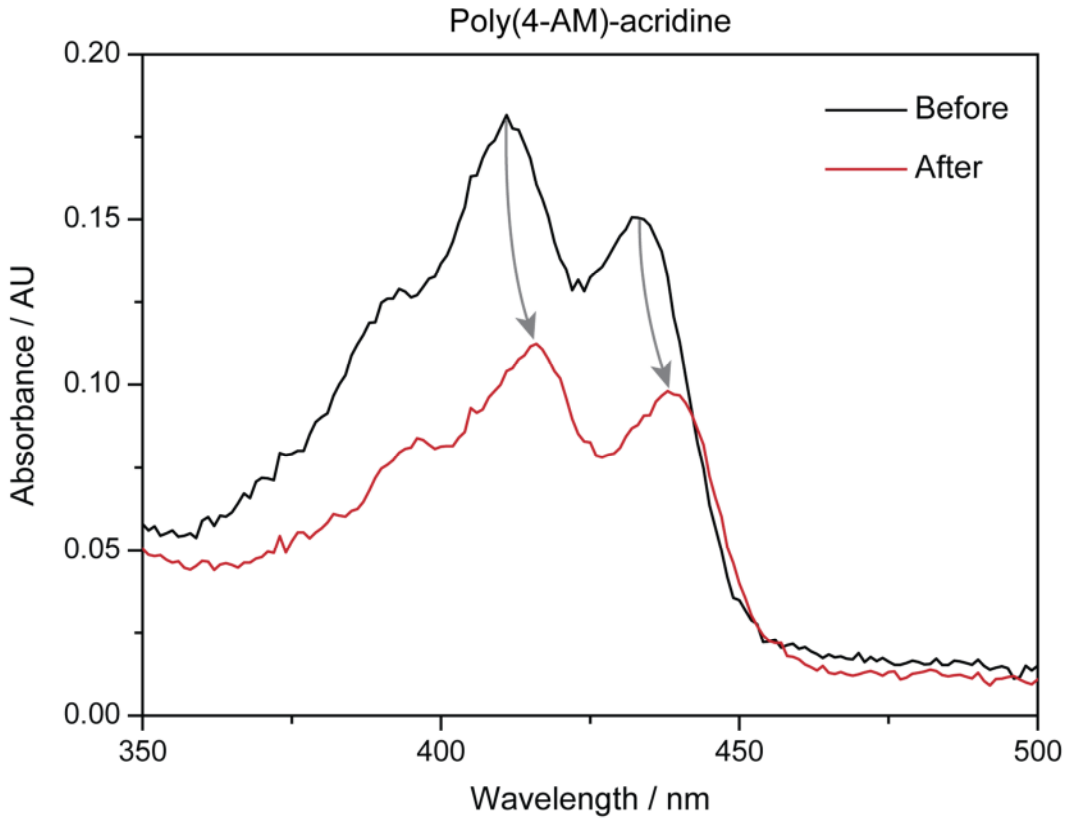

Figure 7.30 UV-vis spectra showing the effect of adding ctDNA (at a ratio of 18.7 base pairs per acridine) to an aqueous solution of **P27**. Clear hypo- and bathochromicity were observed.

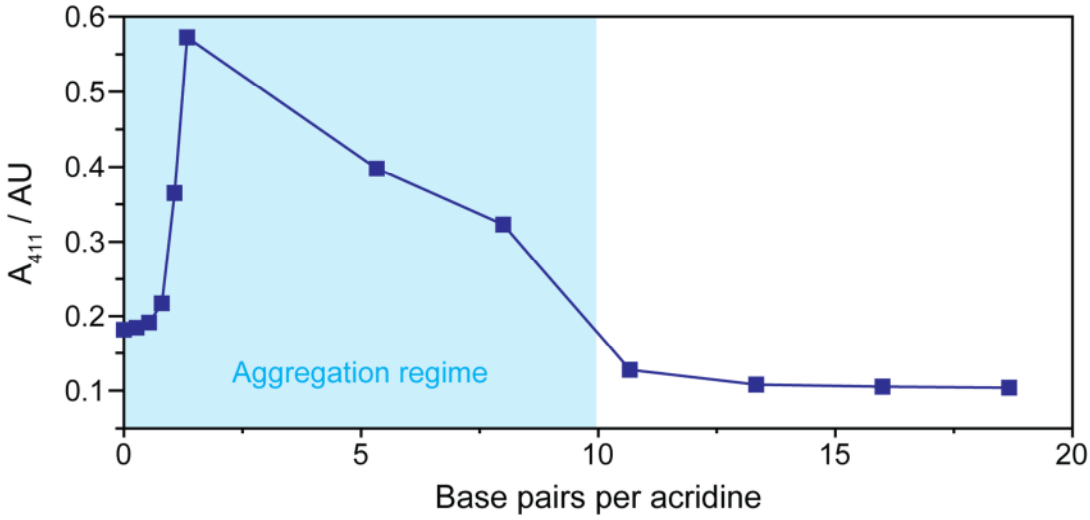

Figure 7.31 Progression of absorbance at 411 nm (A_{411}) with base pair/acridine ratio for **P27** interacting with ctDNA at 30°C in water. The aggregation regime (blue highlighted region) is the range in which the A_{411} value was larger than the starting value, indicating clouding of the solution.

When compared to Figure 7.22, it is evident that the aggregation regime (the area where the

absorbance was higher than the initial value) was much larger for **P27**, extending up to nearly ten base pairs per acridine group (in the case of **P25** and **P26** the aggregation regime extended up to only 1 base pair per acridine). This is surprising given the structural similarity between **P25** and **P27**. It is possible that the extra steric bulk of the morpholine group made aggregation more severe. Certainly, the polymer–DNA interaction was highly sensitive to changes in polymer structure.

By the point at which enough DNA had been added to reverse the aggregation process, the acridine groups had been effectively saturated, so collection of useful titration data (and therefore estimation of K_a) was impossible. The increased degree of aggregation also gave rise to the noise observed in the UV spectra.

7.2.v Synthesis of DNA–polymer brush structures using intercalation

It was reasoned that intercalation of the acridine group should occur regardless of the length of the DNA strand, so the possibility of using a short, perfectly defined segment of dsDNA (instead of the very long and ill-defined genomic ctDNA) was explored. A 63 base pair DNA sequence (dss1) was purchased and used to perform an identical UV-vis titration series to that described above using **P25a** – see Figure 7.32 for the base sequences of the component strands of dss1 (s1 and s1').

```
s1  = 5'- AGG CAG TTG AGA CGA ACA TTC CTA AGT CTG AAA
      TTT ATC ACC CGC CAT AGT AGA CGT ATC ACC -3'

s1' = 5'- GGT GAT ACG TCT ACT ATG GCG GGT GAT AAA TTT
      CAG ACT TAG GAA TGT TCG TCT CAA CTG CCT -3'
```

Figure 7.32 Base sequences of the component strands of dss1 – the double stranded DNA used for intercalation work.

First, the dss1 was assembled from the strands s1 and s1'. This was achieved by heating equimolar amounts of each strand in 1 × TM buffer (100 mM Tris, 6 mM $MgCl_2$) to 95°C for twenty minutes, then allowing the solution to cool slowly to room temperature

overnight. The concentration of the duplex (80 μM) was such that the solution contained the same concentration of base pairs as the ctDNA solutions used for the other titrations above. Successful annealing of the strands was confirmed by 15 % native PAGE analysis (see Figure 7.33), which revealed a lower-mobility band attributed to the duplex.

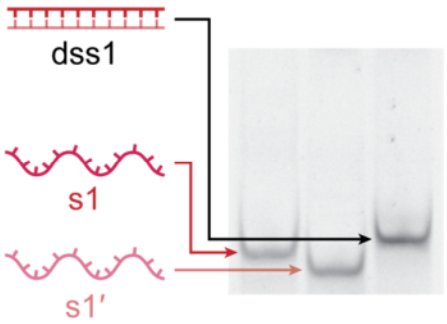

Figure 7.33 15 % native PAGE analysis showing the successful formation of double stranded s1 DNA (dss1 – right-hand lane) from s1 (left-hand lane) and s1 ' (middle lane).

A UV-vis spectroscopy titration was then carried out wherein aliquots of the dss1 solution were added to a solution of **P25a** in water. Figure 7.34 shows the results, which revealed clear hypo- and bathochromicity.

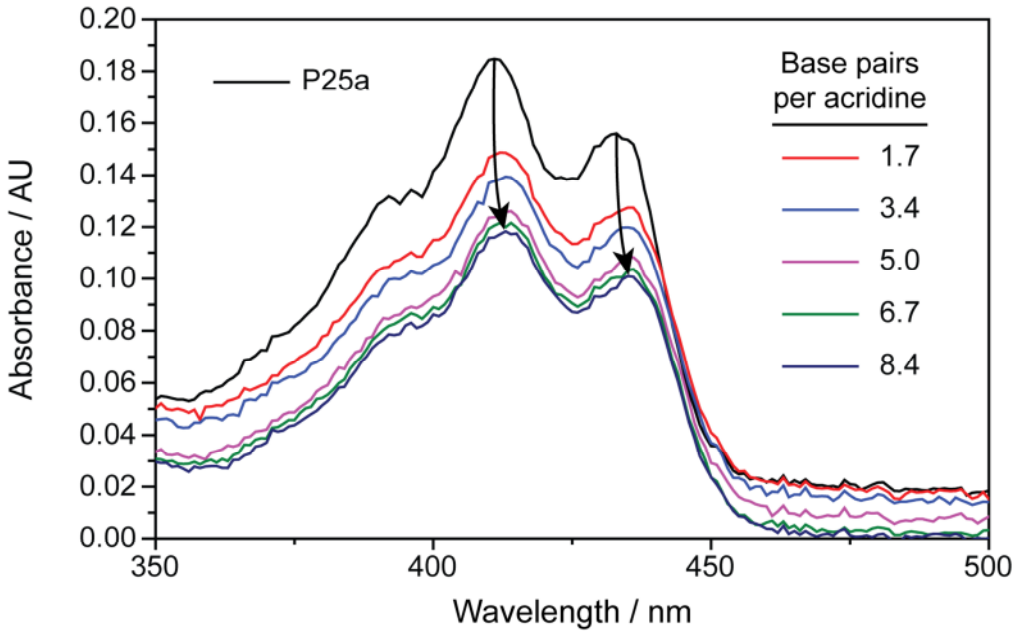

Figure 7.34 UV-vis spectroscopy titration series showing the effect of addition of dss1 to a solution of **P25a**. Hypo- and bathochromicity were observed, as indicated by the black arrows, confirming successful intercalation of the acridine group on the polymer.

This confirmed that intercalation was taking place as expected, and that the shorter length of the DNA had not resulted in significant weakening of the interaction. The solution was also analysed by dynamic light scattering (DLS). It was envisaged that the well-defined nature of the DNA duplex (dss1) might lead to the formation of discrete nanoparticles upon addition of the intercalating polymer (see schematic in Figure 7.35).

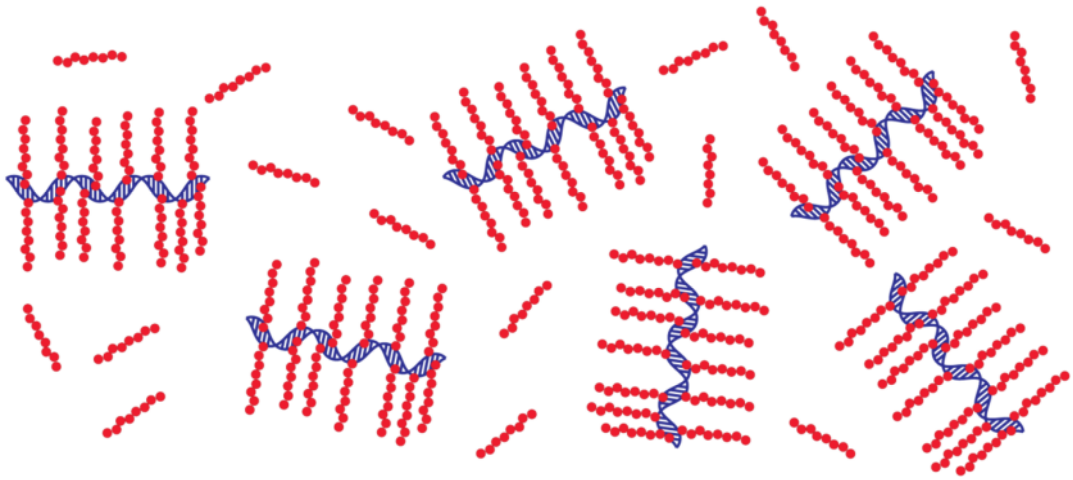

Figure 7.35 Cartoon of the proposed structures formed by the association of polymers containing an acridine end group (red chains) with well-defined double stranded DNA (blue chains) in aqueous solution. Because intercalation is an equilibrium process, free polymer chains would also be present.

However, the results were inconclusive, with multiple populations observed (Figure 7.36). Since the intercalation interaction was an equilibrium process, it is possible that the DLS results were skewed by the large background concentration of free polymer (which may account for the population of particles below 10 nm in diameter).

In an attempt to circumvent this problem, the solution was studied by atomic force microscopy (AFM), dry, on a mica surface. An AFM micrograph of dss1 (Figure 7.37 A) revealed very small particles with the expected height for dsDNA (around 0.9 nm)[22,23] and diameters of around 30 nm, which, taking into account the lateral resolution of the tip (around 10 nm), correlated well with the expected length of a 63 base pair segment of dsDNA (20.9 nm assuming a rise of 0.332 nm per base pair)[24]. AFM analysis of a sample of **P25a** showed that the free polymer did not form structures on its own (Figure 7.37 B);

instead, there was evidence for a thin film of polymer on some areas of the grid (lighter areas in Figure 7.37 B).

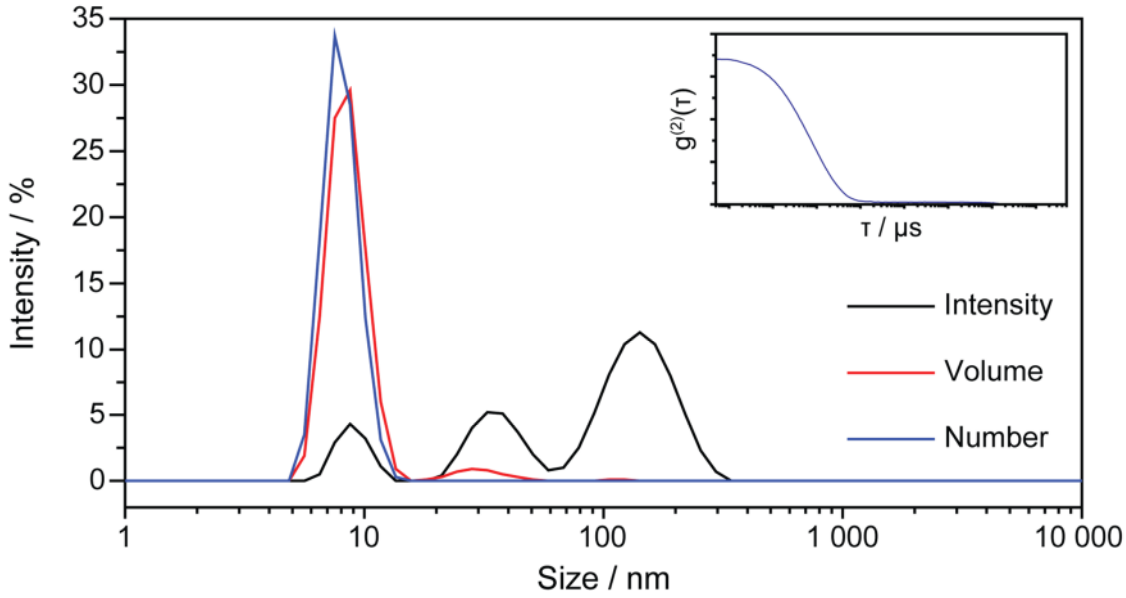

Figure 7.36 DLS analysis by intensity (black), volume (red) and number (blue) of a solution of dss1 in the presence of **P25a** (correlation function inset).

As a final control, poly(DMA) of a similar molecular weight to **P25a** was synthesised using the CTA DDMAT in place of **19**, to give a polymer with the same structure but lacking an acridine group. This was then mixed with dss1 in a ratio of 11.9 base pairs per polymer chain (the same ratio as the final point of the titration of **P25a** with dss1 described above) and analysed by AFM. The results were very similar to those for dss1 alone (Figure 7.37 C), suggesting that there was no significant interaction between the polymer and DNA in the absence of the acridine group at the polymer chain end.

Finally, the solution of **P25a** and dss1 was studied. Upon drying to the AFM substrate, large nanoparticles were observed (Figure 7.37 D). These particles were uniform in diameter (121 ± 17 nm – measurement of 20 particles) and also very flat (with average heights of less than 2 nm) – Figure 7.39 shows a direct comparison between the height plot profiles of dss1 and the dss1–**P25a** nanoparticles. The height plot profile of a single nanoparticle (Figure 7.38) showed a central peak surrounded by a relatively uniform plateau.

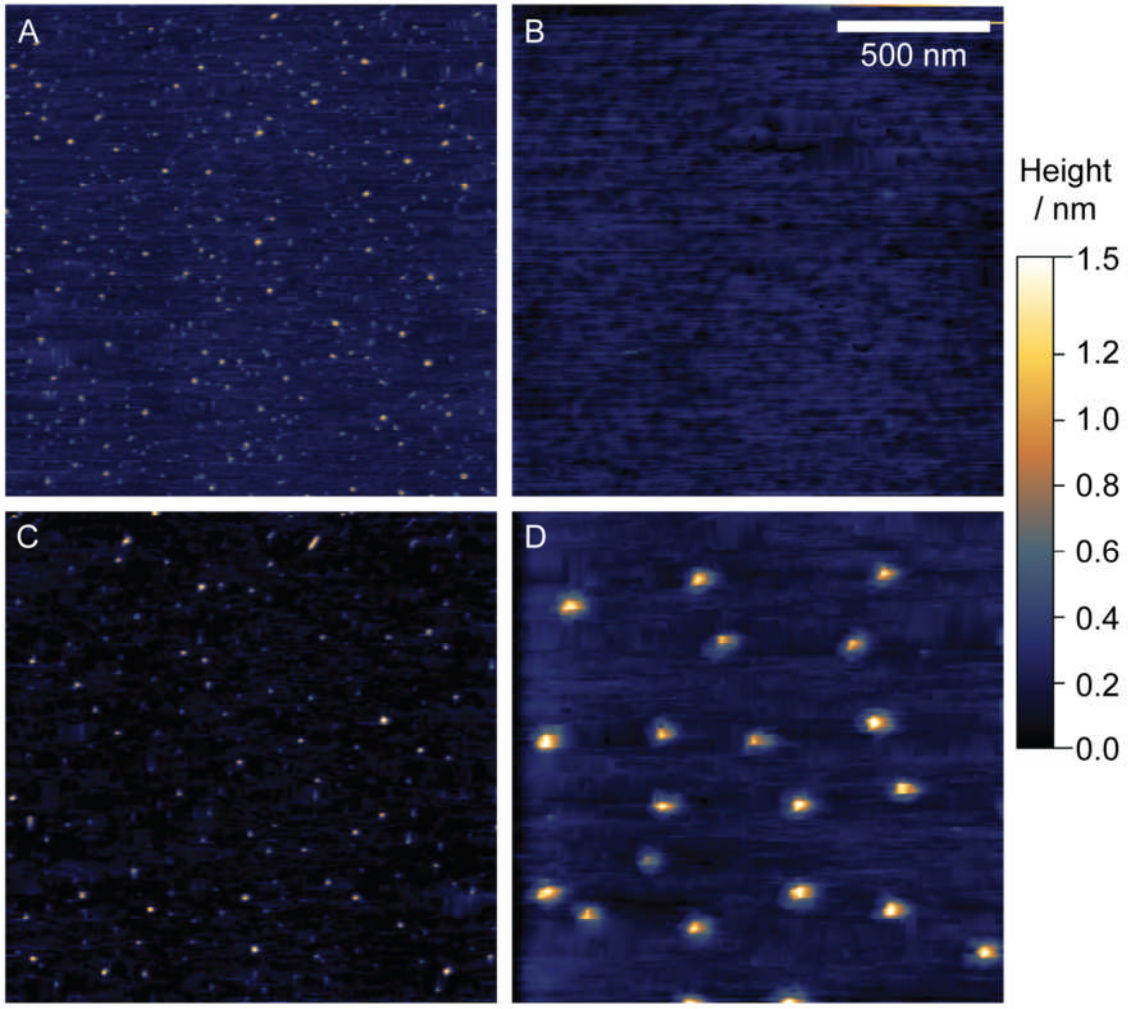

Figure 7.37 AFM micrographs of A: dss1; B: **P25a**; C: dss1 + poly(DMA) (no acridine group); D: dss1 + **P25a**. All images are at the same scale.

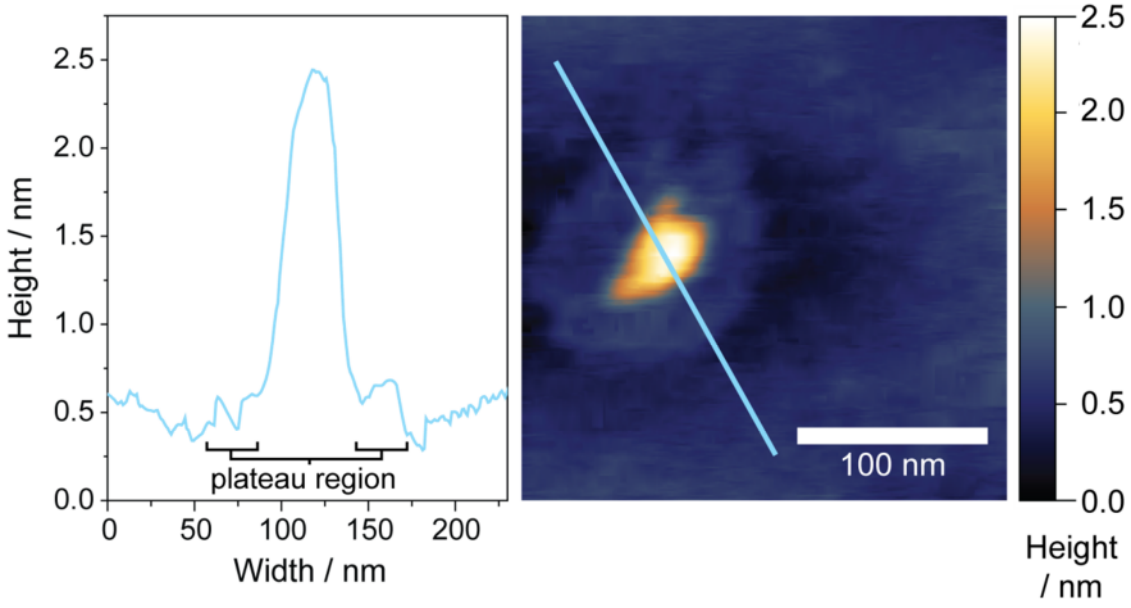

Figure 7.38 AFM micrograph (right) and height plot profile (left) of a single dss1–**P25a** nanoparticle. The light blue line indicates the location of the profile used in the height plot.

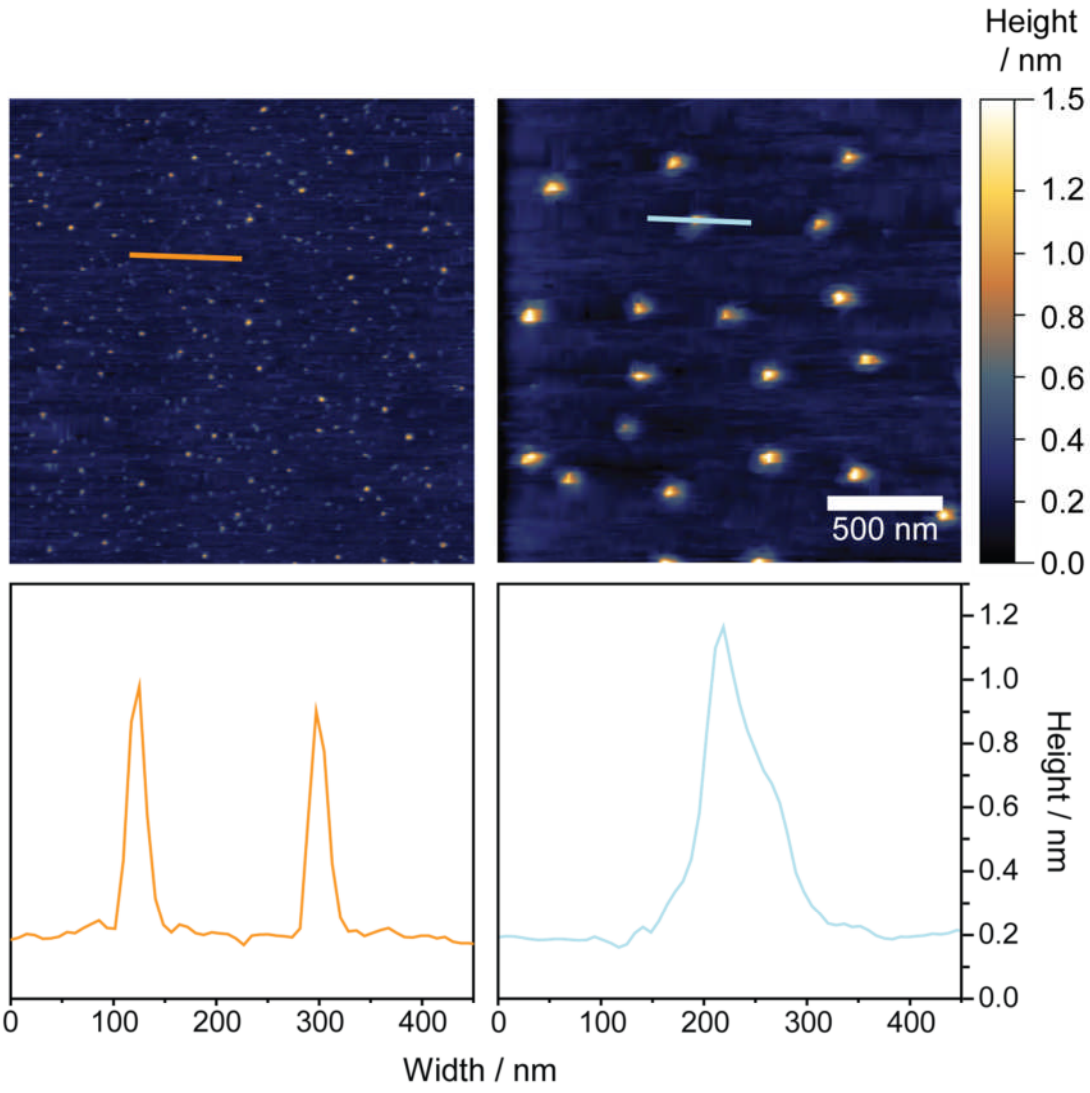

Figure 7.39 Comparison of the height plot profiles of dss1 (left) and dss1 in the presence of **P25a** (right). The AFM micrographs from which the data were taken are shown above the plots, with the location of the plot sample indicated by a solid line. Both images were taken at the same magnification.

Furthermore, the phase contrast diagram (Figure 7.40) suggested that the plateau and central peak were composed of different materials. Taken together, these data suggested that the particles were composed of a central core composed of dss1, surrounded by a corona of **P25a** (see schematic in Figure 7.41). However, the size of the coronae far exceeded that which would have been possible if the particles formed in the manner suggested in Figure 7.35. Instead, it is proposed that as the solution dried to the surface the dss1–**P25a** complexes acted as nucleation sites for the deposition of further **P25a** (see Figure 7.42). This explains the central peak (which corresponded to the original dss1–**P25a**

complex) and surrounding plateau (**P25a** deposited upon drying), and the shallow overall profile of the particles (the central domain had a height of around 1.5 nm – slightly thicker than the expected height for dsDNA – and the surrounding plateau a height of around 0.4 nm – a reasonable thickness for a polymer film).

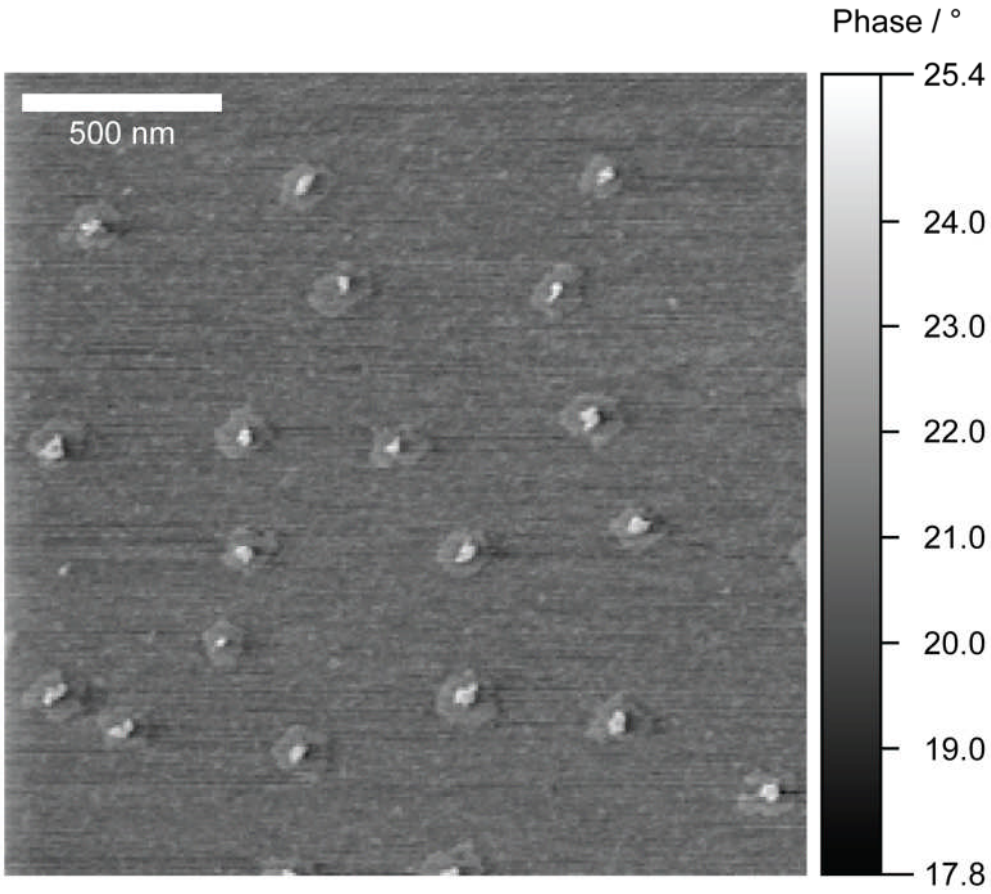

Figure 7.40 AFM phase image of the dss1–**P25a** nanoparticles, showing the difference between the central and outer regions.

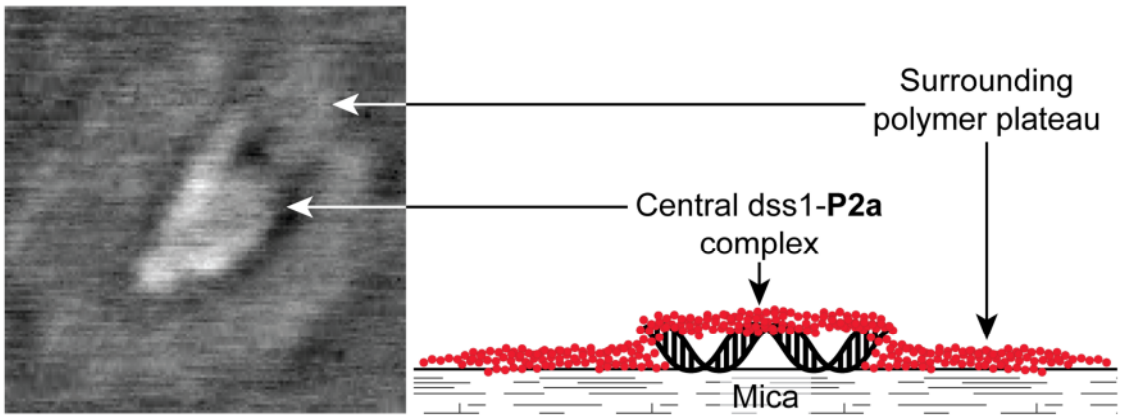

Figure 7.41 AFM phase image (left) of a single dss1–**P25a** nanoparticle. To the right is a cartoon showing the proposed structure, consisting of a central domain of dss1 and **P25a** surrounded by a thin plateau of associated **P25a**.

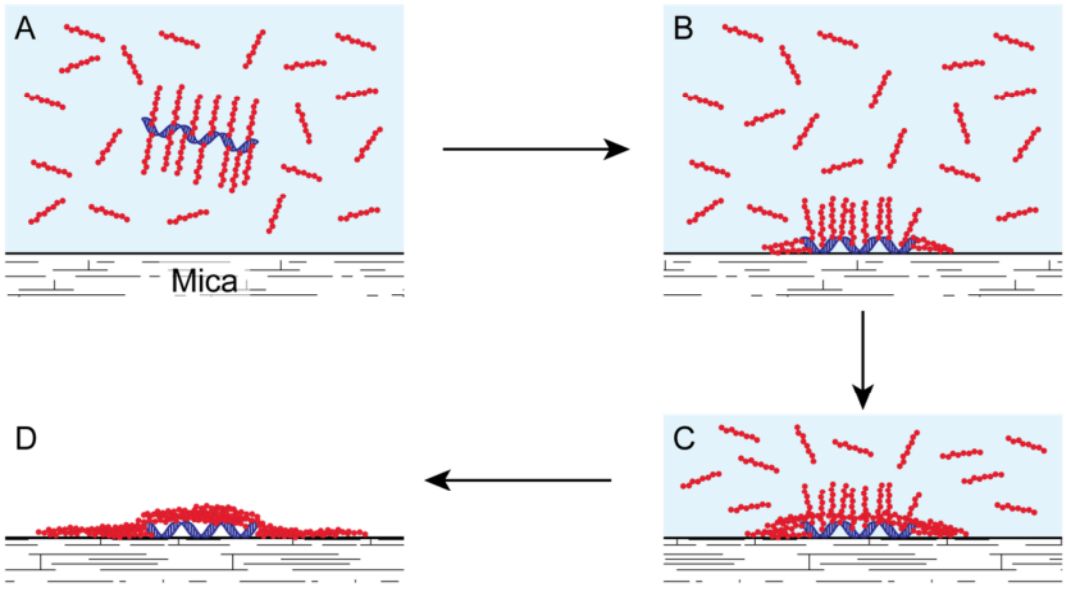

Figure 7.42 Proposed mechanism of formation of the dss1–**P25a** particles observed by AFM. A: the dss1–**P25a** complex exists in solution in the presence of a background concentration of free **P25a**. B: the dss1–**P25a** complex adheres to the AFM substrate. C: as the solution dries, the complex acts as a nucleation site for the deposition of further **P25a**. D: imaging in the dry state shows a large particle composed of a higher central domain containing dss1 surrounded by a low plateau of associated **P25a**.

These results showed that the intercalation interaction could be exploited to create nanoparticles of very uniform size and shape by using well-defined dsDNA as a template.

7.3 Conclusions

The intercalation interaction was exploited to produce non-covalently linked DNA–polymer conjugates. The methyl acridine group was found to be an ineffective R group for the control of the polymerisation of several monomers. However, when this group was incorporated away from the radical polymerisation centre good control was achieved over the polymerisations of NIPAM, DMA, TEGA and 4-AM, to afford polymers containing a terminal acridine group.

These polymers were tested for their interaction with genomic double stranded DNA. Poly(NIPAM)–acridine was found to cause precipitation of DNA even at low concentrations. It was shown that the presence of the acridine group was necessary for this effect to be observed. UV-vis and linear dichroism spectroscopy confirmed that intercalation was, however, occurring. Poly(DMA)–acridine was found to cause DNA precipitation at low DNA concentrations, but this effect was reversed as the concentration of DNA was increased. It was proposed that this was due to the high local concentration of polymer created by intercalation. A UV-vis spectroscopy titration was used to extract an estimate of the association constant, which was found to be only slightly lower than that of the free acridine molecule.

The effect of molecular weight on the association constant was explored, and it was found that doubling the molecular weight approximately halved the strength of intercalation. Poly(TEGA)–acridine was found to have a much weaker interaction than poly(DMA)–acridine of a similar molecular weight, and this difference was attributed to the brush-like structure of the polymer inhibiting the acridine–DNA interaction. Poly(4-AM)–acridine was observed to display intercalation behaviour, but DNA precipitation was too prevalent for the association constant to be quantified. It was proposed that the increased precipitation relative to poly(DMA)–acridine was due to the increased steric bulk of the polymer side chains.

Finally, the intercalation interaction between poly(DMA)–acridine and a short, perfectly-defined sequence of double stranded DNA was observed by UV-vis spectroscopy. Drying of the solution to a mica surface produced very flat, uniform particles that were observed by AFM. Control experiments confirmed that these particles were only formed when the polymer, intercalating end group and DNA were all present. The proposed mechanism of formation is deposition of free polymer around nucleation sites composed of the DNA–polymer complex as the solution dries. These data strongly supported the conclusion that the polymer and DNA were interacting *via* the acridine group, and demonstrated the interesting consequences of using a perfectly-defined DNA sequence in combination with a non-covalently bound polymer.

7.4 Experimental

7.4.i Materials & Methods

For general materials and methods details, see the Appendix. AIBN was recrystallised twice from methanol prior to use. NIPAM was recrystallised from toluene prior to use. DMA and HEA were passed through a neutral alumina column to remove the radical inhibitor prior to use. TEGA was synthesised according to a previously published procedure.[25] 4-AM was distilled prior to use. LD spectroscopy was performed on a Jasco J-815 circular dichroism spectropolarimeter at room temperature using a custom-built 80 μL Couette flow cell. 10 × TM buffer consisted of 1 M Tris and 60 mM $MgCl_2$.

7.4.ii Acridin-9-ylmethyl dodecyl carbonotrithioate, 17

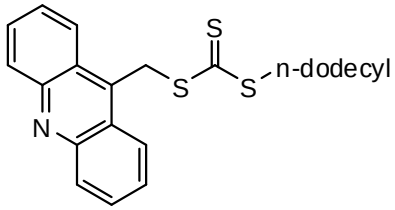

To a suspension of caesium carbonate (0.132 g, 0.40 mmol) in acetone (1 mL) was added dodecanethiol (88 μL, 0.37 mmol) and carbon disulfide (66 μL, 1.10 mmol) and the mixture stirred for 90 minutes. To the bright yellow suspension was added 9-bromomethylacridine (0.050 g, 0.19 mmol) and acetone (0.5 mL) and stirring continued for a further hour, after which time a further portion of 9-bromomethylacridine (0.050 g, 0.19 mmol) and acetone (0.5 mL) was added. The mixture was stirred for 5 hours at room temperature, then filtered and the solvent removed *in vacuo*. The crude residue was purified by recrystallisation from methanol to yield the product as orange crystals (0.066 g, 38 %). ^{1}H NMR (400 MHz, $CDCl_3$) δ 8.26 (d, *J* = 9 Hz, 2H, Ar*H*), 8.19 (d, *J* = 9 Hz, 2H, Ar*H*), 7.80 (t, *J* = 8 Hz, 2H, Ar*H*), 7.61 (t, *J* = 8 Hz, 2H, Ar*H*), 5.57 (s, 2H, ArCH_2S), 3.44 (t, *J* = 7 Hz, 2H, SCH_2CH$_2$), 1.74 (quin, *J* = 7 Hz, 2H, SCH$_2$CH_2), 1.40 (m, 2H, SCH$_2$CH$_2$CH_2), 1.37-1.20 (br m, 18H, alkyl chain CH$_2$), 0.88 (t, *J* = 7 Hz, 3H, CH_3) ppm. ^{13}C NMR (100 MHz, $CDCl_3$) δ 221.2 (*C*=S), 148.6, 130.6, 130.1, 126.8, 125.3, 123.8, 37.4, 33.7, 31.9, 29.6, 29.6, 29.5, 29.4, 29.1,

28.9, 28.0, 14.1 ppm. ESI MS calcd. for $C_{27}H_{35}NS_3$ $[M+H]^+$ 470.2004; observed 470.2000. IR (ν_{max} / cm^{-1}): 2918, 2849, 1470, 1093, 1062, 799, 755, 713.

7.4.iii RAFT polymerisations using CTA 17

Polymerisations of NIPAM, styrene and methyl acrylate were attempted using CTA **17**; an example procedure follows. NIPAM (0.200 g, 1.77 mmol), **17** (0.008 g, 0.02 mmol) and AIBN (0.3 mg, 2 μmol) were all dissolved in DMF (0.4 mL) and transferred to an oven-dried ampoule. The solution was subjected to four freeze-pump-thaw cycles to remove oxygen, sealed under an atmosphere of nitrogen and placed in an oil bath preheated to 65°C for 24 hours. Monomer conversion was measured by ^{1}H NMR and any isolated polymer product was analysed by SEC, eluting with THF.

7.4.iv 5-(acridin-9-ylamino)pentan-1-ol

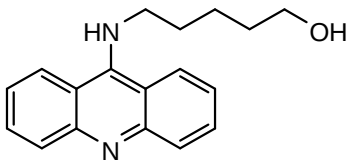

5-(acridin-9-ylamino)pentan-1-ol was synthesised as previously reported.[9] 9-Chloroacridine (0.3350 g, 1.57 mmol) and 5-amino-1-pentanol (0.4044 g, 3.92 mmol) were dissolved in anhydrous DMF (3.35 mL). The solution was thoroughly degassed by three successive freeze-pump-thaw cycles, sealed under nitrogen and heated to 100°C for 5 hours. The reaction was allowed to cool and then water (20 mL) was added and the organic components extracted into dichloromethane (3 × 20 mL). The organic layer was washed with saturated $NaHCO_3$ solution (20 mL), and brine (20 mL), and dried (Na_2SO_4). The drying agent was removed by filtration and washed on the filter with dichloromethane (2 × 10 mL). The solvent was removed *in vacuo* to afford the product as an orange solid (0.3717 g, 85 %). ^{1}H NMR (300 MHz, $CDCl_3$) δ 8.09 (d, J = 9 Hz, 2H, Ar*H*), 8.03 (d, J = 10 Hz, 2H, Ar*H*), 7.64 (t, J = 8 Hz, 2H, Ar*H*), 7.34 (t, J = 8 Hz, 2H, Ar*H*), 3.84 (t, J = 7 Hz, 2H, CH_2OH), 3.68 (t, J = 6 Hz, 2H, CH_2NH), 1.84 (quin, J = 7 Hz, 2H,

CH_2CH$_2$NH), 1.68-1.52 (m, 4H, CH_2CH$_2$CH$_2$OH) ppm. ^{13}C NMR (100 MHz, $CDCl_3$) δ 23.23 (*C*H$_2$CH$_2$CH$_2$OH), 31.18 (*C*H$_2$CH$_2$OH), 32.09 (*C*H$_2$CH$_2$NH), 50.51 (*C*H$_2$NH), 62.35 (*C*H$_2$OH), 115.99 (Ar*C*), 123.02 (Ar*C*), 123.05 (Ar*C*), 128.01 (Ar*C*), 130.44 (Ar*C*) ppm. ESI MS calcd. for $C_{18}H_{20}N_2O$ $[M+H]^+$ 281.2; observed 281.2. IR (ν_{max} / cm^{-1}): 739, 754, 1076, 1262, 1430, 1507, 1559, 2850, 2912, 3328.

7.4.v 5-(acridin-9-ylamino)pentyl 2-(dodecylthiocarbonothioylthio)-2-methylpropanoate, 19

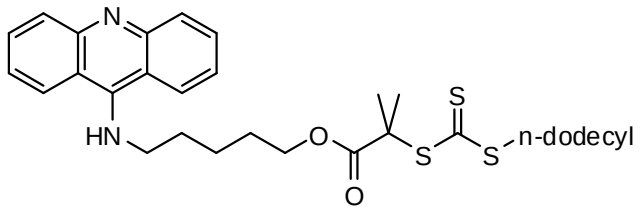

DDMAT (0.260 g, 0.71 mmol), 5-(acridin-9-ylamino)pentan-1-ol (0.200 g, 0.71 mmol), EDCI (0.137 g, 0.71 mmol) and DMAP (0.044 g, 0.36 mmol) were dissolved in a mixture of $CHCl_3$ (5 mL) and DCM (5 mL) and the solution bubbled with nitrogen for 30 minutes. The reaction was then sealed under nitrogen and stirred at room temperature for 24 hours, after which a further portion of EDCI (0.1368 g, 0.71 mmol) was added and the reaction allowed to stir for a further 24 hours. The solvent was removed *in vacuo*. Saturated $NaHCO_3$ solution (15 mL) was added and the products were extracted into DCM (3 × 15 mL). The organic layer was washed with water (2 × 20 mL), and brine (20 mL) and then dried (Na_2SO_4). The drying agent was removed by filtration and washed on the filter with DCM (2 × 10 mL). The solvent was removed from the filtrate *in vacuo* and the residue taken up in a mixture of 9:1 EtOAc/MeOH (15 mL) to precipitate the acridine starting material and EDCI by-product, which were then removed by filtration. The solvent was again removed *in vacuo* and the residue purified by silica gel column chromatography, eluting with EtOAc/MeOH (40:1) and triethylamine (0.1 %). **19** was isolated (R_f 0.15) as a very viscous orange liquid (0.2353 g, 53 %). ^{1}H NMR (300 MHz, $CDCl_3$) δ 8.09 (d, *J* = 9 Hz, 2H, Ar*H*), 7.96 (d, J = 9 Hz, 2H, Ar*H*), 7.56 (m, 2H, Ar*H*), 7.31 (m, 2H, Ar*H*), 6.02

(br s, 1H, N*H*), 4.13 (t, *J* = 6 Hz, 2H, CH_2O), 3.87 (t, *J* = 7 Hz, 2H, NHCH_2), 3.19 (t, *J* = 7 Hz, 2H, SCH_2), 1.90 (m, 2H, NHCH$_2$CH_2), 1.73 (m, 2H, CH_2CH$_2$O), 1.68 (s, 6H, C(CH_3)$_2$), 1.57 (m, 2H, NHCH$_2$CH$_2$CH_2), 1.45 (m, 2H, SCH$_2$CH_2), 1.15-1.35 (br m, 18H, SCH$_2$CH$_2$(CH_2)$_{18}$CH$_3$), 0.87 (t, *J* = 7 Hz, 3H, S(CH$_2$)$_{11}$CH_3) ppm. ^{13}C NMR (100 MHz, CDCl$_3$) δ 221.7 (*C*=S), 173.0 (*C*=O), 152.1, 147.8, 130.5, 127.9, 123.2, 123.1, 116.0, 65.7, 56.0, 50.6, 37.0, 32.0, 31.1, 29.7, 29.6, 29.5, 29.4, 29.1, 28.9, 28.1, 27.9, 25.4 (C(*C*H$_3$)$_2$), 23.5, 22.7, 14.2 ((CH$_2$)$_{11}$*C*H$_3$) ppm [1 signal due to C's 12 missing because of overlap]. ESI MS calcd. for $C_{35}H_{50}N_2O_2S_3$ $[M+H]^+$ 627.3107; observed 627.3108. IR (ν_{max} / cm^{-1}): 752, 814, 1062, 1126, 1155, 1258, 1465, 1559, 1731, 2852, 2922.

7.4.vi Measurement of the extinction coefficient

To measure the extinction coefficient the following dilutions of the molecule of interest were made in either acetonitrile or water: 5, 7.5, 10, 25, 50, 75 and 100 μM. The absorbance at the wavelength under investigation was then recorded for each solution and absorbance plotted versus concentration. Using the equation

$$A = \varepsilon c l$$

where A is the absorbance, ε is the extinction coefficient, c is the concentration and l is the path length of the UV-vis spectrometer cell, ε could be determined by plotting A versus c for a series of known c values and taking the gradient of the resultant line of best fit.

7.4.vii Measurement of reaction kinetics for the polymerisation of NIPAM with 19

19 (55 mg, 0.09 mmol), NIPAM (1 g, 8.84 mmol) and AIBN (2 mg, 0.01 mmol) were dissolved in DMF (1.5 mL) are the mixture degassed by three successive freeze-pump-thaw cycles, then sealed under nitrogen. A 100 μL aliquot was removed every thirty minutes and analysed by ^{1}H NMR spectroscopy and DMF SEC. M_n values were estimated using PMMA calibration standards.

7.4.viii Poly(NIPAM)

19 (55.4 mg, 0.09 mmol), NIPAM (1 g, 8.84 mmol) and AIBN (1.5 mg, 0.01 mmol) were mixed in DMF (1.5 mL) and the solution degassed by three successive freeze-pump-thaw cycles. After warming to room temperature and sealing under an atmosphere of nitrogen, the reaction vessel was placed in an oil bath heated to 65°C for 2.5 hours. The polymer solution was diluted with THF (~1 mL) and precipitated into diethyl ether (300 mL) cooled with dry ice, and collected by filtration to yield the product as a yellow solid (370.9 mg, 55 %[§§]), which was then analysed by DMF SEC using PMMA calibration standards (M_n 6.3 kDa, Đ 1.15). ^{1}H NMR ($CDCl_3$, 400 MHz) 8.22 (m, 2H, acridine *H*), 8.07 (m, 2H, acridine *H*), 7.71 (m, 2H, acridine *H*), 7.37 (m, 2H, acridine *H*), 7.60-5.60 (br m, PNIPAM N*H*), 3.98 (br s, PNIPAM C*H*$(CH_3)_2$), 3.32 (m, 2H, SCH_2), 2.6-0.8 (br m, PNIPAM backbone *H*), 1.12 (br s, PNIPAM CH(CH_3)$_2$), 0.87 (t, J = 7 Hz, 3H, S$(CH_2)_{11}$CH_3) ppm.

7.4.ix Poly(DMA)

Two molecular weights of poly(DMA) were synthesised. What follows is an example procedure. **19** (20.0 mg, 32 μmol), DMA (327.0 mg, 3.3 mmol) and AIBN (0.5 mg, 3 μmol) were mixed in 1,4-dioxane (1.26 mL) and the solution degassed by three successive freeze-pump-thaw cycles. After warming to room temperature and sealing under an atmosphere of nitrogen, the reaction vessel was placed in an oil bath heated to 65°C for four hours. The polymer was precipitated from pet. ether 40-60 (100 mL) cooled in an ice bath and allowed to settle. The solvent was decanted and the solid re-dissolved in 1,4-dioxane (2 mL), then precipitated again into pet. ether 40-60 (100 mL) cooled in an ice bath. The mixture was centrifuged and the solvent decanted to afford the product as a yellow solid (98 mg, 46 %[***]), which was analysed by DMF SEC using PMMA calibration standards (M_n 6.7 kDa, Đ 1.13). ^{1}H NMR ($CDCl_3$, 400 MHz) 8.19 (br m, 2H, acridine *H*), 8.09 (br m, 2H,

§§ Based on 62 % monomer conversion as assessed by ^{1}H NMR spectroscopy at the end of the polymerisation.

*** Based on 65 % monomer conversion as assessed by ^{1}H NMR spectroscopy at the end of the polymerisation.

acridine *H*), 7.67 (br t, 2H, acridine *H*), 7.35 (br m, 2H, acridine *H*), 4.20-3.80 (br m, 4H, end group NCH_2 and $(CH_3)_2CO_2CH_2$), 3.32 (br m, 2H, SCH_2), 3.25-2.20 (br m, PDMA C*H*CON$(CH_3)_2$), 2.15-0.95 (br m, PDMA backbone *H*), 0.78 (t, *J* = 7 Hz, 3H, $S(CH_2)_{11}CH_3$) ppm.

7.4.x Poly(TEGA)

19 (20.0 mg, 32 μmol), TEGA (651.4 mg, 3.2 mmol) and AIBN (0.5 mg, 3 μmol) were mixed in DMF (1.3 mL) and the solution degassed by three successive freeze-pump-thaw cycles. After warming to room temperature and sealing under an atmosphere of nitrogen, the reaction vessel was placed in an oil bath heated to 65°C for seven hours. 18 MΩ water (9 mL) was added and the solution dialysed against water (MWCO 1 000 Da) for two days, incorporating five water changes. The product was isolated by freeze-drying as a yellow solid (308 mg, 66 %[†††]), which was analysed by DMF SEC using PMMA calibration standards (M_n 10.1 kDa, Đ 1.22). ^{1}H NMR ($CDCl_3$, 400 MHz) 8.18 (m, 2H, acridine *H*), 7.68 (m, 2H, acridine *H*), 7.37 (br t, 2H, acridine *H*), 4.17 (br s, PTEGA CO_2CH_2), 3.63 (br s, PTEGA OCH_2), 3.53 (br t, PTEGA $CO_2CH_2CH_2$), 3.37 (br s, PTEGA CH_3), 2.31 (br m, PTEGA C*H*CO_2), 2.10-1.00 (br m, PTEGA backbone *H*), 0.87 (t, *J* = 7 Hz, 3H, $S(CH_2)_{11}CH_3$) ppm.

7.4.xi Poly(4-AM)

19 (44.4 mg, 71 μmol), 4-AM (0.5 g, 3.5 mmol) and AIBN (1.2 mg, 7 μmol) were mixed in 1,4-dioxane (1.5 mL) and the solution degassed by three successive freeze-pump-thaw cycles. After warming to room temperature and sealing under an atmosphere of nitrogen, the reaction vessel was placed in an oil bath heated to 70°C for five hours. The solution was diluted with 18 MΩ water (50 mL) and dialysed against deionised water, incorporating five water changes. The product was isolated by freeze-drying as a pale yellow solid

[†††] Based on 72 % monomer conversion as assessed by ^{1}H NMR spectroscopy at the end of the polymerisation.

(335.0 mg, 84 %[##]), which was analysed by DMF SEC using PMMA calibration standards (M_n 8.4 kDa, Đ 1.15). ^{1}H NMR ($CDCl_3$, 400 MHz) 8.12 (br m, 2H, acridine *H*), 8.03 (br s, 2H, acridine *H*), 7.64 (br s, 2H, acridine *H*), 7.33 (br m, 2H, acridine *H*), 4.20-3.00 (br m, P4-AM NCH_2CH_2O), 2.90-2.20 (br m, P4-AM C*H*C=O), 2.20-1.00 (br m, P4-AM backbone *H*), 0.87 (t, *J* = 7 Hz, 3H, S$(CH_2)_{11}$CH_3) ppm.

7.4.xii Poly(HEA)

19 (27 mg, 43 μmol), HEA (495 μL, 4.3 mmol) and AIBN (2 mg, 13 μmol) were mixed in methanol (1 mL) and the solution degassed by four successive freeze-pump-thaw cycles. After warming to room temperature and sealing under an atmosphere of nitrogen, the reaction vessel was placed in an oil bath heated to 60°C for twenty-one hours. The polymer was precipitated into *n*-hexane and diethyl ether (1:1) and collected by filtration to yield the product as a yellow solid (129 mg, 27 %[§§§]), which was analysed by DMF SEC using PMMA calibration standards (M_n 22.9 kDa, Đ 1.89). ^{1}H NMR (CD_3OD, 300 MHz) 8.35 (t, *J* = 8 Hz, 2H, acridine *H*), 7.85 (m, 2H, acridine *H*), 7.74 (t, *J* = 8 Hz, 2H, acridine *H*), 7.41 (t, *J* = 7 Hz, 2H, acridine *H*), 4.13 (br s, PHEA CO_2CH_2), 3.72 (br s, PHEA CH_2OH), 2.41 (br s, PHEA C*H*CO_2), 2.10-1.00 (br m, PHEA backbone *H*), 0.86 (t, *J* = 7 Hz, 3H, S$(CH_2)_{11}$CH_3) ppm.

7.4.xiii Measurement of the association constant, K_a

This section details the derivation of the equations used to calculate the association constant for the acridine-containing polymers with ctDNA.

The total concentrations of DNA base pairs and acridine in the solution ($[BP]_0$ and $[Acr]_0$) are related to the concentrations of free acridine, free base pairs and base pair–acridine complex as shown in Equation 7.4.

$$[Acr]_0 = [Acr] + [BP–Acr]$$

[##] Based on 80 % monomer conversion as assessed by ^{1}H NMR spectroscopy at the end of the polymerisation.
[§§§] Based on 95 % monomer conversion as assessed by ^{1}H NMR spectroscopy at the end of the polymerisation.

$$[\mathrm{BP}]_0 = [\mathrm{BP}] + [\mathrm{BP{-}Acr}]$$

Equation 7.4 Definition of the total concentration of acridine ($[\mathrm{Acr}]_0$) and base pairs ($[\mathrm{BP}]_0$) in terms of the concentrations of free acridine, free base pairs and base pair–acridine complex.

The mole fraction, $f_{\mathrm{BP{-}Acr}}$, of base pair–acridine complex in solution is defined according to Equation 7.5. Note that $f_{\mathrm{BP{-}Acr}}$ is defined in terms of the concentration of free acridine, not free DNA. This is because, in the case of the UV-vis titrations above, the acridine concentration was kept almost constant throughout the experiment, which simplifies the analysis.

$$f_{\mathrm{BP{-}Acr}} = \frac{[\mathrm{BP{-}Acr}]}{[\mathrm{Acr}] + [\mathrm{BP{-}Acr}]} = \frac{[\mathrm{BP{-}Acr}]}{[\mathrm{Acr}]_0}$$

Equation 7.5 Definition of the mole fraction, $f_{\mathrm{BP{-}Acr}}$, of base pair–acridine complex present in solution.

Using Equation 7.2 and Equation 7.4, the mole fraction can then be re-written as shown in Equation 7.6.

$$f_{\mathrm{BP{-}Acr}} = \frac{K_a[\mathrm{BP}]}{1 + K_a[\mathrm{BP}]}$$

Equation 7.6 Expression of the mole fraction of base pair–acridine complex present in solution as a function of the association constant and the concentration of free base pairs.

The mole fraction of base pair–acridine complex is related to its concentration by Equation 7.7.

$$[\mathrm{BP{-}Acr}] = f_{\mathrm{BP{-}Acr}}[\mathrm{Acr}]_0$$

Equation 7.7 Relation of the mole fraction of base pair–acridine complex to its concentration.

The observed change in absorbance, ΔA, can be written as shown in Equation 7.8, where $\varepsilon_{\Delta\mathrm{BP{-}Acr}}$ is the 'delta extinction coefficient' – essentially the difference between the extinction coefficients of the free acridine and the acridine when complexed to a base pair.

$$\Delta A = \varepsilon_{\Delta \mathrm{BP-Acr}}[\mathrm{BP-Acr}]$$

Equation 7.8 Expression of the observed change in UV-vis absorbance (ΔA) in terms of the concentration of the base pair–acridine complex and the delta extinction coefficient.

By substituting in Equation 7.6 and Equation 7.7, and noting that $\Delta A_{\mathrm{max}} = \varepsilon_{\Delta \mathrm{BP-Acr}}[\mathrm{Acr}]_0$, an expression for ΔA in terms of K_a and free base pair concentration can then be obtained, as shown in Equation 7.3.

$$\Delta A = \frac{\Delta A_{max} K_a [\mathrm{BP}]}{1 + K_a [\mathrm{BP}]}$$

Equation 7.9 The relation between ΔA and free base pair concentration used to extract the association constant, K_a, for the interaction between ctDNA and **P25a** from UV-vis spectroscopy data.

7.4.xiv UV-vis spectroscopy titrations to determine K_a

A 1.5 mL solution of acridine-containing polymer (**P24**-**27**) was made up at 20 μM (calculated using the extinction coefficient of the acridine group) by diluting a 1 mM acetonitrile stock solution with 18 MΩ water. The sample was heated to 30°C within the UV-vis spectrometer (with stirring) and the UV-vis spectrum recorded. DNA (10 μL, 5 mM concentration of base pairs in 1 × TM buffer) was added and the mixture allowed to equilibrate for two minutes before repeating the UV-vis measurement. This process was repeated until the desired amount of DNA had been added. The data were analysed and manipulated using OriginLab 8.5 graphing and analysis software, using a non-linear least squares method with Equation 7.3 to calculate K_a.

7.4.xv LD spectroscopy

A 1.5 mL solution of acridine-containing polymer (**P24**-**27**) was made up at 20 μM (calculated using the extinction coefficient of the acridine group) by diluting a 1 mM acetonitrile stock solution with 18 MΩ water. The LD spectrum was then recorded. ctDNA (1 μL, 5 mM in 1 × TE buffer) and 18 MΩ water (49 μL) were added and the

mixture shaken by hand for one minute before repeating the LD measurement. Measurements were also made of solutions to which had been added 2, 3, 4, 5, 10, 20, 30, 40 and 50 μL of the ctDNA solution. In each case an appropriate amount of 18 MΩ water was added so that the total volume of liquid added to the polymer solution was 50 μL.

7.4.xvi Assembly of dss1

The double stranded DNA dss1 was assembled from the component strands (s1 and s1') as follows. s1 (50 μL, 200 μM in water) and s1' (50 μL, 200 μM in water) were mixed with 18 MΩ water (12.5 μL) and 10 × TM buffer (12.5 μL). The solution was heated to 95°C for twenty minutes and then left to cool slowly in the heating block to room temperature. Formation of the double helix was confirmed by 15 % native PAGE analysis.

7.4.xvii AFM

A solution of the dss1–**P25a** complex was studied by AFM as follows. **P25a** (1.5 mL, 20 μM in water) was mixed with dss1 (50 μL, 80 μM in 1 × TM buffer) and the mixture allowed to equilibrate for two minutes. The solution was diluted one hundred-fold with 18 MΩ water and immediately deposited onto freshly-cleaved mica and allowed to air-dry at room temperature. The sample was then placed inside the atomic force microscope and analysed in tapping mode. Solutions of dss1, **P25a** and dss1 in the presence of poly(DMA) without an acridine end group were also analysed using this procedure.

7.5 References

(1) Schleif, R. *Science* **1988**, *241*, 1182.

(2) Reddy, B. S. P.; Sondhi, S. M.; Lown, J. W. *Pharmacol. Ther.* **1999**, *84*, 1.

(3) Krpetić, Ž.; Singh, I.; Su, W.; Guerrini, L.; Faulds, K.; Burley, G. A.; Graham, D. *J. Am. Chem. Soc.* **2012**, *134*, 8356.

(4) Su, W.; Schuster, M.; Bagshaw, C. R.; Rant, U.; Burley, G. A. *Angew. Chem., Int. Ed.* **2011**, *50*, 2712.

(5) Su, W.; Bonnard, V.; Burley, G. A. *Chem. A Eur. J.* **2011**, *17*, 7982.

(6) Singh, I.; Wendeln, C.; Clark, A. W.; Cooper, J. M.; Ravoo, B. J.; Burley, G. A. *J. Am. Chem. Soc.* **2013**, *135*, 3449.

(7) Marques, M. A.; Doss, R. M.; Foister, S.; Dervan, P. B. *J. Am. Chem. Soc.* **2004**, *126*, 10339.

(8) Snyder, R. D.; McNulty, J.; Zairov, G.; Ewing, D. E.; Hendry, L. B. *Mutat. Res., Fundam. Mol. Mech. Mutagen.* **2005**, *578*, 88.

(9) Imoto, S.; Hirohama, T.; Nagatsugi, F. *Bioorg. Med. Chem. Lett.* **2008**, *18*, 5660.

(10) Maeda, M.; Nishimura, C.; Umeno, D.; Takagi, M. *Bioconjugate Chem.* **1994**, *5*, 527.

(11) Umeno, D.; Kano, T.; Maeda, M. *Anal. Chim. Acta* **1998**, *365*, 101.

(12) Umeno, D.; Maeda, M. *Anal. Sci.* **1997**, *13*, 553.

(13) Moad, G.; Rizzardo, E.; Thang, S. H. *Aust. J. Chem.* **2005**, *58*, 379.

(14) Skrabania, K.; Miasnikova, A.; Bivigou-Koumba, A. M.; Zehm, D.; Laschewsky, A. *Polym. Chem.* **2011**, *2*, 2074.

(15) Hicks, M. R.; Kowalski, J.; Rodger, A. *Chem. Soc. Rev.* **2010**, *39*, 3380.

(16) Estevez-Torres, A.; Baigl, D. *Soft Matter* **2011**, *7*, 6746.

(17) Lerman, L. S. *Proc. Natl. Acad. Sci. U. S. A.* **1971**, *68*, 1886.

(18) Vasilevskaya, V. V.; Khokhlov, A. R.; Matsuzawa, Y.; Yoshikawa, K. *J. Chem. Phys.* **1995**, *102*, 6595.

(19) Mayama, H.; Iwataki, T.; Yoshikawa, K. *Chem. Phys. Lett.* **2000**, *318*, 113.

(20) Yim, H.; Kent, M. S.; Mendez, S.; Lopez, G. P.; Satija, S.; Seo, Y. *Macromolecules* **2006**, *39*, 3420.

(21) Lyles, M. B.; Cameron, I. L. *Biophys. Chem.* **2002**, *96*, 53.

(22) Hansma, H. G.; Sinsheimer, R. L.; Li, M.-Q.; Hansma, P. K. *Nucleic Acids Res.* **1992**, *20*, 3585.

(23) Hansma, H. G.; Revenko, I.; Kim, K.; Laney, D. E. *Nucleic Acids Res.* **1996**, *24*, 713.

(24) Arnott, S.; Chandrasekaran, R.; Birdsall, D. L.; Leslie, A. G. W.; Ratliff, R. L. *Nature* **1980**, *283*, 743.

(25) Ryu, J.-H.; Roy, R.; Ventura, J.; Thayumanavan, S. *Langmuir* **2010**, *26*, 7086.

Conclusion

This work has shown that conjugation of synthetic polymers to DNA in organic solution is challenging. The commonly-used strategies of amide coupling and the thiol Michael addition reaction were shown to be ineffective for the efficient production of DNA–polymer conjugates.

The inverse electron demand Diels–Alder reaction between tetrazine and norbornene was used for the first time to produce DNA–polymer conjugates, and this strategy was shown to be effective in organic solution. However, the time-consuming synthesis and instability of the precursor compounds limited the general appeal of this approach.

The copper-catalysed azide–alkyne cycloaddition reaction was developed to provide a highly efficient synthetic route to DNA–polymer conjugates. With use of the correct catalyst and conditions, yields of over 90 % could be achieved at low DNA concentrations, in organic solution and without the need for a solid support. Efficient conjugation of a variety of polymers was demonstrated, including the highly hydrophobic polymer poly(styrene). Additionally, internal polymer-modification of a DNA strand was achieved – this was the first time this has been demonstrated in high yield.

Conjugation of a DNA tetrahedron-forming DNA strand to a temperature-responsive polymer led to the creation of a novel surfactant-like molecule capable of stabilising the formation of well-defined, discrete nanoparticles of the polymer at elevated temperatures. The formation of this material was only possible due to the combination of the unique properties of both parts of the conjugate: the structure-directing nature of the DNA strand and the stimuli-responsiveness of the polymer.

The use of a non-covalent interaction for the production of DNA–polymer conjugates was explored in depth for the first time. This approach was used to produce well-defined hybrid nanoparticles by using a known sequence of double stranded DNA as a template.

The straightforward preparation of these particles is an attractive feature of this system, and it is hoped that this will lead to practical applications, which could include delivery of therapeutic DNA.

It is hoped that the relatively straightforward synthesis of the conjugate precursor compounds demonstrated here (azide- and alkyne-modifications can already be purchased for made-to-order DNA strands, and these functionalities are simple to incorporate at a polymer chain end) will mean that more polymer research groups begin to explore the possibilities that these novel materials offer. With the plethora of polymer structures and DNA architectures now available, this work has only scratched the surface of what is possible.

Future Work

Having established an effective and highly efficient conjugation chemistry for the synthesis of DNA–polymer conjugates, future work will concentrate on exploring its use for the incorporation of further novel polymers into DNA hybrid materials. Whilst it was shown that poly(styrene) could be conjugated efficiently, other hydrophobic polymers were not explored. The use of a polymer with a lower glass transition temperature would be of interest here, for the synthesis of more dynamic DNA–polymer micelles. The use of polymers responsive to stimuli other than temperature – for example poly(2-(*N*,*N*-diisopropylamino) ethyl acrylate) (responsive to pH) – should also be investigated.

The DNA tetrahedron used in the hybrid nanoparticles should be exploited to its fullest potential. This might include altering the dimensions of the tetrahedron (for instance by making it larger or asymmetrical) or using it to encapsulate enzymes or drug molecules. Additionally, the attachment of temperature-responsive polymers to different DNA nanostructures such as the origami tile will be explored, since it is envisaged that this could lead to some novel aggregation behaviour.

Finally, the templating observed using the intercalation interaction will be exploited to produce well-defined polymer nanotubes by permanent crosslinking of the polymers attached to the double stranded DNA. In this way, the length could be controlled very precisely, simply by changing the length of the DNA duplex used.

Appendix

Materials & Methods

Size exclusion chromatography (SEC)

DMF SEC data were obtained in HPLC grade DMF containing 1 mg mL^{-1} lithium bromide at 323 K, with a flow rate of 1.0 mL min^{-1}, on a set of two Varian PLgel 5 μm Mixed-D columns (7.5 mm diameter), with guard column. THF SEC data were obtained in HPLC grade THF containing 2 % triethylamine at 293 K, with a flow rate of 1.0 mL min^{-1}, on a set of two Varian PLgel 5 μm Mixed-D columns (7.5 mm diameter), with guard column. $CHCl_3$ SEC data were obtained in HPLC grade $CHCl_3$ at 293 K, with a flow rate of 1.0 mL min^{-1}, on a set of two Varian PLgel 5 μm Mixed-D columns (7.5 mm diameter), with guard column. SEC data were analysed using Cirrus SEC software calibrated using poly(methyl methacrylate) standards (690-271 400 Da) or poly(styrene) standards (162-371 100 Da).

NMR spectroscopy

^{1}H, ^{19}F and ^{13}C NMR spectra were recorded on Bruker DPX-300 or -400 spectrometers at 293 K. Chemical shifts are reported as δ in parts per million (ppm) and referenced to the residual solvent resonances ($CDCl_3$ ^{1}H: δ = 7.26 ppm; ^{13}C δ = 77.16 ppm. d_6-DMSO ^{1}H: δ = 2.50 ppm; ^{13}C: δ = 39.52 ppm).

IR spectroscopy

IR measurements were collected on a PerkinElmer Spectrum 100 FT-IR spectrometer. Solid samples were crushed and then applied to the FTIR sensor; liquid samples were applied as a small droplet.

UV-vis spectroscopy

UV-vis measurements were collected on a PerkinElmer Lambda 35 spectrometer using a Hellma TrayCell with a 1 mm path length adapter or, for cloud point measurements, with a

quartz cell with a 1 cm path length. DNA solution concentrations were determined using UV-vis absorption measurements at 260 nm and the known extinction coefficient supplied by the manufacturer, except in the case of calf thymus DNA, where an average base pair extinction coefficient of 6 600 M cm^{-1} was used.

Mass spectrometry

ESI mass spectra were collected on a Bruker Esquire2000 ESI-MS machine using either methanol (for small molecules) or a 1:1 mixture of 2-propanol and 50 mM ammonium acetate (for DNA samples) as solvent. MALDI-ToF mass spectra were collected on a Bruker Ultraflex II MALDI-ToF machine using 3-hydroxypicolinic acid as the matrix.

Electrophoresis

Electrophoresis involves the movement of charged molecules through a gel (typically composed of either poly(acrylamide) or agarose) by an electric current. Molecules are separated based on their mass-to-charge ratio and also the shape they adopt in solution. Larger molecules travel more slowly through the gel as the size of the pores limits the number of paths they can take through it. For single stranded DNA (ssDNA) the mass-to-charge ratio remains constant regardless of the length of the sequence and a random coil conformation is adopted in solution; ssDNA is therefore separated based solely on mass. If secondary structure is present then this can affect the way a molecule moves through the gel. For example, double stranded DNA (dsDNA) has a rigid rod shape in solution, which is more compact than a random coil and thus moves more quickly through the gel than ssDNA of the same mass. Native electrophoresis allows retention of secondary structure (i.e. DNA hybridisation interactions); denaturing electrophoresis using a hydrogen-bonding small molecule such as urea to remove all secondary structure from the sample – therefore, only random coil ssDNA is observed using this technique.

Native polyacrylamide gel electrophoresis (PAGE) was carried out with 1 × Tris-Acetate EDTA (TAE) as running buffer at 4°C and constant voltage of 200 V, loading with

glycerol/bromophenol blue loading buffer. Denaturing PAGE was carried out using gels containing 8.3 M urea, with 1 × Tris-Borate EDTA (TBE) as running buffer at a constant voltage of 300 V, loading with formamide/bromophenol blue/xylene cyanol loading buffer. All gels were run using a Bio-Rad Mini-Protean Tetra System apparatus, and visualised using SYBR Gold nucleic acid stain, purchased from Invitrogen, under UV transillumination with a UVITEC UVIdoc HD2 gel documentation system. For both native and denaturing PAGE, samples were diluted so that approximately 1 pmol of DNA was added to each lane of the gel (typically 10 μL of a 100 nM solution). Agarose gels contained 2 % agarose, were loaded with glycerol/bromophenol blue loading buffer and run using a Bio-Rad Mini-Sub® Cell GT System apparatus. Yields were estimated by densitometry using the Image-J image analysis package by taking the area under the peak of interest and dividing it by the area under all DNA-containing peaks.

1 × TAE buffer consisted of 40 mM Tris-acetate and 1 mM EDTA. 1 × TBE buffer consisted of 89 mM Tris-borate and 2 mM EDTA. 1 × TE buffer consisted of 10 mM Tris-HCl and 1 mM EDTA. The native loading buffer consisted of 25 % glycerol and 0.05 % bromophenol blue in 1 × TE buffer, and was diluted five-fold before use. The denaturing loading buffer consisted of 90 % formamide, 0.5 % EDTA and 0.05 % bromophenol blue and xylene cyanol in 18 MΩ water.

HPLC

HPLC analyses were performed on a Varian 920-LC™ integrated liquid chromatography system. Chromatography was performed on a Waters XBridge™OST C18 2.5 μm 4.6 × 50 mm column heated to 40°C (for DNA strands) or 24°C (for DNA–polymer conjugate). Flow rate was set at 1 mL min^{-1} with a linear gradient of the following buffers: Buffer A, 0.1 M triethylammonium acetate, 5 % acetonitrile, pH 7.0; buffer B, 0.1 M triethylammonium acetate, 70 % acetonitrile, pH 7.0. Fractions collected were combined and concentrated using an Eppendorf concentrator plus.

Dynamic Light Scattering

Hydrodynamic diameters (D_h) and size distributions of nanoparticles were determined by DLS on a Malvern Zetasizer Nano ZS operating at 24°C or 40°C with a 4 mW He-Ne 63 nm laser module. Disposable plastic sizing microcuvettes were used. Measurements were made at a detection angle of 173° (back scattering), and the data analysed using Malvern DTS 5.02 software, using the multiple narrow modes setting. All measurements were made in triplicate, with at least 10 runs per measurement.

Transmission Electron Microscopy

Cryogenic Transmission Electron Microscopy samples were examined using a Jeol 2010F TEM operated at 200 kV and imaged using a GatanUltrascan 4000 camera. Images were captured using Digital Micrograph software (Gatan). A 3 μL droplet of the sample solution was rapidly transferred to a holey carbon-coated copper grid, and blotted to remove excess solution. Subsequently, the grid was plunged into liquid ethane to vitrify the sample. The temperature of the cryogenic stage was maintained below −170°C, using liquid nitrogen, during imaging. Graphene oxide (GO) imaging was performed on 400 mesh lacy carbon films with deposited GO films, using a JEOL 2000FX TEM operated at 200kV equipped with a Gatan Orius digital camera. A solution of the particles (2 μL) was deposited on the GO surface and allowed to air dry before imaging. Where appropriate, particle size analysis was performed using ImageJ.

DNA structures and sequences

The sequences of the DNA strands used in this work are given below. The colour coding corresponds to that used throughout the text. All sequences are given 5' to 3' unless otherwise stated. The structures of the modifications (where available) are also given. All modifications (except for the internal alkyne) were incorporated at the 5' end of the DNA strand.

s0: GCC CGA AAT ACC CCG TTA GAA A

s0': TTT CTA ACG GGG TAT TTC GGG C

s1: AGG CAG TTG AGA CGA ACA TTC CTA AGT CTG AAA
TTT ATC ACC CGC CAT AGT AGA CGT ATC ACC

s1': GGT GAT ACG TCT ACT ATG GCG GGT GAT AAA TTT
CAG ACT TAG GAA TGT TCG TCT CAA CTG CCT

s2: CTT GCT ACA CGA TTC AGA CTT AGG AAT GTT CGA
CAT GCG AGG GTC CAA TAC CGA CGA TTA CAG

s2-alkyne: CTT GCT ACA CGU(alkyne) TTC AGA CTT AGG AAT
GTT CGA CAT GCG AGG GTC CAA TAC CGA CGA TTA
CAG

s3: GGT GAT AAA ACG TGT AGC AAG CTG TAA TCG ACG
GGA AGA GCA TGC CCA TCC ACT ACT ATG GCG

s4: CCT CGC ATG ACT CAA CTG CCT GGT GAT ACG AGG
ATG GGC ATG CTC TTC CCG ACG GTA TTG GAC

Acrylamide:

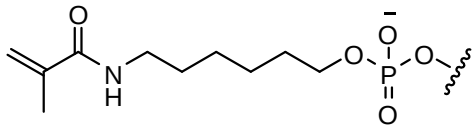

Alkyne:

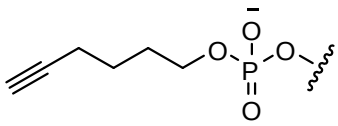

Amine:

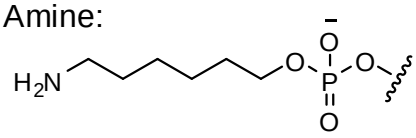

Alkyne (internal):

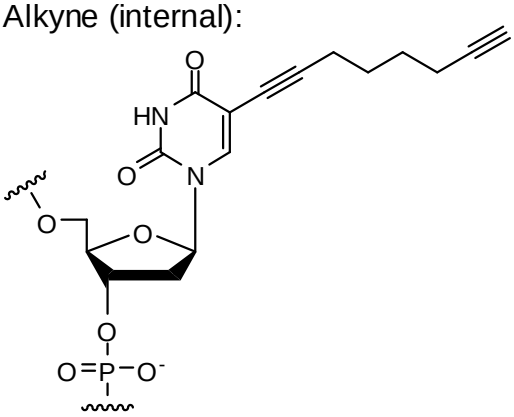

FAM:

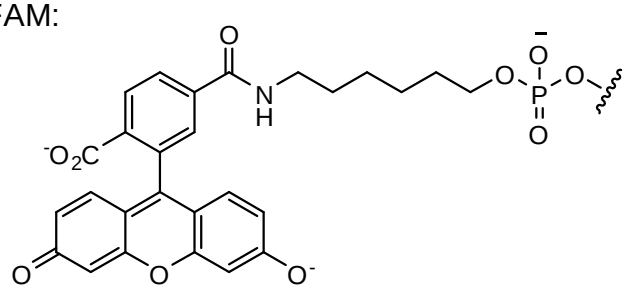

TAMRA: